UNIVERSIDAD DE EXTREMADURA

TESIS DOCTORAL

Comunicación Celular basada en la Vía de Señalización de Notch.

Antuca de los Ángeles Callejas Marín

Doctorado en Biomarcadores de Salud y Estados Patológicos.

Conformidad de los Directores:

Fdo.: **Carlos Lois** Fdo.: **Matías Hidalgo Sánchez**

2021

AUTORIZACIÓN PARA LA PRESENTACIÓN DE LA TESIS DOCTORAL

CARLOS LOIS, RESEARCH PROFESSOR AT BIOLOGY AND BIOLOGICAL ENGINEERING DIVISION AT THE CALIFORNIA INSTITUTE OF TECHNOLOGY, Y **MATIAS HIDALGO SANCHEZ,** PROFESOR TITULAR DEL ÁREA DE BIOLOGÍA CELULAR DE LA UNIVERSIDAD DE EXTREMADURA.

CERTIFICAN:

Que la presente Tesis Doctoral, titulada: **Comunicación Celular basada en la Vía de Señalización de Notch** (**"Cell-cell Interaction based on Notch Signalling Pathway"**, de la que es autor la Lda. **Antuca de los Ángeles Callejas Marín** ha sido realizada en "Biology and Biological Engineering Division at the California Institute of Technology" y en el Departamento de Anatomía, Biología Celular y Zoología de la Universidad de Extremadura bajo sus direcciones.

Revisado el presente trabajo, los directores consideran que tiene la calidad científica necesaria para ser defendido ante el tribunal que se designe al efecto, por lo que:

AUTORIZAN la presentación de la Tesis Doctoral para su defensa.

Y para que conste y surta sus efectos en el expediente correspondiente, expedimos la presente certificación en Badajoz a 10 de Enero de 2021.

Fdo.: **Carlos Lois** Fdo.: **Matías Hidalgo Sánchez**

FINANCIACIÓN

Esta tesis doctoral fue realizada por el que suscribe en “Biology and Biological Engineering Division at the California Intitute of Technology” y en el Departamento de Anatomía, Biología Celular y Zoología de la Universidad de Extremadura bajo y ha sido financiada por los siguientes proyectos:

TITULO DEL PROYECTO: TRACT: **A TOOL TO INVESTIGATE BRAIN CONNECTIVITY AND TO GENETICALLY MANIPULATE NEURONS CONNECTED BY SYNAPSES.**

ENTIDAD FINANCIADORA: **National Institutes of Healths (NIH); (**1RF1MH117825-01)

INVESTIGADOR PRINCIPAL: **Carlos Lois**

Me enseñaron que el camino del progreso no era Rápido ni fácil.
(Marie Curie)

Es siempre recomendable percibir claramente nuestra ignorancia.
(Charles Darwin)

ACKWOLEDGEMENT (AGRADECIMIENTOS).

Con estas líneas en inglés y castellano quiero expresar mi más sincero agradecimiento a todas aquellas personas que a lo largo de estos años han hecho posible que llegue al fin del inicio de una nueva etapa, como es la Tesis Doctoral.

First of all, I would like to thank my PhD advisors, Dr Carlos Lois and Dr Matias Hidalgo Sanchez, for their mentoring and support throughout the years. Dr Carlos Lois thanks for all your advice and open my vision in some scientific fields with your knowledge, curiosity, and many ideas.

Special thanks to all my colleagues in Carlos Lois' laboratory for their knowledge and feedback. I want to make a special mention of Walter, Aubrie, Ellsa, Soomin, Ting-Hao and Tarciso. My research would not be possible without their help. Walter, thanks for all your help with programming and statistical analysis and thanks for the talks in front of the computer for so many hours, it was fun! Aubrie, Ellsa and Soomin thanks for your work, time and availability all the time. Without you, many constructs would not be possible to make. Ting-Hao, thanks for your knowledge and explanations about transgenic flies. Walter, Aubrie and Ellsa thanks for your comradeship with me.

I also would like to thank Tino Pleiner, a postdoctoral in Rebeca Voorhees´ lab for explanations and help with immunoprecipitations and availability. Also, I have to thank Jeff, Brett and Dr Tsui-Fen from Proteome Exploration Laboratory at California Institute of Technology. Thank so much Dr Tsui-Fen Chou, without your knowledge and availability seven days a week mass spectrometry experiments would not be possible.

Thanks to Caltech Biological Imaging Facility (Andres Collazo and Giada Spigolon) and Flow Cytometry Facility at Caltech for your offering all the time answering any questions.

Many thanks to all my friends in Worcester and Pasadena. Elena, Pía and Andrés, I will miss you a lot. I had a great time in Worcester with you. Elsy and Nicolas, Luisa and Aaron, Julie and Gustavo and Sofía and Mathew for all the good times we had together. My life would not have been so good without you. Thanks, Nicolas, for calling our attention in September 2016, since then we have built a great friendship. Mathew and Sofia, Disneyland is different for me since I met you. Thanks for your spontaneity every time we spent times together it has been so much fun. Luisa and Aaron, Julie and Gustavo an unexpected friendship which I will miss.

Por supuesto no puedo dejar estas líneas sin agradecer a cada una de mis *Pacensillas*, por todos los momentos vividos, poquitos, pero intensos, que me dan ese aire fresco lleno de energía y vitalidad para continuar y mirar hacia delante. Gracias por vuestro apoyo en todo momento, por vuestros consejos y carrera profesional Nereida y Mónica, por vuestra fuerza y constancia Ana, Fabiola y Débora, por tu ternura y tu ejemplo de vida Belén, y Carmen por tu tesón. Gracias a todas por vuestras vidas, sin vosotras nada sería igual.

Gracias a las Florecillas, que también han sido esa fuente de energía "biológica" sin descanso.

Gracias a mi GRAN Familia. Gracias, PAPÁ, sin tu ejemplo ni tu vida esto no hubiese sido posible. Gracias por empujarme y dar el primer paso determinante que me llevo a continuar mi carrera científica y no dejarla. Gracias por aquel momento de agosto del 2014: "*debes continuar tu vida, nadie más que tú conoce y construirá tu futuro".* Gracias, por tu lucha incesante y tu alegría y felicidad constante. Gracias por enseñarme a como uno TIENE QUE VIVIR LA VIDA. Allá donde estés solo puedo decirte GRACIAS PAPÁ. Mamá, fuente de lucha y perseverancia. Gracias por ser mi gran bastón y sostén en estos años donde un inmenso océano nos ha separado. Gracias por no dejar que abandone y continuar en el camino a pesar de las piedras GRANDES. Gracias por ser mi MAYOR EJEMPLO DE VIDA. GRACIAS, MAMÁ POR SER EL HOMBRO QUE NUNCA FALLA. GRACIAS POR TU CONFIANZA. Hermanos, gracias por vuestra confianza incondicional en mí, por creer en mí, por allanarme el camino hacia la meta. GRACIAS POR SER COMO SOIS, por vosotros continuo.

Y finalmente, GRACIAS LUIS. Gracias por que sin ti este trabajo no hubiese sido imposible. Gracias por tu apoyo y soporte incondicional; hasta en los momentos más oscuros siempre has sacado una luz para alumbrar el camino. Gracias por no dejarme salir de este, a veces complicado, camino y continuar sin NADA a cambio. Gracias por levantarme y empujarme en momento cruciales, porque sin ti este camino hubiese sido casi imposible. Gracias por los momentos y más felices y con más luz que he vivido en todos estos años, tú has sido el protagonista. GRACIAS por tu constancia, y por tu ayuda sin descanso en esta Tesis Doctoral, tú la has hecho posible. GRACIAS POR SER TÚ.

A mi Padre y a mi Madre
A mis hermanos

A Luis

TABLE OF CONTENTS

ABBREVATIONS

Activation domain (AD)

Adeno-associated virus 2 (AAV2)

Alpha-*myosin heavy chain* (alpha-*MHC)*

Amino acid (aa)

Amyloid precursor protein (APP)

Ankyrin (ANK)

Antennal and mechanosensory motor center (AMMC)

Arginine vasopressin receptor 2 (AVPR2)

Arbitrary units (a.u.)

Biomembrane Force Probe (BFP)

Biotinylated dextran amines (BDAs)

Cacophony Calcium channel (CAC)

Cadherin-related protein 2 (CDHR2)

Canine adenovirus type 2 (CAV-2)

Cholera toxin subunit B (CTB)

Central nervous system (CNS)

Delta like ligand (Dll)

Delta like 4 (Dll4)

Delta/Serrate/LAG-2ligands (DSL)

Destabilizing domain (DD)

Dihydrofolate reductase (DHFR)

DNA binding domain (DBD)

Early T-cell precursor ALL (ETPALL)

E-cadherin (epithelial cadherin)

E. coli DHFR (ecDHFR)

Electron microscopy (EM)

Embryonic lethal abnormal visual system (elav)

Endoplasmatic reticulum (ER)

Extracellular domain (ECD)

Focal adhesion kinase (FAK)

G protein-coupled receptors (GPCRs)

Genetically encoded calcium indicators (GECIs)

GFP reconstitution across synaptic partners (GRASP)

Glycoprotein (GP)

Heat-shock promoter (HSP-70)

Heterodimerization domain (HD)

Horseradish peroxidase (HRP)

Human continuous activation recognition (hCAR)

Intercellular adhesion molecule 5 (ICAM-5)

Intracellular domain (ICD)

In vivo biotin labelling of intercellular contacts (iBlinc)

Juxtatransmembrane domain (jTMD)

Kuzbanian (kuz)

Leucine zipper (LZ)

Ligand Binding Domains (LBDs)

Ligand independent activation (LIA)

Light microscopy (LM)

LIN12-Notch repeats (LNR)

Matrix metalloproteinases (MMPs)

Milliseconds (ms)

Muscle LIM protein (MLP)

Neurexin1 (Nrx1)

Neuronal cell adhesion molecule (NCAM)

Neuropeptide pigment-dispersing factor (PDF)

Neural synaptobrevin (nSyb)

Notch Extracellular Truncation (NEXT)

Notch Intracellular Domain (NICD)

Notch negative regulatory region (NRR)

Olfactory receptor neurons (ORNs)

Patient derived xenograft (PDX)

Period protein (PER)

Photoactivatable green fluorescent protein (PA-GFP)

Photoactivatable light microscopy (PALM)

Phytohemagglutinin-L (PHA-L)

Pico Newtons (Pn)

Pigment-dispersing factor (PDF)

Plasma membrane (PM)

Projection neurons (PNs)

Proline (P), glutamic acid (E), serine (S) and threonine (T) degradation domain (PEST)

Protocadherin-15 (PCDH15)

Regulated intramembrane proteolysis (RIP)

Relative Fluorescent Units (RFU)

Relative centrifugal force (rcf)

RNA interference (RNAi)

S1 loop-out (S1LO)

Sensory Organs Precursor from (SOP)

Sentrin/SUMO-specific proteases (SNEP)

Serial-section transmission electron microscopy (ssTEM)

Single-chain antibody domain (SCAD)

Single-strand binding protein from E. coli (ssB)

Single strand-DNA (ssDNA)

Stimulated emission depletion microscopy (STED)

Stochastic optical reconstruction microscopy (STORM)

Small Ubiquitin-like Modifier (SUMO)

Synaptic tagging with recombination (STaR)

Synthetic Notch (synNotch)

T-cell acute lymphoblastic leukemia (T-ALL)
T cell receptor (TCRβ)

Telencephalin (TLN)

Tetracycline transactivator (tTA)

TEV protease cleavage site (TCS)

Tobacco etch virus (TEV)

Transactivation domain (TAD)

Transcellular activation of transcription (TRACT)

Transmembrane domain (TMD)

Transmission electron microscopy (TEM)

Trimethoprim (TMP)

Tumor necrosis factor alpha-converting enzyme (TACE)

Tyrosine-kinase receptor (RTK)

Units (U)

Upstream Activating Sequence (UAS)

Ventral nerve cord (VNC)

Von Willibrand factor (vWF)

Wheat germ agglutinin (WGA)

β-amyloid protein precursor (βAPP)

ABSTRACT

The comprehensively mapping of the connectivity of various neural circuits across numerous brain regions and many organisms is a major goal of modern neuroscience. There is a general agreement that solving a circuit's wiring diagram is a crucial step towards understanding how the brain works together and how brain function is affected if any neuronal structure is disrupted. For that, the rising of neural mapping technology is essential to elucidate brain connectivity. Transcellular activation of transcription (TRACT) is a novel genetically encoded neurotracer technique based on the logic of the Notch signalling pathway developed by Carlos Lois laboratory. Once the synthetic receptor interacts with its ligand, a couple of sequentially proteolytic cleavages are triggered to release its intracellular fragment and regulate the downstream reporter gene's expression. Although this technique works to detect some connections between neuronal and glial cells in the *Drosophila* brain, the system still presents a high level of background ligand independent activation in the receiver cells, decreasing the signal-to-noise ratio. To improve the efficiency of the system, we engineered different domains of the Notch receptor. We have found that localizing the ligand and receptor to the synaptic cleft enhances the system's inducibility. Among all the modifications analyzed, we have found that the Notch negative regulatory region (NRR) domain is not required for Notch receptor activation. Also, the juxtatransmembrane domain (jTMD), a short sequence of only 12 aa, can act as mechanosensor in the absence of the NRR domain. Furthermore, the Notch jTMD from other species, other transmembrane proteins, and even multiple artificial sequences without any specific structure or sequence can also act as mechanosensory. These results indicate that short amino acid sequences are capable of sensing mechanical forces. These mechanisms can be shared in many proteins, suggesting that mechanical force may regulate many more cellular processes than previously suspected.

RESUMEN

Conocer el mapa de las conexiones neuronales de numerosas regiones del cerebro es un objetivo importante de la Neurociencia actual. En la comunidad Neurocientifica existe un acuerdo general de que resolver el cableado de un circuito neuronal es un paso crucial para comprender cómo funciona el cerebro en conjunto y cómo se ve afectada la función cerebral en el caso que se vea afectada cualquier estructura neuronal. Por este motivo, las nuevas técnicas de mapeo neuronal son esenciales para dilucidar la conectividad cerebral. La activación transcelular de la transcripción (TRACT) es una novedosa técnica de trazado neural codificada genéticamente, y basada en la lógica de la vía de señalización Notch desarrollada por el laboratorio Carlos Lois. Una vez que el receptor sintético interactúa con su ligando, se desencadenan un par de escisiones proteolíticas secuenciales para liberar su fragmento intracelular y regular la expresión de los genes controlados por dicho dominio intracelular. Aunque esta técnica funciona para detectar algunas conexiones entre las células neuronales y gliales en el cerebro de *Drosophila*, el sistema aún presenta un alto nivel de activación independiente del ligando en las células receptoras, lo que disminuye la relación entra la inducción dependiente de ligando y la señal independiente de ligando. Para mejorar la eficiencia de dicho sistema, hemos modificado diferentes dominios del receptor Notch, descubriendo que la localización del ligando y el receptor en sinapsis mejora la inducibilidad del sistema. Entre todas las modificaciones analizadas, hemos encontrado que el dominio de la región reguladora negativa Notch (NRR) no es necesario para la activación del receptor Notch. Además, el dominio juxtatransmembrana (jTMD), una secuencia de tan solo 12 aa, puede actuar como mecanosensor en ausencia del dominio NRR. Además, el Notch jTMD de otras especies, otras proteínas transmembrana e incluso múltiples secuencias artificiales sin ninguna estructura o secuencia específica también pueden actuar como mecanosensores. Estos resultados indican que pequeñas secuencias de aminoácidos son capaces de detectar fuerzas mecánicas. Estos mecanismos pueden compartirse en muchas proteínas, lo que sugiere que la fuerza mecánica puede regular muchos más procesos celulares de los que se sospechaba anteriormente.

CHAPTER 1

GENERAL INTRODUCTION

Unicellular organisms appeared on earth 2 billion years ago, before the first multicellular organism. It could be because, in a multicellular organism, all cells need to communicate with each other to work together and get benefits from the environment. The elaboration of complex and efficient signalling mechanisms may explain the delay of multicellular organisms emergent on earth. Intercellular signals, interpreted by complex machinery in the responding cell, allow each cell to determine its position and specialized role in the body and ensure, for example, that each cell differentiates only when its neighbours dictate that it should do so. The importance of such "social control" of cell differentiation becomes apparent when intercellular communication fails and results in a developmental disease.

1.1. General Principles of Cell Signalling.

Social communication among unicellular organisms has been broadly studied in eukaryotes cells such as yeast. For instance, yeasts normally lead to independent lives. However, they can communicate and influence one another's proliferation in preparation for sexual mating. For example, in the budding yeast Saccharomyces cerevisiae when a haploid individual is ready to mate, it secretes a peptide mating factor that signals cells of opposite mating types to stop proliferating and prepare to conjugate. The subsequent fusion of two haploid cells of the opposite mating type produces a diploid cell, which can then undergo meiosis and sporulate to generate haploid cells with new assortments of genes (Marsh et al. 1991; Kurjan 1992).

In multicellular organisms, social communication is quite different from that observed in unicellular organisms because the cells are part of a tissue that, in turn, forms an organ. Therefore, cells in a multicellular organism are embedded in a tissue that is subjected to multiple signals coming from surrounding cells in the same organ or cells located in other organs. Signals received by a cell can regulate its physiology (proliferation, differentiation, migration, metabolism, or death), coordinating the tissue functions. Most of the molecules involved in cell signalling are chemicals, such as hormones, neurotransmitters, and growth factors that bind to specific proteins called receptors (signalling molecules) on the surface or within the cell. Generally, signals are secreted to the extracellular space by exocytosis from an **emitter cell**. Then, the signal binds to a specific protein call receptor in the receiver cell,

which activates an intracellular signal that changes the cells' behaviour. In other cases, the signal molecule can diffuse through the plasmatic membrane and bind to an intracellular receptor (Hardie, 1991; Snyder, 1985).

1.2. Cellular Communication Strategies.

Signal molecules emitted by an **emitter cell** are recognized by specific receptors on the **receiver cell** that is located far away from the signal source or may act as local mediators, affecting only cells in the immediate environment of the signalling cell. Based on these characteristics, cell signalling can be carried out using different strategies (Alberts et al. 2002; Reece et al. 2014; Calvo 2015):

- ***Autocrine signalling***: Local type signalling where a cell sends a message to itself. The signal molecule release by the emitter cell bind back to its own receptors. This type of signalling may seem strange, but it is essential for cells to maintain their integrity and divide properly. Autocrine signalling is most efficient when several neighbours' cells perform it simultaneously, encouraging to respond coordinately as a group. Therefore, a group of cells will produce a higher concentration of a secreted signal than a cell alone. This type of signalling is crucial during development and helps cells reinforce their identity.

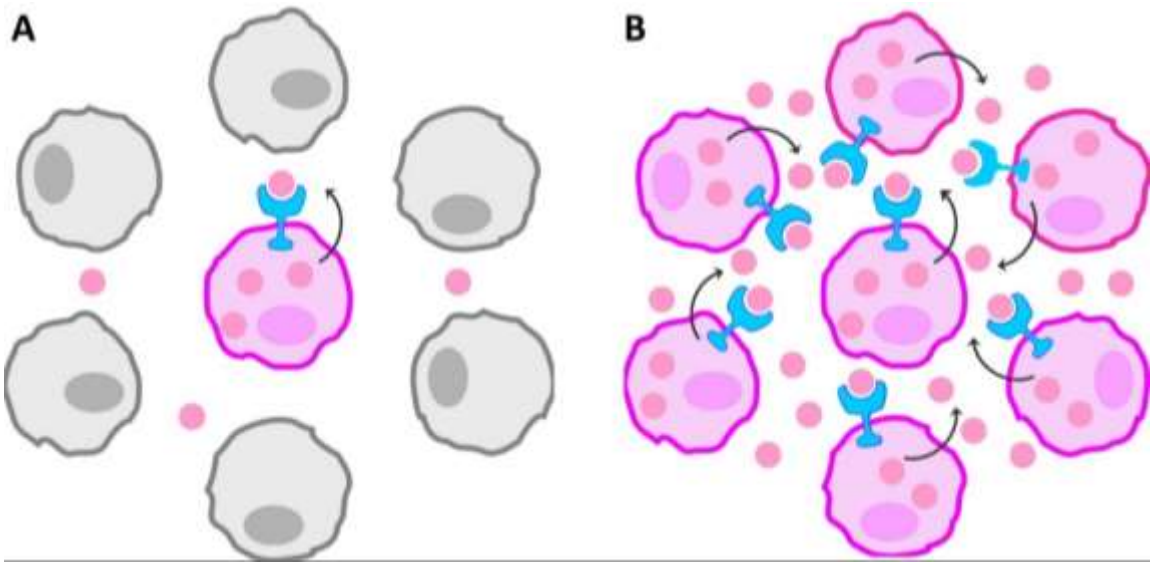

Figure 1.1 Autocrine signalling. (A) Cell signalling in which a cell secretes a chemical messenger that binds to a receptor on that same cell. (**B)** Community effect of the autocrine signalling.

- ***Paracrine signalling***: Local type signalling that affects only cells at a short distance, where the signal molecule is recognized by the same or different type of receiver cells surrounding the emitter cell that send the signal. Paracrine signalling permit cells to coordinate their activities locally with their neighbours. This type of cellular signalling is found in many tissues, being essential during development when one group of cells induces neighbouring cells to determine which identity to adopt (Cooper and Cooper 2000).
- ***Neurotransmitter signalling***: An example of paracrine signalling is the communication between neurons. When a neuron fires an action potential, an electrical impulse moves along its axon triggering neurotransmitters' release, the neuronal ligands. Neurotransmitters are small hydrophilic molecules that bind to the receiver cell's receptors (another neuron or another specialized cell type) after being released by the emitter neuron into the synaptic cleft to cause a particular effect (Hardie 1991).

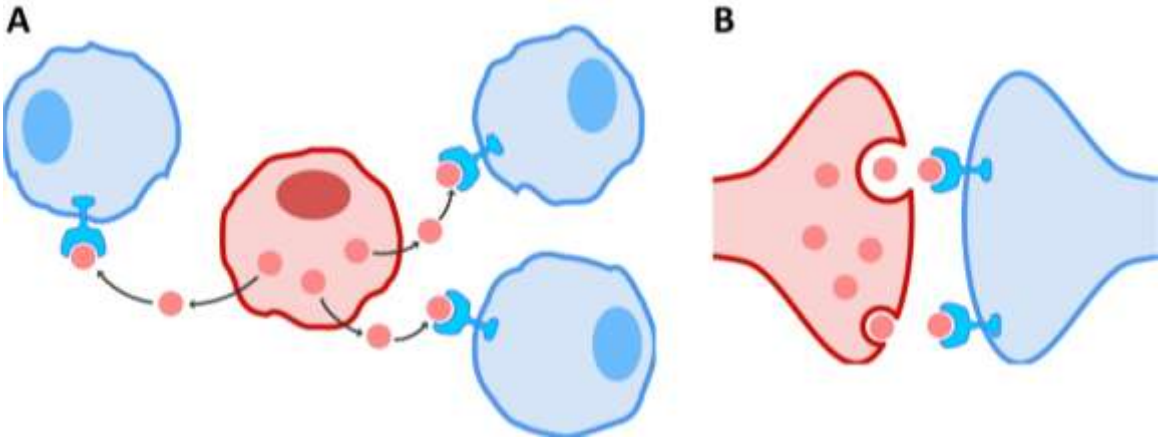

Figure 1.2. Paracrine signalling. (A) Emitter cell releases a molecule signal that binds to the receptor on the surface of closer receiver cells. **(B)** Synaptic signalling between two neurons where the emitter neuron releases neurotransmitters recognized by the downstream (receiver) neuron.

- ***Hormonal (or endocrine) signalling***: Sometimes cells need to transmit signal too far from their location, and often they use the circulatory system. In this case, the emitter cells are known as endocrine cells. They are cells specialized in the hormonal secretion (the ligand) that belong to endocrine organs. Hormones are secreted to the bloodstream and travel through the circulatory system until they reach the receiver cell, usually in places away from the emitter cell (Hardie 1991).

- ***Gap junctions:*** Some cells connect their cytoplasm to a nearby cell through small channels, specialized cell-cell junctions. Although it is a more direct signalling method because it avoids the plasma membrane barrier, it has an important limitation on the signal molecule's size. This channels only allow the diffusion of small signalling molecules, called intracellular mediators. Small molecules, such as ions, can move between cells, but large molecules, such as proteins or DNA, cannot fit through channels without special help (Caveney 1985).
- ***Direct cell-cell or cell-substrate contacts***: In this case, a cell communicates with the neighbouring cell through direct contact between molecules in the plasma membrane of both cells, which are recognized by a key-lock mechanism. It can also occur through direct contacts of its membrane proteins with specific molecules of the extracellular matrix.

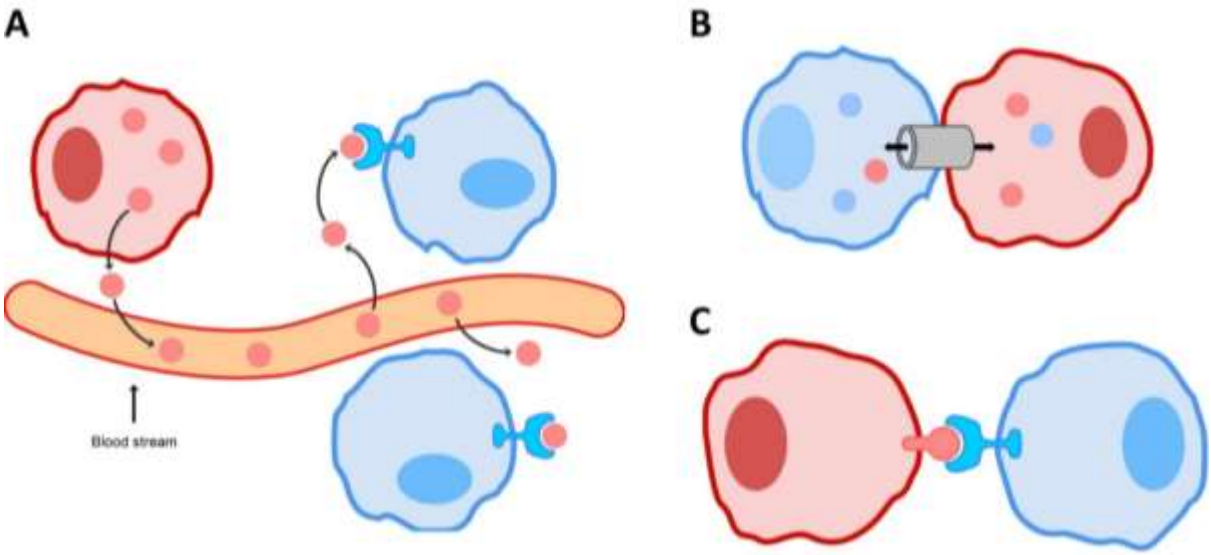

Figure 1.3. (A) *Endocrine signalling* where the hormone (signal molecules) disperses through the bloodstream toward different tissues. (**B)** *Gap junction signalling*, the signal molecules diffuse between two cells by small channels connecting their cytoplasm. (**C)** *Direct cell-cell contact*, ligand and receptor are on the surface of two nearby cells.

Although the signalling mechanisms are quite diverse, they all share several general characteristics that are summarized below (Alberts et al. 2002; Reece et al. 2014; Calvo 2015):

- Cells respond to the signal through specific receptors that can be located **(i)** on the ***plasma membrane*** (membrane receptor), thus recognizing hydrophilic molecules that cannot cross the plasma membrane by diffusion. **(ii)** In the ***cell cytoplasm*** (cytoplasmic

receptor) which recognize hydrophobic molecules that can cross the plasma membrane and bind to their receptors.

- Extracellular signals are transformed into intracellular signals when the ligand binds to the receptor. Intracellular signalling is initiated and transmitted directly to the nucleus, to activate the transcription of specific genes that were silenced. It will end with the translation of the genes in proteins which modify the cell physiology. In other occasions, intracellular signalling does not involve the transcription of new genes, but the response takes place directly through cytoplasmic proteins' activation.
- In some cases, the transmission of intracellular signals from the membrane receptor to the nucleus occurs in a multiple cascade mode. The receptor activates molecules that, in turn, will activate other "downstream" factors. Therefore, this process is called intracellular signalling cascade. This term applies to membrane receptors-dependent signalling. In the absence of signal, the receptor and intracellular signalling molecules remain in an inactive state. After receiving the extracellular signal, the different intracellular factors are activated and are turned on sequentially as molecular switches. Once the signalling cascade has acted, the signalling machinery returns to its inactive state. Therefore, it is a mechanism of "on" and "off".

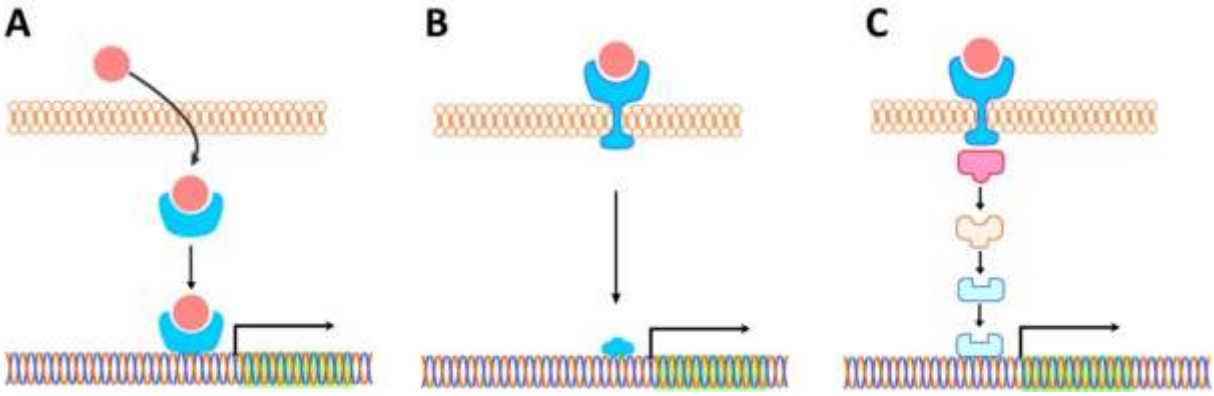

Figure 1.4. Signalling transduction. (A) Hydrophobic ligands diffuse through the plasma membrane and bind to an intracellular receptor that activates the expression of certain genes. Hydrophilic signal molecules bind to receptors on the cells surface, and the intracellular signal can occur directly from the receptor **(B)** or by a signalling cascade **(C).**

- Cells also present several strategies to prevent signalling pathway activation. **(i)** Direct inactivation of the receptor by its endocytosis and their subsequent degradation in the lysosomes, which stop signalling by removing the receptor from the membrane,

or the inactivation of the receptor by blocking proteins. In this case, it is common that the same signalling product act as a stop. **(ii)** Inactivation of downstream signalling. Many of the proteins involved in the intracellular cascade are protein kinases that phosphorylate specific amino acid residues of other proteins activating them and transmit the signal downstream. The inactivation of these proteins happens by eliminating their phosphate group through the action of phosphatase enzymes, causing them to return to their initial state. In some cases, protein phosphorylation does not always have an activating effect since it produces protein inactivation. The mechanisms of inactivation are, in any case, essential for cell physiology to prevent a constant activation of the signalling, which could cause cellular alterations, as occur in certain diseases.

- Cell response results from integrating multiple signals through the receptors present in the cell (intra- and extracellular receptors). This response depends on the set of signals that reach them and the concentration of each signalling substance. The types of signals received by a cell are determined by the tissue in which it is located and by its own responsiveness, which implies the presence of specific receptors that recognize the signal. For example, the combination of several favourable external signals can induce cell proliferation. However, the concurrence of other signals can result in the differentiation of each cell towards a lineage with different morphological and functional characteristics. Another set of external signals or the presence of certain factors can trigger programmed cell death through apoptosis. It is a common phenomenon in tissues to regulate cell number and maintain cell homeostasis.

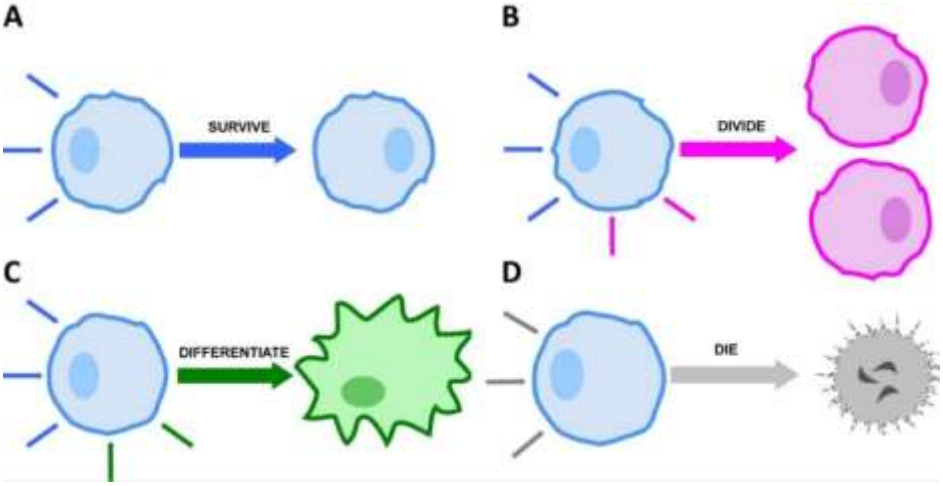

Figure 1.5. Activation of cellular response. The signals received by a cell determine the timing of **(A)** cell survive, **(B)** proliferation, **(C)** cell division and **(D)** apoptosis.

- Some signals can induce distinct responses in different cell types. An example is acetylcholine, which acts as a neurotransmitter and as a hormone. In the heart, acetylcholine causes a decrease in heart rate; however, it promotes muscle contraction in skeletal muscle, while in epithelial cells of the salivary glands, it stimulates secretion. This phenomenon is due to different types of receptors that recognize the same signal or the same receptor with intracellular signalling that can follow divergent pathways, leading to different responses.

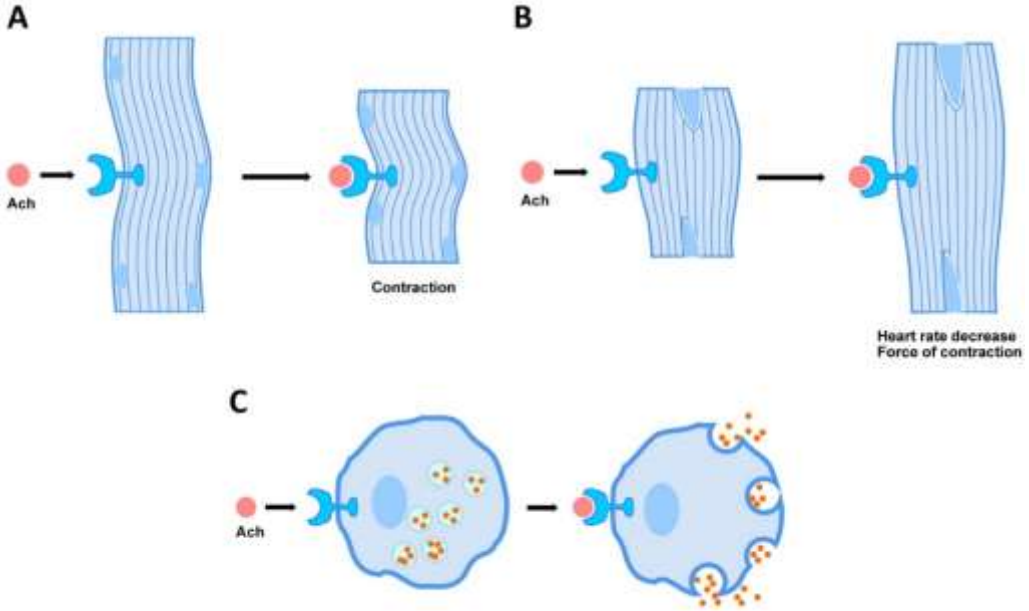

Figure 1.6. A ligand can generate distinct responses in different cells. Acetylcholine can induce **(A)** contraction or **(B)** relaxation of particular muscle, as well as **(C)** secretion release.

CHAPTER 2

TRACT SYSTEM IMPLEMENTATION

(Transcellular activation of transcription)

INTRODUCTION

2.1.1. General Introduction.

The basic working unit in the brain is the neuron. Humans brains houses tends of billions of neurons. Neurons are the most polarized cells in the body, and they present axon and dendrites emerging from the soma with different structures and functions. The cell nucleus and cytoplasm are in the cell body (soma). Dendrites present multiple branched processes and dendritic spines, which receive the neuronal signalling by the receptor on their surface (synapse). Axons usually are a single long process that transmits the neuronal signal by releasing neurotransmitters into the synapse (Takano et al. 2015).

As we mentioned in the general introduction from 1st Chapter, neurons transfer information to long distances through their axons connecting with their neuronal partner by paracrine signalling. Therefore, neurons release neurotransmitters (signal molecules) to influence cells located far away from their soma. The structures of neurons make it extremely difficult to tell which neurons are stimulated by a given neuron's action potential.

In the last decade, a central goal of neuroscience research is to understand the cell-type-specific connections between different regions and the detailed circuit organization within them, **the connectome** (Xu et al. 2020). The brain connectome (or "*wiring diagram of the nervous system*") is essential to understand how different regions of the brain work together and how brain function is affected if any neuronal structure is disrupted (Sporns et al. 2005). Neural mapping experiments have helped to elucidate some of these connections between neurons. For example, anterograde tracers allow the visualization of neurons and their targets, usually starting in the cell bodies and travelling down axons to their postsynaptic targets. Nevertheless, retrograde tracers progress in the opposite direction, from the axon terminals back to their cell bodies. Anterograde and retrograde transport of neural tracers owe their directional specificity to differential intracellular transport pathways in neurons (Figure 2.1) (Maday et al. 2014).

2.1.2. Conventional Tracers for Neural Circuit Mapping.

For more than a century, neuroscientists have been mapping brain connections. In the 1850s, one of the first neuroanatomical method used to investigate neuronal projections was based on Wallerian degeneration of axons that progressively degenerate in a retrograde fashion and reveal tracts that project distally from the site of the lesion (Waller and Owen 1850). In the 1940s, Walle Nauta developed a silver staining method for enhancing degeneration-based signals, which was the dominant approach until the 1960s (Nauta and Gygax 1951, 1954; de Olmos et al. 1981), when chemical tracers were developed. These chemical tracers included radiolabelled amino acids allowed auto-radiographic tracing of axonal connections in the central nervous system (CNS) (Taylor and Weiss 1965; Lasek et al. 1968; Cowan et al. 1972). For instance, radiolabelled 2-deoxyglucose accumulate in the active neurons allowing them to detect physiologically functional regions of the brain. This technique was used effectively to map projections of the visual cortex, such as ocular dominance columns without the requirement of damaging the tissue of interest (Hubel et al. 1977; Tootell et al. 1988). Shortly after that, scientists developed and identified a suite of retrograde tracers (Figure 2.1A), including horseradish peroxidase (HRP; (Kristensson and Olsson 1971, 1975), cholera toxin subunit B (CTB; (Trojanowski et al. 1981), tetanus toxin (Trojanowski et al. 1981), and fluorogold (Schmued and Fallon 1986); and anterograde tracers (Figure 2.1B) such as biotinylated dextran amines (BDAs; (Glover et al. 1986) and phytohemagglutinin-L (PHA-L; (Gerfen and Sawchenko 1984), as well as those that labelled both inputs and outputs, for example, wheat germ agglutinin (WGA; (Trojanowski 1983). In the mid-1980s, stable fluorescent retrobeads with low toxicity were also developed for retrograde tracing experiments (Katz et al. 1984). These non-viral conventional tracers have been used in the past few decades to investigate and elucidate the neuroanatomy and connectivity in different species (Lanciego and Wouterlood, 2020). These tracers were essential to get our current neuroanatomy knowledge of the brain.

An important limitation of the conventional tracers is that they label bulk neuronal connections based on the soma or axon terminal location, so they are mostly limited to mapping global connectivity. Besides, conventional tracers label all the cells

in the injection site and usually do not have enough resolution to identify the synaptic partner of the labelled neurons. In contrast, viruses can be targeted to specific cell types using genetic strategies, for example, via specific expression of a viral receptor or by expressing recombinase proteins in specific cells type to direct infection to those cells (Choi et al., 2010; Wickersham et al., 2007; DeFalco et al., 2001; Lo and Anderson, 2011). In some cases, viruses can be engineered to express some conventional molecule tracers, such as WGA, within interest cell type (Gradinaru et al. 2010). This strategy initiates a new era where modern neuroscience replaces the traditional method to deliver chemical tracers by targeted viral-genetic methods.

2.1.3. Neuronal Tracers based on Viruses.

In the last decades, neuroanatomists have taken advantage of the virus physiology to study microcircuit, where neurons connect with their neighbour neurons or neurons in a close nucleus. It helped to solve the main limitation of conventional neuronal tracers where injection spot is in the same order of magnitude than the microcircuit of study

To use viral vectors as transsynaptic tracers, the virus needs to replicate in the infected cell (emitter cell), and the virions produced are transmitted among neurons transsynaptically. An example of these transsynaptic viruses are the original forms of the herpes virus, rabies virus and pseudorabies virus (Ugolini et al. 1989; Kelly and Strick 2000; Card and Enquist 2001). The herpes virus can be used as an anterograde or retrograde tracer depending on the specific virus strain used to infect neurons. (Zemanick et al. 1991; Card et al. 1992; Levine et al. 1994; Moore et al. 1995; Sun et al. 1996). Nevertheless, rabies and pseudorabies viruses are transmitted only retrogradely (Astic et al. 1993; Ugolini 1995; Kelly and Strick 2000). Due to the toxicity or lethality that these transsynaptic viruses produce in the infected cell, their use has been more limited for biosafety concern. However, the deletion of essential genes for virus replication made these viruses safer. To address this issue, the rabies virus was genetically modified to infect the desired cell types specifically and spread only to monosynaptically connected inputs by injecting two different vectors into the brain (Wickersham et al. 2007; Chatterjee et al. 2018). Cell specificity was obtained using transgenic mice that

express the Cre enzyme in the neuronal type of interest. Then, the first injection with a non-replicant virus will activate the expression of the EnvA receptor (TVA) and rabies glycoprotein (G) upon Cre enzyme activity. A second injection with rabies virus particles carrying a deletion of its glycoprotein-G selectively labels a genetically defined cell population where virion replicates, incorporates the glycoprotein and propagates to the presynaptic neurons (Figure 2.1C) (Wickersham et al. 2007).

Some of the "replication-incompetent" viral vectors can be used as retrograde tracers. They can infect neurons by their axon terminals and travel to their cell body, beginning to express a gene of interest without spreading to nearby neurons. The viruses most used as retrograde tracers are the canine adenovirus type 2 (CAV-2; Li et al., 2018; Soudais et al., 2001) and a serotype of the adeno-associated virus 2 (AAV2; Naidoo et al., 2018; Tervo et al., 2016; Tordo et al., 2018).

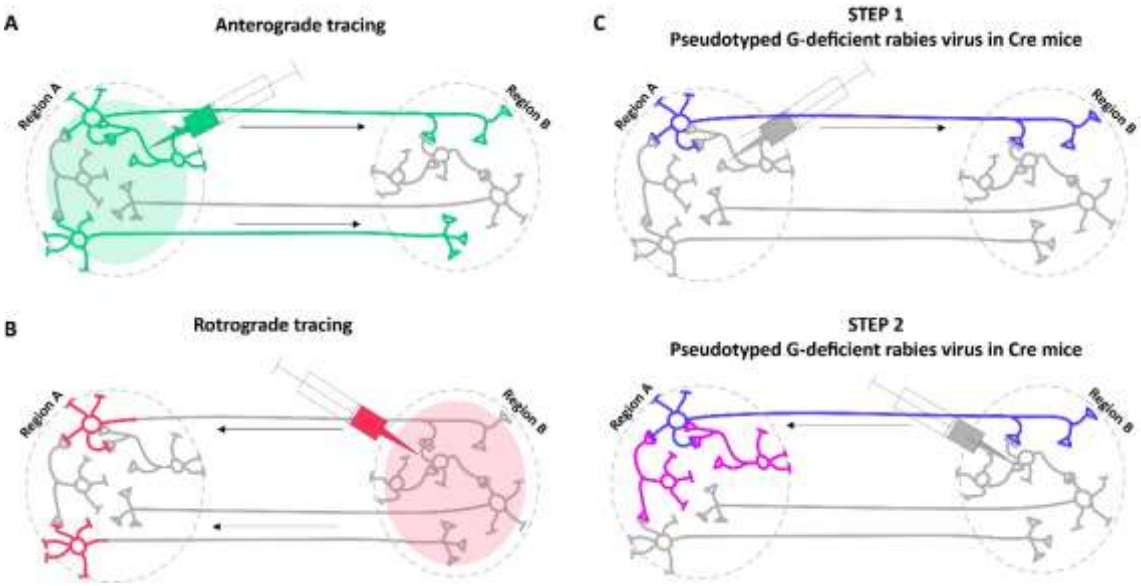

Figure 2.1. Anterograde, retrograde and transsynaptic tracers. (A) Anterograde tracing, tracers such as PHA-L, BDA or WGA-HRP injected in region A label efferent neurons including axon terminals in region B. In the injection site projection neurons and interneurons are labelled and indistinguishable from each other. **(B)** Retrograde tracing, tracers such as CTB label projection neurons irrespective of their neurochemical phenotype. **(C)** Step 1, injection in region A of a virus carrying the G protein that is expressed in specific neurons upon Cre recombinase activity. Step2, injection on region B a pseudotyped G-deficient rabies virus that go retrogradely infect first order neurons and proceed transsynaptically to second-order neurons

2.1.4. Methods to Study the Connectome in the Drosophila melanogaster Brain.

Although the connectome originated with the pioneering reconstruction of the entire *C. elegans* nervous system by electron microscopy (EM) in 1980, it has expanded to other organisms, such as *Drosophila* and mouse. The C. elegans nervous system, comprised of just over 1,000 neurons, is relatively simple to analyze. Furthermore, due to its fast generation time and reproductive peculiarities, *C. elegans* is an outstanding model for genetic analysis. However, there are a few issues that limit the usefulness of *C. elegans* for nervous system studies. First, *C. elegans* has a very limited behavioural repertoire. Second, *C. elegans* neurons lack voltage-gated sodium channels and consequently do not fire action potentials. Neurotransmitter release in *C. elegans* occurs via graded depolarizations mediated by voltage-gated calcium channels, a mechanism that is not shared by vertebrates or most invertebrates. Finally, electrophysiological recordings in *C. elegans* are notoriously challenging. Consequently, it is difficult to establish correlations between synaptic activity and behaviour in C. elegans.

On the other hand, the mouse is an attractive model for neuroscience. It is the most genetically tractable mammal, and there is strong conservation of physiology and anatomy between the rodent and human brain. Besides, despite its relatively slow generation time, the techniques for genetic manipulation and electrophysiological recordings in mice are highly sophisticated. However, the mouse brain has more than 100,000,000 neurons, making it very difficult to analyze and understand the structure and dynamics of its nervous system

The *Drosophila* brain, by comparison, only has around 100,000 neurons. The simplicity of its brain combined with the sophisticated tools available for genetic manipulation allows scientists to map entire circuits in *Drosophila* at the cellular level. At the same time, *Drosophila* exhibits more sophisticated behaviour and circuitry than do *C. elegans*, making the study of its nervous system pertinent to understanding our own. In fact, some of its brain circuits, such as the olfactory circuit, show significant overlaps in organization and function with equivalent circuits in the mammalian brain. Ultimately, the *Drosophila* brain is an excellent model system for understanding how the connectome gives rise to function and behaviour. As a result, many new methods to

investigate neurons' connectivity have been developed to use in *Drosophila*. These methods can be broadly divided into two groups: those based on electron microscopy (EM) analysis of brain tissue, and those based on genetic techniques.

2.1.4.1. Electron Microscopy.

EM represents the gold standard for analysis of brain structure. Due to its high resolution, EM can unambiguously identify synapses. EM uses accelerated electron beams instead of light as its source of illumination and can consequently reveal biologic tissue's ultrastructure with XY-resolution as high as 2 nm. Chemical synapses can be visually identified from EM image because synaptic vesicles are concentrated at the presynaptic site.

There are several variations of EM that can be used to study brain connectivity, but the one that has been used most extensively by neuroanatomists is serial-section transmission electron microscopy (ssTEM). For this technique, biologic tissue is fixed, stained, embedded in resin, and then serially cut into sections around 40 nm thick with an ultramicrotome. The resulting sections are collected and visualized by transmission electron microscopy (TEM), which measures the electrons that pass through the sample. TEM offers the best XY-resolution of all EM methods. After images are generated from serial sections, they are first aligned along the XY-axis. Then, cellular membranes and organelles are identified and marked in a process known as segmentation. Finally, the segmented images are linked across the Z-axis for 3D-reconstruction of neurons. Though the initial steps (sectioning, imaging, alignment, and segmentation) can be automated with varying degrees of success, reconstructing and proofreading a 3D-model from serial images requires hundreds of hours of skilled labour and represents the limiting step (Chklovskii et al. 2010; Schneider-Mizell et al. 2016).

The resolution of EM reconstructions offers two main advantages over other connectomic techniques. First, EM reconstructions can yield a comprehensive understanding of a small neuronal circuit. For instance, the EM volume generated from the antennal lobe of *Drosophila* larva identified over 38,000 synapses among 160 neurons (Berck et al. 2016). Second, the high resolution of EM leads to a quantitative assessment of neural circuits. Because EM reconstructions can reveal the size and the

number of synapses that exist between neurons, EM can provide an estimation of the strength of the connection between neurons.

Although EM is a powerful method, it has several significant limitations. First, for tissues to be analyzed by EM, they need to be fixed, which prevent the direct combination of EM with functional analysis by electrophysiological or optical recordings. Second, EM is extremely time and labour-intensive. For reference, the seminal reconstruction of the *C. elegans* connectome took several years to complete for one single specimen. Similarly, EM reconstructions of the larval antennal lobe (Berck et al. 2016), the adult optic medulla (Takemura et al. 2013), and the A2 and A3 segments of VNC (Butcher et al. 2012) provide detailed connectomic data but only in localized circuits and for single samples.

2.1.4.2. Light Microscopy.

Unlike electron microscopy cannot be used to examine live tissue, long-distance connections, or investigates large numbers of samples, light microscopy (LM) can partially solve this bottleneck. However, the resolution of LM is restricted to the wavelength of light used to illuminate the samples (400–600 nm). However, recently developed techniques such as stimulated emission depletion microscopy (STED) (Hell and Wichmann, 1994; Klar and Hell, 1999), photoactivatable light microscopy (PALM), and stochastic optical reconstruction microscopy (STORM) (Nienhaus and Nienhaus 2014; Yamanaka et al. 2014) allow investigators to image the brain at subdiffraction limit resolution. STED uses patterned illumination to restrict light emission to a small region, while PALM and STORM use spare photoactivation of fluorophores to achieve a similar goal (Huang et al. 2010). At this resolution, subcellular structures such as individual neurotransmitter vesicles can be discerned. Although these methods' resolution is still lower than that of TEM, LM offers two significant advantages. First, LM can be directly combined with genetic methods for labelling cells by expressing fluorescent proteins. Second, LM can be used in live animals with parallel electrophysiological and optical imaging techniques. This allows researchers to combine structural and functional information in a way that EM cannot.

Several methods, including synaptic tagging with recombination (STaR) (Figure 2.2), use genetic labelling of synaptic sites to identify putative synaptic contacts between neurons (Kremer et al. 2010; Christiansen et al. 2011; Chen et al. 2014; Mosca and Luo 2014). These methods have been used to study the variation in the synaptic organization among individuals in different conditions and at different developmental stages, and to compare changes in connectivity caused by mutations (Christiansen et al. 2011; Chen et al. 2014; Mosca and Luo 2014; Liu et al. 2016; Akin and Zipursky 2016). In these methods, pre- and postsynaptic markers need to be genetically fused with different tags, such as fluorescent proteins, or tags that can be detected by immunocytochemical stainings, such as V5, HA, or OLLAS tag. Therefore, by analyzing pre- and postsynaptic markers' proximity, putative synaptic sites can be revealed directly by LM imaging. Moreover, as in most methods that depend on LM, fluorescent protein-tagged synaptic markers allow the monitoring of changes in synapses in the same animal over time by live imaging using methods such as 2-photon microscopy (Chen et al. 2014).

To precisely analyze pre- and postsynaptic markers' proximity, especially in regions with dense synapses, super-resolution microscopy methods may be required. It combined with the proper image analysis methods; the tagged synapses' spatial organization can be analyzed with resolving powers that approach those of EM. However, because of the influence of light scattering and spherical aberrations, only the top 1–3 mm of the sections can be imaged to obtain the optimal resolution. For this reason, reconstructing the connectome from a large piece of the brain by super-resolution microscopy would still be time-consuming. However, if super-resolution microscopy could be combined with methods that allow for imaging in thick tissues, such as tissue clarification techniques (CLARITY, SeeDBD2, Scale…), it would benefit the processes to analyze the synaptic organization in large brain regions.

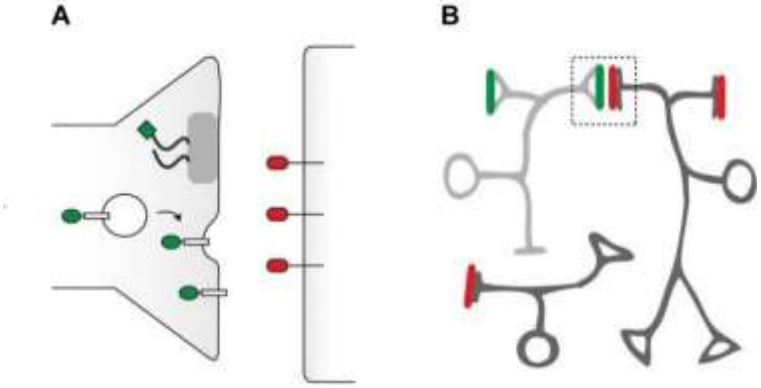

Figure 2.2. Visualization of synapses by genetically tagging synaptic proteins. (A) Fluorescent proteins or epitope tags can be targeted to synaptic membranes by fusion to synaptically localized proteins. For example, tags fused to Brp (curly black line) or synaptic vesicular proteins (white rectangle) will localize to the presynaptic terminal (left). There are no pan-neuronal postsynaptic markers, but tags (red oval) fused to neurotransmitter receptors such as Ort have been successfully used in the past. (B) The axon terminal (triangle) of the presynaptic neuron of interest (light gray) is marked with tags that are fused to presynaptic proteins (green). A different tag (red) is expressed at the postsynaptic sites of candidate partner neurons (dark gray). The proximity of these two distinct tags (green, red) is assessed to verify the synaptic connection.

2.1.4.3. GFP Reconstitution Across Synaptic Partners (GRASP).

GRASP is a genetic method used to identify cell contacts and synapses in living animals (Feinberg et al. 2008). It was initially developed in *C. elegans*, but it has been subsequently applied to the study of *Drosophila* brain connectivity. GRASP labels synapses based on the proximity of the pre- and postsynaptic plasma membranes. In the CNS synapses, two synaptic partners' membranes are typically separated by less than 100 nm of extracellular space, which is known as the synaptic cleft. This distance can be spanned by transmembrane proteins expressed in the two interacting neurons. As the name implies, GRASP is based on the reconstitution of 2 fragments of the split-GFP across the synapses of interacting neurons. Each of the two non-fluorescent split-GFP pieces is added to carrier transmembrane proteins. The two fragments of the split GFP assemble into a fluorescent form only when the membranes are sufficiently close to permit carrier proteins to span the intercellular gap. One fragment of the split GFP, spGFP1–10, is 214 aa long while the second fragment, spGFP11, is just 16 residues long. The spGFP11 fragment can, therefore, be inserted into many different proteins without affecting their function.

In initial experiments in *C. elegans,* each GFP fragment was fused to the extracellular domain of the cell adhesion molecule CD4 (Feinberg et al. 2008). However, this molecule is homogeneously distributed throughout the plasma membrane, without any specificity for synaptic sites. As a result, GRASP implementation led to GFP reconstitution throughout the membrane, including non-synaptic contact sites (Figure 2.3A). To improve the system's specificity, one or both GRASP components were fused to synaptically localized proteins, restricting GFP reconstitution to synapses (Figure

2.3B). Gordon and Scott (2009) demonstrated that GRASP works efficiently in flies by using it to detect cell-cell contact at the synapses between olfactory receptor neurons (ORNs) and projection neurons (PNs). The power of fly genetics has allowed the GRASP system to be expanded for studying neuron-muscle connections (Itakura et al. 2015; Hasegawa et al. 2016), the visual circuit (Lin et al. 2016), the circadian rhythm circuit (Cavanaugh et al. 2014; Gorostiza et al. 2014), and the olfactory circuit (Masuda-Nakagawa et al. 2014).

A recent modification of the GRASP system has taken advantage of the properties of some synaptic proteins that are displayed on the membrane only after the release of neurotransmitters (Macpherson et al. 2015). To limit GFP reconstitution to active synapses, the investigators fused spGFP1–10 to the extracellular domain of N-synaptobrevin (nSyb), which is exposed to the synaptic cleft only after vesicle release (nSyb::spGFP1–10). They tested this implementation by expressing nSyb::spGFP1–10 in ORNs and its GRASP partner CD4::spGFP11 broadly in PNs. GFP was reconstituted at synapses after artificial stimulation with KCl or natural stimulation with cognate odorants, demonstrating that nSyb::GRASP can preferentially label active synapses in *Drosophila* brain.

The GRASP system is a powerful technique, but it has three significant **limitations**. First, the reconstituted fluorescence is often weak, making it difficult to detect *in vivo*. The reconstitution of GFP can be detected in fixed tissue using immunofluorescence with different GFP antibodies that can selectively detect spGFP1–10, spGFP11, or the reconstituted GFP. However, immunostaining requires fixing the tissue, and thus it precludes the combination with functional methods such as electrophysiological or optical recordings. Second, the interaction between the sp11 and sp1–10 fragments are irreversible and can artificially render permanent cell-cell contacts that are natively transient. Third, GRASP reveals the point of contact between cells, but it does not allow for genetic manipulation of synaptically connected neurons, a feature that would be invaluable for functional analysis of circuitry.

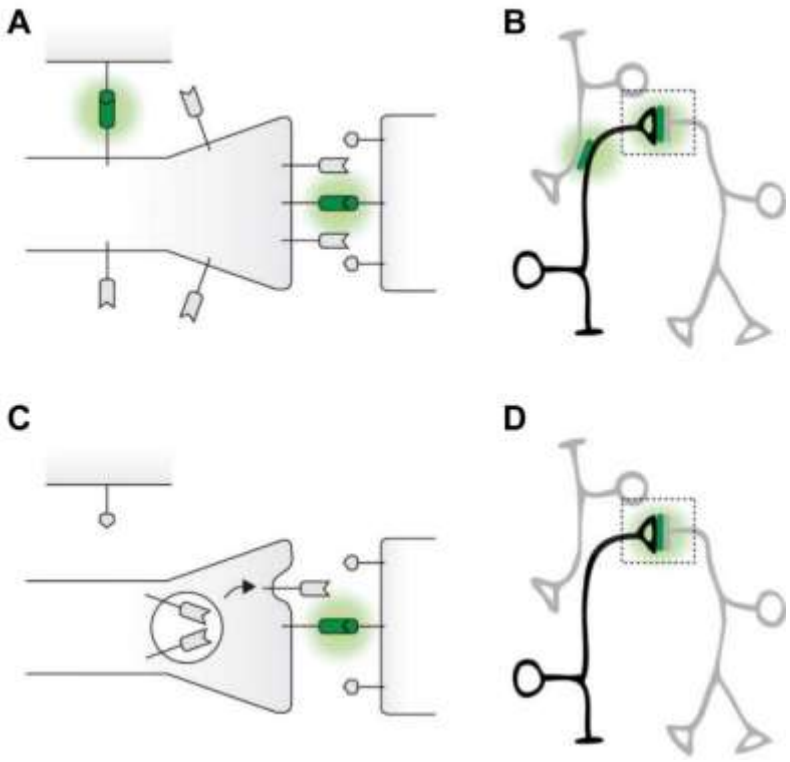

Figure 2.3. GFP Reconstitution Across Synaptic Partners (GRASP). (A) CD4::spGFP1–10 (dented rectangle) is distributed homogeneously throughout the presynaptic neuron's membrane. As a result, GFP reconstitution (green) can occur at the synapse (right) as well as at sites of non-synaptic contact (top). **(B)** A presynaptic neuron (black) expressing CD4::spGFP1–10 makes contact with 2 neurons (gray) expressing CD4::spGFP11. GFP reconstitution occurs at all sites of membrane contact and is not specific to synapses. **(C)** nSyb::spGFP1–10 (dented rectangle) is localized to synaptic vesicles. Upon synaptic release, nSyb::spGFP1–10 is exposed specifically to the synaptic cleft. As a result, GFP reconstitution (green) only occurs at synaptic sites when synaptic vesicles fuse. **(D)** A presynaptic neuron (black) expressing nSyb::spGFP1–10 makes contact with 2 neurons (gray) expressing CD4::spGFP11. GFP reconstitution occurs at the synapse but not at the site of non-synaptic contact.

2.1.4.4. Photoactivatable Fluorescent Protein.

When using GRASP or STaR to analyze synaptic contacts, putative pre- and postsynaptic neurons have to be known a priori so that the transgenic proteins can be expressed precisely in these neurons. Therefore, these strategies cannot be used to discover novel synaptic partners in an unbiased manner. In contrast, a photoactivatable green fluorescent protein (PA-GFP) is an ideal tool for finding novel synapses, and has been successfully used in *Drosophila* (Ruta et al. 2010; Lai et al. 2012; Fişek and Wilson 2014; Clowney et al. 2015). For further implementation of this technique, a neuron of

interest (first-order neuron) must be marked with dye or fluorescent proteins to outline its neurites. PA-GFP is genetically expressed pan-neuronally, or more narrowly in candidate subsets of neurons that are hypothesized to be connected to the first-order neuron. By spatially restricting the application of UV light to specific dendrite or axon arborizations of the first-order neuron, only the PA-GFP in neurites of partner neurons is converted from a weakly fluorescent state to a strong one (>100-fold increase) (Patterson and Lippincott-Schwartz 2002). Gradually, the activated PA-GFP diffuses from the neurites to the cell body highlighting the morphology of the entire neuron (Figure 2.4A). Recently, two new enhanced variants of PA-GFP, SPA-GFP and C3PA-GFP, have been generated, with the latter having the strongest fluorescence (Ruta et al. 2010).

One caveat of this approach is that any neuron with dendrites or axons in the illuminated region can be highlighted even if they do not synapse with the first-order neuron (Figure 2.4B). Therefore, electrophysiological recordings or genetically encoded calcium indicators (GECIs) are required to confirm the existence of synaptic connections between the highlighted neurons and the first-order neuron. Newly developed PA-GECIs have the characteristics of PA-GFP (high contrast of fluorescence intensity after photoactivation) and GECIs (high-sensitivity of calcium detection) (Berlin et al. 2015). PA-GECIs could provide a more convenient way to investigate connectivity by allowing researchers to initially identify the potential synaptic partners and subsequently test their functional connectivity in the same animals.

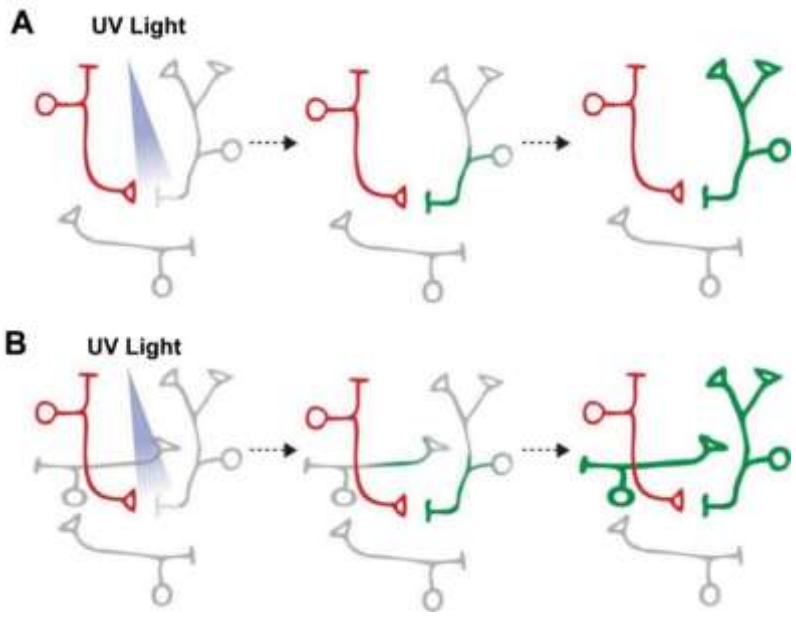

Figure 2.4. Detection of synaptic partners by photoactivatable green fluorescent protein (PA-GFP). (A) A neuron of interest (red) is first highlighted with dye or fluorescent proteins to mark its neurites while PA-GFP is expressed in all candidate partner neurons (gray). When UV light is applied just outside the neurite of the highlighted neuron, PA-GFP in its synaptic partner (green) is converted to a strongly fluorescent state. The converted PA-GFP then diffuses throughout the partner neuron, highlighting its entire morphology. **(B)** One of this technique's pitfalls is that UV light stimulation can also activate PA-GFP in bystander neurons. In this scenario, PA-GFP in 2 neurons (green) is activated, but only one is synaptically connected to the neuron of interest (red). In practice, functional studies need to be performed to confirm the candidate synaptic connections identified with PA-GFP.

2.1.4.5. Transsynaptic Tracers.

Transneuronal tracing in mammals has benefited from the availability of specific neurotropic viruses that are selectively transported across synapses. Herpes simplex virus type 1, pseudorabies virus, and rabies virus have all successfully been used to elucidate neural connections in mice (Nassi et al. 2015). Non-viral tracers such as C-fragment of tetanus toxin or wheat germ agglutinin (WGA), can be expressed as transgenes into specific "source" neurons, and transferred across their synapses (Huh et al. 2010). The transfer of tracing agents may occur in an anterograde (from the source neuron's axon to its postsynaptic partner) or retrograde (from the source neuron's dendrite to its presynaptic partner) manner. In particular, WGA has been used successfully as a transneuronal tracer in multiple species, including *Drosophila* (Tabuchi et al. 2000).

WGA is a lectin protein that binds specific sugar moieties of glycoproteins covering eukaryotic cell membranes. WGA is transported preferentially to the axon terminal, where it is secreted and endocytosed by the postsynaptic partner of the source neuron. It can be repeatedly passed along a circuit of connected neurons. Then, WGA can be visualized by staining or by conjugation to horseradish peroxidase. However, this multi-synaptic transport of WGA may not give a clear interpretation of data. Because only a small fraction of the WGA from the source neurons jumps across the synapse, and WGA does not replicate, the little WGA that reaches the synaptic partner can be challenging to detect. To solve this problem, adeno-associated viruses (AAV) encoding WGA fused with Cre recombinase, WGA-Cre, has been used in combination with Cre-

dependent reporters in mice to amplify the WGA signal (Gradinaru et al. 2010; Libbrecht et al. 2017). However, this strategy does not seem to work robustly in mammals, and it remains to be tested whether parallel strategies such as WGA-Flp or WGA-Gal4 can be used in *Drosophila*.

2.1.4.6. TANGO.

Several recently developed genetic tools have adopted the molecular mechanisms of Delta-Notch signalling pathways to monitor and modify interacting cells. The Delta-Notch pathway plays significant roles in the control of cell fate during development through cell-cell interactions. Notch receptor includes a set of EGF motif repeats at its N-terminus, followed by a key structural element called the Notch negative regulatory region (NRR), which is located in the extracellular domain (ECD), just outside of the transmembrane domain (TMD) (Gordon et al. 2007). Without Delta binding, the NRR is folded in such a way that a cleavage site (called S2) is inaccessible to the action of ubiquitous metalloproteases such as Kuzbanian (in *Drosophila*) or tumour necrosis factor-a-converting enzyme (TACE) or ADAM17 (in vertebrates) (Tiyanont et al. 2011). Upon Delta-Notch binding, it is hypothesized that the mechanical force generated by the endocytosis of Delta partially unfolds the NRR, exposing the S2 cleavage site to metalloproteases (Tiyanont et al. 2011; Meloty-Kapella et al. 2012; Stephenson and Avis 2012; Gordon et al. 2015). After S2 cleavage, a subsequent cleavage (called S3) by the ubiquitous metazoan γ-secretase complex occurs in the TMD, within the lipid bilayer (Brou et al. 2000; Mumm et al. 2000), which releases the intracellular domain (ICD). Then, the released ICD translocate to the nucleus, regulating the transcription of cell fate related genes (Struhl and Adachi 1998, 2000).

The Tango assay is one such tool derived from the molecular logic of Delta-Notch signalling. It was initially developed to monitor the interaction of a receptor of interest with its ligand or agonist in the extracellular space. In the Tango assay, three exogenous genetic elements are introduced into a receiver cell. The first element is an engineered protein consisting of a transmembrane receptor fused to an intracellular transcription factor separated by a cleavage site that is recognized by a site specific protease, such as tobacco etch virus (TEV) protease. The second element is a protein fusion consisting of

the before mentioned protease linked to a protein that associates with the receptor upon agonist-binding. The third element is a reporter gene that can be activated by the transcription factor. The binding of the agonist recruits the protease to the receptor. Then, the protease frees the transcription factor from its membrane anchoring, allowing it to reach the nucleus and activate transcription of the reporter cassette which results in a visual indication of receptor activation (Barnea et al., 2008).

Tango assays were initially developed to monitor receptor activation in G protein-coupled receptors (GPCRs), receptor tyrosine kinases, and steroid hormone receptors, *in vitro*. In designing the Tango assay for GPCRs, the human arginine vasopressin receptor 2 (AVPR2) was used as a model. The receptor was fused to a transcription factor by a TEV protease cleavage site (TCS), and the TEV protease was linked to human β-arrestin2, which associates with AVPR2 upon receptor activation. When these two chimeric constructs and a reporter gene were introduced into a cell line, the Tango-modified AVPR2 induced the reporter gene expression upon binding to its respective agonist. The GPCR Tango assay has since been adopted for use in the *Drosophila* nervous system. The assay can be used to both screens which circuits are responsive to a specific neurotransmitter (Tango-map) and identify the postsynaptic partners of known neurons (Tango-Trace) that use GPCRs as neurotransmitter receptors.

Inagaki et al. (2012) applied the Tango-map assay to dopamine receptors in the *Drosophila* nervous system to investigate the neural circuits on which dopamine acts (Figure 2.5A, B). They were able to detect the expression of the GFP reporter in receiver cells that expressed the modified dopamine receptor upon their activation by dopamine. Next, they used this technique to explore which neurons received dopamine signalling following starvation periods to determine how hunger affects neuromodulators' action, like dopamine.

The Tango approach was next used to identify synaptic partners of *Drosophila* neurons (Jagadish et al., 2014). They developed a Tango-based technique called Tango-Trace, which enables the trace of synaptic connections of photoreceptor neurons in the

Drosophila visual system. Their goal was to identify the synaptic partners of photoreceptors in the different layers of the optic lobe.

The Tango assay, as described here, has several benefits that make it a versatile, useful tool for visually detecting cell-cell interactions. The assay can be applied to 89 members of the GPCR class, making it suitable for many different cell types. Additionally, if neurotransmitter release can be controlled specifically in presynaptic neurons of interest, as with the trpA1 channel, Tango can allow for the identification of its functional postsynaptic partners. Tango also has several limitations. Although Tango can be adapted for many members of the GPCR family, it is currently restricted to the study of cell-cell interactions mediated by GPCRs. It precludes the use of Tango for studying synapses mediated by ionotropic receptors. Furthermore, Tango requires a priori knowledge of the neurotransmitter used by the presynaptic neuron of interest, preventing its application for unbiased identification of uncharacterized synapses. Second, Tango has caveats that could lead to false identification of connectivity. Theoretically, if the neurotransmitters diffuse outside of the synaptic cleft, neighbouring neurons that express the receptor, but are not synaptically connected to the source neuron may be activated.

Recently, an implementation of the Tango technology has been developed, the trans-Tango (Talay et al. 2017). The main difference between this new trans-Tango strategy and the original Tango system is the use of a membrane-bound ligand targeting the presynaptic site. Thus, the receptor and ligand are exogenous, and pan-neuronally expressed. The human glucagon and its receptor are used for this new Tango implementation.

The trans-Tango signalling pathway is based on four different components (Figure 2.5C). **(i)** The engineered receptor is a fusion of the glucagon receptor, a G protein-coupled receptor bound to the transcriptional activator QF by a linker with the cleavage site from the tobacco etch virus (TEV). **(ii)** The second component is a fusion between the TEV and human β-arrestin2, which is recruited to the receptor upon ligand binding. **(iii)** The reporter is under the transcriptional regulation of QF transcription factor. Therefore, the reporter is expressed upon activation of the pathway. **(iv)** The last

component is a membrane-tethered form of glucagon expressed at the presynaptic site by its binding to neurexin.

The trans-Tango system is specifically activated in postsynaptic neurons to those expressing the ligand, and no reporter expression is detected in the absence of ligand. On the contrary, when the ligand is expressed at the presynaptic site, it will activate the receptor that will trigger the recruitment of hArr::TEV. TEV will cleave the receptor in its target site, and the QF will translocate to the nucleus and induce the reporter's expression. Using this method, the author showed that the number of postsynaptic PNs making synapses with ORNs were higher than previously reported.

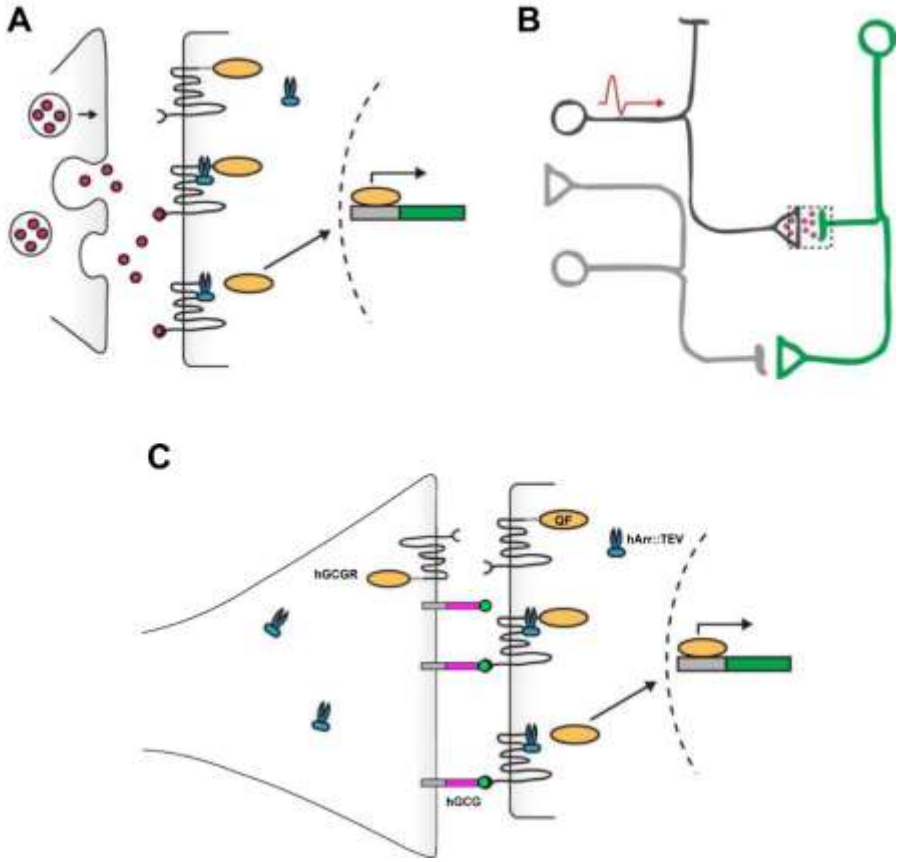

Figure 2.5. Identifying functional synaptic contact using Tango-modified GPCRs. **(A**) When neurotransmitters (red) are released from the active zone of the presynaptic neuron (left), they bind Tango-modified GPCRs on the postsynaptic neuron (right). The binding of neurotransmitter recruits an intracellular protease (blue), that cleaves the transcription factor (orange), which is tethered to the GPCR. This transcription factor then translocated to the nucleus to activate transcription of reporter genes such as GFP (green rectangle). **(B)** After the presynaptic neuron of interest (dark gray) fires an action potential, releases neurotransmitters (pink) that bind to the Tango-modified GPCRs in the postsynaptic neuron. It induces GFP expression in the postsynaptic neuron (green) but not in the bystander neuron (light gray).

2.1.4.7. Transcellular Activation of Transcription (TRACT)

In contrast to Tango, which was designed to monitor interactions of a receptor to its soluble ligand or agonist, other Delta-Notch system applications have aimed at studying the contact between the plasma membranes of neighbouring cells. The Delta-Notch system can be engineered to monitor cell-cell contact without interfering with endogenous signalling. By replacing the EGF repeats with a single-chain antibody domain (SCAD), a synthetic version of Notch can be made to recognize orthogonal ligands, such as CD19 or GFP, instead of Delta. Besides, the Notch ICD can be replaced with an orthogonal transcriptional regulator such as Gal4 or tTA. Ultimately, emitter cells expressing the artificial ligand can trigger the modified Notch receptor's proteolysis in receiver cells by membrane-membrane contact. Used in conjunction with UAS or tetO, membrane-membrane contact can be observed by expressing a reporter gene such as GFP (Figure 2.6A).

This strategy has been used *in vitro* to engineer cell-cell interactions based on their contact (Morsut et al. 2016) and enhance T cell activity against tumour cells in mice (Roybal et al. 2016). Our group has developed a parallel method called transcellular activation of transcription (TRACT), which we have used to investigate neuron-glia interactions in the *Drosophila* nervous system (Figure 2.6B) (Huang et al., 2016). As a proof of concept, we expressed the CD19 ligand in two different subsets of glial cells under either the alrm or repo driver while the receptor was expressed in all neurons. The spatial pattern of each of these drivers is distinct. Whereas the repo driver leads to strong expression of the ligand in many types of glial cells, the alrm driver is relatively specific to astrocytes. Consistent with our expectations, depending on which glial cells were expressing the ligand, different populations of neurons were induced to transcribe GFP. It suggested that TRACT was capable of detecting glia-neuron contact *in vivo*. We tested this in subsequent experiments by restricting ligand expression to few cells. When the receptor was expressed in all astrocytes (under the alrm driver) and the ligand in subsets of neurons with a restricted localization in the brain, we observed GFP expression only in the astrocytes that contact the ligand expressing neurons. For example, expressing the ligand in the ORNs (under the orcodriver) led to GFP expression in the astrocytes surrounding the ORN axons in the antennal lobe. Similarly, expressing

the ligand in neurons that produce the PDF peptide (under the pdf driver) led to GFP induction in a small set of astrocytes bordering PDFC neurons. Our results clearly demonstrate that TRACT is capable of detecting neuron-glia contact in *Drosophila*. In addition, this application of TRACT serves as a much-needed tool for selectively labelling groups of glial cells. Though systems such as MARCM or Flip-Out can be used to sparsely label glial cells in mosaic clones, both systems are inherently stochastic and cannot be used to control gene expression in a stereotypical set of cells. With TRACT, we have shown that it is now possible to readily identify and consistently label subpopulations of glial cells based on their contact with known neuronal types.

Although this observation indicates that TRACT can be used to detect membrane-membrane contact between interacting neurons, it does not guarantee that TRACT can specifically identify synaptic connections, at least in its current implementation. As the GRASP case, it would be necessary to localize the molecular components to pre- and postsynaptic sites. Theoretically, targeting the ligand and/or receptor to synaptic sites will prevent the possibility of receptor activation by membrane-membrane contact at non-synaptic sites (for instance, between fasciculated axons).

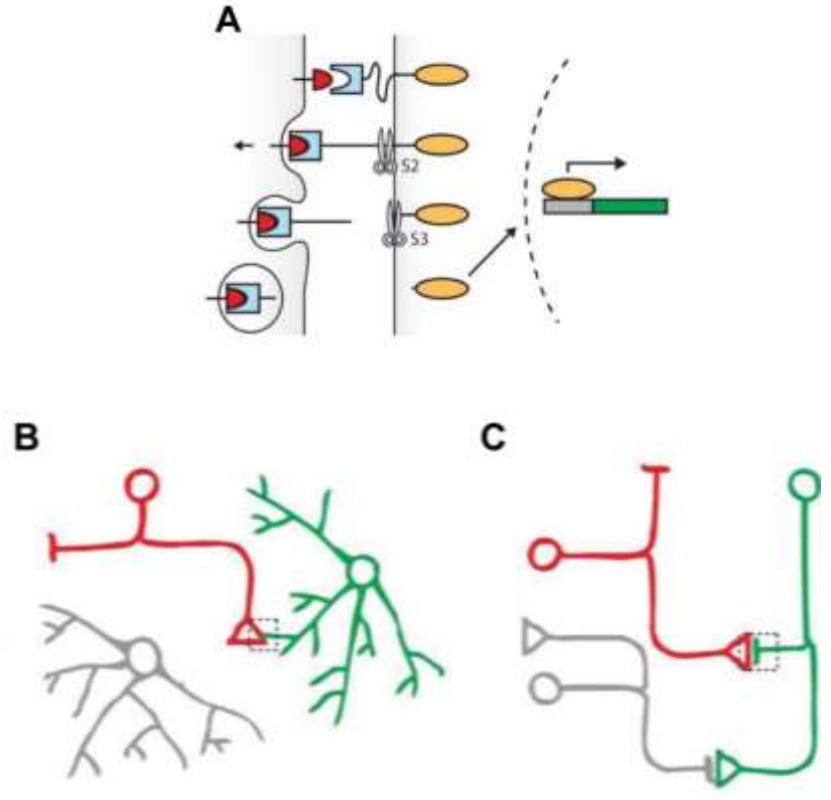

Figure 2.6. Visualizing cell-cell contact using the TRACT method. **(A)** The ligand (red) is localized to the plasma membrane in the cell of interest (left). When the ligand binds to the receptor (light blue) on a neighbouring cell (right), it partially unfolds the NRR to allow for proteolysis of the receptor (S2). S2 induces another proteolysis (S3), liberating the transcription factor (orange oval) fused to the receptor. This transcription factor then translocated to the nucleus to activate transcription of reporter genes such as GFP (green rectangle). **(B)** TRACT can be used in *Drosophila* to detect neuron-astrocyte contact *in vivo*. The artificial ligand is expressed in the neuron of interest (red) while the receptor is expressed in all astrocytes (green, gray). Only the astrocyte in contact with the ligand expressing neuron is induced to express GFP (green). **(C)** With optimization, TRACT could also be used to detect neuron-neuron contact. For anterograde tracing, the ligand needs to be localized to the presynaptic terminal in the neuron of interest (red). If the receptor is expressed at the postsynaptic sites of all candidate neurons (green, gray), only the postsynaptic neuron to the neuron of interest (red) will be induced to express GFP (green). Alternatively, for retrograde tracing, the ligand would be localized at the postsynaptic sites in the neuron of interest, and the receptor would be localized at the presynaptic sites of all candidate neurons.

AIMS

The comprehensively mapping of the connectivity of various neural circuits across numerous brain regions and many organisms is a major goal of modern neuroscience. There is a general agreement that solving the wiring diagram of a circuit is a crucial step towards understanding the computations implemented in that circuit. Here, we propose to improve, optimize, and validate a novel technique, developed in our laboratory, to reveal monosynaptic connections arising to or from a genetically labelled neuron of interest (TRAnsynaptic Control of Transcription; TRACT). In this neuronal tracing method, neurons expressing a synaptically targeted artificial ligand (emitter neurons) bind to and activate a genetically engineered synthetic receptor on their synaptic partners (receiver neurons) via interactions in their synaptic cleft. Upon ligand receptor binding at synapses, the receptor is cleaved in its extracellular domain and transmembrane domain, releasing a protein fragment that activates transcription in the synaptic partners.

The first version of TRACT system was used to investigate the interactions between neurons and glial cells in the *Drosophila* central nervous system (Huang et al., 2016). However, the system was not efficient to trace neuronal circuits and presented two main limitations. **(i)** The receptor showed a high ligand independent background in some brain regions; **(ii)** ligand and receptor were expressed all over the neurons' surface, revealing all forms of cell-cell contact, including non-synaptic contacts.

Therefore, in this Chapter of the Thesis, we have addressed the following objectives:

Aim 1: Reduce ligand independent activity of the Notch receptor.

To improve the signal-to-noise ratio of the TRACT system, we will make several modifications to the transmembrane domain, extracellular domain and intracellular domain of the engineered receptor and test their efficiency *in vitro*.

<u>Aim 2:</u> Implementation of the TRACT technique *in vivo*.

Using the olfactory system, a well-known and established neuronal circuit in *Drosophila*, we will determine the ability of the best receptors candidates obtained from the Aim 1, to reveal cellular connections *in vivo*.

<u>Aim 3:</u> Target the ligand and receptor toward the synaptic cleft.

To improve the signal-to-noise ratio of the TRACT system and avoid unspecific activation due to non-synaptic contact, we will engineer the ligand and receptor to be selectively located in the pre- and postsynaptic compartment in emitter and receiver neurons, respectively.

<u>Aim 4:</u> Assess the TRACT system as a retrograde neuronal tracer.

In the first version of the TRACT technique, only anterograde labelling was tested. We will assess the capability of the TRACT system as a retrograde tracer in the *Drosophila* nervous system.

RESULTS

As mentioned in the Introduction from this Chapter, the most commonly used methods to trace cell-cell interaction are: co-localization of fluorescent tags by light microscopy (Chen et al. 2014), serial electron microscopy (Denk and Horstmann 2004), GFP reconstitution across synapses (GRASP; (Feinberg et al. 2008), and trans-Tango (Talay et al. 2017). None of these methods enables long-term genetic modifications of the interacting cells. However, our laboratory has developed a new genetically encoded tool based on the molecular logic of Notch that can analyze cell-cell interactions (TRACT; Huang et al., 2016). At that moment, most of the techniques based on Notch-Delta signalling mechanism had been used *in vitro* to recognize tumour by T cells and to create engineered cells interactions in cells in culture (Gordon et al. 2015; Morsut et al. 2016; Roybal et al. 2016). TRACT has been developed to be the first genetically encoded method to analyze cell-cell interaction *in vivo*, based on the Notch-Delta mechanism.

The TRACT system has shown new insights into neuron-glial interactions and has revealed the potential for complex experiments with the available methods to date. However, the TRACT method still exhibits some ligand independent activation (LIA) problems *in vitro*, and *in vivo* when it is used to label a subset of astrocytes, expressing the receptor 1d3NRRG4 under the promoter alrm (astrocytes-like glial cells marker). Moreover, TRACT does not show all the already well-known connections between neurons and glia in the adult brain of *Drosophila*. Therefore, to improve the efficiency to monitor cell-cell contacts of TRACT, we focused on two strategies: **(i)** receptor optimization to improve its signal-to-noise ratio and surface expression by modifying its ECD, TMD, ICD, and the combination of said receptor with different systems; and **(ii)** targeting the receptor and ligand to the dendrites and axons terminals, respectively.

Our synthetic receptor design is based on the Notch receptor and a bipartite expression system, Gal4-UAS (Upstream Activating Sequence) (Gordon et al. 2015; Morsut et al. 2016). The synthetic receptor maintains the Notch negative regulatory region (NRR) and transmembrane domain (TMD), but both the Notch EGF-like repeats and intracellular domain (ICD) have been replaced by a single-chain antibody domain (SCAD, which is 1d3) (Kochenderfer et al. 2009) and the transcriptional regulator, Gal4 (G4), respectively (Figure 2.7A). This receptor is named 1d3NRRG4. Upon 1d3-mCD19 binding, the NRR partially unfolds, and ADAMs metalloprotease can cleave in the S2 site.

The cleavage of the S2 site triggers a second cleavage (S3) by the ubiquitous metazoan γ-secretase complex in the TMD. After this S3 cleavage, Gal4 releases from the plasma membrane and translocates to the nucleus where it binds to UAS promoter activating gene expression (Figure 2.7B).

A good membrane expression of the 1d3NRRG4 protein is an essential factor since this system is activated by the interaction of the receptor and ligand (CD19) across two plasma membranes. Therefore, the activation of 1d3NRRG4 is limited to the number of molecules on the cell surface. Boosting the amount of receptor on the cell surface by increasing the titer of the lentivirus carrying the receptor, does not help as the receptor overexpression leads ligand independent background (see images on Figure 2.7C) (Yang et al. 2020), while the high expression of synNotch (synthetic receptor of Notch) also correlates with the increase of ligand independent activation.

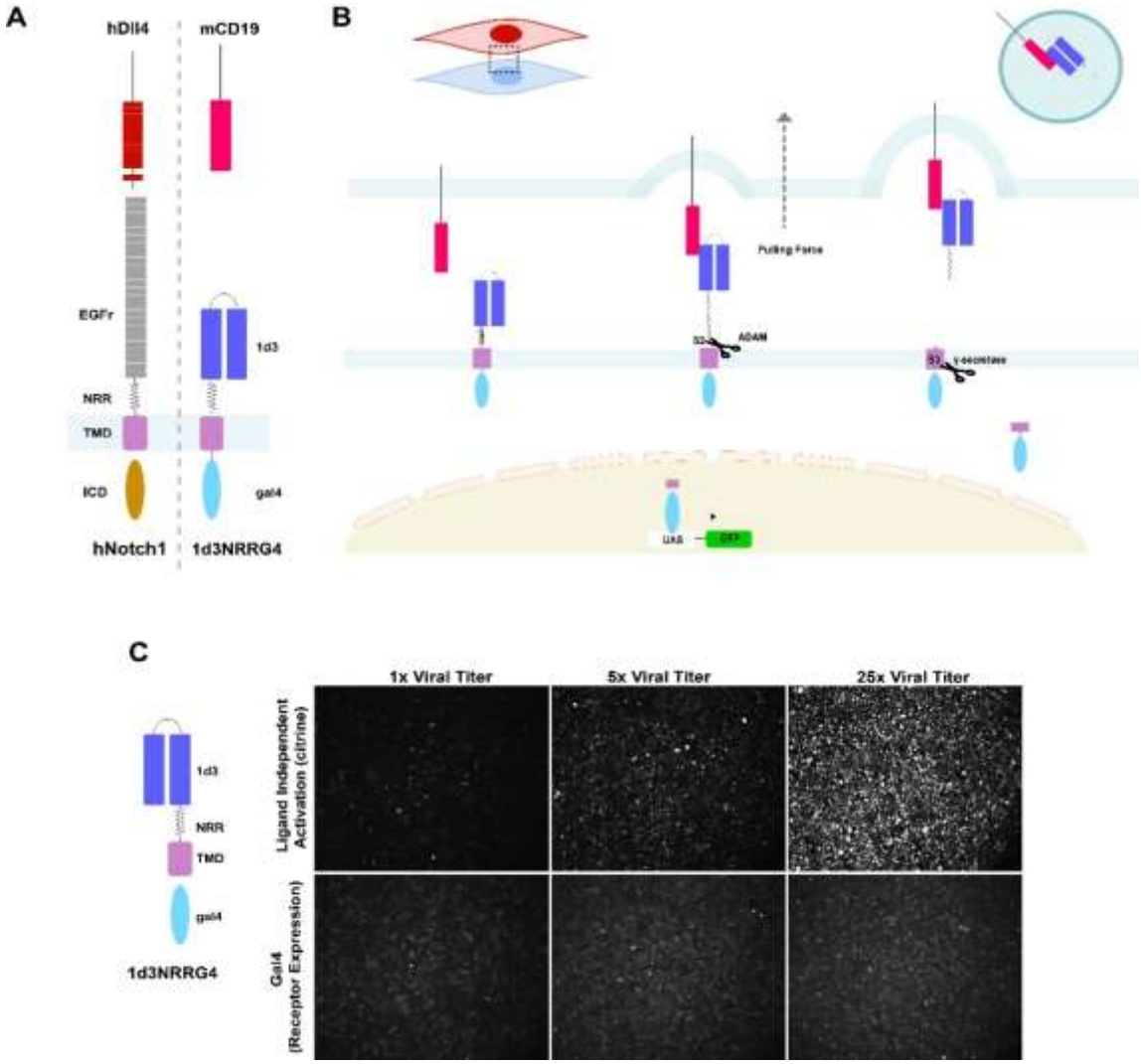

Figure 2.7. TRACT engineered genetic system to record and manipulate cell-cell contacts. (A) Diagram showing ligand (hDll4) and receptor from Notch signalling pathway (left) and synthetic receptor (1d3NRRG4, from TRACT) based on Notch and its ligand mCD19 on the right. **(B)** 1d3NRRG4 activation is based on Delta/Notch signalling pathway. Endocytosis of CD19 ligand binding triggers a conformational change in the 1d3NRRG4 receptor, which induces two cleavages in NRR (S2) and TMD (S3) ADAMs and γ-secretase, respectively. The ICD (Gal4) translocates to the receiver cell's nucleus to activate transcription of downstream genes such as GFP. **(C)** High expression of the receptor (1d3NRRG4) leads an increase of ligand independent activation (LIA).

Following previous results from Ting-Hao, a postdoctoral from Dr Lois' laboratory, 1d3NRRG4 receptor is mostly accumulated in the cytosol (perinuclear region: endoplasmic reticulum (ER) and Golgi apparatus (GA)). By performing immunohistochemistry against the receptor's extracellular domain (1d3 domain) under non-permeabilized conditions, he observed a weak expression of the receptor on the plasma membrane. Moreover, the ligand independent background of this receptor was reduced by ADAMs and γ-secretase blockers TAPI and DAPT, respectively, suggesting their involvement in the ligand independent cleavage of the NRR and the TMD. These results indicate that the synthetic receptors are transported to the cell surface inefficiently, being retained in the ER and/or Golgi complexes. To enhance the receptor trafficking toward the cell surface and improve the efficiency of the TRACT system, we carried out several approaches modifying different receptor domains.

2.3.1. Modifications of the Transmembrane Domain.

Several studies have shown that the properties of transmembrane domains, such as the charge and length, play essential roles in the sorting and transport across different subcellular compartments, influencing the subcellular localization of membrane proteins (Sharpe et al. 2010; Singh and Mittal 2016). For instance, TMDs from proteins in the plasma membrane present a higher hydrophobic length than those TMDs from proteins in the Golgi membrane (Sharpe et al. 2010). Moreover, the abundance of hydrophobic residues changes along the length (structure) of the TMD. Transmembrane domains in the plasma membrane showed that the outer leaflet has an increase in smaller residues and an increase in larger residue for vertebrates and fungi. Therefore, this study suggests that transmembrane proteins with long TMD tend to better localize on the plasma membrane.

Considering the length and amino acid compositions of the TMDs, we modified the TMD from 1d3NRRG4 receptor giving rise to five different modifications of it (Figure 2.8A). The TMD of these modifications is based on the 23 aa of the CD4TMD and last 5 aa from hNotch1TMD, where S3 cleave site is located. We used CD4TMD because it is a glycoprotein known to be transported to the plasma membrane of the immune cells such as monocytes, dendritic or T-helper cells, efficiently. We generated different receptors using either 19 aa or 22 aa from CD4 TMD and adding the last 5 aa from hNotch1 (see Table 1 – ANNEX 1). Moreover, the N-end rule shows that certain amino acids present on the N-terminal of a protein present a longer half-life than other such as Valine that last 100 hours or Cysteine in the opposite site lasting 1.2 hours (Bachmair et al. 1986). Based on this statement, our TMD modifications would present different half-life times due to the amino acid located at the N-terminus after S3 cleavage (see Table 1 - ANNEX 1)

To investigate if the TMD modifications improve the signal-to-noise ratio, we performed ligand receptor interaction experiments. First, we generated cell lines expressing each receptor modifications. Then, we mixed ligand cell lines expressing mCD19mCherry with each receiver cell lines in a 1:1 ratio, unless the experiment conditions are specified. The fold activation between the integrated intensity of the induction versus background from all these modifications reaches a higher fold activation for those receptors with shorter TMD (24aa:7.61-fold; 24aa,+ILE:7.1-fold; and 24aa,+SER: 6.44-fold) than Notch TMD (24aa, 4.95-fold activation) (Figure 2.8B). Furthermore, those receptors, in which the length of TMD is the same as the control, did not show any improvement in the fold increase (27noC:4.3-fold; 27noC,+SER: 2.56-fold). Besides, receptors in which the Cysteines have been deleted, 24 aa and 27noC, present three times and 1.8 times lower background, respectively, than the original receptor regardless of the length of the TMD (Figure 2.8C). This modification helps to bring down the background level, but it would be potentially interesting if the level of the induction would be similar to the control (1d3NRRG4) (Figure 2.8C). Moreover, replacing the Cysteines by Serines (24aa,+SER and 27noC,+SER) showed no significant differences for 24 aa TMD length receptor, and much lower ligand independent activation and induction for 27 aa length (Figure 2.8C). Finally, a 24 aa length TMDs with

Isoleucine (20 hours half-life) did not show an improvement in the fold increase, though reducing the background and the induction compared to Notch1TMD (Figure 2.8B and C). Although decreasing the length of the TMD (24 aa) improves the fold increase, the overall background and induction are lower than the control, showing no promising results (Figure 2.8C). The ideal situation would be a construct in which the ligand independent background would have the same level of 27noC, +Ser or even lower with an induction comparable to the Notch TMD.

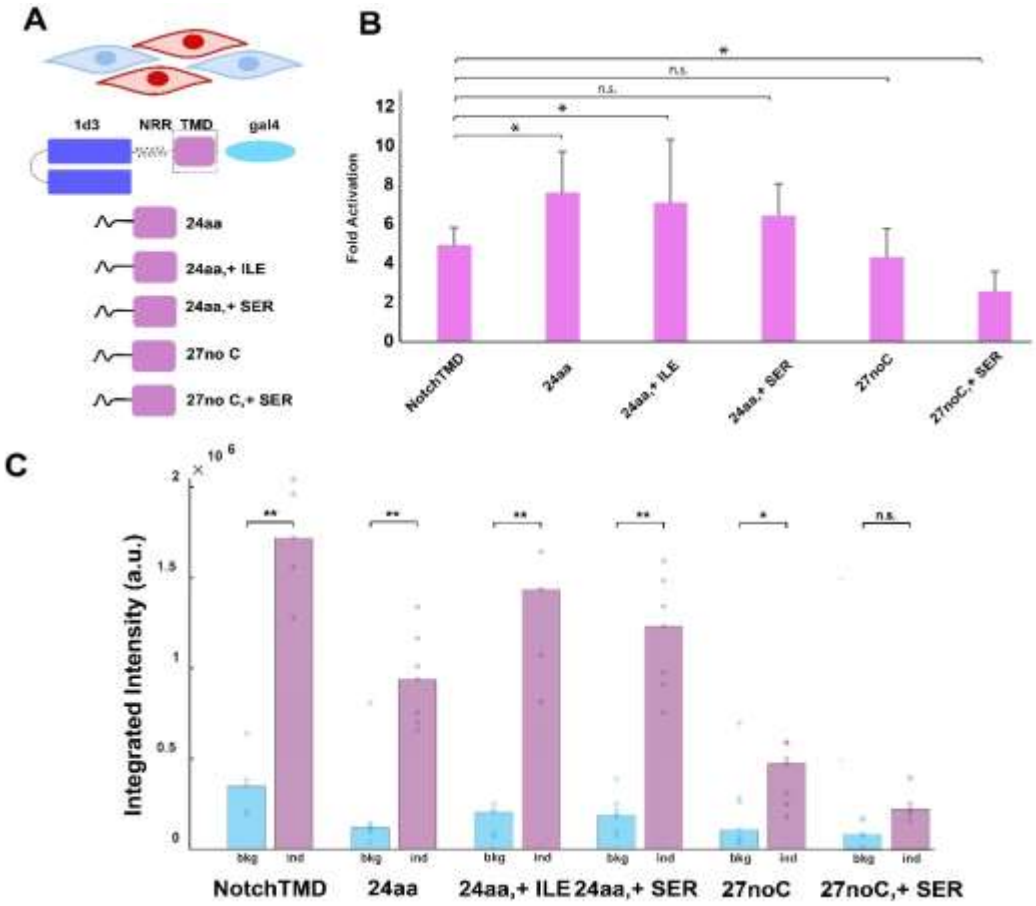

Figure 2.8. Capabilities to induce the reporter gene expression by cell-cell interaction of Transmembrane domain modifications of synthetic receptor 1d3NRRG4. (A) Top: It is shown a diagram of cell-cell interaction experiments where the red cells correspond to emitter cells and the blue cells are the receiver cells. Button: Diagrams showing the different modifications of the TMD. **(B)** Fold Increase of the different modifications of the TMD ((NotchTMD)=4.95-fold (24aa)=7.95-fold; (24aa,+ILE)=7.10-fold; (24aa,+SER)=6.44-fold; (27noC)=4.30-fold; and (27noC,+SER)=2.53-fold). Note that comparisons of each modification with NotchTMD only showed significant differences for 24aa and 24aa,+ILE (p-value(24aa)=0.017; p-value(24aa,+ILE)=0.022; p-value(24aa,+SER)=0.200; p-value(27noC)=0.200; and p-value(27noC,+SER)=0.030) **(C)** Quantification of Integrated Intensity (arbitrary units) of the induction and background for every TMD modifications. These values are normalized based on the same threshold.

p-values from induction vs control comparisons: NotchTMD=0.079; 24aa=0.040; 24aa,+ILE=0.079; 24aa,+SER=0.065; 27noC=0.031; and 27noC,+SER=0.097.

Based on the previous TMD modifications, we also analyzed the hybridized TMD obtained from the direct fusion of CD4 TMD (24 aa) plus 5 aa of hNotch1 (1d3Hyb) (see Table 1 – ANNEX 1). This receptor with hybrid TMD showed a lower ligand independent and dependent activation (Figure 2.9C) than the control 1d3NRRG4. In this case, the fold activation is almost three times higher than the original (Figure 2.9B). This modification suggests that part of the background from the 1d3NRRG4 receptor could come from the conformation and charges of hNotch1 TMD since the receptor still have the last 5 aa from Notch TMD where several S3 cleavages occur (Tagami et al. 2008). Therefore, this receptor would be a great candidate to enhance TRACT system *in vivo* since it provides low ligand independent background and good inducibility (3.4×10^6) compared to the original receptor (4.26×10^6).

2.3.2 Modifications of the Extracellular Domain.

It is known that S1 cleavage of Notch receptor has different effects on the surface expression of Notch1 and Notch2 receptors. Moreover, Notch1 and Notch2 receptors lacking the loop containing the S1 cleavage site (S1 loop-out, S1LO) avoid or resist the proteolytic cut by Furin-like convertase. Although S1LO modification decreases the surface expression and ligand dependent activation of Notch, S1 cleavage is not required for physiologic activation of Notch proteins (Gordon et al. 2007). Then, we decided to modify the original receptor, 1d3NRRG4, by switching the NRR from Notch1 to the S1LO NRR (Figure 2.9A). First, we observed that UASH2BmCit CHO cells expressing 1d3N1S1LO showed weaker mCitrine intensity for ligand independent activity than those expressing 1d3NRRG4 (Figure 2.9C). When 1d3N1S1LO/UAS-H2Bmcit cells were co-cultured with mCD19mCherry cells (ligand), low levels of H2BmCit expression were observed (Figure 2.9C and D) suggesting that the surface expression of this receptor is worse than 1d3NRRG4. My colleague Ting-Hao also showed that the modified receptor with S1LO and TMD from hNotch2 presents similar background and inducibility levels than 1d3N1S1LO without any improvement (Huang 2017). Overall, these results where 1d3N1S1LO still has inducibility despite its poor surface expression, suggest that TRACT

system only requires a minimum amount of the receptor in the plasma membrane to be activated.

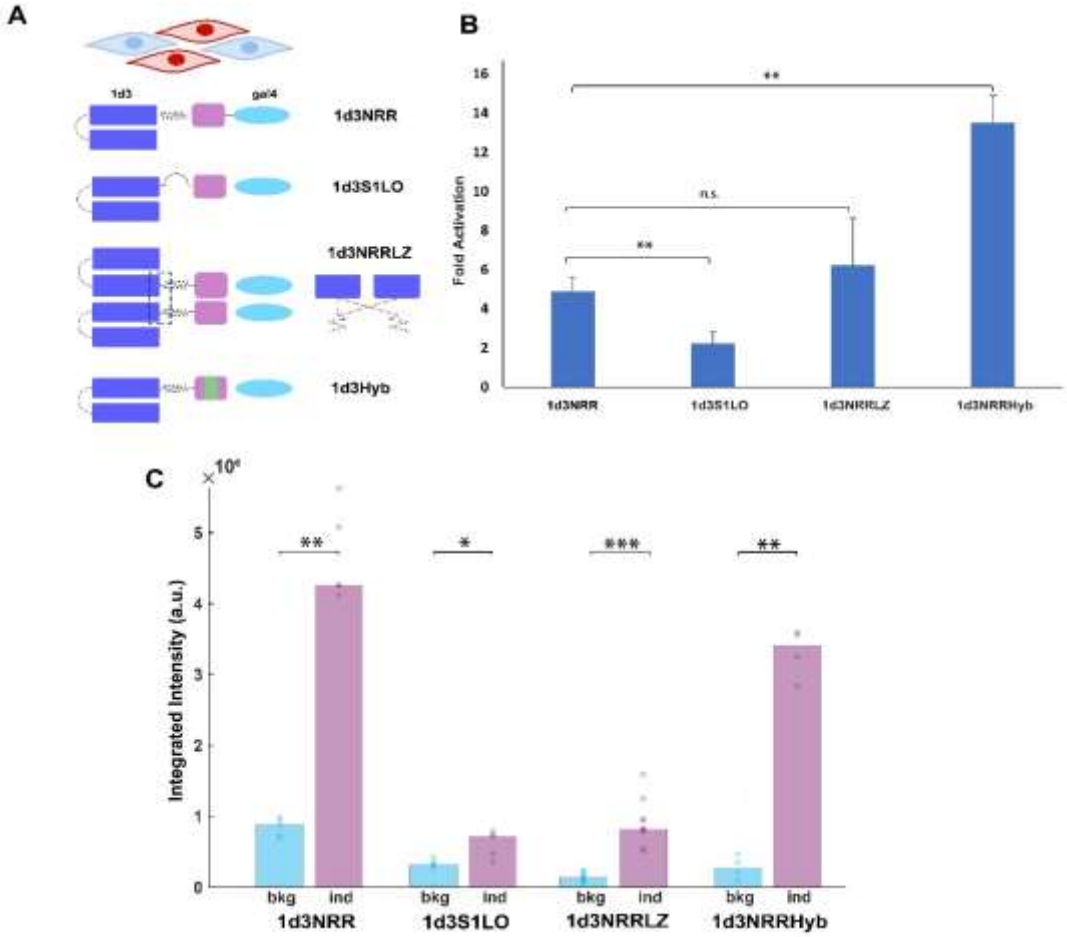

Figure 2.9. Capabilities of the extracellular domain modifications (NRR) of 1d3NRRG4 and 1d3NRRHybTMD to induce gene expression. (A) *Top:* Diagram showing the cell-cell interaction experiment. *Button:* Diagrams showing two different modifications of ECD (1d3S1LO and 1d3NRRLZ) and the 1d3NRRHybTMD. **(B)** Fold increase of the different modifications of the ECD. Note that comparisons of ECD modification with 1d3NRRG4 did not show any improvement (1d3NRRG4=4.86-fold; 1d3S1LO=2.24-fold (p-value=0.007); and 1d3NRRLZ=6.22-fold (p-value=0.206)). Comparison of 1d3NRRHyb with 1d3NRRG4 (13.55-fold) showed significant differences, p-value=0.009. **(C)** Quantification of integrated intensity of the induction and background for every modification, p-values from induction vs control comparisons: 1d3NRRG4=0.079; 1d3S1LO=0.032; 1d3NRRLZ=0.00018 and 1d3Hyb=0.097.

It has been shown in *Drosophila* that the dimerization of Notch1 receptor caused by a 30 aa peptide derived from the yeast (leucine zipper (LZ) from yeast, GCN4) and Notch PEST domain (polypeptide enriched in proline, glutamate, serine and threonine, degradation signal) reduce the ligand independent activation (Struhl and Adachi 2000). Based on this strategy, we decided to investigate the ligand independent activation of a

dimerized receptor (1d3NRRG4) with leucine zipper in the ECD (1d3NRRLZ; Figure 2.9B). The GCN4 motif was inserted between the ECD (1d3) and the NRR of the original 1d3NRRG4. In cell-cell interaction experiments, 1d3NRRLZ receptor showed six times less integrated intensity of the background compared to the control 1d3NRRG4 (Figure 2.9C). The fold activation for this new receptor 1d3NRRLZ (6.22-fold) (Figure 2.9B) is not significantly higher than 1d3NRRG4 (4.98-fold) with a p-value higher than 0.05 due to the level of ligand dependent activation (Figure 2.9C).

On the other hand, it has been reported that adding an extra EGF repeat from hNotch1 to the ECD at the N-terminus of the NRR domain reduce its ligand independent background (Morsut et al. 2016). Considering that observation, we generated three different receptors whit one (EGF30), three (EGF30-33) or six (EGF30-36) EGF repeats from the most C-terminal of Notch located in front of the NRR (Figure 2.10A). The receptors with either three or six EGF repeats in the ECD did not show an improvement reducing the background with a fold increase similar or lower than 1d3NRRG4 (4.97-fold and 5.96-fold, respectively) (Figure 2.10B and C). In contrast, the receptor with one EGF repeat (EGF36) showed a slightly lower background level than 1d3NRRG4 (Figure 2.10C) and a higher level of ligand dependent activation which brings the fold activation to 7.91-fold compared to the control 1d3NRRG4 (6.12-fold activation) (Figure 2.10B). Considering the fold activation increase in the synthetic receptor adding one EGF repeat (EGF36) in its extracellular domain would be an excellent candidate to boost TRACT system *in vivo*.

As mentioned in the transmembrane domain section, the human CD4 glycoprotein has an excellent cell surface expression. For this reason, we decided to create a synthetic receptor using the ECD from human CD4. Therefore, we decided to switch the 1d3 ECD from the original receptor to CD4 (CD4NRRG4, Figure 2.11A) to test if increasing the cell surface level can trigger better ligand dependent cleavage. In addition, the small ubiquitin-like modifier (SUMO protein) of about 100 aa was added between the extracellular domain of CD4 and NRR (CD4NRRSUMOG4). It is known that SUMO protein is well conserved in evolution, and it attaches and detaches from other proteins to modify their functions (Han et al. 2018). In this case, to study a ligand-receptor interaction, we generated cell lines expressing the HIV glycoprotein gp160,

which binds to human CD4 to enable entry of HIV into T-lymphocytes (Mao et al. 2012). The cells expressing the receptors were mixed with emitter cell lines, expressing the gp160 fused to mCherry fluorescent protein. Switching the 1d3 ECD to CD4 ECD does not increase the ligand dependent activation, and the fold increase is as high as 1d3NRRG4 receptor (Figure 2.20B and C). Moreover, the interaction between the CD4 and SUMO does not help to reach a higher fold activation level (5.36-fold) (Figure 2.20B).

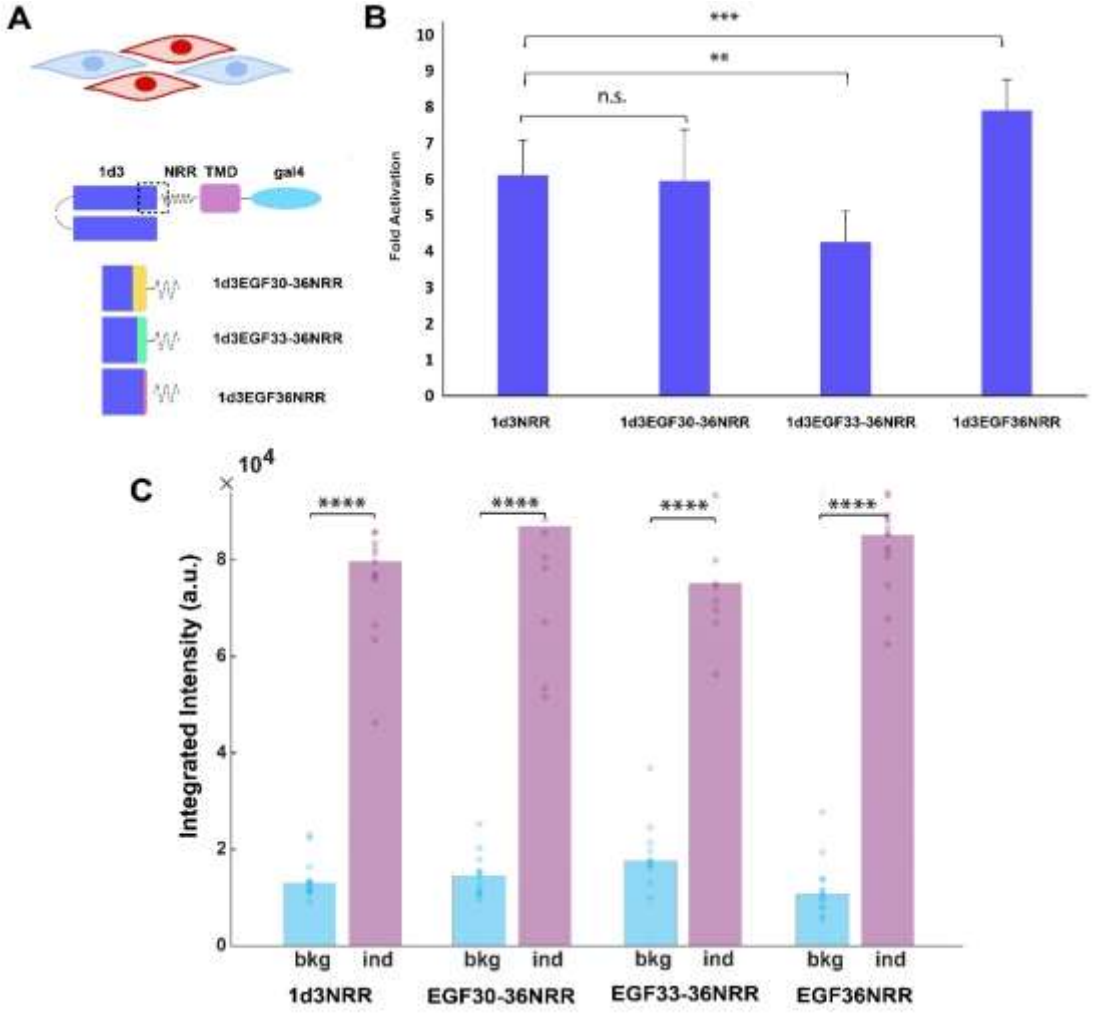

Figure 2.10. Capabilities to induce the reporter gene expression by cell-cell interaction of extracellular domain modifications (EGF repeats) of 1d3NRRG4. (A) *Top:* Diagram showing the cell-cell interaction experiment. *Button:* Diagrams showing the insertion of 6, 3 or 1 EGF between the SCAD (1d3) and NRR domains. **(B)** Fold increase of the different modifications of the ECD. Note that comparisons of ECD modification with 1d3NRRG4 showed a significant increase of the fold activation for 1d3EGF16NRR (1d3NRREGF30-36=5.95-fold, p-value=0.970; 1d3NRREGF33-36=4.27-fold, p-value=0.0037; 1d3NRREGF36= 7.91-fold, p-value=5 x 10^{-4}). **(C)** Quantification of the integrated intensity of the induction and background for every modification. All the modifications showed a significant different (less than 0.0001) between the induction and the background (1d3NRRG4=0.079; 1d3NRREGF30-36=1.64 x 10^{-5}; 1d3NRREGF33-36=8.15 x 10^{-5} and 1d3NRREGF36=1.64 x $10^{-5)}$.

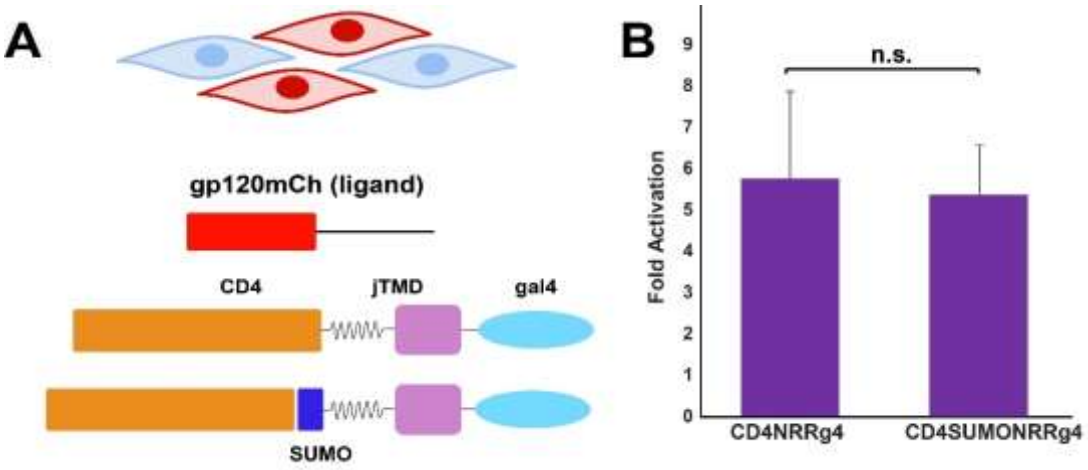

Figure 2.11. Capabilities to induce intracellular signal by cell-cell interaction of engineered receptor based on CD4glycoprotein and SUMO protein. (A) *Top:* Diagram showing the cell-cell interaction experiment. *Button:* Diagrams showing the ECD from CD4 glycoprotein and adding a SUMO-protein between the CD4 and NRR. **(B)** Comparisons of the fold activation did not show any significant difference (CD4NRR=5.36-fold and CD4SUMONRR=5.72-fold; p-value=0.826).

Recently, it has been reported that adding a small hydrophobic sequence of peptides (HGQ**LWF**, RAM sequence) at the N-terminus of the intracellular domain of Notch, significantly reduced the background without affecting the efficiency for the induction (Yang et al. 2020). This RAM sequence is responsible for the loop that binds the ICD to the membrane, "snorkelling" the ICD. Based on these statements, we hypothesized that adding part of this sequence (LWF) to the jTMD of our CD4NRRG4 synthetic receptor could reduce the level of ligand independent activation. The juxtatransmembrane (jTMD) domain, is a small domain next to the N-terminus of the TMD in the extracellular region with a length of 12 aa (QSETVEPPPPAQ; Figure 2.12A). Following a similar strategy, we engineered a receptor in which the jTMD has these three amino acids (RKR) (Figure 2.12A). Due to the positive charges of Arginine (R), the jTMD will be attracted to the negative charges of the plasma membrane surface. The cells expressing either the receptor with the LWF sequence (QSE**LWF**GGGSAQ) or RKR (QSE**RKR**GGGSAQ) sequence in its jTMD did not show a positive effect. In both scenarios, the ligand independent activation is reduced, but the ligand dependent activation is also lower than the control receptor (CD4NRRG4) with a fold activation of 2.55-fold and 2.15-fold, respectively (Figure 2.12B and C). Also, we generated molecular dynamic simulation models of these two new jTMDs and Notch1 (Figure 2.12D), and we did not

observe an overall negative or positive charged peptide compared to NotchjTMD (peptide negative charged).

In summary, from all the analyzed engineered receptors with modifications in the ECD and TMD that showed a low ligand independent activity and strong induction, we selected 1d3NRRHybG4 (which have a low background and excellent induction) to assess TRACT system *in vivo*. Overall, the inefficiency of our receptor modifications to enhance the signal-to-noise signal suggests that the 1d3NRRG4 receptor may suffer a complex regulation of its processing, transport, and activity.

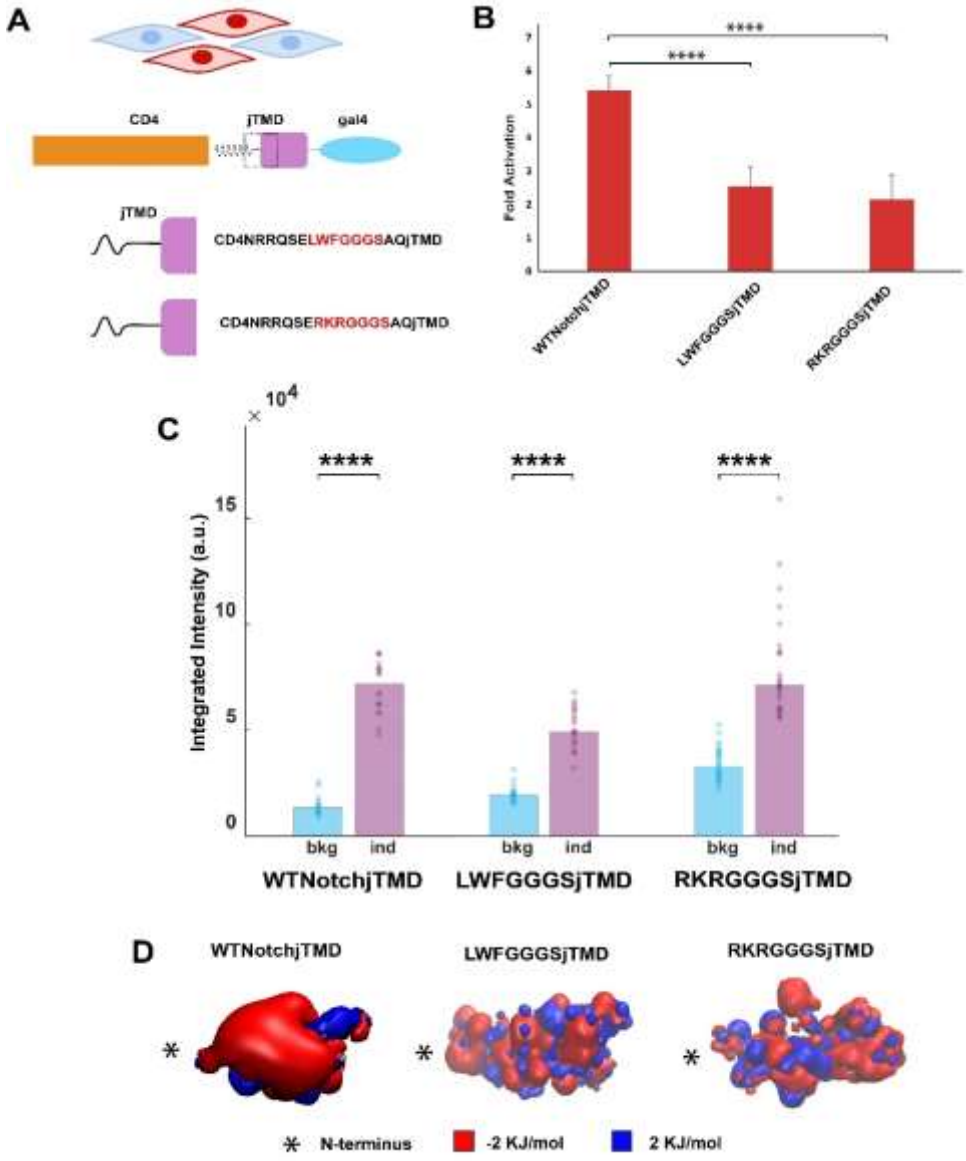

Figure 2.12. Capabilities of juxtatransmembrane domain modifications to induce gene expression by cell-cell interaction. (A) *Top:* Diagram showing the cell-cell interaction experiment. *Button:* Diagrams showing the modifications of the jTMD. **(B)** Fold activation of both LWF ("snorkeling") and RKR peptides modifications in the jTMD, did

not show any improvement (CD4NRR=5.43-fold; CD4NRR**LWF**=2.55-fold; CD4NRR**RKR**=2.15-fold (p-value(LWF)=1.54 x 10^{-7} and p-value(RKR)=4.81 x 10^{-8})). **(C)** Quantification of the integrated intensity of the induction and background for every modification. All the modifications showed a significant different between the induction and the background less than 0.0001: CD4NRR=3.22 x 10^{-7}; CD4NRR**LWF**=6.70 x 10^{-8}; CD4NRR**RKR**=1.40 x 10^{-6} and 1d3NRREGF36=1.64 x 10^{-5}. **(D)** Potential energy surface of **LWF** and **RKR** jTMDs calculated using the published NMR structure and the APBS plugin of the VMD software with CHARMM parameters (see Methods for more details).

2.3.3. Modifications of the Intracellular Domain.

When the receptor 1d3NRRG4 was dimerized using leucine zipper in its ECD, we observed a ligand independent activation lower than the original receptor, and a fold increase slightly higher, not showing a significant difference (see Figure 2.9). It is plausible than the leucine zipper (LZ) in the ECD can cause some changes in the conformation of the receptor ECD that does not allow to be fully induced by the ligand or the interaction with the ligand is not 100% efficient.

The results obtained by dimerization of the ECD using leucine zipper, increase the fold activation because it exhibits a very low ligand independent activation. Then, we generated two different cell lines with a dimerized region in its ICD: One of the receptors has the LZ between the DNA binding domain (DBD) and the activation domain (AD) (1d3NRR-63GS), and the second receptor has the LZ in the C-terminal of the AD (1d3NRR-GCN4icd) (Figure 2.13A). In this case, two ligands need to bind to the ECD of the receptor to activate the signalling pathway of these engineered receptors. Cell-cell interaction experiments using these two ICD modifications presented a lower level of ligand independent activity than control receptor (1d3NRRG4) where the lowest integrated intensity is for GNC4 (0.77 x 10^4) (Figure 2.13C). Moreover, the fold activation in both cases is bigger than the control (6.7-fold) and similar between them: for 1d3NRR-GCN4icd (10.09-fold) and 1d3NRR-63GS (10.20-fold) (Figure 2.13B). Also, the dimerized receptor between the AD and the DBD (1d3NRR-63GS) showed higher induction than 1d3NRR-GCN4icd and the 1d3NRRG4. Although 1d3NRR-63GS might be a great candidate considering the fold activation and induction, the ligand independent background level is not significantly lower than the control. On the other hand, 1d3NRR-GN4icd presents the lowest ligand independent background and higher fold activation

than our control receptor, making this receptor a potential candidate to evaluate our TRACT system *in vivo*.

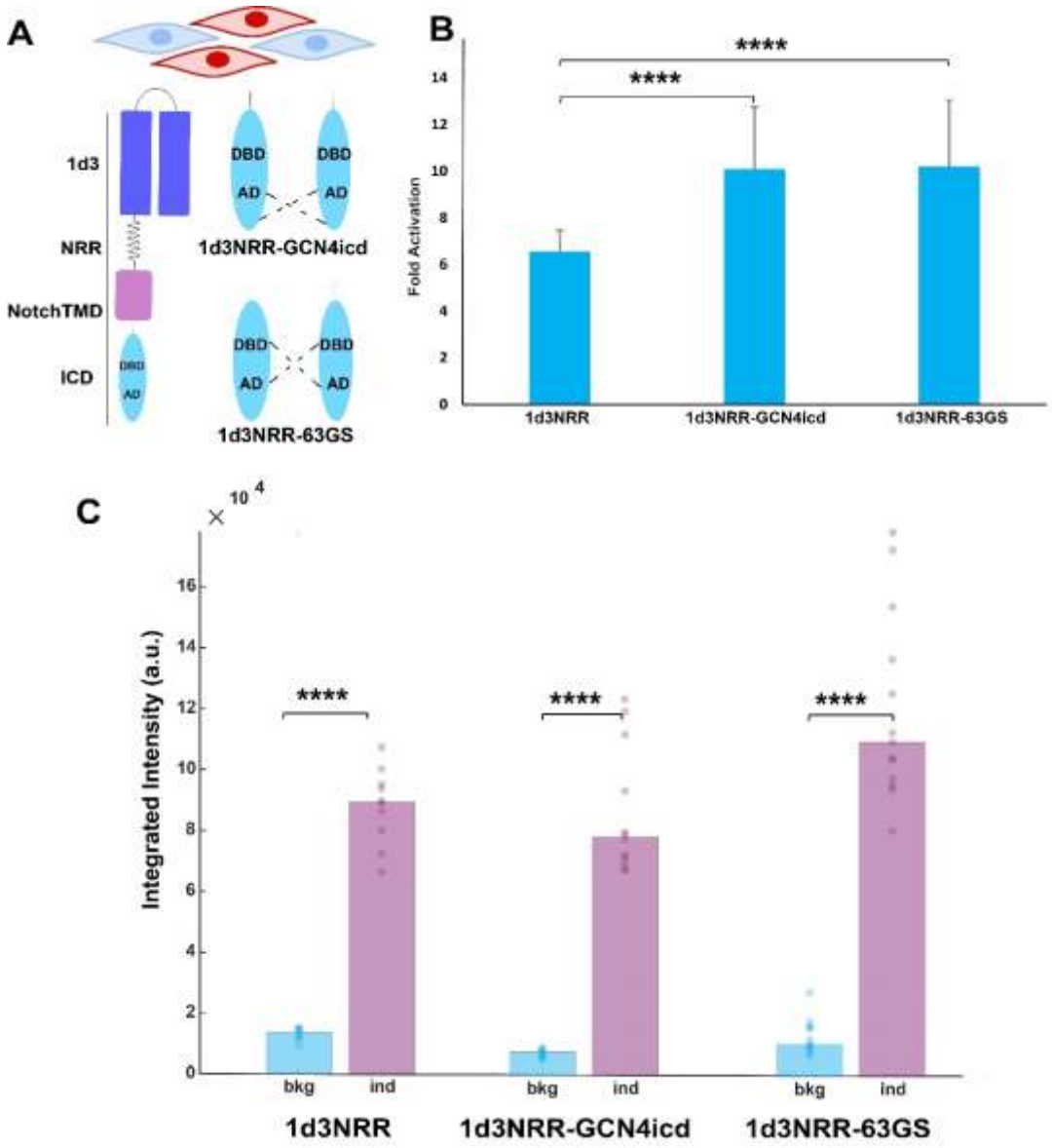

Figure 2.13. Capabilities to induce the reporter gene expression by cell-cell interaction of leucine-zipped ICD of 1d3NRRG4. (A) *Top:* Diagram showing the cell-cell interaction experiment. *Button:* Diagrams showing the junction of the Gal4: after the AD (GCN4icd) or between the DBD and AD (63GS). **(B)** Leucine-zipped receptor ICDs showed a significant increase in their fold activation: 1d3NRRG4=6.56-fold; 1d3NRRGCN4icd=10.09-fold, p-value(GCN4)=8.73 x 10^{-5}; 1d3NRR63GS=10.19-fold, p-value(63GS)=8.21 x 10^{-5}. **(C)** Quantification of the integrated intensity of the induction and background for both ICD modifications. Both modifications showed a significant different between the induction and the background with a p-value less than 0.0001: 1d3NRRG4=1.84 x 10^{-4}; 1d3NRRGCN4icd=1.65 x 10^{-5}; 1d3NRR63GS=3.65 x 10^{-5}.

A similar strategy to receptor dimerization using leucine zippers is the split of the transcription factor. In the last decade, several works used the Split Gal4 system in *C. elegans* and *Drosophila* to control the transgene expression in space and time (Luan et al. 2006; Pfeiffer et al. 2010; Dolan et al. 2017; Wang et al. 2018). The yeast transcriptional factor has two functional independent domains: **(i)** for site specific DNA binding domain (DBD), and **(ii)** activation domain (AD) which cannot activate transcription on its own. Both domains need to join (covalently or non-covalent interactions) to reconstitute the transcription factor and induce gene expression at a specific site (Luan et al. 2006). Split Gal4 method can improve the Gal4-UAS system by expressing the DBD and the AD under the control of different promoters (enhancers), so the transcription of UAS only occurs in cells where both domains are expressed. Then, we engineered two receptors where the AD and DBD are independent intracellular domains of each receptor. The two domains need to be fused by a heterodimerizing leucine zipper fragment, so they bind no-covalently. In this case, we used the DBD in conjunction with two versions of the viral transcription factor VP16: the leucine zipper fragment is placed N-terminal or C-terminal to the activation domain (VP16) (Figure 2.14A).

The cell line expressing both the DBD and ZipVP16 domains (dimerization domain at N-terminus) in 90% of its cells showed a fold activation of 3.95, more than two times lower than 1d3 50% (cell line with 50% of the cells positive for 1d3NRRG4) after 74hours of cell-cell interaction (Figure 2.14B). However, the cell line expressing both the DBD and VP16zip (dimerization domain at C-terminus) in 100% of the cells was not induced after five days of cell-cell interaction experiment (data not shown), so we discarded this version of the heterodimerization domain. Overall, these results indicate a slower activation dynamic when the AD and DBD need to encounter to activate site-specific transcription, which suggests that both domains bind once they are released from the plasma membrane.

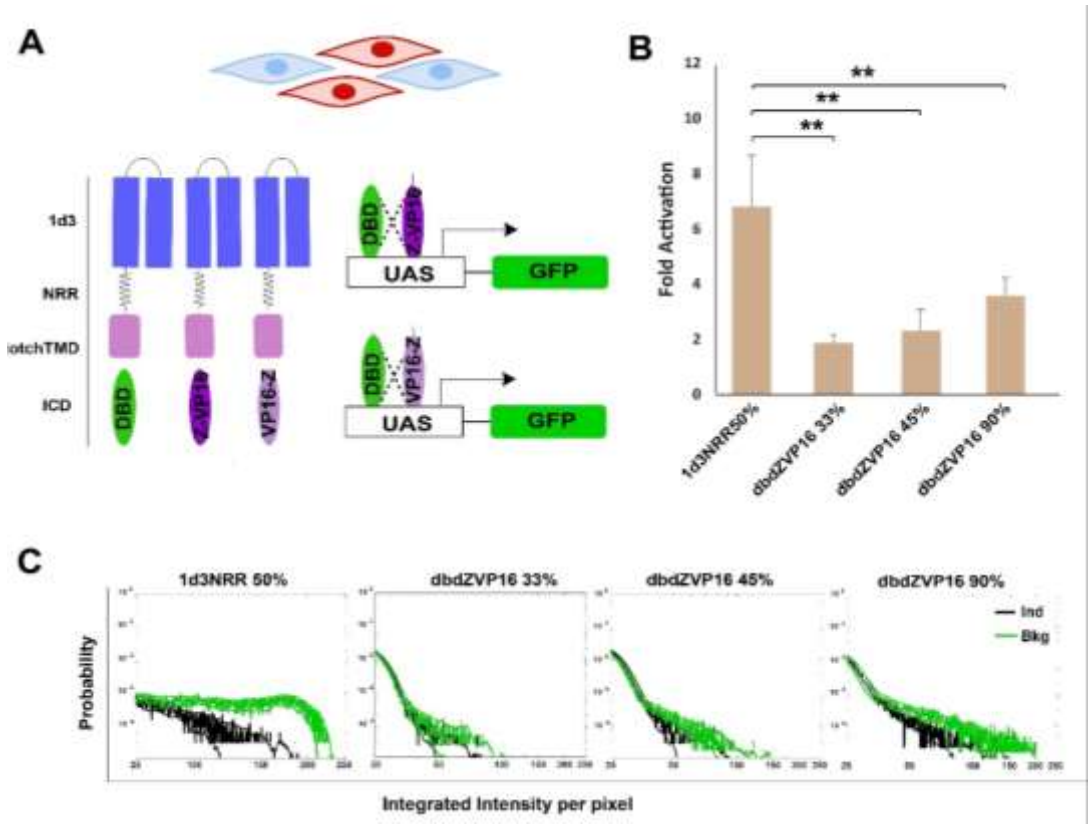

Figure 2.14. Capabilities to induce the reporter gene expression by cell-cell interaction using split Gal4 strategy. (A) *Top:* Diagram showing the cell-cell interaction experiment. *Button:* Diagrams showing three different versions of 1d3NRRG4 where the ICD will be only the DBD or the AD of VP16 with the leucine zipper domain either at the C-terminus or N-terminus. **(B)** Fold activation of leucine zipped receptors did not increase after 72 hour: 1d3NRRG4(50%)=6.5-fold; 1d3NRRZipVP16(33%)=1.78-fold, p-value(33%)=0.002; 1d3NRRZIPVP16(45%)=2.32-fold, p-value(45%)=0.002; and 1d3NRRZipVP16(90%)=3.60-fold, p-value(90%)=0.002. **(C)** Histograms showing the probability to find a cell with a specific intensity. The green trace corresponds to induction, and the black trace corresponds to the background. Note that the background for all the zipped receptor is lower than the cell line expressing the control receptor 1d3NRRG4 in 50%.

2.3.4. Evaluation of Proteases as Ligands of the TRACT System.

It is important to mention that our TRACT system depends on ADAMs and γ-secretase to release the intracellular domain from the plasma membrane. It is known that the proteases are expressed in every cell type, but there is no evidence that their proteolytic activity is the same at different developmental stages or comparable between distinct cell types. Although we have successfully performed neuronal-glia tracing, we also know that the TRACT system does not reliably work for other circuits, particularly for neuron-neuron interaction. It could be the reason why we observed variations in TRACT system efficiency depending on the brain circuit tested (Huang

2017). In order to implement the TRACT system, we developed a new modification of the receptor where the NRR domain was replaced by a motif that can be recognized and cleaved by an exogenous protease (SUMO and Sortase A proteases). In this case, both proteases will act as ligands. These proteases will then cut and shorten the newly engineered receptor when bound to it, and the ICD will be released.

The SUMOylation is a post-translational modification considered a crucial molecular regulatory mechanism involved in several processes such as carcinogenesis or DNA-damage repair. It based on two components: a small ubiquitin-like modifier protein (SUMO) and the SUMO protease. SUMO is a small protein of 100 aa, well conserved in evolution, that attaches and detaches from other proteins to modify their functions. The first step of SUMOylation is the cleavage of SUMO protein by sentrin/SUMO-specific proteases (SNEP) family occurs. After that, several steps involving different enzymes play their roles, and finally, the modified SUMO protein is attached to the substrate for specific post-translational modification (Han et al. 2018). On the other hand, the *Staphylococcus aureus* Sortase A cleaves a surface protein from cell wall carrying a specific motif of 5 aa (LPXTG) between the Threonine and Glycine residues. This cleavage is responsible for wall sorting reaction in almost all Gramm positive and some Gramm negative bacterium or Archaea (Wang et al. 2018).

In this strategy, we designed four different versions of the receptor based on SUMO protease mechanism and one receptor base on Sortase A (Figure 2.15A). We replaced the ECD (SCAD(1d3) and NRR) of our original receptor with **(i)** SUMO protein (1xSUMO), **(ii)** SUMO protein and ubiquitin tag in the intracellular domain (1xSUMOubi), **(iii)** two SUMO proteins (2xSUMO), and **(iv)** CD4 extracellular domain and SUMO protein (CD4SUMO), (Figure 2.15A). The receptor recognized by Sortase A has CD4 plus the small motif of 5 aa (LPETG) as ECD. 1xSUMOubi receptor showed very low background, almost undetectable (Figure 2.15C).

After making the cell line with 1xSUMOGal4 receptor, we observed a high level of ligand independent activation (data not shown). Then, we decided to discard this receptor for further analyses. As proof of principle, we tested whether the activation of our SUMO engineered receptor can be cleavage by adding the commercial SUMO

protease into the culture medium. Increasing concentration of said protease showed the highest fold activation for CD4SUMO receptor (182-fold) when 20 units (U) of the SUMO protease was added, followed by 2xSUMO receptor (49-fold). Almost not induction was shown for 1xSUMOubi receptor (Figure 2.15B). It is important to mention that CD4SUMO has the lowest ligand independent background among the inducible receptors, followed by 1d3NRRG4 (Figure 2.15C). Although 2xSUMO presents higher integrated intensity of induction than CD4SUMO for every concentration of SUMO-protease (Figure 2.15B'), the background is nine times higher than CD4SUMO (Figure 2.15C) which end with a lower level of fold activation than CD4SUMO (Figure 2.15B). Moreover, after mixing the receptor cell lines, CD4SUMO and 2xSUMO, with anchored and secreted SUMO protease cell lines, no induction was observed for any of these receptors (data not shown).

Cysteines residues are essential for the formation of specific thioester during SUMO-conjugation, and all SUMO enzymes involved in conjugating and deconjugating have catalytic Cysteines (Xu et al. 2008). Several studies report that a low concentration of H20H inhibits this conjugation mechanism during SUMOylation and induce reversible oxidative inhibition (Bossis and Melchior 2006). Moreover, (Xu et al. 2008) showed that oxidation produces some modifications of the catalytic domain (Cysteine residues) from the reversible form to irreversible state. We did not see any protease dependent induction when receptor cell lines were co-culture with the protease cell line, suggesting that SUMO protease suffered some sort of oxidation process. Several concentrations of a reducing agent (Dithiothreitol (DTT)) were added into the cell culture medium to prevent SUMO protease oxidation. Only 400 µM of DTT showed a slight increase in the induction dependent activity for both secreted and anchored proteases to the plasma membrane (Figure 2.15D).

Finally, we followed the same strategy that SUMO protease experiments to test the inducibility of CD4LPETG receptor by adding commercial recombinant *Staphylococcus aureus* Sortase A. The fold activation of CD4LPETG receptor with 20U of the recombinant SortaseA is 118-folds (Figure 2.15E) lower than CD4SUMO when the same units of SUMO Protease (Figure 2.15B). Even though the results were not promising, we tested the inducibility of this receptor by mixing it with two different

Sortase A cell lines: anchored and secreted. No induction at all was observed for any of the Sortase A cell lines (data not shown).

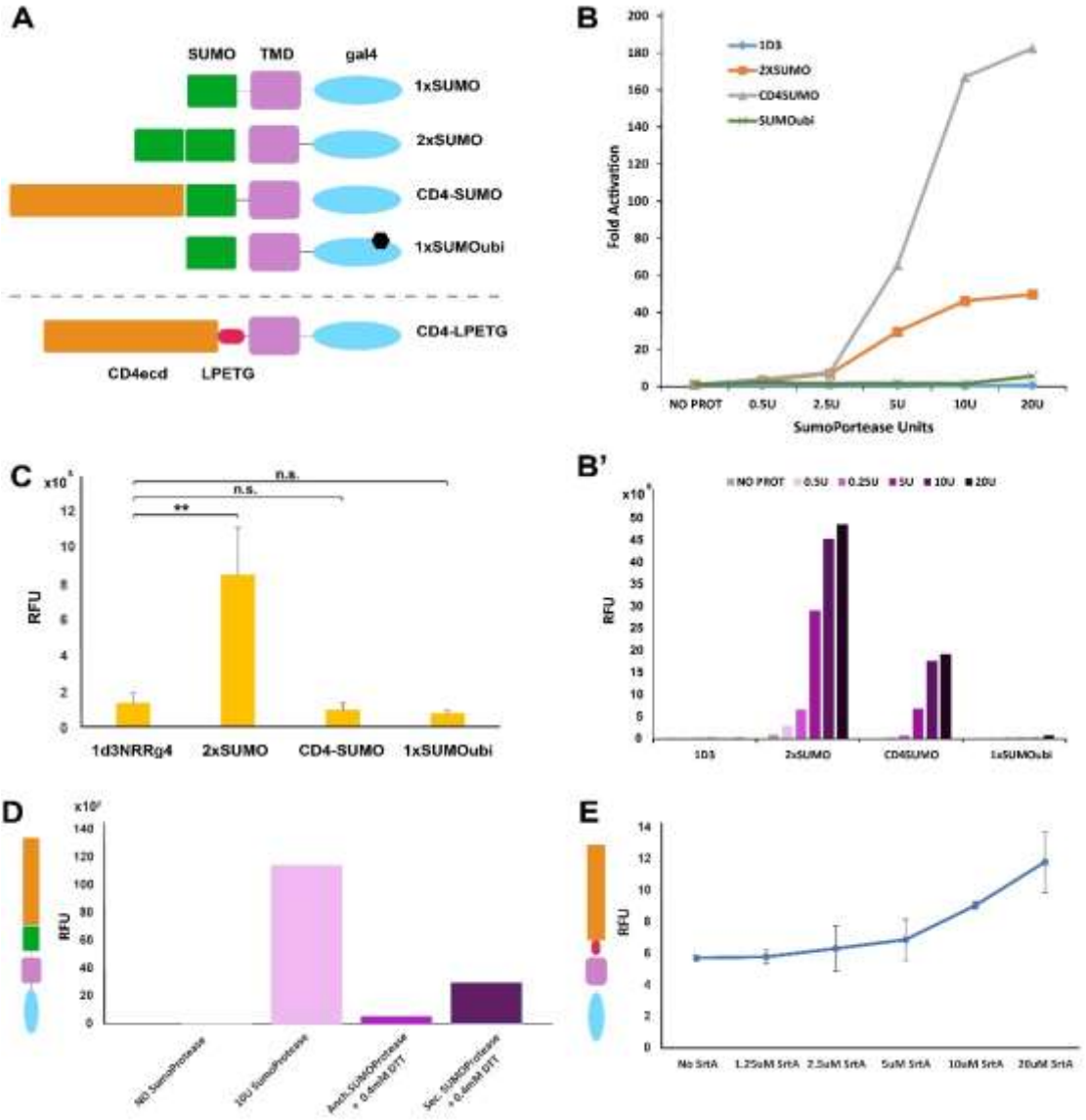

Figure 2.15. Synthetic receptor activation based on SUMO and Sortase A proteases. **(A)** Diagrams showing the addition of SUMO domain or small peptide, LPTEG, to Notch engineered receptor. **(B)** Serial dilutions of recombinant SUMO protease cleave with high efficiency in SUMO protein integrated into CD4SUMO receptor (20U=183-fold and 10U=167-fold) followed by 2xSUMO receptor (20U=49-fold and 10U=46.20-fold). **(B')** Relative fluorescent units (RFP) of the ligand dependent cleavage based on the amount of recombinant SUMO protease added. Note that 1xSUMO receptor has almost no detectable induction. **(C)** Relative fluorescent units of ligand independent activation. 2xSUMO receptor showed a background nine times higher than CD4SUMOreceptor (1d3=1.48 x 10^5, 2xSUMO=9.81 x 10^5, p-value=0.0062; CD4SUMO=1.05 x 10^5 p-value=0.340; 1xSUMOubi=0.82 x 10^5, p-value(1x)=0.035). **(D)** Addition of a reducing agent (Dithiothreitol (DTT)) slightly increases the induction dependent activity of CD4SUMO (anchored=500 RFU and secreted proteases=3000 RFU). **(E)** Serial dilutions of recombinant Sortease A protease cleave efficiently in CD4LPETG receptor (11.8 x 10^2 RFU). Abbreviation: relative fluorescent unit (RFU).

2.3.5. Control of the Receptor Expression by a Destabilizing Domain.

In our previous results, where we have performed different types of modification in distinct receptor domains, we found that receptors with the best fold induction not always correlated with a high induction level. Moreover, reducing the ligand independent activation to minimum levels is critical to increase the fold activation. Furthermore, to reduce the receptor lifetime and in consequence, the ligand independent activation, we engineered a new receptor. We fused the well-known destabilizing domain (DD), dihydrofolate reductase (DHFR) from *E. coli*, which is stabilized by the inhibitor trimethoprim (TMP) to the receptor ICD (Figure 2.16B) (Iwamoto et al. 2010; Cho et al. 2013). Then, the ICD is constantly degraded until the TMP addition to the cell culture medium. Therefore, we assumed that the level of ligand independent activation could be reduced, attaching DHFR sequence to our receptor. DHFR can be controlled in a dose dependent manner by TMP. We created three different receptors in which different versions of DHFRs (DHFR, 100IDHFR, and 100YDHFR) have been fussed to the ICD of the tetracycline control transactivator (tTA) (Figure 2.16A). These two versions of DHFR have mutations that compromise their enzymatic activity and being less efficient: 100iDHFR has a replacement to Isoleucine in aa number 100 and 100YDHFR has a change to Tyrosine in aa number 100 (Adams et al. 1991; Iwamoto et al. 2010). Because one of our main goals is being able to trace cell-cell interaction in mammalians (mice) using our TRACT system, we created a slightly different version of the receptor: the ECD, 1d3, has been replaced by hCAR (a single antibody domain from human continuous activation recognition), while the ICD, Gal4, has been replaced by the tetracycline transactivator protein (tTA), a well-known transcription factor broadly used in mice (tetracycline control expression systems). We used CD19 from human as a ligand, which will recognize the hCAR extracellular domain. For this set of experiments, we analyzed the overall intensity since the reporter expression is cytosolic, making it more complicated to segment the cells. To control the optimal receptor expression, increasing amount of TMP has been tested (data not shown), being 1mM of TMP the best tested concentration for signal-to-noise ratio. We did not observe a significant improvement in the percentage decrease in any of the DHFRs versions as well as for the overall intensity of the ligand dependent background (DHFR=115%; 100IDHFR=30%;

100YDOHFR=no reduction (Figure 2.16C). Although there was no improvement using these modifications of our TRACT system, we decided to move forward and test them in our TRACT system (see explanation in the next section *in vivo* Results).

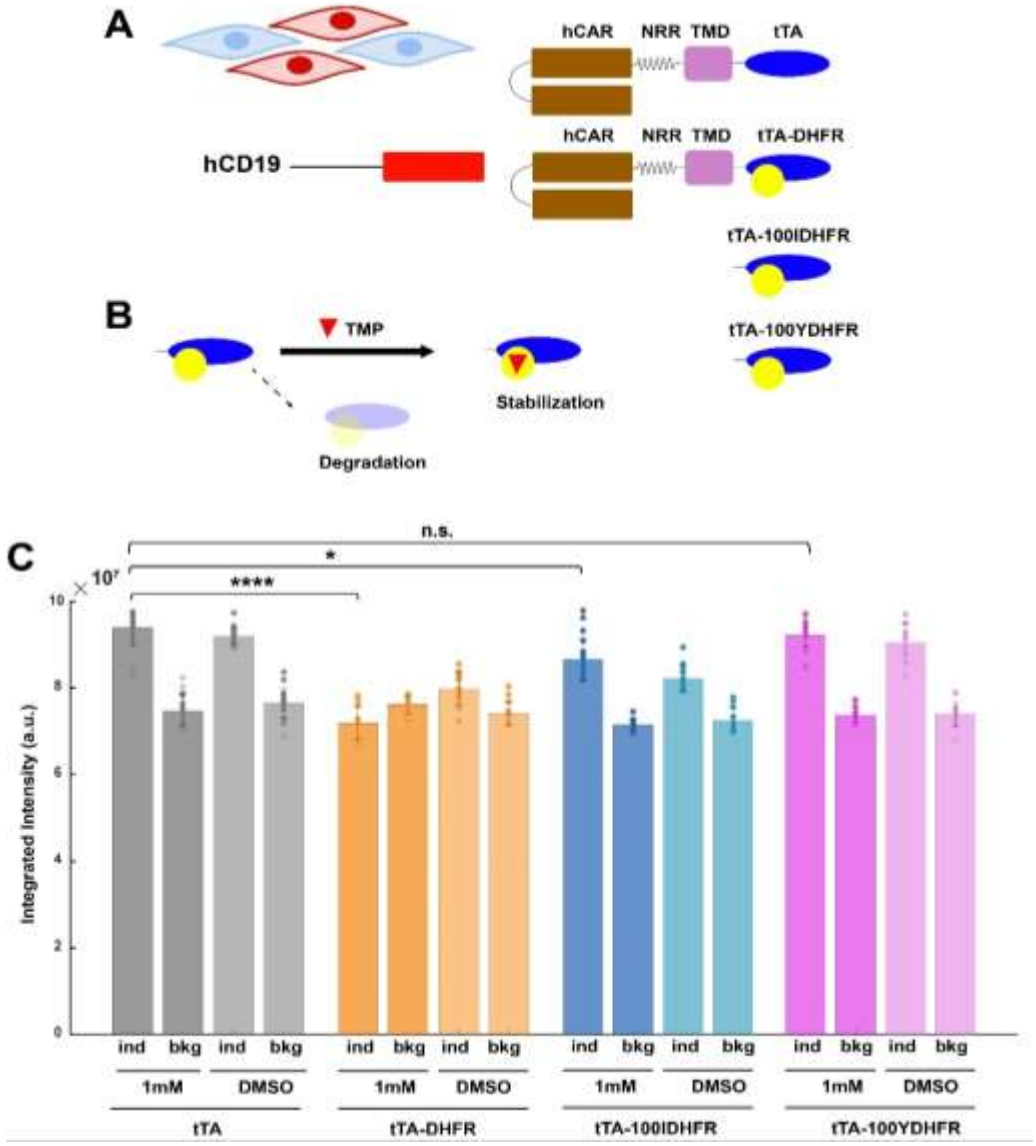

Figure 2.16. Capabilities to induce the reporter gene expression by cell-cell interaction of 1d3NRRG4 receptor couple to DD domain (DHFR). (A) *Top:* Diagram showing the cell-cell interaction experiment. *Button:* Diagrams showing a variant of 1d3NRRG4 where the ECD is replaced by hCAR and the ICD by the tTA. Also showing three modifications of the control receptor where the ICD is fused to three DHFR variants. **(B)** Diagram showing the DHFR mechanism and its inhibition by TMP. **(C)** The overall intensity of induction and background for the three DHFR variants and the control tTA. Note that significant differences were found when DHFR variant was compared to the control but no difference for the other two modifications (100I and 100Y) (DHFR=1.51 x 10^{-5}; 100IDHFR=0.027; 100YDHFR=0.076) (also see Table 7 from ANNEX2).

2.3.6. Strategies to TRACT system implementation in the Drosophila Nervous System.

2.3.6.1. Dihydrofolate Reductase (DHFR).

Similar to the Gal4/UAS system, the LexA/LexAop system has also been broadly used in *Drosophila* (Lai and Lee 2006). The combination of both systems in our TRACT technique allows us to trace more brain circuit. TRACT receptor with the LexA transcription factor as ICD had high levels of ligand independent background (tested in the laboratory by Aubrie de la Cruz, data not shown). Then, we decided to use the DHFR method in these transgenic flies to test if the level of ligand independent background can be reduced. To evaluate the efficiency of DHFR domain in TRACT system, we created the same TRACT receptor with the LexA transcription factor attached to two different modifications of the DHFR domain (DHFR7 and DHFR30), which would post-translationally degrade the receptor. We supplemented the adult flies' food with different TMP concentrations to fine-tune the amount of receptor expressed in the cells and reduce the background while allowing sufficient expression of the receptor to respond to ligand dependent activation. For that, adult flies were given *Drosophila* formula with increasing TMP concentrations (no TMP, 5mM TMP and 10mM TMP) for five days. After the treatment, they were dissected and imaged for reporter signal (GFP). Between these two versions of DHFR, the brains with DHFR30 had significantly lower background (Figure 2.17A and B). However, there was no detectable induction of GFP signal, even when the food was supplemented with 10mM of TMP (Figure 2.17B). On the other hand, brains expressing DHFR7 in two different insertion sites (P2 and P40) showed higher background than DHFR30 (Figure 2.17C and D). In summary, there was no difference between TMP and no TMP conditions due to a large amount of background in both cases that mask the induction of GFP signal. Therefore, similar to our *in vitro* experiments, the DHFR system does not help to implement the TRACT technique.

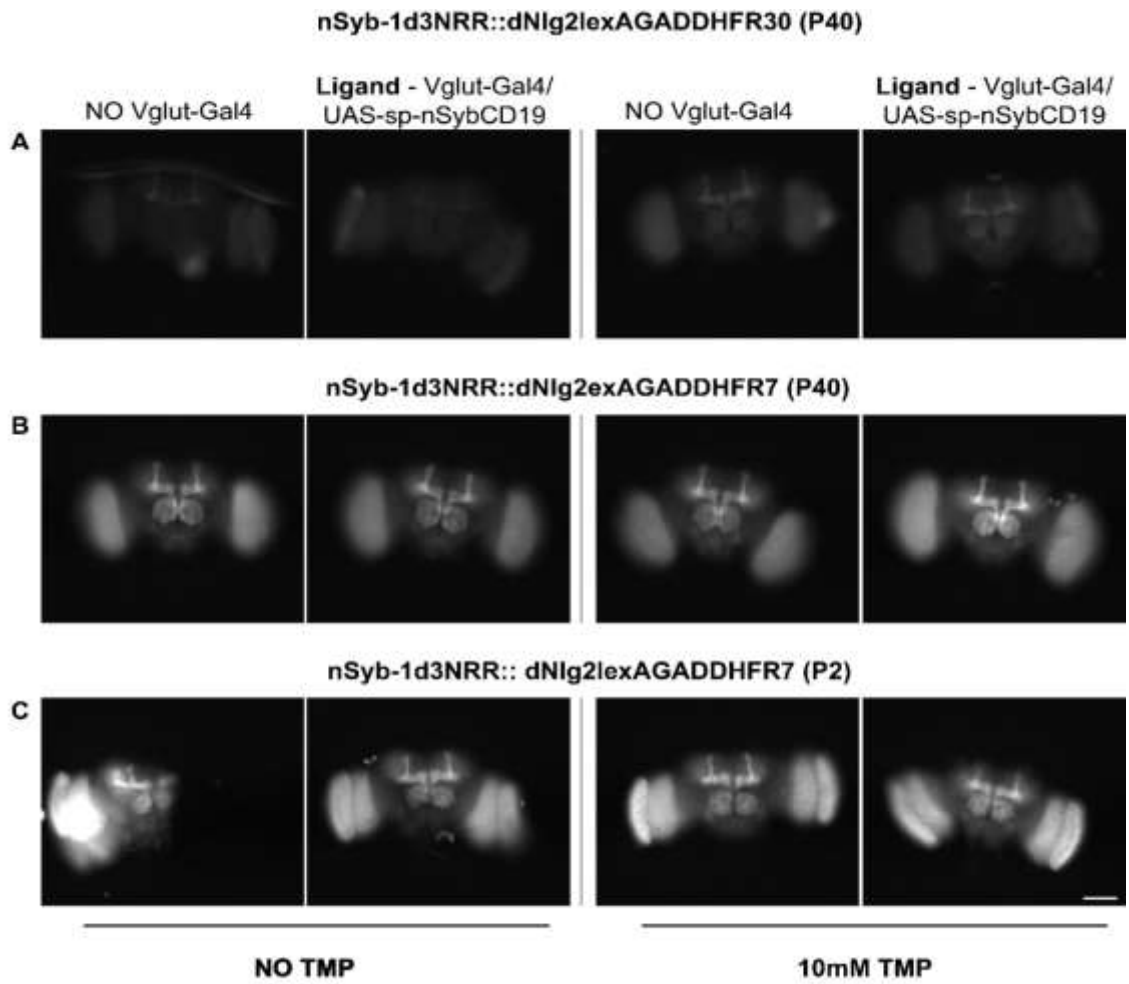

Figure 2.17. Evaluating the DHFR domain coupled to 1d3NRRlexA in *Drosophila*. For all the experiments, we used a pan-neural receptor based on nSyb-1d3NRR::dNlg2lexAGAD. **(A)** Flies expressing the receptor with a DHFR30 version at the P40 insertion site showing the lowest background (No-Vglut-Gal4) and the induction (ligand - Vglut-Gal4/UAS-sp-nSybCD19) without TMP left panel and with TMP right panel. Note that flies supplemented with food containing 10mM of TMP increases GFP signal, but no difference between background and control were detected. **(B)** DHFR7 version at the P40 insertion site showing the background (No-Vglut-Gal4) and the induction (Vglut-Gal4/UAS-sp-nSybCD19) without TMP left panel and with TMP right panel. No apparent differences were observed between no TMP and TMP. Note the high level of the background without TMP. **(C)** DHFR7 version at the P2 insertion site, where the transcription is more active, showing the background (No-Vglut-Gal4) and the induction (Vglut-Gal4/UAS-sp-nSybCD19) without TMP left panel and with TMP right panel**.** No obvious differences were observed between no TMP and TMP. Scale bar: 100µm.

2.3.6.2 Evaluation of the 1d3NRRHybG4 Receptor in the Drosophila Brain.

One of the candidate receptors obtained from our *in vitro* TMD modifications to be tested *in vivo* was the 1d3NRRHybG4 receptor (Figure 2.9). In our first TRACT version,

we always expressed the receptor all over the neurons' membrane without targeting it to the synapse. To enhance the receptor induction by localizing the receptor toward the synaptic cleft, we fused 1d3NRRG4 and 1d3NRRHybG4 receptors to the neuroligin postsynaptic proteins, which is important in synaptic formation and maintenance (Knight et al. 2011; Bang and Owczarek 2013). This neuroligin protein has been used to target exogenous proteins at synaptic sites, in cases such as GRASP or *in vivo* biotin, labelling intercellular contacts (iBlinc) without showing any detectable effect of endogenous synaptic markers (Kim et al. 2011; Yamagata and Sanes 2012; Desbois et al. 2015). Therefore, we included 260 aa residues of the intracellular domain of *Drosophila* neuroligin 2 (dnlg2) between TMD and Gal4 of 1d3NRRG4 and 1d3NRRHybG4 receptors. Then, we generated these new transgenic fly strains: nSyb-1d3NRR::dNlg2ICD::G4 and nSyb-1d3NRRHyb::dNlg2ICD::G4 with V5 tag in the ICD by site-specific insertion at the attP40 site to avoid insertion position effects. We also replaced the neuronal promoter *elav* (embryonic lethal abnormal visual system) with a pan-neuronal promoter in postmitotic neurons, neural Synaptobrevin (*nSyb*). We decided to use this driver because previous results from our laboratory showed that TRACT could only label the antennal lobe local interneurons (LNs) but not the projection neurons (PNs) when the receptor is under the control of elav promoter, and the ligand is expressed on all the olfactory sensory neurons (OSNs).

First, we tested the subcellular localization of the receptor, to confirm the effect of the dNlg2ICD trafficking the receptor at the postsynaptic site. For that, immunostaining against V5 tag was performed showing that nSyb-1d3NRR::G4 (receptor without neuroligin) accumulates in cell bodies and it is absent in the neuropil (area in the nervous system of *Drosophila* composed of axons, dendrites and glial cell) while most of the nSyb-1d3NRR::dNlg2ICD::G4 are expressed in the neurites (Huang 2017).

Any of the receptor variants (nSyb-1d3NRR::G4 and nSyb-1d3NRRHyb::dNlg2ICD::G4) with the reporter 5xUASCD4::tdGFP and the ligand transgene (LexAop-CD19::mCh), showed moderate GFP signals in the dorsal brain (white arrow) and the suboesophageal ganglions (red arrow) in the adult brain (Figure 2.18A and D) coming from the reporter line by itself. Moreover, nSyb-1d3NRRHyb::dNlg2ICD::G4 transgenic flies carrying the LexA driver (OR846b) and ligand

transgene showed no induction (Figure 2.18E). However, flies carrying nSyb-1d3NRR::dNlg2ICD::G4, 5xUAS-CD4::tdGDP and the ligand transgene (LexAop-CD19::mCh) showed strong GFP signal in the antennal mechanosensory motor center (AMMC) (arrowhead in Figure 2.18C), and several neurite arborizations from the antennal lobe neurons (arrow in Figure 2.18C), even without LexA driver to precisely drive the ligand expression (arrow in Figure 2.18B). This level of signal might be due to the basal expression of CD19 even without LexA driver. Moreover, transgenic flies no carrying the LexA driver but with the ligand transgene (LexAop-CD19::mCh) showed moderate GFP signals at the same level than nSyb-1d3NRR::G4 and nSyb-1d3NRRHyb::dNlg2ICD::G4 (Huang 2017). Induction of CD4::tdGFP was observed in neurons (arrow in Figure 2.18C) having the arborizations covered the whole antennal lobe and in AMMC (arrowhead in Figure 2.18C) when CD19::mCh was driven by Or83b promoter in OSNs. On the other hand, preliminary data of transgenic flies expressing 1d3NRRG4 with nlg2 under the control of nSyb showed the TRACT system's capability to trace neuronal circuits *Drosophila*. This TRACT implementation gave rise to the paper: *Tracing neuronal circuits in transgenic animals by transneuronal control of transcription (TRACT)* (Huang et al., 2017).

Figure 2.18. Targeting the 1d3NRRG4 and 1d3NRRHybG4 receptor at the synapse in *Drosophila*. (A) Background of nSyb-1d3NRR::G4 no targeted at the synaptic site of *Drosophila* adult brain. Moderate GFP signal is observed in the dorsal brain (white arrow) and the suboesophageal ganglions (red arrow). **(B)** Background of 1d3NRRG4 targeted at the synaptic site (nSyb-1d3NRR::dNlg2ICD::G4) of *Drosophila* adult brain. Note that the level of background is stronger than nSyb-1d3NRR::G4. Arrowhead indicates mechanosensory motor center AMMC and the arrow show neurite arborization from the antennal lobe. **(C)** Induction of 1d3NRRG4 targeted at the synaptic site (nSyb-1d3NRR::dNlg2ICD::G4) of *Drosophila* adult brain. Note that the induction is observed in the same areas that the background (arrowhead in AMMC, and arrow antennal lobe). **(D)** and **(E)** show the background and induction of nSyb-1d3NRRHyb::dNlg2ICD::G4 targeted at the synapse, respectively. **D** shows low GFP signal in the dorsal brain (white arrow) and the suboesophageal ganglions (red arrow). No induction at all was detected in **E**. Scale bar: 100 µm. Nc82: is a marker of the presynaptic active zone in *Drosophila*.

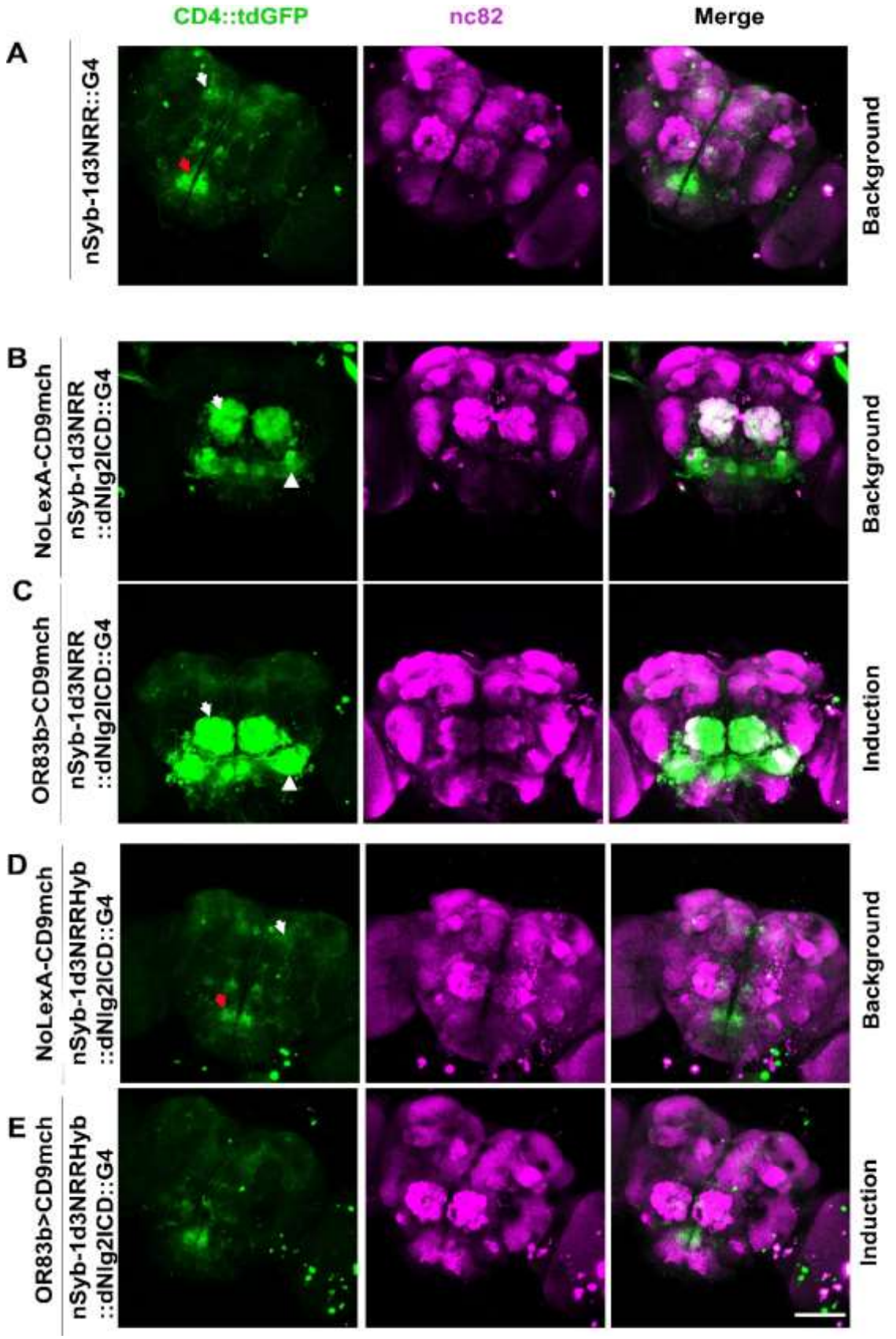
CD4::tdGFP
nc82
Merge
A
nSyb-1d3NRR::G4
Background
B
NoLexA-CD9mch
nSyb-1d3NRR
::dNlg2ICD::G4
Background
C
OR83b>CD9mch
nSyb-1d3NRR
::dNlg2ICD::G4
Induction
D
NoLexA-CD9mch
nSyb-1d3NRRHyb
::dNlg2ICD::G4
Background
E
OR83b>CD9mch
nSyb-1d3NRRHyb
::dNlg2ICD::G4
Induction

2.3.7. *Evaluation of the TRACT efficiency as a retrograde neuronal tracer.*

Above we showed an important improvement of our TRACT system by locating the ligand and receptor at the synapse. But until now, TRACT system has always been used to reveal neuronal circuit in the *Drosophila* brain in an anterograde manner, from presynaptic to postsynaptic neuron. There are currently several retrograded methods to analyze neuronal connections, as we mentioned in the Introduction of this Chapter. In the same way that most of the anterograde tracers, none of these retrograde methods enable long-term genetic modification of interaction between cells. Therefore, TRACT technique brings an excellent opportunity to label retrogradely neuronal connections for the long term. For that, we engineered the TRACT components to become a retrograde genetic tracing technique based on the neuromuscular junctions (NMJ). They are chemical synapses that connect the terminal axon of a motor neuron (presynaptic) to a motor endplate of skeletal fiber (postsynaptic). One of the main features of this type of synapses is the invagination of the sarcolemma at the junction, which increase the surface area facing the synaptic cleft. This type of synapse is ideal for evaluating TRACT system efficiency as a retrograde neuronal tracer because of the extensive surface contact between the axon terminal and the muscle plate.

For the first approach, we expressed the ligand under the control of the α-myosin heavy chain (α-MHC) (MHC-CD19mch) and the 1d3NRRG4 receptor under the pan-neuronal driver (Synaptobrevin, nSyb-1d3NRR::G4). No signal at all was detected either at the axon terminal (neuromuscular junction) or in the ventral nerve cord of *Drosophila* (data not shown). Next, we decided to express the receptor under the control of several motoneurons drivers, allowing us to know the pattern of any signal coming from the ligand dependent or independent activation. Flies carrying any of these drivers did not show any signal from either the induction or the background. In these two approaches, the ligand was expressed all over the membrane of the muscles without targeting it to the synapse. Therefore, we hypothesized that there might be not enough ligand at the synaptic cleft. Moreover, our previous results targeting the receptor to the presynaptic sites increase the TRACT system's sensitivity. In this case, we fused the ligand CD19mch with a presynaptic protein called Neurexin1 (Nrx1) to target the ligand to the pre-synaptic sites. Neurexin1 is the type I transmembrane ligand protein of neuroligin at the

synaptic sites (Knight et al. 2011; Bang and Owczarek 2013). We replaced the Nrx1 extracellular part with the extracellular domain of CD19 (CD19::Nrx1OLLAS). Flies carrying the receptor 1d3NRRG4, the reporter 5XUASCD4::tdGFP and the ligand transgene (CD19::Nrnx1OLLAS) showed very low level of ligand independent background in the ventral nerve cord (VNC) (Figure 2.19B). The VNC contains ascending and descending neurons that receive and integrate sensory information which is involved in generating locomotor actions of *Drosophila* (Mendes et al. 2013; Bidaye et al. 2014; Mamiya et al. 2018). The induction in flies carrying all transgenes and MHC driver showed very few induced axon terminals in Torso muscles (Figure 2.19E and F) and Leg muscles (Figure 2.19G) compared to the number of neurons in the VNC (Figure 2.19D). Although we observed an improvement on labelling axon terminals and neurons in flies carrying the receptor and ligand under the control of MHC driver, many more axon terminals and neurons should be labelled.

We continue working on the improvement of the retrograde TRACT. We changed the circuit and approach to evaluate the retrograde tracing. In this case, the receptor is expressed pan-neuronally at the presynaptic sites, and the ligand is at the postsynaptic site of a specific neuronal population such as the asymmetrical body (driver R72A10). To target the receptor at the presynaptic sites, we fused it to Cacophony Calcium channel α1 subunit in *Drosophila* (CAC) (Kawasaki et al. 2004). It is known that this channel is located at the presynaptic active zones. Moreover, to target the ligand to the postsynaptic site, we fused it to telencephalin (TLN; lexAop-syn21CD19TLNp10) a neuronal surface glycoprotein (intercellular adhesion molecule 5 (ICAM-5)) (Yoshihara et al. 1994; Yoshihara and Mori 1994). TLN is located at the soma-dendritic membrane but not at the axonal membrane (Benson et al. 1998; Mitsui et al. 2005) in neurons within the telencephalon (Mori et al. 1987; Oka et al. 1990). Unfortunately, any GFP induction signal was detected (data from Ting-Hao and Aubrie, Carlos Lois laboratory).

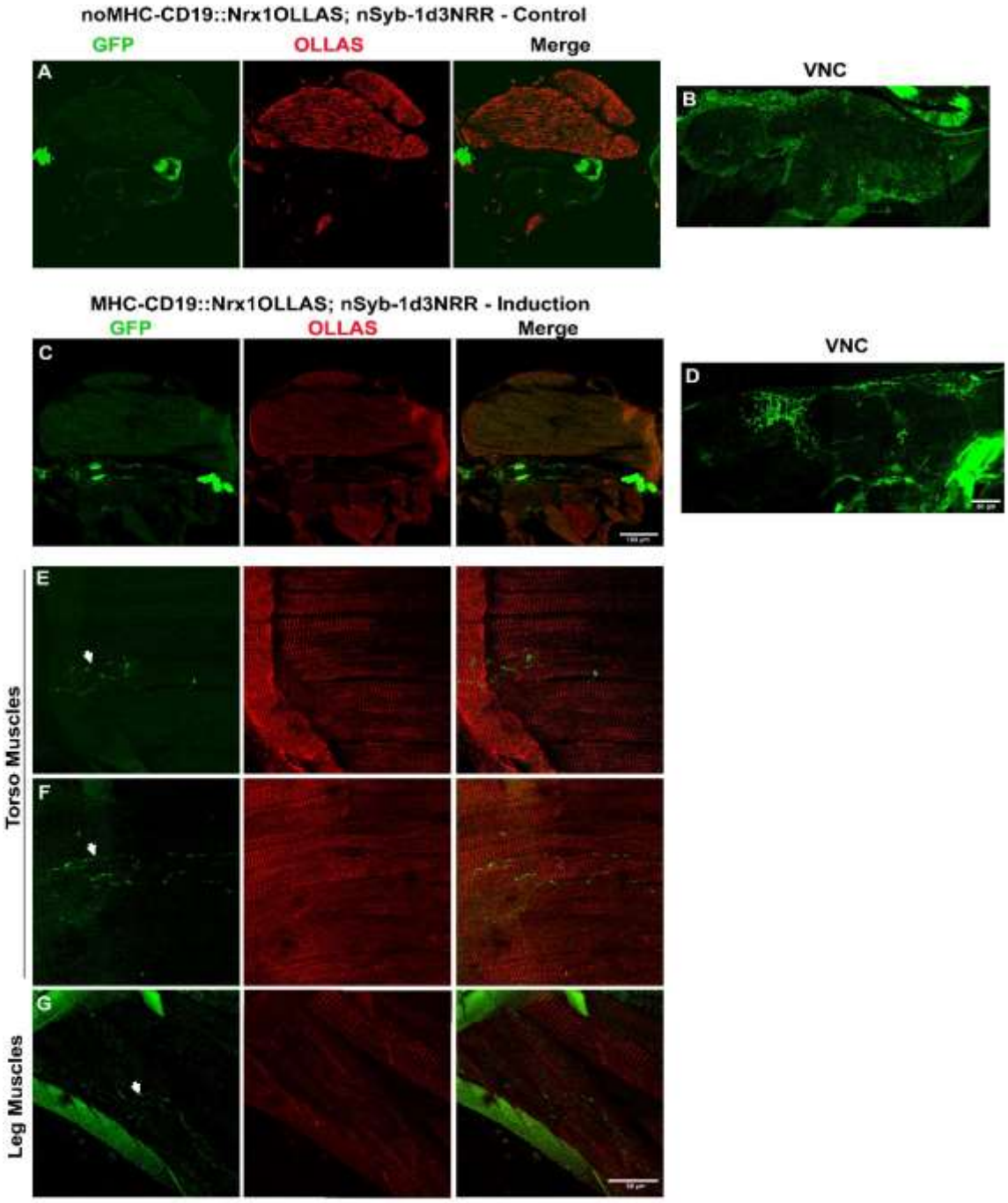

Figure 2.19. Monitoring neuron-muscle connections in the *Drosophila* nervous system. **(A)** Sagittal section of control transgenic fly carrying ligand transgene, receptor transgene and reporter (NOMHC-CD19::Nrx1OLLAS; nSyb-1d3NRRG4). Note the weak GFP signal from ligand independent activation **(B)** compared to **(D)** where the GFP signal is stronger in flies MHC-CD19::nrx1OLLAS; Syb-1d3NRRG4 (induction). **(E)** and **(F)** show axon terminals from induced neurons in the Torso muscles (sagittal section). Same GFP signal was detected in neurons on the leg **(G)** in a sagittal section from *Drosophila*. A and C 10x magnification. Scale bar in C (100µm) for A and C. Scale bar in D (50 µm) for B and D. Scale bar in G (50 µm) is for E, F and G.

Genotypes of flies analyzed in the figures:

FIGURE 2.17

2.17A: nSyb-nlgSNTlexAGADDHFR30(P40)/**Cyo**; 13xlexAopCD4tdGFP(VK33)/ UAS-sp-nSybCD19(P2)

nSyb-nlgSNTlexAGADDHFR30(P40)/**VglutGal4**; 13xlexAopCD4tdGFP(VK33)/ UAS-sp-nSybCD19(P2)

2.17B: nSyb-nlgSNTlexAGADDHFR7(P40)/ **Cyo**; 13xlexAopCD4tdGFP(VK33)/ UAS-sp-nSybCD19(P2)

nSyb-nlgSNTlexAGADDHFR7(P40)/ **VglutGal4**; 13xlexAopCD4tdGFP(VK33)/ UAS-sp-nSybCD19(P2)

2.17C: 13xlexAopCD4tdGFP/**Cyo**; nSyb-nlgSNTlexAGADDHFR7(P2)/ UAS-sp-nSybCD19(P2)

13xlexAopCD4tdGFP/**VglutGal4**; nSyb-nlgSNTlexAGADDHFR7(P2)/ UAS-sp-nSybCD19(P2)

FIGURE 2.18

2.18A: nSyb-1d3NRR::G4V5/5XUAS-CD4::tdGFP; LexAop-CD19mch /+

2.18B: nSyb-1d3NRR:: dNlg2ICD::G4V5/5XUAS-CD4::tdGFP; LexAop-CD19mch /+

2.18C: nSyb-1d3NRR::dNlg2ICD::G4V5/5XUAS-CD4::tdGFP;LexAop-CD19mch/0r83b-LexA::VP16

2.18D: nSyb-1d3NRRHyb:: dNlg2ICD::G4V5/5XUAS-CD4::tdGFP; LexAop-CD19mch /+

2.18E: nSyb-1d3NRRHyb:: dNlg2ICD::G4V5/5XUAS-CD4::tdGFP; LexAop-CD19mch/0r83b-LexA::VP16

FIGURE 2.19

2.19 A and B: NOMHC-CD19::Nrxn1OLLAS; nSyb-1d3NRR/5XUAS-CD4::tdGFP -Control

2.19 C-G: MHC-CD19::Nrxn1OLLAS; nSyb-1d3NRR/5XUAS-CD4::tdGFP -Induction

DISCUSSION

Como mencionamos en la introducción, la interacción entre células es esencial para el desarrollo, así como para el establecimiento y la función de los organismos multicelulares. Por ejemplo, comprender cómo están conectadas las neuronas es uno de los principales desafíos de la neurociencia moderna. Nuestro laboratorio ha desarrollado una técnica novedosa para el trazado neuronal, control transneuronal de la transcripción (TRACT), basada en la proteólisis intramembrana inducida por ligandos de la vía de señalización Notch. Dicho sistema se ha desarrolladp para revelar conexiones monosinápticas que surgen hacia o desde una neurona de interés marcada genéticamente. En la última década, varios trabajos han utilizado los mecanismos moleculares de la vía de señalización Notch para detectar interacciones celulares *in vitro* e *in vivo*, incluyendo nuestro sistema TRACT que se ha utilizado para conocer interacciones celulares entre neuronas y células gliales, y neurona-neurona (Huang et al. 2016, 2017). Por ejemplo, la expresión del ligando en células gliales bajo el promotor alrm induce la transcripción en neuronas en todo el cerebro de *Drosophila* y el cordón nervioso ventral (VNC) (Huang et al. 2016). Además, el sistema TRACT también se ha utilizado para confirmar la conectividad entre las neuronas receptoras olfativas (ORN) y las neuronas de proyección (PN) en el sistema olfatorio de *Drosophila* y para descubrir nuevas conexiones en el circuito circadiano de Drosophila (Huang et al.2017).

Las principales ventajas de utilizar el sistema TRACT como trazador neuronal son las siguientes: **(i)** está totalmente codificado genéticamente permitiendo su uso con alta reproducibilidad en animales transgénicos; **(ii)** es un sistema simple porque solo requiere tres componentes: un ligando, un receptor y un reportero; **(iii)** se puede aplicar en cualquier especie donde la transgénesis sea posible, especialmente en *Drosophila* (St Johnston 2002; Bellen et al. 2010), ratones (Anderson e Ingham 2003; Kile y Hilton 2005) y peces cebra (Fetcho y Liu 1998 ; Patton y Zon 2001); **(iv)** el ligando y el receptor se pueden expresar bajo promotores específicos para ser expresados selectivamente por tipos de células definidos e iniciar la señalización de poblaciones neuronales específicas; **(v)** lo que es más importante, no es tóxico, por lo que se puede utilizar para estudiar neuronas *in vivo*; **(vi)** puede diseñarse para trazar circuitos anterógradamente y retrógradamente localizando el ligando y el receptor en una dirección neuronal presináptica a postsináptica o en dirección opuesta; **(vii)** se puede combinar con

diferentes técnicas como tecnicas electrofisiológicas, imágenes en vivo, optogenética o imágenes de calcio para monitorear la actividad neuronal y estudiar neuronas conectadas sinápticamente *in vivo* o tejido fijo combinándolo con microscopía óptica o electrónica; **(vii)** marcar las neuronas conectadas por completo (dendritas, cuerpos celulares y axones), lo que permite reconstrucciones completas del circuito; **(ix)** también se puede utilizar para manipular genéticamente las neuronas conectadas sinápticamente para estudiar su función. Por ejemplo, cuando se usa Gal4, lexA o tTA como dominios intracelulares, el sistema podría diseñarse para manipular la función neuronal induciendo la transcripción de ARN de interferencia (Mohr et al. 2014), sensores de calcio codificados genéticamente (Chen et al. 2013), optogenética (Yizhar et al. 2011; Kim et al. 2017) o herramientas farmacogenéticas (Urban y Roth 2015). De manera similar, al usar Cre o FLP en el ICD del receptor, TRACT puede permitir la deleción selectiva de genes flanqueados por señales loxP o FRT.

A pesar de las ventajas de este método de rastreo neuronal, hemos observado que el receptor 1d3NRRG4 todavía tiene un alto nivel de activación independiente del ligando *in vitro* e *in vivo*. Por ejemplo, cuando el receptor se expresa bajo el promotor del sistema visual anormal letal embrionario (elav) y el ligando en las ORN, la actividad independiente del ligando es muy fuerte en algunas áreas del cerebro de *Drosophila* no relacionadas, como el “mushroom body”. Además, los reporteros usados in vivo como 10xUAS-myr:: GFP o 5xUAS-CD4::tdGFP producen un alto nivel de fondo cuando no hay receptor TRACT en las moscas (datos no publicados de Ting-Hao). Estos resultados indican que la señal independiente de ligando es una combinación de la actividad del receptor independiente del ligando y la sensibilidad de los reporteros.

Por tanto, la actividad independiente del ligando observado en algún circuito neuronal, donde se utilizó el sistema TRACT, puede ser una consecuencia de varios problemas. **(i)** El receptor 1d3NRRG4 no está correctamente plegado debido a la interacción entre un dominio quimérico como 1d3 y el dominio de la región reguladora negativa (NRR); **(ii)** se ha sugerido que la actividad independiente del ligando de los receptores de Notch es impulsada por su endocitosis de la membrana plasmática (Palmer y Deng 2015). Después de la endocitosis, el receptor de Notch puede reciclarse de nuevo a la membrana o transportarse a los lisosomas y cuerpos multivesiculares

(MVB). Allí, el dominio extracelular de Notch es cortado por la proteasa lisosómica que desencadena la escisión por la γ-secretasa y la liberación del ICD que induce la expresión de genes indicadores; **(iii)** además, varios estudios han demostrado que las mutaciones en NRR que son responsables de T-ALL, generan desestabilización del dominio de heterodimerización (HD) que induce la activación independiente del ligando del receptor Notch (Malecki et al.2006; Sulis et al.2008) . Para que el sistema TRACT sea una técnica de neurotrazado fiable, es esencial reducir y minimizar la activación independiente del ligando del receptor Notch. Si no se mejora, podría generar falsos positivos o efectos externos cuando se utilice para expresar ARN de interferencia (ARNi) o proteínas mutantes, limitando la aplicación de TRACT *in vivo*. En consecuencia, para reducir la actividad independiente del ligando y mejorar la relación entre la inducción y el "background", hemos diseñado diferentes modificaciones en los dominios del receptor basados en nuestro receptor original de TRACT (1d3NRRG4).

Se ha sugerido que la longitud del dominio transmembrana puede afectar la localización de las proteínas en la membrana plasmática, donde las proteínas con un TMD largo tienden a ubicarse mejor en la membrana plasmática (Sharpe et al. 2010; Singh y Mittal 2016). Basándonos en el receptor 1d3NRRG4, modificamos la longitud del TMD (de 23 aa de CD4jTMD a 24 y 27 aminoácidos). Las modificaciones del receptor con un pequeño aumento en la longitud de TMD (23 a 24 aa) aumentaron significativamente el ratio de activación, pero la activación dependiente del ligando fue menor que hNotch1TMD. Por lo tanto, los receptores con los TMD más largos podrían mostrarse mejor en la membrana plasmática, ya que el nivel de activación independiente del ligando es menor que el de hNotch1 TMD, pero también reduce la inducción. Además, el receptor con un TMD de 27 aa compuesto por los 23 aa del TMD de CD4 y los últimos 5 aa del TMD de Notch conteniendo el sitio de escisión S3 mostró la mejor relación inducción-background con un ratio de activación casi tres veces mayor que 1d3NRRG4.

Las mutaciones desestabilizadoras en el dominio de heterodimerización inducen la activación independiente del ligando del receptor Notch (Weng et al. 2004; Mansour et al. 2006; Chiang et al. 2016; McCarter et al. 2018). Las modificaciones del 1d3NRRG4 al reemplazar el NRR con S1LO (bucle de salida S1) y dimerizar su dominio extracelular con un dominio de cremallera de leucina reducen significativamente la activación

independiente y dependiente del ligando, sin mostrar ninguna mejora para la relación inducción-background. Como informa Gordon et al., (2007), estas modificaciones pueden ser un enfoque excelente para bloquear la señalización independiente del ligando de las mutaciones NRR responsables de T-ALL. El dominio hNotch2 NRR es más estable y resistente a mutaciones que pueden inducir la activación constitutiva de hNotch1NRR que el hNotch1 NRR. Se requiere más fuerza para desenmascarar el sitio de escisión S2 en hNotch2 NRR que hNotch1 NRR (Stephenson y Avis 2012). Cuando reemplazamos el dominio NRR por S1LO y el TMD de hNotch2, los niveles de background e inducibilidad fueron similares a 1d3S1LO de hNotch1 sin observar ninguna mejora (Huang 2017).

La interacción entre un dominio sintético diseñado y NRR en el dominio extracelular de 1d3NRRG4 puede causar una inducción independiente del ligando al plegarse mal la proteína. Morsut et al., (2016) demostraron que las repeticiones EGF adicionales ubicadas en el extremo N-terminal de la NRR en un receptor sintético (Synthetic Notch, synNotch) reducen su actividad independiente del ligando. Siguiendo la misma estrategia, también agregamos diferentes números de repeticiones de EGF (30-36aa, 33-36aa y solo 36aa) en el extremo N-terminal de la región NRR, mostrando una reducción del background y un aumento en la actividad dependiente del ligando para el receptor que lleva una repetición de EGF (36º). Además, para mejorar la relación inducción-background, probamos nuevas estrategias mediante la introducción de modificaciones adicionales en el dominio extracelular como agregar proteína SUMO en el extremo N-terminal del dominio NRR o “snorkelling” el jTMD. Ambas modificaciones del dominio extracelular no lograron mejorar la relación entre la activación dependiente e independiente de ligando. Por lo tanto, el background o activación independiente de ligando es independiente de la interacción entre un dominio de unión de ligando sintético y la región reguladora negativa de Notch (NRR).

El sistema Split Gal4 se ha utilizado ampliamente para mapear circuitos cerebrales y controlar la expresión de transgenes en espacio y tiempo en *C.elegans* y *Drosophila* (Luan et al.2006; Pfeiffer et al.2010; Dolan et al.2017; Wang et al.2018). Con este sistema, la actividad de Gal4 se puede restringir a una población de neuronas en la que se requieren dos promotores para expresar el dominio de unión al ADN y el dominio

de activación para activar Gal4 (Luan et al. 2006; Pfeiffer et al. 2010). Por lo tanto, los dos componentes se co-expresan solo en las células donde los dos promotores están activos. Aplicando la lógica del sistema Split Gal4 a la técnica TRACT, dos receptores (uno con el DBD de Gal4 como dominio intracelular y un segundo receptor que tiene el dominio de activación (AD) de Gal4) son necesarios para activar el receptor de TRACT. Por lo tanto, desencadenar cualquier activación independiente de ligando será más complicado que en los receptores 1d3NRRG4 porque al menos dos receptores complementarios deben escindirse para inducir la activación de la señalización. Nuestros resultados mostraron una aparente reducción en la escisión independiente del ligando. Desafortunadamente, la inducción se redujo, lo que llevó a la mitad la activación de los receptores 1d3NRRG4, dependiendo del porcentaje de células transfectadas con DBD y AD.

Se ha demostrado que la actividad independiente del ligando de los receptores Notch es causada por su endocitosis de la membrana plasmática (Palmer y Deng 2015). Una vez que el receptor Notch es internalizado por endocitosis, puede reciclarse de nuevo a la membrana o transportarse a los lisosomas y cuerpos multivesiculares (MVB). Luego, el ECD de Notch es escindido por la proteasa lisosomal que desencadena la escisión por la γ-secretasa y libera el ICD. Debido a que nuestros receptores sintéticos se basan en la señalización Notch, unimos la pequeña proteína ubiquitina al ICD del receptor para evitar su transporte a los lisosomas o MVB, y por lo tanto, se evita el background procedente de la escisión de la γ-secretasa en los lisosomas. El receptor 1xSUMOubi mostró un nivel de activación independiente de ligando muy bajo (casi no detectable), pero no hubo inducción en absoluto. Observamos resultados similares cuando se unió un motivo ubi al dominio ICD del receptor 1d3NRRG4 (datos no mostrados).

La enzima dihidrofolato reductasa (DHFR) se ha utilizado ampliamente como una herramienta para el control temporal y espacial de la expresión génica para comprender cómo se desarrollan y funcionan los circuitos neuronales en ratones, *Drosophila* o gusanos. En *Drosophila*, existen herramientas poderosas como los sistemas de expresión bipartita para controlar la expresión génica de forma selectiva y tener control temporal sobre varios factores de transcripción como Gal4, QF y LexA. Además, los sistemas de

expresión inducible dependientes de la temperatura se han diseñado utilizando un promotor inducible por calor para un gen diana (Lis et al. 1983), así como factores de transcripción sensibles a la temperatura (Gal80ts) que inhiben la expresión del gen Gal4 a bajas temperaturas (18°C), pero no una temperatura alta (29°C) (McGuire et al. 2003). Siguiendo una estrategia similar, se ha desarrollado un sistema químicamente inducible basado en DHFR en *Drosophila* (Sethi y Wang 2017), donde la expresión génica se controla en etapas postraduccionales, similar al utilizado para controlar proteínas diana en ratones y gusanos (Iwamoto et al. 2010; Cho et al. 2013; Sando et al. 2013). Una de las ventajas de este sistema es que DHFR puede ser inhibido por trimetoprima (TMP) dependiente de la dosis para controlar la cantidad de proteínas en la célula, lo que lo hace realmente útil para el sistema TRACT. Además, TMP no requiere dimerización con otra proteína para ser activa. Este inhibidor tiene muy pocos efectos fuera del objetivo en mamíferos, inhibiendo *E. coli* DHFR (ecDHFR) mucho más fuertemente que el DHFR endógeno de mamífero y controla la estabilidad de las proteínas en el sistema nervioso central, respectivamente (Schrader et al. 2010). Los receptores del sistema TRACT que llevan diferentes variantes de DHFR en su dominio intracelular no mostraron ninguna mejora en el nivel de escisión independiente del ligando *in vivo* o *in vitro*. Las células que expresan la variante WT-DHFR de *E.coli* no mostraron ningún nivel de inducción indicando una fuerte eficiencia de degradación. Con base a estudios anteriores, también se probaron otras dos variantes de WT-DHFR (100I y 100Y) (Adams et al. 1991; Iwamoto et al. 2010; Cho et al. 2013). Se sabe que la actividad enzimática de estas variantes está comprometida para reducir la eficiencia de degradación. Ambas variantes presentaron niveles similares de intensidad en comparación con el control (hCARNRRtTADHFR) sin mostrar ninguna mejoría.

El sistema TRACT se basa en la vía de señalización Notch. La activación del receptor Notch necesita la acción de dos proteasas ubicadas en la membrana plasmática. Las proteasas de ADAM escinden el sitio S2 dentro del dominio NRR y la γ-secretasa escinde el sitio S3 en el dominio transmembrana para liberar el ICD de la membrana plasmática. Para reducir la activación de la escisión independiente del ligando del sitio S2, reemplazamos el dominio NRR por la proteína SUMO o el motivo LXPTG que se reconocen por las proteasas SUMO y Sortease A, respectivamente. En este

caso, las proteasas actúan como ligando en la célula emisora, evitando la inducción del receptor antes de exponerse al ligando. Nuestros resultados solo mostraron un rango razonable para la relación inducción-background cuando el receptor sintético (CD4SUMO) se induce mediante la adición de proteasas recombinantes en el celular, pero no se detectó inducción en absoluto cuando las enzimas se secretaron o anclaron a la membrana plasmática.

Uno de los mejores receptores sintéticos de TRACT (1d3NRRHybG4) con una mejor relación inducción-background *in vitro* se utilizó para evaluar la eficacia de la técnica TRACT en el sistema olfativo de *Drosophila*. Aunque 1d3NRRHybG4 mostró un mejor ratio de activación con una activación independiente del ligando mucho menor que 1d3NRRG4, este receptor no mostró inducción *in vivo*. Una de las razones por las que este receptor no mostró ninguna activación dependiente de ligando detectable podría ser el promotor específico que controla su expresión (*nSyb*). Este promotor neuronal puede que no sea lo suficiente fuerte para producir suficientes moléculas del receptor. Este problema podría resolverse expresando el receptor bajo el control de un promotor pan-neuronal más fuerte como *elav*. Sin embargo, utilizando *nSyb* y agregando un péptido señal *neuroligin*, nlg2, al receptor para dirigirlo al sitio postsináptico, el sistema TRACT mejoró la relación entre la inducción y el background y su eficiencia para conocer la red neuronal en el cerebro de *Drosophila* (Huang et al. al.2017). Sugiere que la localización del ligando y el receptor en las sinapsis es más importante para mejorar la activación de TRACT que aumentar la expresión de los receptores.

Además, la versatilidad del sistema TRACT tolera cambiar la localización del ligando y el receptor para usar la misma técnica como trazador retrógrado. Por lo tanto, TRACT se está implementando para convertirse en una técnica de rastreo genético retrógrado. Nuestros resultados donde el ligando está expresado en el sitio presináptico de las sinapsis músculo-neurona y el receptor se expresaba panneuronalmente, marcaron pocos terminales axónicos en comparación con los resultados esperados. Todos los axones de las motoneuronas que inervan los músculos debieran estar marcados. Además, en la segunda estrategia en la que el ligando se expresa en el sitio postsináptico de una población neuronal específica, como el cuerpo asimétrico, no

mostró ninguna inducción (datos no publicados de Aubrie y Ting-Hao). En este caso, el sistema TRACT retrógrado no funcionó con estas últimas modificaciones, probablemente porque el factor de transcripción Gal4 no se transporta de manera eficiente y la cantidad de ligando puede no ser suficiente. El uso de un promotor más fuerte para el ligando como R53D12-lexA en el cuerpo elipsoide podría aumentar la eficiencia de la inducción retrógrada.

El cuerpo elipsoide de *Drosophila* es una subestructura compleja central involucrada en funciones de integración sensorial y coordinación motora. Debido a que la combinación de modificaciones previas no funcionó, nos preguntamos si el receptor retrógrado (en el sitio presináptico) no se muestra correctamente en la superficie celular. En este caso, podríamos utilizar el ligando retrógrado (en el sitio postsináptico) para activar un receptor anterógrado. Hemos encontrado que el receptor anterógrado no está localizado al 100% en el sitio postsináptico. Para abordar esta hipótesis, utilizamos el receptor anterógrado que se ha utilizado en el experimento anterior (nSyb-nlgn1d3NRRG4) y el ligando retrógrado (lexAop-syn21CD19TLNp10). En este caso, se detectó algún nivel de inducción, por lo que el ligando retrógrado funcionó, lo que sugiere que el receptor retrógrado no está funcionando correctamente. Para asegurarnos de que el sistema TRACT funcione retrógradamente, lo probaremos en el circuito neuronal entre las neuronas de proyección y el (MB), conexión ”mushroom body” que son más especializadas, directas y conocidas en el cerebro de *Drosophila*.

Podemos anticipar que el receptor TRACT podría rastrear neuronas de tercer orden que combinan receptores con dominios de unión de ligandos diferentes y otros dos ligandos, de manera anterógrada. La neurona de segundo orden expresará el receptor en el sitio postsináptico que será reconocido por el ligando mCD19mCherry localizado en el sitio presináptico de la neurona de primer orden. El dominio intracelular de este receptor (Gal4) se trasladará al núcleo e inducirá la expresión de GFP y un segundo ligando (gp120), que se dirigirá al sitio presináptico de la neurona de segundo orden. Este ligando activará el receptor CD4NRRQF en el sitio postsináptico de la neurona de tercer orden. El dominio intracelular (QF) se trasladará al núcleo y se unirá a QUAS activando la transcripción de proteína fluorescente como mTurquoise.

Además, TRACT también podría ser utilizado para bloquear o anular genes durante el desarrollo y la invasión del cáncer durante la metástasis al reemplazar el ICD del receptor con recombinasas como Cre, FLP que inician la expresión de ARNi.

CONCLUSIONS

After performing several modifications of different domains of the TRACT receptor, localize the ligand and the receptor towards the synaptic cleft, as well as assess the capacity of the TRACT system as a retrograde neuronal tracer, we have reached the following conclusions:

1. The addition of the EGF motif 36 between the Notch negative regulatory region and the single chain antibody domain (SCAD; 1d3) improves the signal-to-noise ratio by 7.91-fold activation, showing a slight decrease in the ligand independent activity.
2. Switching the NRR by S1LO domain, and snorkelling the juxtatransmembrane (jTMD) reduces the background but does not improve the signal-to-noise ratio.
3. Adding the leucine zipper domain between the NRR and the 1d3 extracellular domain reduces the background bringing the fold activation to similar levels as the control receptor (1d3NRRG4).
4. Changing the SCAD by CD4 glycoprotein does not show any improvement in the signal-to-noise ratio, as well as the location of the SUMO protein between CD4 and NRR domain.
5. The transmembrane domain (TMD) modification of the 1d3NRRHybG4 receptor, shows a fold activation almost three times higher than the control receptor 1d3NRRG4.
6. Binding intracellular domain by leucine zipper of two 1d3NRRG4 receptors shows an increase of 10 points for the fold activation.
7. Considering the results of all receptor modifications, we validated the 1d3NRRHybG4 and 1d3NRRDHFR receptors in the *Drosophila* olfactory system. The transgenic flies carrying 1d3NRRHybG4 receptor do not show any GFP signal. However, both DHFR transgenic flies showed high ligand independent activation levels, making it impossible to distinguish the ligand dependent activation.
8. Ligand and receptor localization at the pre- and postsynaptic site, respectively, shows a significant improvement of the TRACT technique to reveal neuronal circuits in the *Drosophila* brain.
9. Retrograde TRACT technique is not efficient to reveal neuronal connections in neuro-muscle junctions.

Tras realizar varias modificaciones de diferentes dominios del receptor TRACT, localizar el ligando y el receptor en sinapsis, así como evaluar la capacidad del sistema TRACT como trazador neuronal retrógrado, hemos llegado a las siguientes conclusiones:

1. La adición del motivo EGF 36 entre la región reguladora negativa de Notch y el dominio de unión al ligando (SCAD; 1d3) mejora la relación entre la inducción y el background en 7,91 veces, mostrando una ligera disminución en la actividad independiente del ligando.
2. Cambiar el NRR por el dominio S1LO y ¨snorkelling¨ el dominio juxtatransmembrana (jTMD) reduce el background pero no mejora la relación entre la activación dependiente e independiente de ligando
3. La adición del dominio de cremallera de leucina (leucine zipper) entre el NRR y el dominio extracelular 1d3 reduce el background llevando la activación a niveles similares a los del receptor control (1d3NRRG4).
4. El cambio del dominio SCAD por la glicoproteína CD4 no muestra ninguna mejora en la relación inducción / background, así como la ubicación de la proteína SUMO entre el dominio CD4 y NRR.
5. La modificación del dominio transmembrana (TMD) del receptor 1d3NRRHybG4, muestra un nivel de activación casi tres veces mayor que el receptor de control 1d3NRRG4.
6. La unión del dominio intracellular de dos receptores 1d3NRRG4 mediante la cremallera de leucina muestra un aumento de 10 puntos en el nivel de activación.
7. Considerando los resultados de todas las modificaciones de los receptores, se validaron los receptores 1d3NRRHybG4 y 1d3NRRDHFR en el sistema olfativo de *Drosophila*. Las moscas transgénicas que llevan el receptor 1d3NRRHybG4 no muestran ninguna señal de GFP. Sin embargo, las moscas transgénicas con dos variaciones de DHFR mostraron altos niveles de activación independiente del ligando, lo que hizo imposible distinguir la activación dependiente del ligando.

8. La localización de ligandos y receptores en el sitio presináptico y postsináptico, respectivamente, muestra una mejora significativa de la técnica TRACT para trazar circuitos neuronales en el cerebro de *Drosophila*.
9. El sistema TRACT retrógrado no es eficaz para revelar conexiones neuronales en las sinapsis neuromusculares.

CHAPTER 3

INTRINSICALLY DISORDERED PEPTIDES ACT AS LIGAND-DEPENDENT MECHANOSENSORS

INTRODUCTION

Cells are considered the basic unit of life that play complex and specialized functions. In the same way, we can communicate and receive stimuli from the outside world through the five senses; these tiny life units can perceive stimuli such as chemical sensing, temperature, or mechanosensing from their environment, encoding distinct functions. For instance, mechanical forces provide an essential route for communication among cells and their microenvironment.

3.1.1. Mechanical Tension in Cells.

Mechanosensing is an important and widespread biological process that allows organisms to perceive and respond to environmental changes (Ellison and Brun 2015). Mechanical forces influence tissues to produce the final morphology of an organism through processes of mechanotransduction. Moreover, it is known that this process of mechanotransduction has an essential function in cellular behaviour such as migration, growth, or tissue regeneration (Iskratsch et al. 2014). There are a wide variety of mechanical interactions in cells: cell-cell interaction, cell-matrix adhesions, oscillating pressure in blood vessels, stretch in beating heart, muscle tension or bloodstream (flow) pressure. These forces generated by cells regulate many physiological processes, including the selection of optimal antibodies, sorting of chromosomes and organelles within the cell, and blood clotting in response to turbulence. Accordingly, cells have evolved specialized proteins capable of sensing these forces such as filamin like talin (Giannone et al. 2003), focal adhesion kinase (FAK; Sawada and Sheetz, 2002); muscle LIM protein (MLP; Knöll et al., 2002), Von Willebrand factor (VWF; Sadler, 1998) or Notch receptor (Parks et al., 2000).

An excellent example of mechanosensor is the Von Willebrand factor, a glycoprotein secreted by endothelia cells and megakaryocytes, described in 1926 by the physician Erik von Willebrand (von Willebrand, 1926). It is present in the plasma and endothelium playing an essential role in hemostasis and thrombosis. The domain A1 of VWF factor (VWFA1) can detect the shear force caused by bloodstream that triggers its deployment, allowing ADAMTS13 access to A2 domain and cleaves it and transduces a signal/cell response(Sadler 1998, 2005). The platelets (glycoprotein (GP)Ib-IX complex) will bind to VWFA1 promoting the coagulation and stopping blood flow when a healing

process is required at the injury site (Ellison and Brun 2015). The VWFA1 domain plays a remarkable role in initiating thrombus formation under pathological shear rates (Rana et al. 2019).

3.1.2. Notch Signalling Pathway.

A well-known mechanotransduction process involved in cell communication is the Notch signalling pathway, a highly conserved cell signalling system present in most animals. The Notch protein is a transmembrane type I receptor that span in the cell membrane containing several domains, each of them with distinct and unique functions. It has been studied for more 100 years since John Dexter discovered the appearance of notches at the wing margins of *Drosophila* for the very first time. Although, the alleles of the gene involved in this notches wing were identified in 1917 (Morgan 1917), the Notch protein as a receptor involved in *Drosophila* neurogenesis was identified almost three decades later (Artavanis-Tsakonas et al. 1983; Wharton et al. 1985; Kidd et al. 1986; del Amo et al. 1993). The Notch receptor is involved in a variety of process in development, physiology (differentiation, proliferation, or migration) and diseases such as cancer. Furthermore, it is known that its dysregulation causes several diseases, including leukaemias.

Notch receptor has very simple design that provides a lineal cell-cell communication, sending information from the cell surface to the nucleus in three very straightforward steps: **(i)** Its extracellular domain (ECD) recognizes the ligands on the surface of neighbouring cells, that **(ii)** trigger two cleavages in its structure (extracellular and transmembrane cleavages) **(iii)** releasing the intracellular domain (ICD) from the plasma membrane and translocating to the nucleus to transduce the signal sent by the surrounding cells. Therefore, the Notch pathway is a direct signalling without any secondary messenger or signal amplification (Figure 2.7B, Chapter 2). Notch pathway is evolutionarily conserved throughout metazoans. In mammals, there are four Notch receptors (1-4) and five canonical ligands [Delta-like ligand (Dll1, 3, 4; or Delta/Serrate/LAG-2 ligands (DSL)] and Jagged (Jagged-1, -2) (Kopan and Ilagan 2009). Furthermore, it is well known that each ligand triggers a specific effect of Notch Receptor. For example, Dll1 mutant mice (knockout) present embryonic lethality

because Dll4 cannot replace Dll1 in many tissues (Preuße et al. 2015). Due to its simplicity, it is remarkable that Notch receptor participates in cell-cell communication regulating so many different cellular behaviour mechanisms (stem cell maintenance, specification of cell fate, differentiation, proliferation, and apoptosis). Moreover, its pleiotropic effects in distinct organs, and its interaction with a different regulator in a context-specific manner, mask its simplicity (Henrique and Schweisguth, 2019). This complex regulation in time and space between several Notch receptors and ligands difficult its study in mammals and some vertebrates. However, most of the Notch signalling pathway studies have been focused on *Drosophila melanogaster* which has only one Notch receptor and two ligands (Delta (Dl) and Serrate (Ser)); but its conservation level with their mammals' orthologues is relatively high (Kopan and Ilagan 2009; Zacharioudaki and Bray 2014).

3.1.2.1 Notch Receptor: Synthesis and Splicing on the Plasma Membrane.

Notch receptor is first synthesized as a 300 to 350-kDa type I single-pass transmembrane glycoprotein. During its transport to the cell surface, the Notch receptor precursor (pre-Notch) is first proteolytically cleaved by a Furin-like convertase at the S1 in the Golgi apparatus (trans-Golgi network). After this cleavage, both subunits heterodimerize noncovalently to create the mature form of Notch receptor on the plasma membrane (120KDa fragment (p120) plus 200KDa fragment (p200)), in an autoinhibited conformation (Blaumueller et al. 1997; Logeat et al. 1998). The Furin-like convertase belongs to the Subtilisin/Kexin family with a tissue-specific distribution except for the Furin that is ubiquitously expressed. Mutations of the main processing site of Notch1 (S1) (RQRR sequence → to AAAA mutation) prevent the Furin cleavage action, producing a full-length protein that does not reach the cell surface. Furthermore, when *Lovo* cells (epithelial cells from adenocarcinoma of the colon) which express no functional Furin (mutation in the coding region) were transiently transfected with Notch1, only the full-length of the Notch precursor was detected (Logeat et al. 1998). However, it has been suggested a Notch 1 signalling independent on Furin activity in mammals (Bush et al. 2001) and *Drosophila* (Kidd and Lieber 2002).

Based on Notch1 and Notch2 crystal packing study, Gordon et al., (2009b) showed for the first time that S1 cleavage site lay on small unstructured region inside the heterodimerization domain (HD), and most importantly, they showed that Furin-S1 site almost does not affect both receptors' conformation. They also observed that the Notch1 receptor lacking the S1 loop does not reach the cell surface (reduced by 5 to 10-fold). In contrast, Notch2 mutant receptor (no S1 loop) has normal trafficking to the plasma membrane. They observed Notch signalling activation upon ligand-binding in both cases, suggesting that Furin-S1 cleavage is not essential for Notch activation.

Interestingly, Notch hybrid molecules expressed in *Drosophila* (Notch receptor from *Drosophila* with mouse S1 site) reached the cell surface as a heterodimer. In contrast, only the unprocessed hybrid murine Notch receptor (a mouse Notch receptor with the *Drosophila* S1 cleavage site) reached the plasma membrane. Although the *Drosophila* Furin can process the mouse S1 site, the murine Furin cannot process *Drosophila* S1 region because it lacks the cleavage consensus site (Kidd and Lieber 2002). Moreover, expression of Notch receptors without the S1 cleavage site partially rescue the Notch loss of function in *Notch* null transgenic fly embryos (Kidd and Lieber 2002), showing activation of Notch receptor even without Furin cleavage. However, reducing or blocking the *Drosophila* Furin convertases showed a normal Notch processing *in vitro* and *in vivo*, suggesting that different enzymes can play the Furin role in *Drosophila* (Lake et al. 2009). Although there are two main Furin cleavage sites identified in *Drosophila* (F1 (RKNK) and F2 (RLKK)), the only mutation on F2 site showed a decrease in the production of heteromeric Notch on the cell surface (Gordon et al. 2009b; Lake et al. 2009).

In mammals, it has been shown that the unprocessed Notch1 receptor can suppress the myogenesis in a Notch1-dependent myogenic differentiation model, but it cannot trigger the signalling. Moreover, overexpressing mutant Notch1 receptor resistant to the Furin-cleavage showed similar results. It is important to mention that this suppression effect may be due to the low endogenous level of Notch1 (Bush et al. 2001).

3.1.2.2. Notch Receptor Structure.

Notch transmembrane receptor is anchored to the plasma membrane and can be divided into three main domains: **(i)** a large extracellular domain (ECD), **(ii)** a transmembrane domain (TMD), and **(iii)** a small intracellular domain (ICD) (Figure3.1A).

First, the ECD compromises several repeats in its amino acid sequence, similar to that of epidermal growth factor (EGF-like). The EGF repeats responsible for the ligand-binding site are EGF11-13 that contain a Ca^{2+}-dependent binding consensus sequence (Hambleton et al. 2004). The number of EGF repeats which are O-glycosylated varies among species, and many of them have an additional consensus sequence for Ca^{2+} binding (cd EGF). Experiments of site-directed mutagenesis of EGF11, 12 and 13 showed that only the loss EGFr 12 eliminates the extracellular domain's binding to the ligand Dll1 (Cordle et al. 2008). Later, it was identified that the residues L504 and V513 in *Drosophila* Notch and L468 and I477 in EGF12 of human Notch1 were key amino acids in this EGF repeat for Notch binding to the ligand (Whiteman et al. 2013). Secondly, there is a domain called Notch negative regulatory region (NRR) in the ECD, located c-terminus to the EGF repeats. It is a 300 aa domain that contains a cleavage site, called S2, inside the heterodimerization domain (HD) that can be cleaved by ubiquitous membrane-bound metalloproteases of the ADAM family. The NRR region also contains 3 Lin12/Notch repeats which protect the S2 cleavage site in an autoinhibition state and the HD (region most frequently mutated in T-cell acute lymphoblastic leukaemia (T-ALL)) surrounding the S1 cleavage site (Gordon et al. 2007, 2009a). (Figure 3.1A).

Third, the Notch TMD is also a well-conserved α-helix structure that extends 29 amino acids containing the S3 cleavage site recognized by γ-secretase (Haass and Selkoe 1993). It has been suggested that the juxta-transmembrane domain, the connection between NRR and TMD, present a flexible structure (Deatherage et al. 2015). Finally, the ICD is translocated to the nucleus and transduce the Notch signal. This ICD is divided into several regions: RAM domain, seven ankyrin (ANK) repeats flanked by two nuclear localization signals, a transactivation domain (TAD), and a PEST (proline (P), glutamic acid (E), serine (S) and threonine (T) domain) region thought to regulate protein degradation (Sanchez-Irizarry et al. 2004) (Figure3.1A).

3.1.2.3. Molecular Mechanism of Notch Signalling Pathway.

Notch receptors located on the receiver cells' surface are activated by the ligand situated on the neighbouring emitter cells' surface. This type of cell-cell activation is known as a trans-activation (both proteins are in different cells). In the absence of ligand, the Notch negative regulatory region (NRR) is folded burring the S2 cleavage site, located between the TMD and S1 site, making it inaccessible to the action of metalloproteases such as Kuzbanian (in *Drosophila*) or TACE (Tumor necrosis factor—Converting Enzyme) in vertebrates (Qi et al. 1999; Schlöndorff and Blobel 1999; Tiyanont et al. 2011). It has been hypothesized that the ligand-receptor binding induces a mechanical force generated by the ligand endocytosis, triggering the NRR unfolding and exposing the S2 site which is then cleaved by ADAM metalloproteases (Tousseyn et al. 2009; Tiyanont et al. 2011; Meloty-Kapella et al. 2012; Gordon et al. 2015). After S2 cleavage, only a short domain of 12 amino acids (aa) long of Notch ECD, the juxtatransmembrane domain (jTMD), remains above the membrane. This shortening of the Notch ECD triggers an intramembrane cleavage by the γ-secretase (regulated intramembrane proteolysis (RIP)) in the so-called S3 site (Brou et al. 2000; Mumm et al. 2000). Later, the Notch intracellular domain loses its membrane anchorage and translocate to the nucleus, activating the transcription of target genes (activate transcription) (Struhl and Adachi 1998, 2000). Therefore, the ligand-receptor binding and subsequent endocytosis of ligand-receptor complex induce regulated intramembrane proteolysis (RIP) to generate a transcriptional effector (Kopan and Ilagan 2009).

3.1.3. Notch Negative Regulatory Region (NRR).

The first step on the Notch pathway that involves the ligand-binding complex processing and the force induced by the ligand endocytosis is essential to understand how the subsequent mechanisms are triggered. Previous studies have demonstrated that the key component controlling the Notch transmembrane receptor's activation is Notch negative regulatory region (NRR) (Gordon et al. 2007). This region switches between an inactive state where S2 cleavage site, located in the heterodimerization domain (HD), is protected by three LIN12-Notch repeats domains (LNR A-C) to an active

unfolding NRR, making S2 site accessible to ADAMs metalloproteases (Gordon et al. 2007, 2009a; Xu et al. 2015). The crystal structure from Notch1, 2 and 3 NRR showed similar conformations where the LNR domains buried the S2. Moreover, the three Notch receptors require a substantial movement in the LNR domains. Deletions of each LNR domains showed that LNR-A and B and the linker between them are essential to prevent the cleavage of the S2 site by ADAMs metalloproteases and need to be removed from the S2 site before the cleavage occurs (Gordon et al. 2007, 2009b, a) (Figure 3.1B). Other studies showed that the deletion or mutations on LNR domains cause gain of function phenotype (Greenwald and Seydoux 1990). Moreover, mutations in Notch1 NRR that induce ligand-independent cleavage are very often found in certain type of leukemias (Weng et al. 2004). Therefore, it is extremely important to control the ADAMs access to the S2 cleavage site.

The heterodimerization domain (HD) of the NRR is divided into two subunits (HD-N and HD-C) connected by an extensive hydrogen-bonding network into an α/β sandwich structure. The S1 Furin-cleavage site is located between HDs and presents a poorly conserved loop (Gordon et al. 2009b) while the S2 site is located in the HD-C subunit (Gordon et al. 2007). Furthermore, activating mutations that disturb the HD domain's stability and lead to aberrant ligand-independent activation are responsible for diseases such as leukemias (Malecki et al. 2006; Gordon et al. 2007) (they well be discussed later in this chapter).

Although the overall NRR structure is the same in the three Notch receptors, some detailed differences may play a role in their sensitivity of a particular activation. Three conserved tryptophan residues stabilize the connection between the LNR A and B in Notch receptors, but it is reinforced in Notch1 and Nocth2. Moreover, in Notch 3 receptor, the LNR-C is packed closer to the HD domain because of the replacement of a salt bridge between LNR-C and the first helix of the HD domain with a hydrogen bond (Lovendahl et al. 2018).

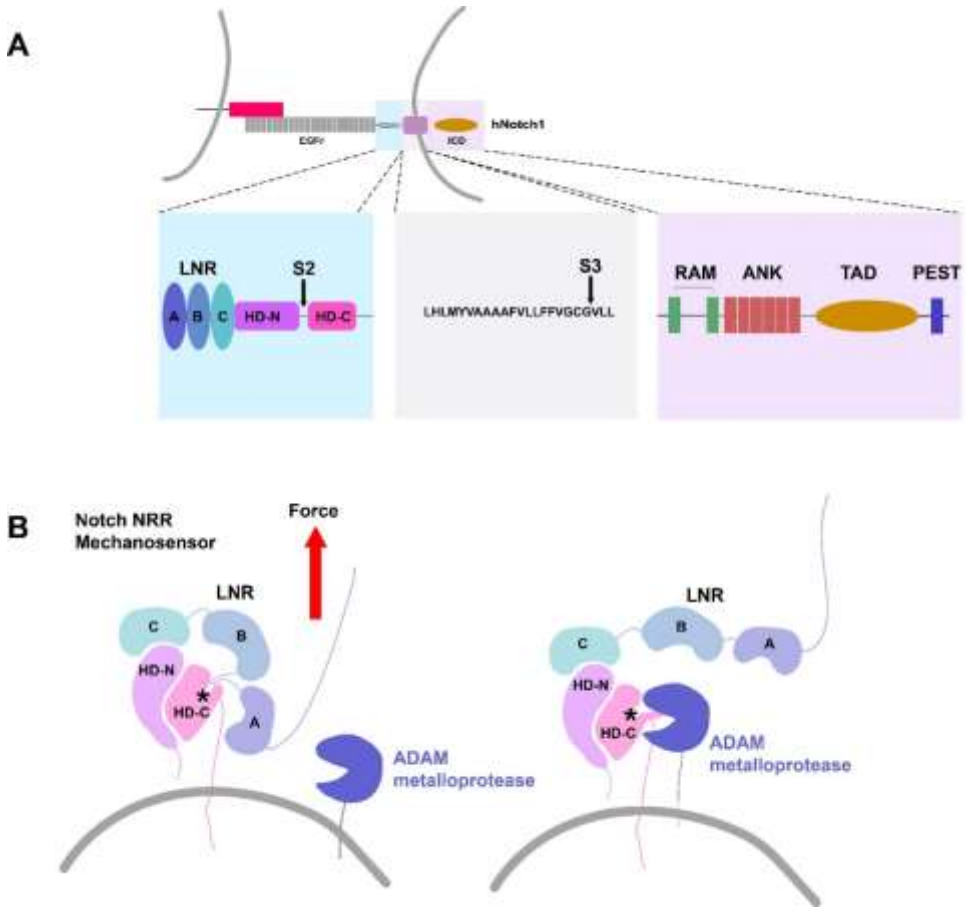

Figure 3.1. Different domains of Notch receptor. (A) Diagram of ligand-receptor interaction where the NRR, TMD, and ICD are shown in higher magnification to distinguish the different subunits in detail. Adapted from Gordon et al. 2007. **(B)** Schematic representation of Notch negative regulatory region. On the left, the inactive site where the S2 cleavage site is protected. After a pulling force is applied by ligand endocytosis, the S2 cleavage site is accessible by ADAMs metalloproteases (on the right panel). Asterisk represents the S2 cleavage site. Adapted from Gordon et al., 2015.

3.1.3.1. S2 cleavage site.

The S2 site is in a small hydrophobic pocket plugged the by three highly conserved residues derived from the linker that connects LNR A and B. Also, the hydrophobic interactions between the second LNR and the HD occlude the metalloproteases access. Moreover, it is suggested that LNR domains induce stabilization to the NRR through its interactions with the HD and must be displaced to unmask the S2 in the HD (Gordon et al. 2009b). This conformational change in the structure of NRR likely requires a lot of energy; more consistent with mechanical force activation than allostery. Then, the S2 cleavage is recognized and cleaved by a

metalloprotease (ADAMs) in response to ligand binding that induces a conformational change (Mumm et al. 2000; Parks et al. 2000a). The cleavage by ADAMs will leave a short version of Notch receptor with only 13 amino acids in its extracellular domain (Notch Extracellular Truncation (NEXT) or juxtatransmembrane domain, jTMD). Furthermore, human genetic studies have also shown that mutations inside NRR, destabilize NRR, expose the S2 cleavage site, and activate Notch in a ligand-independent manner.

ADAMs proteases, originally also known as metalloproteinase/disintegrin/cysteine-rich proteins (MDC), are membrane bound Zinc-dependent metalloproteases that regulate the activity of transmembrane signalling molecules (van Tetering and Vooijs 2011) (Teetering and Voojis 2014). For substrate proteolysis, ADAMs require a Zn^{2+} ion, and their activity can be inhibited by broad-spectrum Zn^{2+}-chelating drugs such as hydroxamate-type inhibitors (van Tetering and Vooijs 2011) (Teetering and Voojis 2014). According to their catalytic sites, these zinc-dependent metalloproteases are subdivided into several groups, where ADAMs proteases belong to the Metzincins superfamily of metalloproteases (Seals and Courtneidge 2003; Giebeler and Zigrino 2016). This Metzincin superfamily is further divided into another 4 subfamilies according to small differences in the catalytic site and the presence of additional domains: matrixins (matrix metalloproteinases, MMPs), adamalysins (ADAM, ADAMTS and class III snake venom proteins), astacins (BMP1/TLL proteins and meprins) and bacterial serralysins (Stöcker et al. 1995; Huxley-Jones et al. 2007). The structure of the ADAMs consists of a prodomain, a metalloprotease domain, a disintegrin domain, a cysteine-rich domain, an EGF-like domain, a transmembrane domain, and a cytoplasmic tail (Seals and Courtneidge 2003) (Figure 3.2A). They play an essential role in protein "shedding" (proteolytic ectodomain release) regulating diversity membrane proteins' function.

Among all different ADAMs, ADAM10 and ADAM17, also called tumour necrosis factor alpha-converting enzyme (TACE), have been studied for their variety of functions in diverse types of transmembrane proteins such as Notch receptor and ligand, NCAM (neural cell adhesion molecule, E-cadherin (epithelial cadherin), RTKs (Tyrosine-kinase receptor), and APP (amyloid precursor protein) among others.

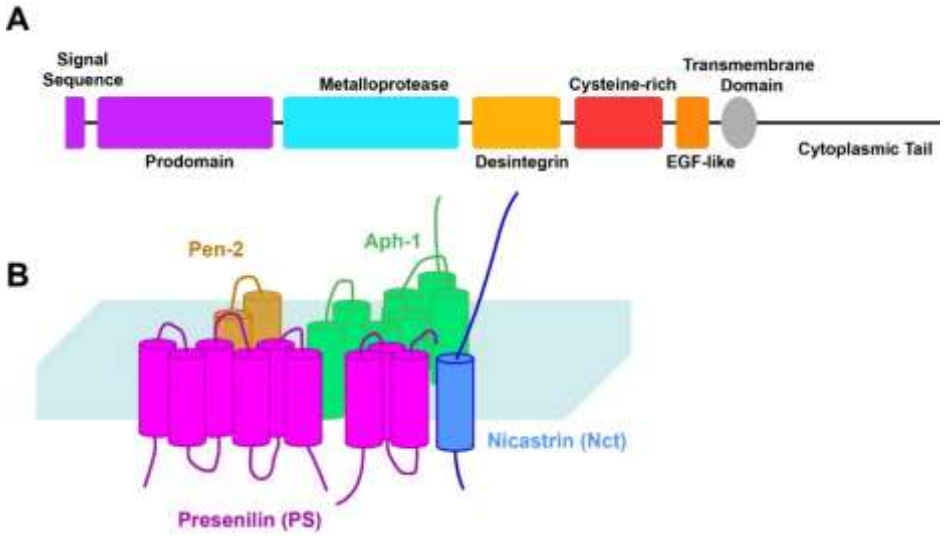

Figure 3.2. Structure of ADAM and γ -secretase complex. (A) Schematic Representation of ADAM 10 showing the different domains and **(B)** diagram showing the four essential subunits of the γ-secretase complex on the plasma membrane.

ADAM 10 and 17 are essential for the activation of Notch signalling either by ligand-dependent or independent induction, respectively. They cleave the S2 site facilitating the subsequent cleavages at S3 site in the TMD by the γ-secretase complex (Rooke et al. 1996; Sotillos et al. 1997; Lieber et al. 2002; Jarriault and Greenwald 2005). In *Drosophila*, *Kuzbanian (kuz*), the fly ortholog of ADAM10, regulates the Notch cleavage involved in neurogenesis, growth, and patterning of the imaginal disc (Rooke et al. 1996; Sotillos et al. 1997; Lieber et al. 2002). *Kuz* mutants' flies have a neurogenic defect similar to those observed in *Drosophila* mutant Notch (Rooke et al. 1996). Studies in C. elegans have shown that the inactivation of sup-17 (ADAM10 ortholog) or adm-4 (ADAM17 ortholog) has no strong effect on Notch signalling. However, the combined inhibition of both ADAMs, induces a Notch loss-of-function phenotype (Jarriault and Greenwald 2005). It suggests that another ADAMs related proteases could have redundant activity in the absence of *adm-4* and *sup-17*. Moreover, knockout ADAM10 mouse dies at embryonic day 9.5 (E9.5) while ADAM17 deficient mouse dies at birth without phenocopying Notch1 mutant mice (Peschon et al. 1998; Horiuchi et al. 2007). *In vitro* studies showed that defects in ADAM10 did not show ligand induced signalling in mammalian cells (Bozkulak and Weinmaster 2009). In contrast, ADAM17 activity lost did not significantly diminish S2 cleavage. Several studies confirm these results about

ADAM functions depending or not on ligand binding activation in different organs (Tian et al. 2008; Glomski et al. 2011; Tsai et al. 2014).

Moreover, it is well known that ADAM10 and 17 are essential for developmental and physiological processes (Tousseyn et al. 2006; Reiss and Saftig 2009). For example, ADAM10 is a regulatory element of E-cadherin transmembrane glycoprotein shedding, regulating its activation (Maretzky et al. 2005). In addition, it has been shown that ADAM17 proteolytic cleavage of NCAM induces the neurite outgrowth (Kalus et al. 2006) while ADAM10, stimulated by ephrinA5, can induce the growth cone of NCAM (Brennaman et al., 2014). Moreover, the ectodomain of ErbB4 is sheeded by ADAM17, causing the subsequent γ-secretase cleavage of the remnant peptide to release intracellular domain (ICD) (Zeng et al. 2007; Toonen et al. 2016).

3.1.3.2. S3 Cleavage Site.

After the cleavage of the Notch receptor in the S2 site (heterodimerization domain of the NRR) by ADAMs, NEXT is cleaved in its TMD at the S3 by γ-secretases, releasing the Notch intracellular domain (NICD) which is translocated to the nucleus and interact with CSL (CBF1, Suppressor of Hairless, Lag-1). In the absence of NICD, CSL repress transcription of Notch target genes, and after its interaction with NICD is converted into a transcriptional activator of the Notch signalling pathway downstream genes (Jarriault et al., 1995; Kao et al., 1998; Schweisguth, 2004; Struhl and Adachi, 1998).

The Notch S3 site's cleavage is carried out by aspartyl proteases, which belong to presenilin family, that are part of a large protease complex called γ-secretases (PS/γ-secretase; Haass and Selkoe, 1993; Selkoe and Wolfe, 2007). γ-secretases are composed of a catalytic subunit (presenilin-1 or presenilin-2) and accessory subunits (Pen-2, Aph1, and nicastrin) which are transmembrane proteins (Figure 3.2B). This enzyme mediates the degradation of transmembrane domains from different types of transmembrane proteins such as Notch and β-amyloid protein precursor (βAPP) (Xia and Wolfe 2003; Koo and Kopan 2004); as well as E-cadherin, N-cadherin, ErbB4, or ephrin-B2 (Ni et al. 2001; Marambaud et al. 2002, 2003; Georgakopoulos et al. 2006).

Elegant experiments by Huppert et al., (2000) showed a single point mutation next to the S3 site in Notch1 receptor leads embryonic lethality in mice, similar to the effects observed in Notch1 knockout. Mice deficient either for one catalytic subunit of γ-secretases complex or both (presenilin-1/presenilin-2) showed a substantial reduction in Notch Intracellular Domain (NICD) generation (De Strooper et al. 1999). Mammals and worms present two presenilin-1 and presenilin-2 (PS1 and PS2) that are similar but exclusive in the γ-secretase complex whereas flies have a single presenilin protein (PS) (van Tetering and Vooijs 2011).

It has been suggested that there is a variety of S3 cleavage sites in the mouse Notch1 receptor which differs depending on the subcellular location (Tagami et al. 2008). Among the different S3 cleavage sites found (NICD-V), NICD-L(+1), NICD-L(+2), NICD-S(+3)) the highest relative intensity peak shown in mass spectrometry spectrum was obtained for NICD-S(+3) (between Leu1746 and Ser1747) suggesting that NICD-S(+3) may be the main S3 cleavage site in cells *in vitro* and fetal mouse tissue (Figure 3.3) (Tagami et al. 2008). However, NICD-S(+3) showed a weaker activation of Notch signalling compared to NICD-V (cleavage between Gly1743 and Val1744), being the latter more stable than NICD-S(+3). Furthermore, the ratio of NICD-V vs NICD-S(3+) was higher in the plasma membrane (PM) fraction than in endosome fraction indicating that cleavage at NICD-V occurs mainly on the PM and NICD-S(+3) in the endosomes.

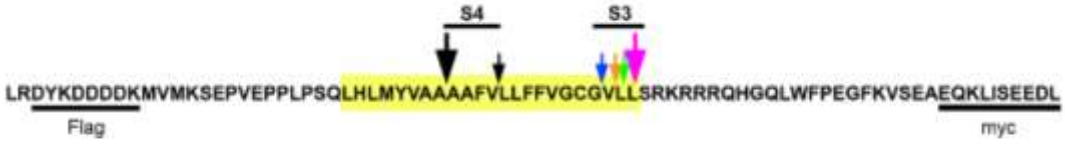

Figure 3.3. Schematic Representation of S3 cleavage sites and S4 within Notch1 transmembrane domain. It was adapted from Tagami et al., 2008.

In addition to S3 cleave site, mass spectrometry analysis reveals that there is an additional cleavage (S4) in the middle of the TMD in the center of four sequential alanine residues (between Ala1731 and Ala1732) (Figure 3.3) (Okochi et al. 2002). Experiments, where S3 cleavage site was mutated, have shown a reduction of the NICD. The S4 site's cleavage mediated by γ-secretase is dependent on S3 site integrity S4 cleavage happens after S3 cleavage (Chandu et al. 2006).

3.1.3.3. Mechanical Allostery (NRR as Mechanosensor).

The allosteric regulation is a natural mechanism that induces structural changes, in a protein-protein interaction, where the protein binding is transmitted to another site causing a conformational change of the protein structure. This term was first described by Jacob and Monod (1961). It is complicated that allosteric regulation plays a role for Notch receptor activation because the ligand-binding site on the EGF repeats 10-12 is far from the NRR, which is the domain where conformational changes occur. It has been suggested that only the ligand binding to the receptor does not trigger Notch receptor activation (Varnum-Finney et al. 2000). Therefore, different types of allostery mechanisms are necessary to unmask the S2 site. Genetic and biochemical studies have indicated that the ligand-receptor complex's endocytosis is required for this conformational change in the Notch receptor (Gordon et al. 2007; Musse et al. 2012).

The first evidence that Notch activation requires endocytosis was observed in Shibire mutant *Drosophila* (Shibire, encodes a *Drosophila* homolog of dynamin)(Seugnet et al. 1997). It is known that dynamin is essential for releasing the endocytic vesicle from the plasma membrane (PM). Although it was described that ligand endocytosis is actively involved in Notch proteolysis, it was no clear the specific function of ligand endocytosis to activate Notch signalling (Parks et al., 2000). Two models were proposed for ligand-endocytosis mechanisms to trigger conformational changes and activate the Notch pathway (Figure 3.4):

1. Recycling model: This model proposes that the ligand on the plasma membrane is no active to transduce a signal and has to be internalized and recycled back to the cell surface (Wang and Struhl 2004, 2005; Weinmaster and Fischer 2011; Musse et al. 2012). Epsin (endocytic adaptor) is required to recruit the ubiquitinylated ligand before its endocytosis for this internalization process. Later, the ligand changes from an inactive to an active state, and it is repositioned to the cell surface, where it can activate Notch in the adjacent cells. The statement of this model is supported by several studies where in sensory organs precursor from *Drosophila* (SOP), the ligand trafficking from basal to apical requires ubiquitylation in association with recycling cofactors components

before the ligand is displayed on the cell surface to activate the Notch receptor (Jafar-Nejad et al. 2005; Emery et al. 2005; Benhra et al. 2010). It has been reported that this ligand recycling process dependent on a specific cellular context. For example, Rab11 and Sec15 are required in ligand recycling for SOP cell fates (Jafar-Nejad et al. 2005; Emery et al. 2005), but Rab11 and Rab5 are not needed for the ligand expressing cell to trigger Notch signalling in developing eye or germlines (Windler and Bilder 2010; Banks et al. 2011). Based on these studies, the ligand recycling pathway is no essential for all Notch-dependent processes, despite that this ligand trafficking through the recycling pathway is required for SOP cell fates.

2. Pulling force model: The concept of pulling force generated by emitter cells appear for the first time performing *in vitro* experiments with *Drosophila* S2 cells (Fehon et al. 1990). This model proposed that after the ligand-bind to the receptor, this ligand's endocytosis on the sender cells produces a mechanical force to pull the Notch receptor. This pulling induces conformational changes in Notch receptor that allow the proteases access to several cleavage sites and trigger several proteolysis events to end with the Notch intracellular domain (NICD) release. In this model, Epsin is required for ligand endocytosis (D'Souza et al., 2008; Nichols et al., 2007). Epsins act as endocytic adaptors that contribute to the membrane bending and, therefore, regulate the endocytosis process (Sen et al. 2012). It has been reported that the ligand is polyubiquitinated upon Notch receptor binding, inducing the formation of Epsin depending endocytic structures (Hansson et al. 2010; Weinmaster and Fischer 2011). Moreover, studies in zebrafish showed that the replacement of the Delta ICD by a ubiquitinated motif could induce ligand polyubiquitylation that triggers its internalization (Itoh et al. 2003) while an unique ubiquitinated motif generates a weak Notch signal (Wang and Struhl 2004).

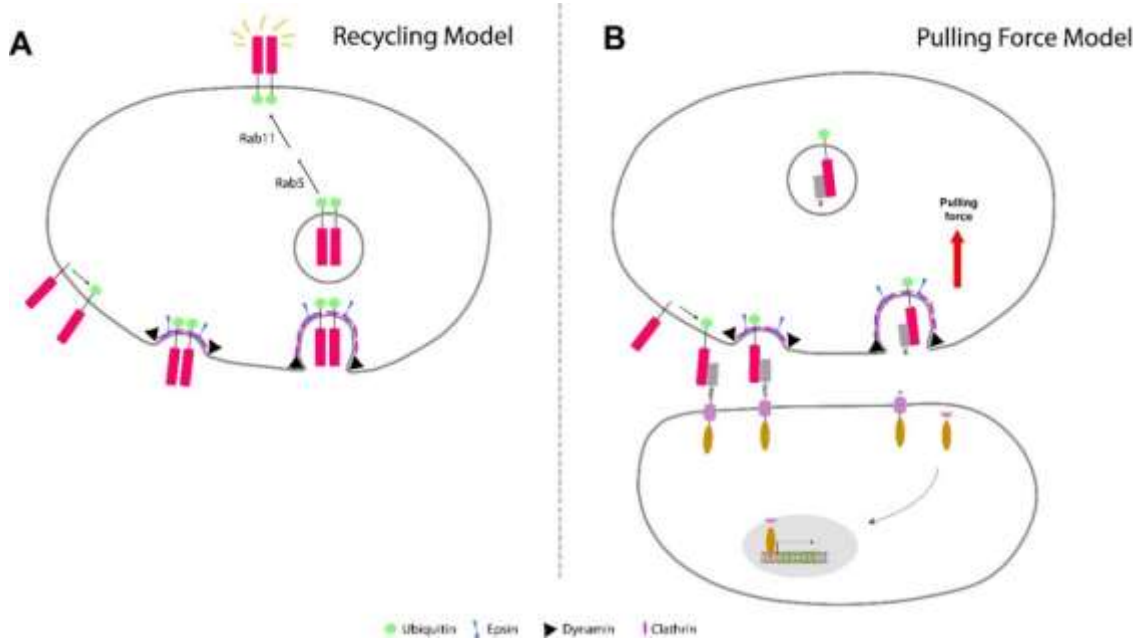

Figure 3.4. Schematic representation of the recycling model (A) and pulling force model (B) to activate Notch signalling. The ligand must go through an endocytosis process to be activated and induce Notch signalling **(A).** In the pulling force model, the ligand endocytosis previous ubiquitination will produce a pulling force that induces a change of Notch receptor to activate its signalling pathway **(B)**.

Although both models required ligand endocytosis to activate Notch signalling pathway by two different mechanisms, the most accepted is the pulling force or mechanotransduction model (Parks et al., 2000). In these experiments, they observed that Notch receptor-Delta ligand complexes aggregate on emitter cells (trans-endocytosis), suggesting that Notch activation is dependent on Delta endocytosis (Nichols et al. 2007; Shaya et al. 2017). This mechanical activation model was supported by experiments where adding a soluble ligand does not induce Notch activation (Varnum-Finney et al. 2000). Significantly, Notch Extracellular domain transendocytosis was inhibited when there is no ligand endocytosis, showing defects in flies and mammalian cells (Nichols et al., 2007; Parks et al., 2000).

In general, proteins in the cell are on the nanometers order, so the forces that induce their structural and conformational changes are in a range between sub-pN to pN (Lovendahl et al. 2018). Moreover, studies doing simulations with high membrane tension showed that the force to pull the membrane into a tube-shape is 100–200 pN (Walani et al. 2015) which can be reduced to 10 pN by the assistance of coat proteins inducing a specified curvature on the plasma membrane (Hassinger et al. 2017). Several

biophysical methods have been developed to measure these types of pulling force *in vitro*: optical and magnetic tweezers, immobilized tensions sensors, and bio-membrane force probes (Lovendahl et al. 2018). The primary strategy of these techniques is tethering the protein of interest to a bead so the position of said bead can be manipulated.

In the last 5-10 years, several studies have focused on measuring the Notch signalling pathway's mechanical force *in vitro*. In that respect, several predictions have been hypothesized: **(i)** the force to induce the S2 cleavage should be within the physiologic force, **(ii)** the binding of the ligand must not be enough to trigger Notch activation, **(iii)** the ligand endocytosis force should be sufficient to induce the structural changes of NRR and expose the S2 site, and **(iv)** the ligand-receptor binding complex should be strong enough to avoid any rupture during the force delivery. Considering these predictions, the methods used to address these hypotheses have been focused on measuring the following forces: **(1)** force required to expose S2 cleavage site, **(2)** force to trigger Notch activation, **(3)** the force exerted by ligand endocytosis, and **(4)** force response of ligand-receptors binding (bonds) (Figure 3.5).

1. Force to expose the S2 cleavage site.

The force required to expose S2 site within an isolated Notch1NRR was measured by magnetic tweezers (Figure 3.5D, bottom panel). This experiment showed that a force range between 3.5–5.4 pN is needed to induce proteolytic sensitivity (Gordon et al., 2015). This range of force is inside the physiologic forces, and it is similar to the force required (8 pN) to induce protease sensitivity of the Willebrand factor A2 domain (Zhang et al. 2009).

2. Force to trigger Notch Activation.

It has been suggested that ligand endocytosis provides the mechanical force necessary to unmask the S2 site. Thus, the force involved in Notch activation should be similar to ligand endocytosis. To measure this pulling force, in 2013 Wang and Ha bound the DSL ligand to a DNA strand which is annealed to a complementary strand attached to a glass surface (TGT duplex DNA sensor; Figure 3.5C, top panel). Changing the DNA

sequence will create an "unzipping" force of the resulting DNA duplex than can be modulated, leading digital force sensors that will be broken at different forces. If the DNA duplexes are unzipped, there is no Notch activation because the force between the plated ligand and Notch expressing cells is bigger than the DNA duplex's rupture force. Since the lowest magnitude sensor ruptured is at 12pN, the Ha lab did not find any of their DNA duplexes unzipped.

On the other hand, using magnetic tweezers, Notch activation was observed on the order of 2pN (Figure 3.5D top panel; Gordon et al., 2015). For this measurement, cells expressing Notch receptor were seeded at different heights in 96 well plates. Magnetic beads coated with recombinant Delta-like 4 (Dll4) were added to cell culture, and a lid with magnets was placed over the cells. Notch activation based on the magnet distance (as a function of force) can be measured with luciferase transcriptional readout. However, this experiment is not reliable to measure the ligand-receptor interaction force because it comprises multiple of these interactions.

This limitation was addressed by tagging Notch to a magnetic plasmonic nanoparticle (MPN) specifically synthesized for monovalent interaction (Seo et al. 2017)**.** They used MPNs conjugated with Dll1 ligand to target Notch1 receptor or benzylguanine-conjugated MPNs targeting a SNAP-tag Notch1 fusion (Figure 3.5D, middle panel). They observed that forces between 1 and 9 pN activate monovalent Notch.

Nano Yoyo single strand-DNA (ssDNA) method, a variation of the TGT duplex sensor (Figure 3.5C, bottom panel), where DNA is wrapped around the single-strand binding protein from *E. coli* (SSB) (Chowdhury et al. 2016) showed activation of Notch1 by Dll1 in a force range between 4 pN and 12 pN. This force range is similar to what previous systems have been reported. In contrast, forces lower than 4pN can activate Notch when Dll4 binds to it (Luca et al. 2017).

3. <u>Force of ligand Endocytosis.</u>

To measure the ligand endocytic force, polystyrene beads coated with Notch1 receptor are trapped by a laser tweezer (Figure 3.5B). Then, the forces required for ligand endocytosis will pull the bead into the cell expressing Dll1 ligand. The force

needed to balance this endocytic internalization of the ligand, which varies between 2 to 10 pN, was determined by applying an opposite force to the beads (Meloty-Kapella et al. 2012).

4. Force response of ligand-receptors binding.

Notch activation and ligand endocytosis forces are in the range 1-9 pN; therefore, ligand-receptor complex rupture force should be higher. Using optical tweezers (Figure 3.5B), it has been reported that the force required to rupture the binding between Dll1 expressing cells and Notch1-Fc coated beads were between 16 to 18 pN (Shergill et al. 2012). Therefore, the ligand-receptor complex remains intact under the force required to unmask the S2 cleavage site. In addition, using a Biomembrane Force Probe (BFP) spectroscopy (Figure 3.5E), it has been shown that the lifetime of bonds between the ligands Jagged1 or Dll4 to Notch receptor is enhanced in response to an increasing force between 0 pN to 10 pN (Luca et al. 2017). In the BFP spectroscopy technique, one micropipette aspirates a ligand-coated red blood cell while a second micropipette has a receptor coated-bead. The phenomenon observed in this experiment is called "catch-bond" which also occurs in T-cell receptor signalling (Chen et al. 2017). When protein interactions happen under force can show either this "catch-bond" behaviour or the opposite, the force reduces the binding lifetime (Lovendahl et al. 2018).

Most of the knowledge of the mechanical pulling force required to induce Notch signalling pathway comes from force spectroscopy and molecular tension sensors experiments but testing this pulling force model in vivo is challenging due to several uncontrollable variables. However, a genetic mosaic strategy in *Drosophila* has shown strong evidence about the requirement of a mechanical pulling force generated by Delta endocytosis to activate Notch (Langridge and Struhl 2017). They have also proved that chimeric ligand-receptor binding pairs can enter the Epsin-Clathrin pathway and activate its receptors, showing that NRR act as allosteric modulators and none other parts of Notch receptor has this ability. Therefore, NRR may act as a force sensor being cleaved in response to a specific force threshold as the spectroscopy force experiments have shown. Based on this statement, any mechanosensor that can be cleaved at the same force range that NRR could activate Notch signalling. For example, unfolding the subunit

A2 from von Willibrand factor (vWF) requires a force greater than 8 pN. Chimeric receptor composed of follicle-stimulating hormone (FSH) in its ECD and A2 subunit replacing NRR was not activated by Delta-FSH. However, mutant versions of this A2 domain in this chimeric receptor need lower force threshold for unfolding, enabling cleavage in a ligand-dependent manner (Langridge and Struhl 2017). These results suggest that the pulling force from Delta ligand endocytosis is sufficient for the mutant versions. Still, it is not clear if the cleavage of A2-WT (wild-type) involves the *Drosophila* ADAM/TACE family.

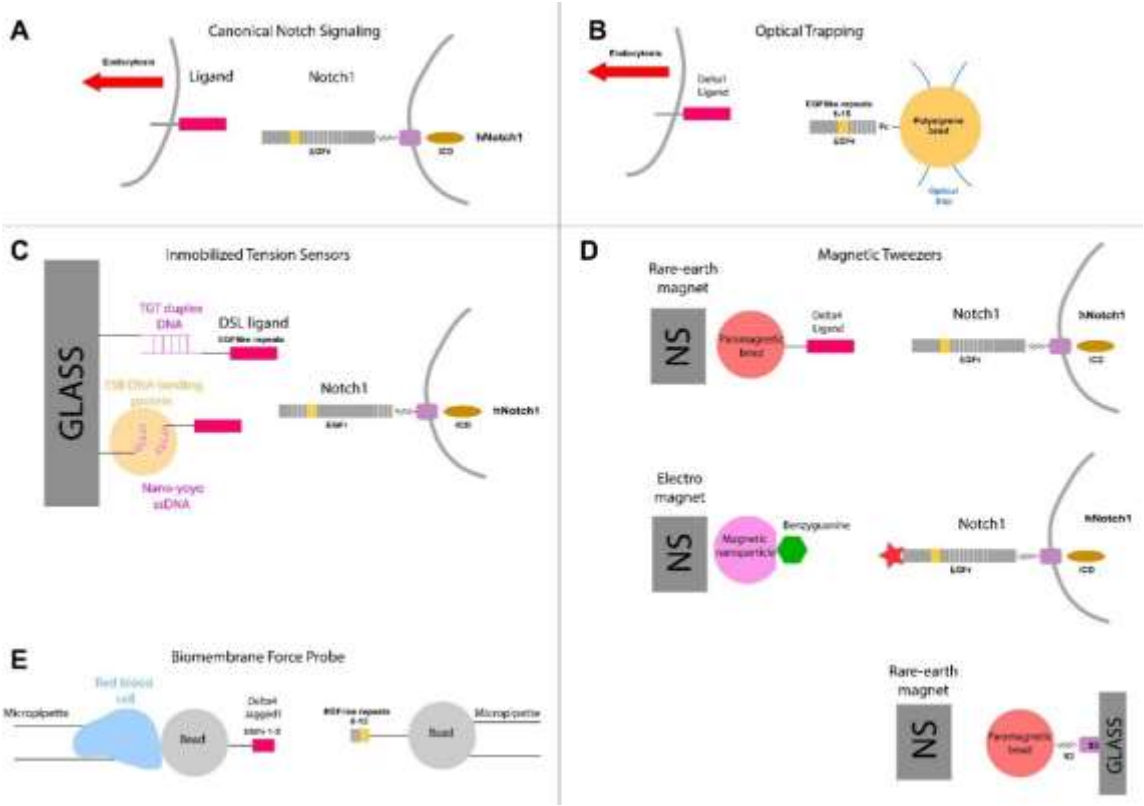

Figure 3.5. Force spectroscopy and molecular tension sensor experiments. Schematic representations of different *in vitro* experimental approaches to measure the mechanical pulling force involved in Notch signalling activation. **(A)** Canonical Notch signalling where the pulling force is coming from ligand endocytosis**. (B)** Optical trapping experiments where polystyrene beads are coated with a recombinant protein of hNotch1 receptor and bound to optical trap measuring the pulling force exerted from Ligand endocytosis. **(C) Top panel:** tension-gauge-tether (TGT) force sensors. A ligand is attached to a DNA strand which is annealed to a complementary DNA strand fixed to a glass. The force of the DNA duple can be modified by changing the DNA sequence. **Bottom panel:** Single strand DNA (ssDNA) wraps around the ssDNA binding protein (ssBD) from *E. coli*. One end of this complex is attached to the surface (glass) trough ssBD, and the other end has the ligand. When a force is applied, the ssDNA is unoiled or unrolled. **(D)** Three different experiments based on magnetic tweezer are shown: **Top**: Cells expressing Notch1 receptor were plated on 96 well plate at different heights and

beads coated with Dll4 ligand were added to the cells. A plate with magnets was covering the cells. **Middle:** Notch1 is tagged with SNAP protein at its N-terminal to bind with magnetic plasmonic nanoparticles (MPN) that are synthesized for monovalent interaction (Benzyguanine). **Bottom:** Magnetic beads coated with anti-SUMO were bound to biotinylated NRR with SUMO tag attached. This biotinylated NRR is bound to a surface with streptavidin. **(E)** Biomembrane Force Probe experiments. It consists of two micropipettes: One then aspirates a red blood cell coated with a ligand and the second one aspirates a coated bead with the receptor (EGF repeats 8-12). If the receptor beads are pulled away, the ligand exerts a force in the red blood cell, which is measured.

3.1.4. Notch in Cancer.

Next-generation cancer cells genomes experiments have revealed three main patterns types on Notch mutations in various human tumours. Human Notch1 was first described as an oncogene with the discovery of the first pattern of Notch mutations: rare chromosomal translocation which generates constitutively active *NOTCH1* allele in T-cell acute lymphoblastic leukaemia/lymphoma (T-ALL; Ellisen et al., 1991). This translocation produces a chimeric gene with the 3'end of Notch fused to enhancer elements of the T cell receptor (TCRβ) gene, completely removing the NRR coding sequence. This mutated humanNotch1 receptor undergoes ligand independent proteolysis and constitutively production of NICD. Later, more frequent point mutations, in-frame deletion and insertions were identified (Weng et al. 2004). These mutations also disrupt the NRR conformation, and therefore they also trigger ligand independent Notch1 proteolysis and activation. Moreover, Notch is the most mutated gene in murine T-ALL models (Aster et al., 2008).

The second pattern of mutations such as frameshift, nonsense, or alternative splicing mutations affects the NICD, specifically the PEST domain occurring in the absence of NRR mutation from the fist pattern (Aster et al. 2017). This type of mutations mainly produces B cell tumours such as chronic lymphocytic leukaemia (Puente et al. 2011; Fabbri et al. 2011), splenic marginal zone lymphoma (Kiel et al. 2012), and mantle cell lymphoma (Kridel et al. 2012), as well as occasional diffuse large B cell lymphomas (Lee et al. 2009; Arcaini et al. 2015) and peripheral T cell lymphomas, such as adult T-cell leukaemia/lymphoma (Pancewicz et al. 2010).

The third pattern of mutations affects to the N-terminal regions of Notch1 receptor. Disruptive nonsense, frameshift, or point substitutions produces loss of function of Notch receptor. These mutations cause the loss of functions of Notch triggering squamous cell carcinomas of the lung and skin (Wang et al. 2011), head and neck (Agrawal et al. 2011), esophagus (Agrawal et al. 2012), and also seen in small cell lung cancers (George et al. 2015).

Although Notch mainly acts as an oncogene in lymphoid neoplasms, it also can play a function as a tumour suppressor in different types of neoplasm (myeloid neoplasms) (Klinakis et al. 2011; Nowell and Radtke 2017).

3.1.4.1. NRR in T-cell Acute Lymphoblastic Leukemia (T-ALL).

T-cell acute lymphoblastic leukaemia (T-ALL) is an aggressive malignant neoplasm that arises from bone marrow or immature thymocytes cells in the thymus. 60% of the T-ALL cases arise from chromosomal translocations which produce the activation of Notch1 constitutively (Ellisen et al., 1991). Since the discovery of Notch as oncogene responsible for T-ALL, many more investigations have extended this research, and confirming the implication of the Notch signalling dysregulation in adult T-ALL (Asnafi et al. 2009; Mansour et al. 2009; Trinquand et al. 2013; Vadillo et al. 2018). Ligand independent activation is the most common mechanism of activation in these types of leukaemias where NRR mutations expose the S2 cleavage site of Notch1 receptor, activating it in the absence of the ligand. Notch1 is the primary responsible oncogene for most of the T-ALL oncogenic subtypes (Weng et al. 2004) except for early T-cell precursor ALL (ETPALL) which is a primitive form of T-All (Coustan-Smith et al. 2009). In this type of leukaemias, Notch1 mutation is less frequent (11-38%).

These Notch1 mutations can be classified into two clusters based on the protein region where the mutation occurs. These two clusters dysregulate the Notch signalling trough different mechanisms (See Figure 3.6).

Cluster 1: This group harbours the most common Notch1 mutations in human T-ALL (Weng et al. 2004; Mansour et al. 2006; Chiang et al. 2016; McCarter et al. 2018) that affects to the heterodimerization domain of the NRR (amino acid substitution and

in-frame insertions) and the juxtatransmembrane domain (jTMD, in-frame insertions). Mutations in this region cause ligand independent Notch1 signalling and can be classified in 3 mechanistic types:

- *Class 1 mutations*: Affect the heterodimerization domain (HD). It can be caused by amino acid substitutions and short deletions or insertions. It is divided into two subtypes: *Class 1A mutations* where the extracellular domain is separated from the transmembrane domain. *Class 1B mutations* which induce structural changes of the HD increasing the S2 site exposure (Malecki et al. 2006).
- *Class 2 mutations* are insertions of short peptides next to the C-terminal end of the HD that duplicate the S2 cleavage site (e.g., A1721_V1722InsARLGSLNIPYKIEA) or a juxtamembrane expansion (JME) which is caused by an insertion of 17 amino acids peptide (QAVEPPPPAQLHFMYVA) at position 1740 of Notch1 receptor (Malecki et al. 2006; Sulis et al. 2008).
- *Class 3 mutations:* Affect the third LNR located in the NRR, and it disconnects this LNR from the HD, possibly due to loss of calcium (Gordon et al. 2009b). Together, all these mutations induce ligand independent changes that unmask the S2 cleavage site and generate the active form of Notch intracellular domain (NICD).

Cluster 2: The second hotspot of Notch1 mutations corresponds to nonsense or frameshift mutations (insertion or deletions) that affect the C-terminal PEST domain which regulates the degradation of NICD (Chiang et al. 2006, 2016). Mutations in this region depend on ligand activation. These mutations stabilize the active fragment from Notch (NICD) and therefore Notch activation is increased. Specifically, PEST mutations remove the Degron site (a small portion of the protein which regulates the degradation rates) that are phosphorylated for different types of kinases (Chiang et al. 2016; McCarter et al. 2018) and targeted by the E3 ubiquitin-ligase f-box and WD repeat-containing protein 7 (FBXW7) (O'Neil et al., 2007; Pagliaro et al., 2020; Thompson et al., 2007). Therefore, mutations either in PEST or FBXW7 increase the half-life of NICD and stabilize it.

If mutations from cluster 1(NRR) and 2 (PEST-FBWX7) occurs in cis (at the same time), Notch activation is increased, which occurs in 20% of patients. However, Notch mutations in PEST without NRR mutations happen in 23% of patients (Weng et al. 2004).

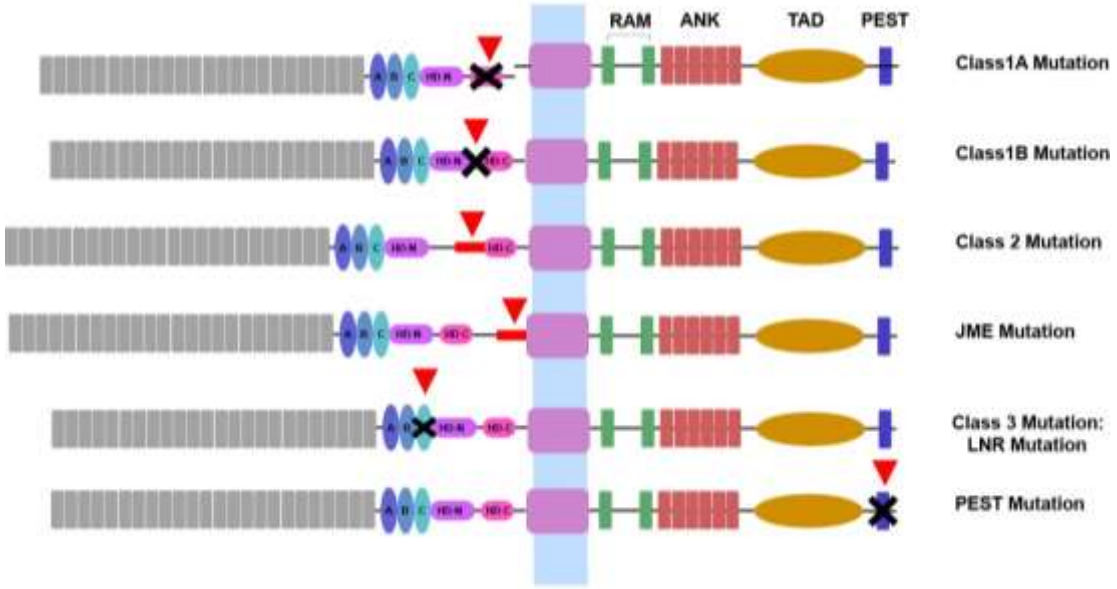

Figure 3.6. T-ALL mutations in NRR and ICD. Diagram simplifying the different mutations found on T-ALL in the LNR repeats, affecting heterodimerization domain (HD): Class 1, 2 and a novel juxtamembrane expansion (JME) mutation and in a subunit of the ICD (PEST).

As mentioned above, Notch mutation affecting the NRR of the Notch receptor is active in a ligand-independent manner, while mutations affecting PEST domain depend on ligand signal. However, some studies have suggested that ligand interactions with WT-Notch receptor can induce Notch activation in T-ALL. For instance, NRR mutations that trigger cleavage of Notch3 have not been observed even though they showed detectable Notch3 activation in 12 out of 24 patient-derived xenograft (PDX) samples and in 2/40 primary T-ALL samples. Therefore, this Notch3 activation might be a mutation ligand independent and dependent (Bernasconi-Elias et al. 2016). This suggestion is in line with studies showing that Notch3 receptor has the highest propensity for activation because its NRR conformation is less tightly closed in the autoinhibition state (Xu et al. 2015). Moreover, mutated NRR domain activates Notch signalling constitutively and responds to ligand-based on cell-based assay (Malecki et al. 2006). Besides, it has been shown that PDX with mutated or WT-Notch receptor responded to ligand stimulation (Armstrong et al. 2009). One strategy to treat this type

of ligand-dependent mutations would be by ligand inhibitors. For example, WT-Notch receptor signalling was inhibited by anti-Dll4 antibody in mice (Minuzzo et al., 2015) suggesting that ligand stimulations may play an important role in T-ALL.

AIMS

Cells are surrounded by a membrane that serves as a barrier between the inside of a cell and its environment. Moreover, in the cell surface there is a wide variety of proteins that inform the cell about different signals from the surrounding environment. Proteins reach the cell plasma membrane by a process named membrane trafficking pathway involved in transporting newly synthesized proteins in the endoplasmic reticulum to their destination, such as the plasma membrane and other organelles. Besides, membrane trafficking pathway also involves the internalization of extracellular component or plasma membrane proteins for recycling or degradative regulation.

Previous studies have shown that the Notch negative regulatory region (NRR) domain may be essential to regulate the surface display of native Notch receptor. For instance, Notch2 receptor lacking the S1loop has a regular display on the membrane while very few mutant S1loop Notch1 receptors can reach the cell surface (Gordon et al., 2009). Although few Notch1 receptors get the membrane, they can induce Notch activation, suggesting that S1 cleavage site is not necessary to trigger Notch signalling. Moreover, previous results from our laboratory showed that the original synthetic receptor (1d3NRRG4) was inefficiently displayed on the plasma membrane producing a high level of ligand independent background (Huang 2017).

On the other hand, *in vivo* experiments highlight that TRACT system presents different sensitivity in distinct neuronal circuits tested in *Drosophila* brain. This efficiency variations may occur because of the synaptic cleft length change between neuronal circuits. For instance, if the synaptic cleft separation is too large, the ligand and receptor interactions would be inefficient, and the induction would be almost undetectable. At the same time, if the synaptic cleft is too short, the ligand and receptor may not interact with each other.

To enhance the receptor display on the cell plasma membrane and boost the sensitivity of the TRACT system *in vivo*, in this Chapter of the Thesis, we have addressed the following objectives:

<u>Aim 1:</u> Determine the importance of Notch negative regulatory region (NRR) in the membrane trafficking pathway of the Notch receptor.

To improve the localization of the Notch receptor in the cell surface, we will generate Notch receptors without the NRR domain, in addition to engineered new chimeric receptor with several membrane proteins and test their induction efficiency *in vitro*.

<u>Aim 2:</u> Assess the implication of the S2 cleavage site distance from the cell surface for Notch activation.

To evaluate the importance of the S2 cleavage site distance from the cell membrane in the activation of the Notch receptor, we will generate Notch receptors with different lengths to separate or shorten S2 site and test their induction efficiency *in vitro.*

RESULTS

Previous works in our laboratory have observed that the engineered receptors used in TRACT technique was inefficiently displayed on the plasma membrane and produced a high level of ligand independent activation of the receptor. We hypothesized that our engineered receptors' inefficient plasma membrane display and ligand independent background activation could be due to their chimeric nature. For instance, there could be interference between the two extracellular domains from different proteins, LBD (from a single-chain antibody domain) and NRR (from Notch), along with their transit from the endoplasmatic reticulum (ER) to the plasma membrane. Indeed, several lines of evidence indicate that the NRR domain may be important to regulate the surface display of native Notch molecules. Notch receptor is a heterodimer encoded by a single gene, which is cleaved into the so-called S1 site within the NRR by Furin-like proteases (Gordon et al. 2009b). The two polypeptide chains of Notch are held together by disulfide bonds within the NRR. To investigate the possibility that the poor display of engineered receptors was due to the interference between the LBD and NRR in chimeric constructs, we compared the effects of including or omitting the NRR downstream the LBD on the ligand independent background activation of our engineered receptors.

3.3.1. Depletion of NRR Domain from Synthetic and Notch Receptors.

To investigate the role that NRR play in the ligand independent background, we generated two hybrid proteins: **(i)** hCARNRRG4 contains an LBD that recognizes the human CD19 (Porter et al. 2011) (hCD19), the 300 aa of NRR from hNotch1, the jTMD (12 aa) and TMD (24 aa) from hNotch1 and the yeast transcription factor Gal4 in its ICD. **(ii)** hCARnoNRRG4 contains the hCAR LBD, the jTMD and TMD of hNotch1 and Gal4, but does not have the NRR (Figure 3.7A). We observed no significant differences in the cell membrane display between hCARnoNRRG4 and hCARNRRG4 (data not shown), and that hCARnoNRRG4 had a level of ligand independent background higher than hCARNRRG4 (Figure 3.7C). Surprisingly, we observed that cells expressing hCD19 (the ligand that is recognized by the hCAR LBD) activated cells expressing hCARNRRG4 (the hybrid receptor with NRR) less efficiently than hCARnoNRRG4 (the hybrid receptor without NRR) (3.9-fold vs 10.68-fold respectively) (Figure 3.7B). The level of ligand independent activation for hCARnoNRRG4 is higher than the receptor with the NRR domain, suggesting that NRR plays a role in preventing the activation without the

presence of the ligand (Figure 3.7C and D) as has been observed in T-cell acute lymphoblastic leukemias (T-ALL; Ellisen et al., 1991).

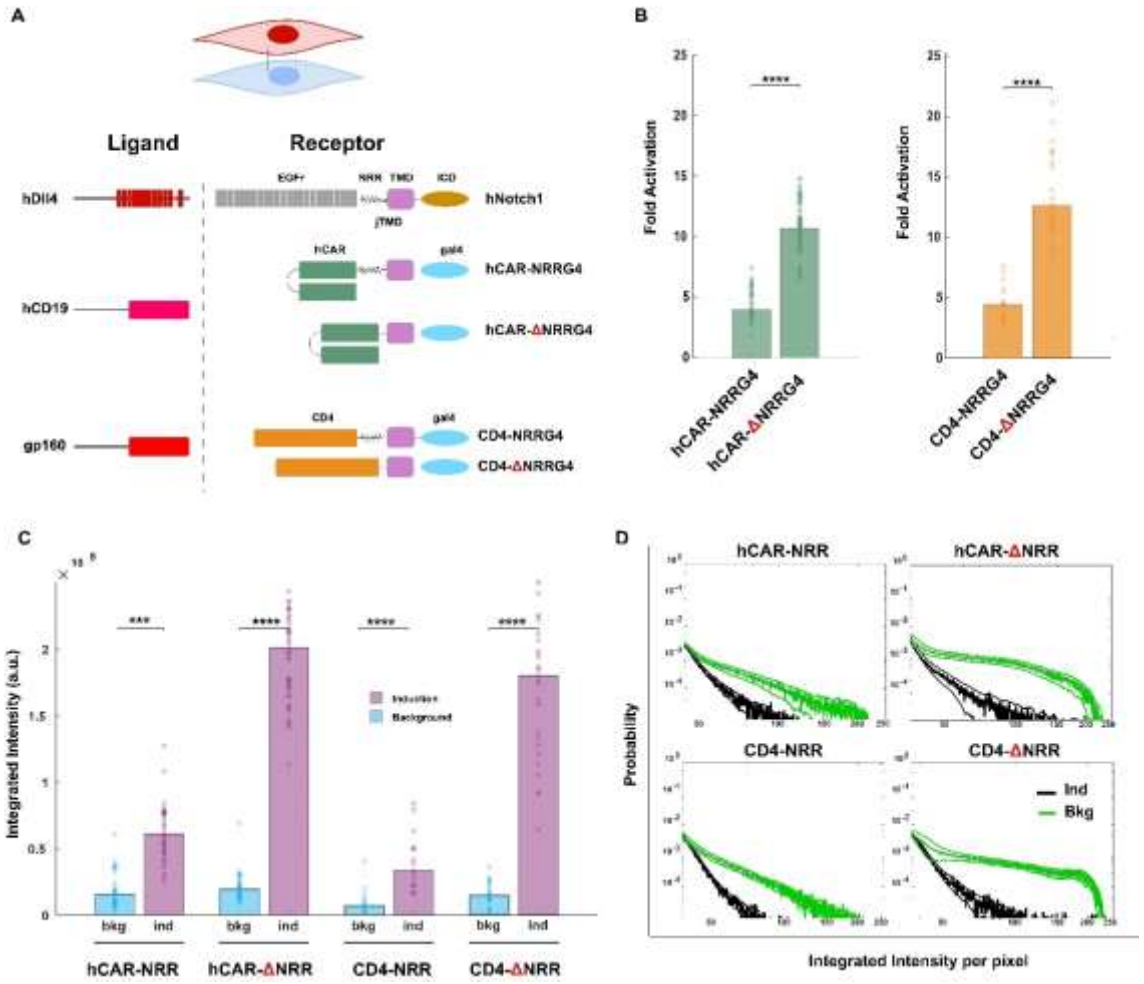

Figure 3.7. Ligand dependent activation of synthetic receptors without NRR. (A) Diagram showing ligand (hDll4) and receptor from Notch signalling pathway (top), and synthetic receptor (hCAR and CD4, as extracellular domain) with and without NRR, and its ligand hCD19 and gp160, respectively (middle and bottom). **(B)** Fold activation of synthetic receptors with and without NRR (left graphs hCAR as extracellular domain and right graph CD4). Note the significant difference between receptor carrying NRR or not for both extracellular domains (hCARNRRG4=4.35-fold, hCARnoNRRG4=10.68-fold, p-value=6.5 x 10^{-5}; CD4NRRG4=4.90-fold, CD4noNRR=12.06-fold, p-value=3.69 x 10^{-8}). **(C)** Integrated intensity of induction and background showing higher significant differences for receptors without NRR (see table 1 from ANNEX 3). P-values between induction and background integrated intensity: hCARNRRG4=1.95 x 10^{-12}; hCARnoNRRG4=3.12 x 10^{-15}; CD4NRRG4=7.54 x 10^{-6}; CD4noNRRG4=3.03 x 10^{-10}. **(D)** Histograms showing normalized probability distribution of intensities above the threshold (median is shown as solid lines and standard deviation shown as thin lines). The green trace is ligand dependent activation, and the black trace is ligand independent activation.

Because hCARnoNRRG4 did not contain the NRR, we wondered whether the hCAR domain could act as a ligand dependent mechanosensor playing a similar role than the NRR domain from Notch receptor. To test this idea, we generated new hybrid receptors containing or lacking the NRR, in which the LBD was switched from hCAR to the ECD from the human CD4 glycoprotein (Figure 3.7A). **(i)** CD4NRRG4 contains the ECD from the CD4 followed by the hNotch1 NRR, jTMD and TMD of hNotch1 and Gal4. **(ii)** CD4noNRRG4 includes the ECD from the CD4 followed by the jTMD and TMD of hNotch1 and Gal4 but does not contain NRR. We produced cells expressing CD4NRRG4 and CD4noNRRG4, by placing them on a plastic surface coated with an antibody that recognizes CD4, we confirmed that immobilized ligand could trigger activation of this engineered receptor. Again, we observed that CD4NRRG4 and CD4noNRRG4 had comparable levels of induction, despite the fact that CD4noNRRG4 did not have the NRR domain (Figure 3.10C). This result indicates that it is possible to obtain ligand dependent cleavage of engineered molecules without NRR and two different LBDs (CD4 or hCAR). Also, we observed that adding the antibody against the ECD of CD4 or hNotch1 into the cell culture medium failed to slightly activate the synthetic receptors and Notch receptors with and without NRR, indicating that activation of our engineered receptors requires a mechanical force that cannot be generated by ligands in solution (Figure 3.8).

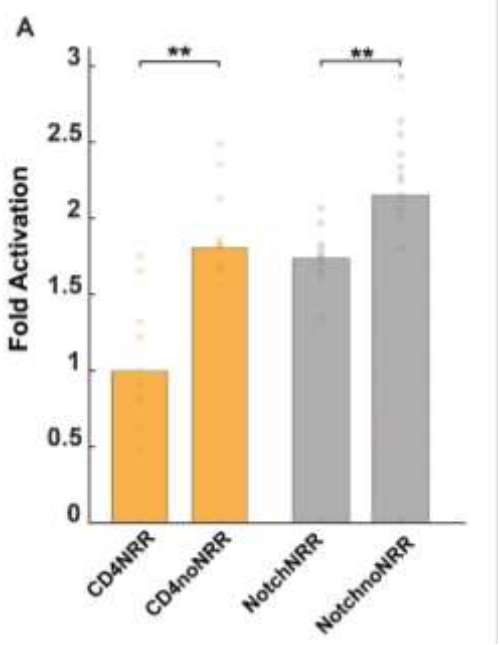

Figure 3.8. Ligand independent activation by antibody solution. Fold activation of the engineered receptors and Notch receptors with and without NRR. Very low fold activation is shown for both sets of constructs with and without NRR (CD4NRR=1.00±0.39-fold, CD4noNRR=1.69±0.28-fold; p-value=1.01 x 10^{-3} and

NotchNRR=1.63±0.17-fold and NotchnoNRR=2.17±0.18-fold; p-value=6.53 x 10^{-3}). The fold activation results from dividing the integrated intensity of the receptors' background by the integrated intensity of the reporter cell line by itself.

In addition, our result also suggests that receptor activation is force dependent. It is possible that the binding between the immobilized anti-CD4 antibody and the CD4noNRRG4 could trigger activation of the receptor because the binding of antibody-antigen is essentially irreversible, and it may generate stretching forces that are not seen under physiological conditions. To study the ligand-receptor interaction with binding forces commonly observed in physiological conditions, we generated cell lines expressing the HIV glycoprotein gp160 (Mao et al. 2012), which binds to human CD4 to enable entry of HIV into T-lymphocytes. After mix cells expressing gp160 with cells carrying CD4NRRG4 or CD4noNRRG4, we observed activation of both receptors (Figure 3.7B). CD4noNRRG4 showed a higher level of background and higher integrated intensity activation (Figure 3.7C and D). Moreover, CD4noNRRG4 showed a fold activation almost three times higher than CD4NRRG4 (12.04-fold versus 4.8-fold; Figure 3.7B) with no significant differences in the cell membrane display between both receptors (Figure 3.9).

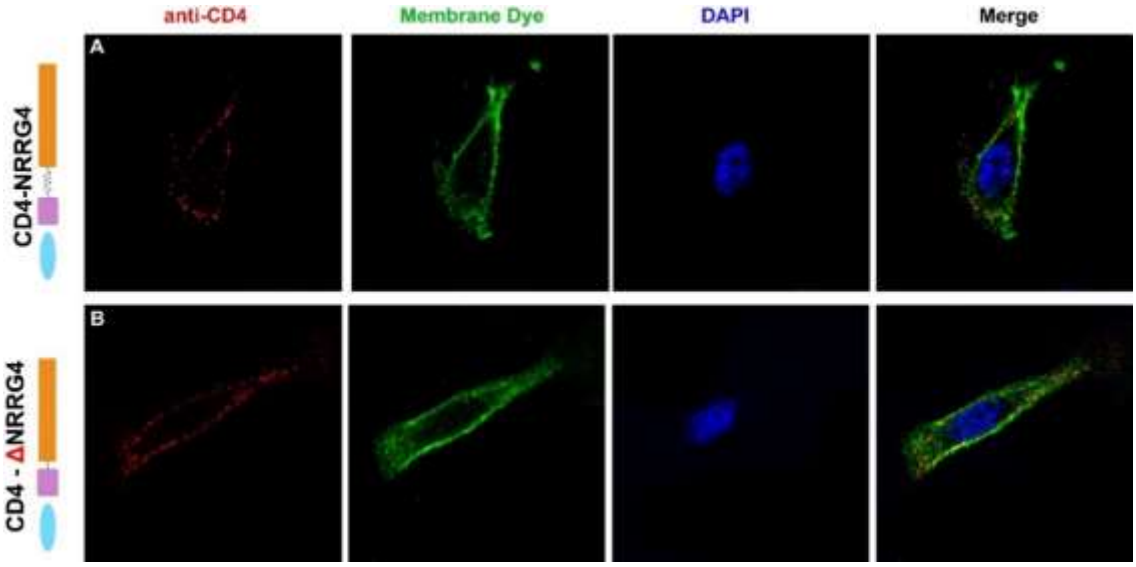

Figure 3.9. Cell membrane display of CD4NRRG4 and CD4noNRRG4. (A) CD4 labeling the extracellular domain of CD4NRRG4 receptor did not show differences compared to CD4noNRRG4 **(B).**

These results are unexpected because the ECDs of hCARnoNRRG4 or CD4noNRRG4 do not contain the canonical S2 site (in the NRR) that is usually cleaved upon ligand-receptor interaction in the Notch signalling pathway. Next, we examined whether the activation of hybrid receptors lacking NRR occurs by a mechanism similar to Notch receptor, requiring ADAM proteases (for an S2-like cleavage), and γ-secretase (for an S3 cleavage). First, we added a cocktail of ADAM protease blockers to the cell culture medium: Batismastat, GM6001 and TAPI (Figure 3.10A). In this case, we observed a strong reduction of ligand dependent activation of CD4NRRG4 and CD4noNRRG4 receptors upon ligand binding (Figure 3.10B and C). This reduction is stronger than the engineered receptor with NRR (CD4NRR=81.30% vs CD4noNRR=93.34%). Because ADAM protease blockers are not strictly specific for any individual member of the ADAM metalloproteases, we generated cell lines in which the ADAM10 gene (the key ADAM member involved in ligand dependent Notch activation) was knockout by CRISPR/CAS9 (Figure 3.11A). We observed that CD4NRRG4 or CD4noNRRG4 did not exhibit ligand dependent cleavage in ADAM10 knockout cell lines (Figure 3.11C) (85% reduction vs 115% reduction, respectively). In addition, the western blot for the ablation of ADAM10 in CD4NRRG4 and CD4noNRRG4 cell lines showed no presence of ADAM10 protein vs the control cell lines infected with scramble CRISPR/CAS9 (Figure 3.11B). These observations indicate that although there is no NRR or canonical S2 site in the CD4noNRRG4 receptor, the interaction of CD4noNRRG4 with gp160 triggers an S2-like cleavage similar to that observed when Notch receptor binds to its ligands (delta, jagged and serrate). Second, the γ-secretase blocker DAPT completely abolished the reporter's activation upon CD4NRG4 or CD4noNRRG4 interaction with its ligands (107% vs 98%, Figure 3.10B and C), indicating that the activation of the receptor required intramembrane proteolysis mediated by γ-secretase. Therefore, these results suggest that the CD4noNRRG4 receptor activation occurs by a similar mechanism observed in Notch-ligand interactions, even though the NRR domain is not present in this engineered receptor.

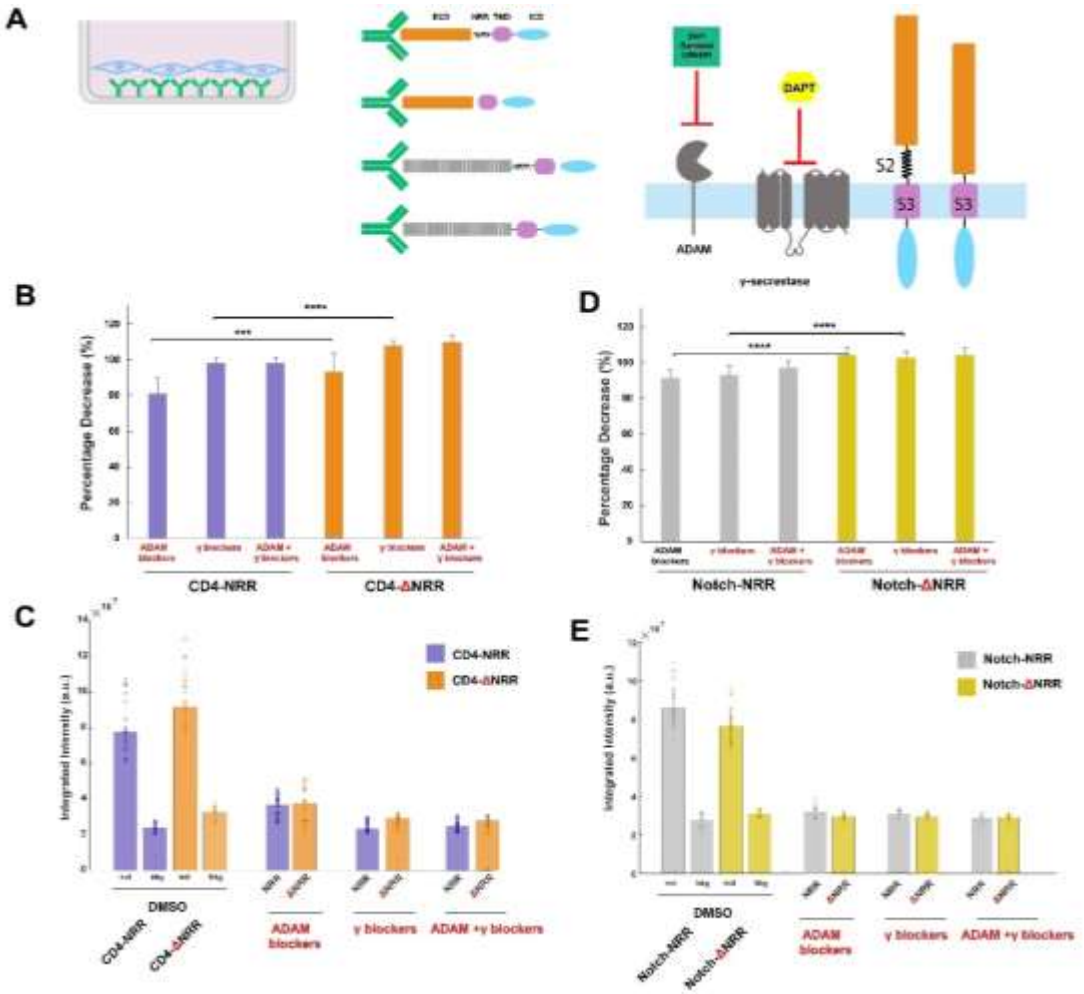

Figure 3.10. Effect of ADAM and γ-secretase blockers on ligand dependent activation of synthetic and original Notch with and without NRR. (A) *(Left)* Diagram showing the interaction between the receptors, and *(Right)* antibody against the extracellular domain and the different blocker inhibiting ADAM or γ-secretase. **(B)** Percentage decrease of the induction from synthetic receptors because of different blocker. Note that ADAM blockers reduce the induction by 81.30% for CD4NRRG4 and 93.34% for CD4noNRRG4; p-value=3.50 x 10^{-4} while DAPT reduce 98.15% for CD4NRRG4 and 107.76% CD4noNRRG4; p-value=7.31 x 10^{-8}, respectively. In addition, comparison of ADAM and gamma blockers for CD4NRR (p-value=1.45x10^{-7}) and CD4noNRR (p-value=1.34x10^{-5}). **(C)** Overall intensity of induction, background, and reduction of the induction for CD4NRR (purple) and CD4noNRR (orange). **(D)** Percentage decrease of the induction from Notch receptors because of different blockers. Note that ADAM blockers reduce the induction by 91.72% for NotchNRRG4 and 104.48% NotchnoNRRG4; p-value=4.46 x 10^{-8}, while DAPT reduces the induction by 93.29% for NotchNRRG4 and 102.76% NotchnoNRRG4, p-value=4.17 x 10^{-7}, respectively. In addition, comparison of ADAM and gamma blockers for NotchNRRG4 (p-value=0.174) NotchnoNRRG4 (p-value=0.796). **(E)** Overall Intensity of induction, background and reduction of the induction for NotchNRR (gray) and NotchnoNRR (green).

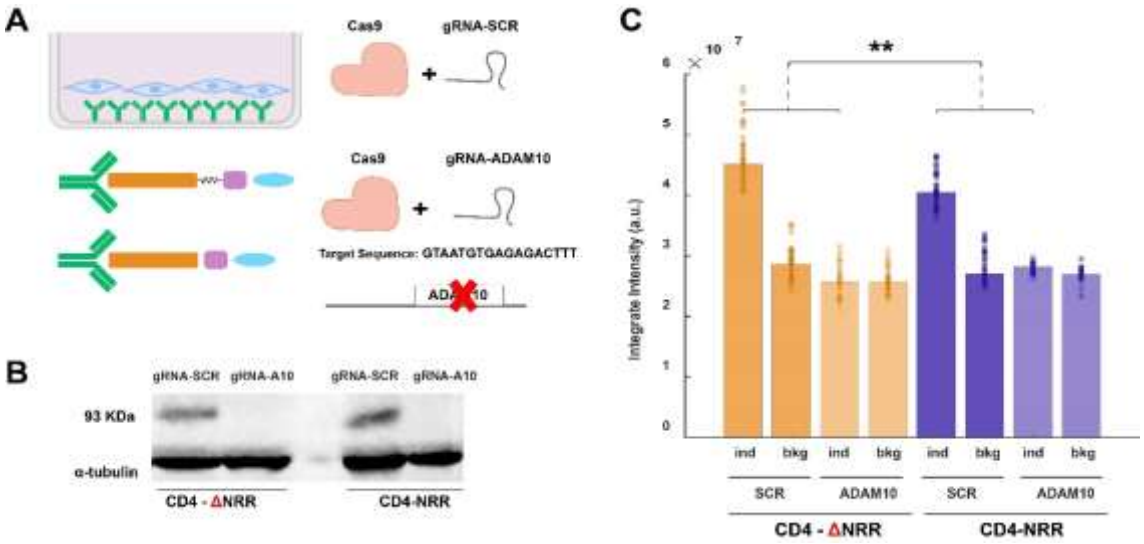

Figure 3.11. Effect of ADAM10 protease ablation. (A) *Left:* Diagram showing how the cell lines and experiment were performed. *Right:* Strategy to ablate ADAM10 protease in CD4NRRG4 and CD4noNRRG4 cell lines. **(B)** Western blot showing the ablation of ADAM10 protein from receptor cell lines infected with CRISPR-Cas9 and a gRNA against ADAM10 gene. A scramble gRNA was used as control. α-tubuline was shown as a control (55KDa). **(C)** Percentage decrease of ligand dependent activity when ADAM10 is knockout. Note that CD4noNRRG4 showed a percentage decrease of 115.86% compared to 80.84% for CD4NRRG4, p-value=0.0072.

Our data showed that engineered receptors lacking NRR can be activated by ligand binding through a similar mechanism to that observed in Notch pathway. To investigate whether the NRR domain is essential for triggering Notch signalling by ligand binding, we engineered new receptors using Notch1 receptor. The ECD can be subdivided into three main domains: the LBD consisting of 36 EGF repeats, the NRR domain, and the jTMD (Kopan and Ilagan 2009). To further examine the role of NRR on Notch signalling pathway, we generated the following constructs: **(i)** the receptor named 1-36NRRjTMDG4 or NotchNRRG4, encoding the 36 EGF repeats of human notch1 ECD, the hNotch1 NRR, the jTMD and TMD of hNotch1 and Gal4, and **(ii)** the receptor named 1-36noNRRjTMDG4 or NotchnonRRG4, encoding the 36 EGF repeats of hNotch1 ECD, the jTMD and TMD of hNotch1 and Gal4, without NRR (Figure 3.12A). We investigated the inducibility of the modified Notch receptor, with and without NRR domain, using two methods: **(a)** coated antibody that recognizes the N-terminus domain of hNotch1 (Figure 3.10A, D and E), and **(b)** cell-cell interaction using as ligand a cell line expressing human Delta4, one of the ligands for Notch (Figure 3.12A). We observed that NotchNRR present higher fold activation than NotchnoNRR (Figure 3.12B) due to the ligand

independent cleavage. The induction showed pretty similar levels of integrated intensity for both receptors (Figure 3.12C and D). Furthermore, we observed that the activation of the hNotch1 receptor lacking NRR could also be inhibited by the ADAM metalloprotease blockers (batismastat, GM6001 and TAPI) 104.08% compared to 91.72% for NotchNRRG4 (Figure 3.10D and E). This result suggests that even in the absence of NRR domain, or a S2 site, ligand binding to 1-36noNRRjTMDG4 receptor triggers a cleavage mediated by ADAMs metalloproteases. Moreover, the γ-secretase blocker DAPT completely abolished the reporter's activation for NotchNRRG4 and NotchnoNRRG4 (93.29% vs 102.76%, Figure 3.10D and E), indicating that the activation of Notch receptor without NRR also requires intramembrane proteolysis mediated by γ -secretase. These experiments indicate that both engineered hybrid receptors (hCARnoNRRG4 or CD4noNRRG4) and hNotch1 receptor (1-36noNRRjTMDG4) lacking the NRR domain can be induced by ligand dependent cleavage. Paradoxically, even though there is no canonical S2 cleavage site in the hCARnoNRRG4, CD4noNRRG4, or 1-36noNRRjTMDG4 constructs, ligand dependent induction is inhibited for all these receptors by the ADAM blockers. Our results suggest that receptors lacking the NRR domain present a potential S2-like site cleaved in a ligand dependent manner.

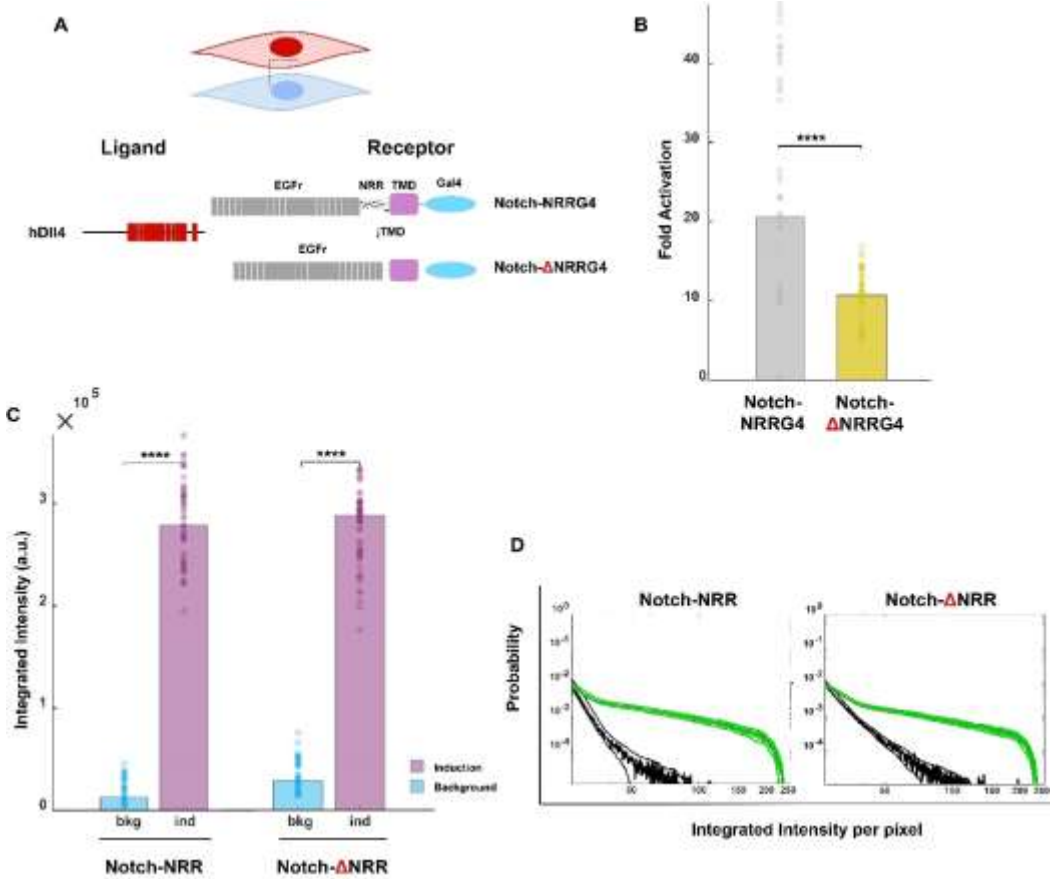

Figure 3.12. Ligand-dependent activation of Original Notch receptor without NRR. (A) Diagram showing original Notch receptor with and without NRR and its ligand Dll4. **(B)** Fold activation of both receptors. Notice that NotchnoNRR showed a fold activation lower than NotchNRR (NotchNRR=20.49-fold; NotchnoNRR=10.80-fold; p-value=1.49 x 10^{-7}) due to the ligand independent activation of NotchnoNRR. **(C)** Note that both receptors' ligand dependent activity reaches a pretty similar level, being the main difference the background integrated intensity (p-value between induction and background, NotchNRR=3.30 x 10^{-18}; NotchnoNRR=3.55 x 10^{-21}. Integrated intensity: NotchNRR: bkg=1.22 x 10^4±1 x 10^4, ind=2.79 x 10^5±0.45 x 10^5; NotchnoNRR: bkg=2.88 x 10^4±1.50 x 10^4, ind=2.89 x 10^5±0.57 x 10^5. **(D)** Histograms indicated the distribution of the probability to find an induced cell with specific integrated intensity above the threshold. The green trace is ligand dependent activation, and the black trace is ligan independent activation.

3.3.2. Replacement of Human Notch1 jTMD

The hNotch1 jTMD included in our receptors is composed of 12 aa (QSETVEPPPPAQ) starting after the canonical hNotch1 S2 cleavage site (Ala/Val) until the first amino acid of the TMD (Leu). To investigate whether the cleavage of our engineered receptors was happening on the jTMD or the TMD, we generated two new constructs: **(i)** CD4noNRRCD4jTMDG4, which contains the CD4 ECD, including the CD4 LBD, the CD4 jTMD followed by the hNotch1 TMD and Gal4 ICD, and **(ii)** CD4noNRRN1jTMDG4, which includes the CD4 LBD, both the jTMD and TMD of hNotch1 and Gal4 ICD (Figure 3.14A). In cell-cell interaction experiments, we observed that a cell line expressing CD4noNRRCD4jTMDG4 receptor (containing the CD4 jTMD) had no induction upon mixing with cells expressing the ligand gp160 (1.09-fold activation). In contrast, a cell line expressing the CD4noNRRN1jTMDG4 receptor (containing the hNotch1 jTMD) had >10-fold induction (11.94-fold) upon ligand binding (Figure 3.14B). This result indicates that the hNotch1 TMD is not sufficient for the engineered receptors' ligand dependent activation. Instead, it suggests that the 12 aa of the hNotch1 jTMD could contain an S2-like cleavage site acting as a ligand dependent mechanosensor.

Next, we investigated whether the jTMD of the Notch receptors from different species can also act as ligand dependent activation domains. We generated new synthetic receptors in which the jTMD from chicken Notch1, Xenopus Notch1, zebrafish Notch1, human Notch2, and *Drosophila* Notch were placed between CD4 ECD and

hNotch1 TMD (CD4noNRR**ch**jTMDG4, CD4noNRR**x**AjTMDG4, CD4noNRR**zf**jTMDG4, CD4noNRR**hN2**jTMDG4, and CD4noNRR**d**jTMDG4) (Figure 3.13A). In cell-cell interaction experiments, we observed that Notch jTMDs from different species were sufficient to induce ligand dependent cleavage of the hybrid receptors in the absence of NRR domain (Figure 3.13B). Interestingly, receptors with the jTMD from chicken, Xenopus and zebrafish showed a fold activation almost identical among them (7.42-fold, 7.93-fold, and 7.48-fold, respectively) but lower than hNotch1 jTMD (11.63-fold) (Figure 3.13B). However, hNotch2 and *Drosophila* jTMD showed a fold increase almost 3 times lower than CD4noNRRG4 (observe the ligand independent activation) (Figure 3.13B and C). The distribution of the probability to find a cell with a certain intensity is shown in Figure Sup. 3.13 ANNEX4. These experiments indicate that short sequences (12aa) as the jTMD of different Notch receptors can act as ligand dependent mechanosensors when are placed in heterologous molecules. Besides, molecular dynamics of the aa sequence of the jTMD from the different species, showed that the core of these jTMDs exhibited a strong electronegative (negative charged amino acid placed N-terminal to the plasma membrane) surface similar to human Notch1 which may help them to stick out from the membrane. However, *Drosophila* jTMD has the negative charged amino acid next to the plasma membrane Glutamic Acid (E) (Figure 3.13D).

Figure 3.13. Ligand dependent induction by Notch jTMD from different species. (A) Diagram showing the amino acid sequences of the Notch jTMD from different species. **(B)** Fold activation of the Notch jTMD of different species showed that chicken, zebra fish and Xenopus present a similar fold activation among them and lower than hNotch1jTMD. hNotch2 and *Drosophila* jTMD also showed lower activation levels while dNotchNOpro has the lowest fold activation (hNotch1=11.63-fold, hNotch2=4.16-fold, p-value(hN2)=3.85 x 10^{-10}; chNotch=7.43-fold, p-value(ch)=1.65 x 10^{-7}; zfNotch=7.97-fold, p-value(zf)=5.10 x 10^{-6}; xNotch=7.48-fold, p-value(x)=8.10 x 10^{-7}; dNotch=3.77-fold, p-value(d)=7.35 x 10^{-10}; and dNotchNOpro=2.53-fold, p-value(NOpro)=3.12 x 10^{-10}). **(C)** Integrated intensity for the background and induction indicated that most of the species except hNotch1 had a higher ligand independent activation, showing a significant difference for *Drosophila* and its derivate; see table 2A from ANNEX 3 (p-values between induction and background, hNotch1=7.36 x 10^{-20}, hNotch2=8.00 x 10^{-10}, chNotch=1.06 x 10^{-13}, zfNotch=6.60 x 10^{-14}, xNotch=3.04 x 10^{-13}, dNotch=3.06 x 10^{-9}, and dNotchNOpro=6.05 x 10^{-9}). **(D)** Dynamic model predictions of electrostatic charges for different Notch species jTMD.

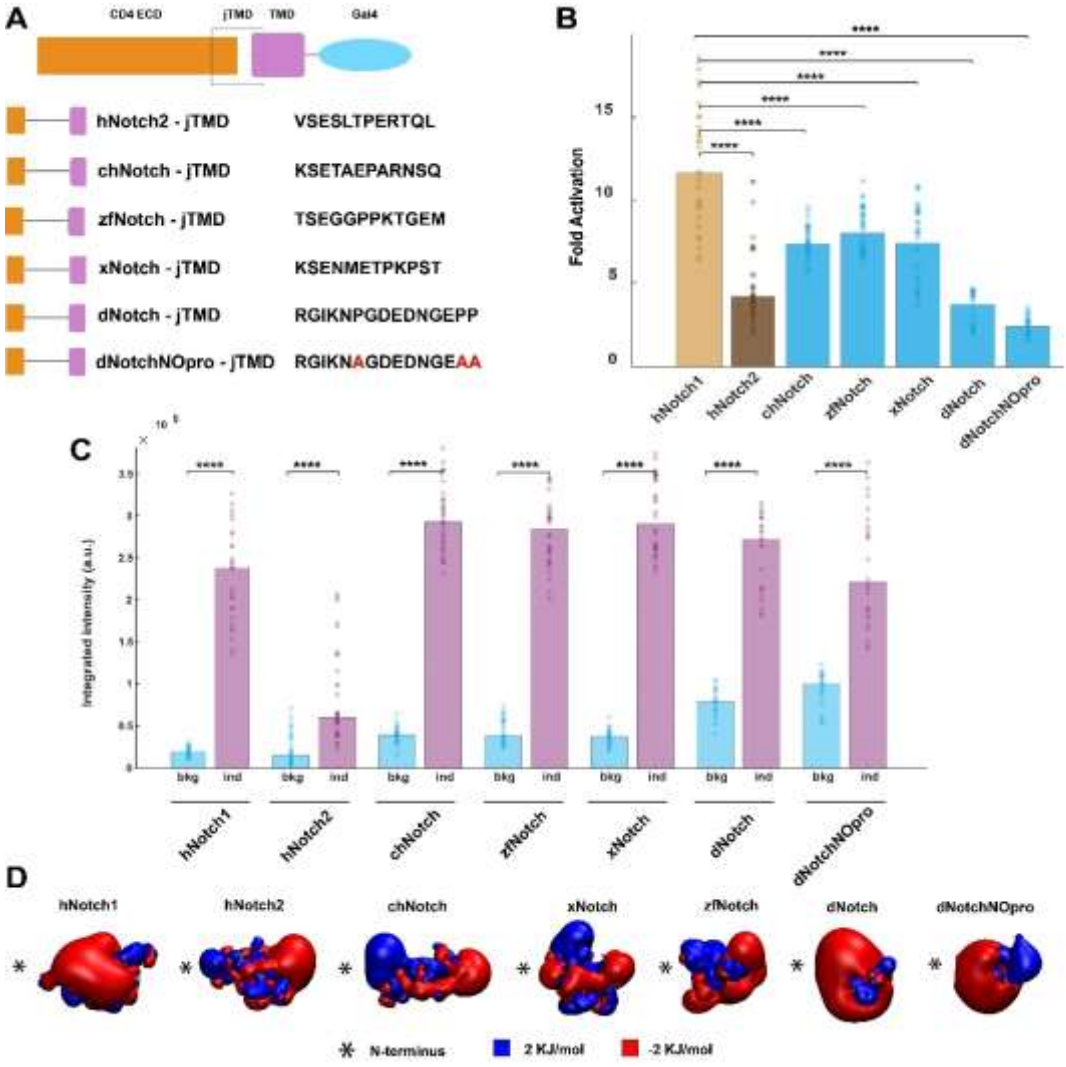

To test whether the jTMD from other molecules unrelated to Notch could act as mechanosensors, we generated constructs encoding the CD4 LBD followed by 12 aa of the jTMD from E-Cadherin, NCAM, and erBb4 (long and short), the hNotch1TMD and Gal4 ICD (CD4noNRRE**Cadh**jTMDG4, CD4noNRR**NCAM**jTMDG4, CD4noNRR**shorterbB4**jTMDG4, and CD4noNRR**longerbB4**jTMDG4) (Figure 3.14A). It has been reported that these three membrane proteins can be cleaved by ADAMs proteases, although the mechanism of activation is mechanosensing independent (Maretzky et al. 2005; Higashiyama et al. 2011; Brennaman et al. 2014). By cell-cell interaction experiments, we observed that cells expressing CD4noNRRE**Cadh**jTMDG4, CD4noNRR**NCAM**jTMDG4, CD4noNRR**shorterbB4**jTMDG4 receptors were activated upon mixing with cells expressing the ligand gp160 (8.23-fold, 6.49-fold, and 6.43-fold, respectively). This result indicates that short jTMD sequences from cell surface molecules other than Notch receptor can be grafted onto hybrid molecules to render

them ligand inducible (Figure 3.14B). On the other hand, CD4noNRR**longerbB4**jTMDG4 did not show any activation despite the high ligand independent activation (Figure 3.14C). It is possible that having so much background, the receptor cannot be induced because it had reached the maximum level of activation. Cell line expressing a lower level of CD4noNRR**longerbB4**jTMDG4 receptor showed approximately 3 times less ligand independent background, but they were not induced (see Figure Sup. 3.14 from ANNEX 4, CD4noNRR**longerbB4**jTMDG4 (-5x)). In addition, molecular dynamic models of the sequence of aa of the jTMD of these membrane proteins were predicted using VMD software (Figure 3.14D). The receptors that were activated upon ligand binding showed an electronegative surface.

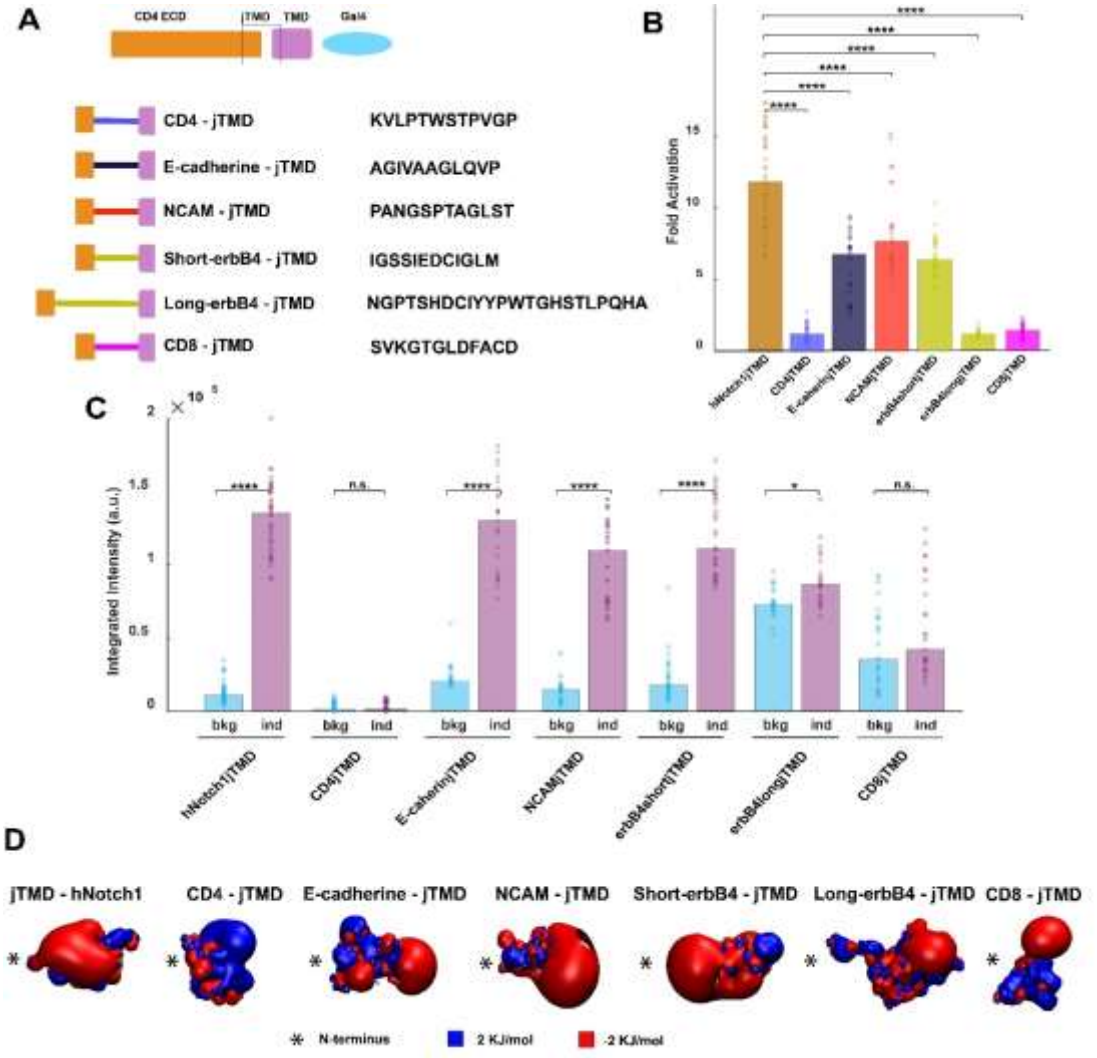

Figure 3.14. Ligand dependent induction by jTMD of different membrane proteins. (A) Schematic representation showing the jTMDs from different membrane proteins and their amino acid sequences. **(B)** Fold activation showing that CD4jTMD, CD8jTMD, and erbB4longjTMD are not induced (1.09-fold, 1.40-fold, and 1.68-fold, respectively). E-

cadherinjTMD, NCAMjTMD, and shorterbB4jTMD showed similar fold activation but lower than hNotch1jTMD (6.49-fold, 8.24-fold, and 6.43-fold, respectively). **(C)** CD4jTMD showed the lowest integrated intensity for the background and induction compared to CD8jTMD and erbB4longjTMD that are also not induced (p-values between induction and background, CD4jTMD=0.2807, CD8jTMD=0.093, and erbB4longjTMD=0.01). Note that the induction and background for E-cadherinjTMD, NCAMjTMD, and erbB4shortjTMD is similar than hNotch1jTMD but the fold activation is lower as shown in **B** (p-values between induction and background hNotch1jTMD=3.12 x 10^{-15}, E-cadherinjTMD=3.03 x 10^{-3}, NCAMjTMD=7.46x10^{-6}, erbb4shortjTMD=4.79x10^{-5}). See table 4A from ANNEX 3. **(D)** Dynamic model predictions of electrostatic charges for the different membrane proteins jTMDs. Note that CD4jTMD present an overall positive charge compared to the rest of jTMD of the different membrane proteins.

3.3.3. Modifications of Human Notch1 jTMD sequence.

In hNotch1, the S2 site inside NRR is cleaved between Ala and Val, which are located 14 and 13 aa upstream of the TMD, respectively. However, constructs missing the NRR domain but maintaining the 12 aa of the hNotch1 jTMD (after Val) still showed induction. A cursory inspection of the sequence of the different jTMDs does not reveal any obvious motif or pattern (see electrosurface predictions in Figure 3.15D) but we noticed that the amino acid Proline appeared in those sequences with a higher frequency than expected in a random distribution. Proline is the only amino acid that can be present in either cis or trans conformation in a polypeptide. Moreover, previous experiments have indicated that Proline isomerization is responsible for various conformational changes in proteins, during folding, upon neurotransmitter binding to receptors, or in cytoskeletal proteins under tension (Schmidpeter et al. 2015). Therefore, we decided to change the Prolines in the jTMD of dNotch (Figure 3.13) and hNotch1 (modif.6 in Figure 3.15) and observed that the Pro-Ala jTMD maintained their ability to act as ligand dependent activating domains (Figure 3.13B and Figure 3.15B, respectively). It suggests that perhaps there is no stringent requirement in the sequence of different jTMDs to act as ligand dependent cleavage domains. To further investigate whether there are critical aa sequences in the hNotch1jTMD for mechanotransduction of the receptor signalling, we generated several constructs with the following modifications of the hNotch1jTMD(QSETVEPPPPAQ): **(i)** Q***A***ETVEPPPPAQ (switching S to A, modif. 1), **(ii)**Q***E***ETVEPPPPAQ (switching S to E, modif. 2), **(iii)** QS***S***TVEPPPPAQ (switching E to S, modif. 3), **(iv)** QSETVE***AAAAAA*** (switching PPPPAQ to

AAAAA, modif. 4), and **(v)** QSET***AAAAAAAA*** (switching VEPPPAQ to AAAAAAA, modif. 5) (Figure 3.15A). Furthermore, we replaced the entire hNotch1 jTMDby 12 Alanies and 12 Glicines, two simple and unstructured polypeptides. None of the first three modifications in the sequence of the jTMD impaired the ligand induced activation of the receptors (Q***A***ET 9.98-fold, Q***E***ET 10.16-fold, QS***S***T 10.33-fold versus hNotch1jTMD 11.96-fold) (Figure 3.15B). However, switching either the last 6 aa or 8 aa to Alanine at the C-terminus reduced the fold activation from almost 12 points to 5 points (modifs. 4 and 5 in Figure 3.15B). Moreover, the level of ligand independent activation for these two constructs is more than 3 times higher that hNotch1jTMD (Figure 3.15C and Fig.Sup3.15) (see Table 5A from ANNEX 4 for values). In addition, we analyzed whether the composition of the overall charges for the modifications of hNocth1jTMD may affect the conformation of these different peptides (Figure 3.15D). These molecular dynamic prediction models showed an overall negative charge of the jTMD for all the modifications except for 12A and 12G, which are nonpolar amino acids. Finally, to test the hypothesis that even sequences with any random structure could act as mechanoreceptors, we generated constructs in which the jTMD consisted of a stretch of 12 Ala or 12 Gly, two sequences which do not possess any defined structure. Interestingly, even these jTMDs exhibited ligand triggered activation, albeit it was significantly weaker than that observed with the hNotch1-jTMD (approximately 3-fold versus 12-fold). Several studies predict polyAlanine polypeptide to be an alpha helix. However, it seems that the alpha helix is not so stable in aqueous solution, and it exists as a mixture of helices and other conformers (Lewis et al. 2001). This hypothesis may explain why there is some cleavage (Figure 3.15B), even the few times that the helix does form.

Figure 3.15. Ligand dependent induction from several modifications of the hNotch1jTMD. (A) Schematic representation showing the different modifications of the hNotch1jTMD (QSETVEPPPPAQ). **(B)** Similar fold activation was observed for modif. 1(Q***A***ETVEPPPPAQ), modif. 2(Q***E***ETVEPPPPAQ), modif. 3(QS***S***TVEPPPPAQ), and modif. 6 (QSETVE***AAAA***AQ) without significant difference compared to hNotch1jTMD (hNotch1jTMD=11.96-fold; modif. 1=9.95-fold; modif. 2=10.16-fold; modif. 3=10.33-fold; modif. 6=9.62-fold). Note that modifications at the C-terminus reduce the fold activation by two times (modif. 4 (QSETVE***AAAAAA***)=5.80-fold; modif. 5

(QSET***AAAAAAAA***)=4.77-fold), while undefined structure such as modif. 7 (12 Ala) or modif. 8 (12 Gly) bring the fold activation to approximately 3 points (modif. 7=3.52-fold; modif. 8=3.24-fold). **(C)** Integrated intensity for the background and induction indicated that modifs 4, 5, 7, and 8 presented higher levels of background than the hNotch1jTMD, (see table 5A from ANNEX 3) (p-values between induction and background: hNotch1jTMD=6.51 x 10^{-12}; modif. 1=1.55 x 10^{-6}; modif. 2=3.02 x 10^{-12}; modif. 3=1.66 x 10^{-6}; modif. 4=1.64 x 10^{-5}; modif. 5=1.24x10^{-5}; modif. 6=6.60 x 10^{-14}; modif. 7=3.23 x 10^{-17}; modif. 8=1.62 x 10^{-20}). **(D)** Model of electrostatic charges predictions for the different modifications of hNotch1jTMD showed similar overall charged except for modif. 7 and 8 (polypeptides with 12Ala and 12Gly, respectively) where their overall electrostatic charges were neutral due to the non-polar characteristic of these amino acids.

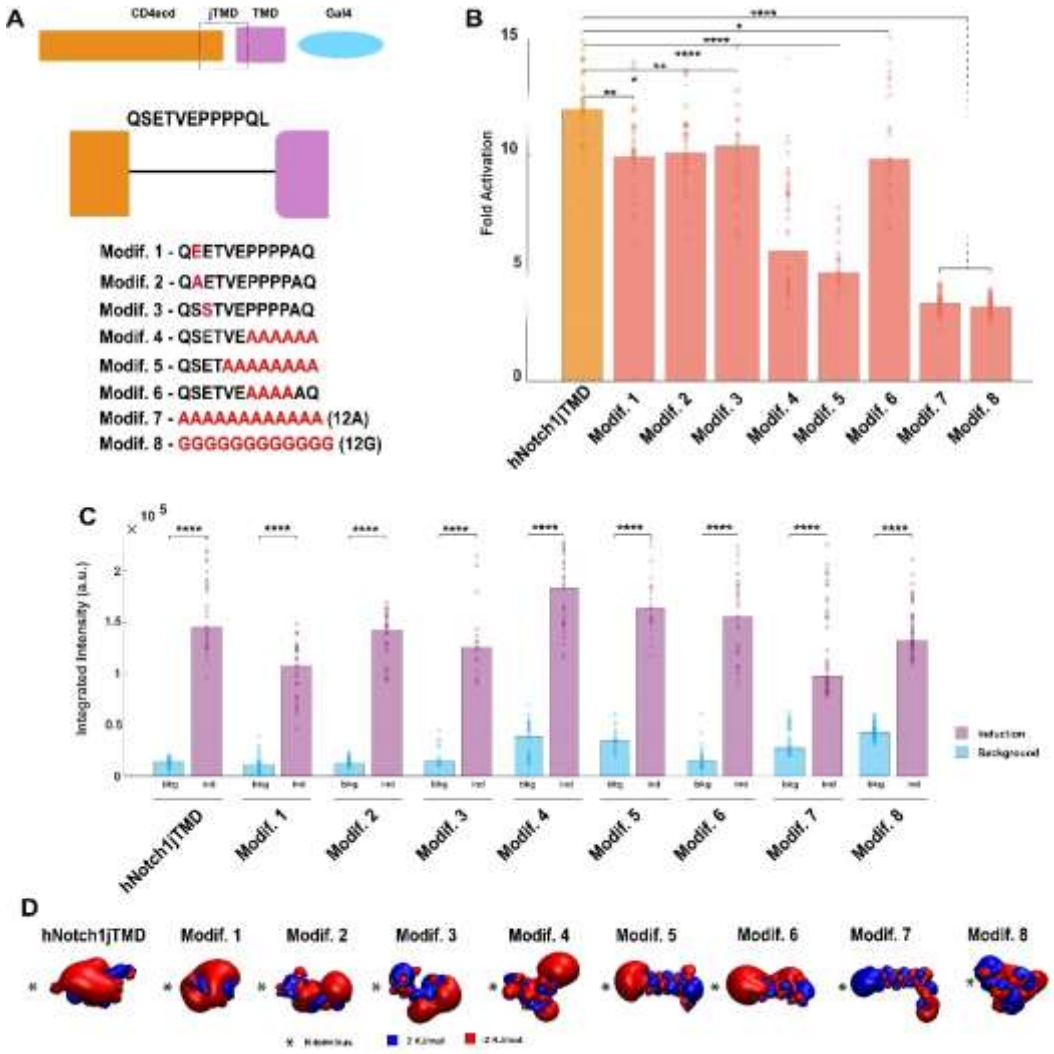

As we described above, many short sequences could act as mechanoreceptors when the hNotch1jTMD switched them, but we also found that the CD4jTMD could not perform this function. Besides, we observed that engineered receptors containing the CD4 LBD followed by 12 aa jTMD from CD8 could not be induced upon ligand binding (Figure 3.14B and C).

It is known that proteins have different conformation depend on their aa sequences and the charge of them. Molecular dynamic simulation models of the CD4jTMD (KVLPTWSTPVGSP), CD8jTMD (SVKGTGLDFACD) and hNotch1jTMD (QSETVEPPPPAQ) showed that the CD4jTMD appeared to be compacted (overall positive charged domain). In contrast, the hNotch1 jTMD was more stretched due to the overall electronegative charges (CD4jTMD has a strong electropositive surface compared to hNotch1jTMD) (Figure 3.14D). Moreover, the molecular dynamic simulations suggested that the compaction of the CD8jTMD was due to the presence of (Lysine) K and (Glycine) G in its sequence SV***K***GT***G***LDFACD, and a strong negative charge on the C-terminus (Aspartic acid, D), next to the membrane. In contrast, the simulations suggested that the presence of two glutamic acids (E) in the hNotch1jTMD contributed to its being an elongated peptide (Figure 3.14D). To evaluate if the K and G in CD8jTMD (SV**K**GT**G**LDFACD) determined its compaction and hence its lack of inducibility, we generated constructs in which the K and G from CD8jTMD were inserted into the equivalent positions of the hNotch1jTMD (modif. 1 – QS**K**TV**G**PPPPAQ). We also added the last 6aa of CD8jTMD to the previously modified receptor (modif. 2 – QS**K**TV**GLDFACD**) (Figure 3.16A). These modifications of hNotch1jTMD did not show any inducibility (1.57-fold and 1.82-fold, respectively) (Figure 3.16B), suggesting that either the K and G from CD8jTMD abolished inducibility, or that the two glutamic acids (E) in hNotch1jTMD (QSETVEPPPPAQ) are necessary for inducibility. To investigate whether these two Es in the hNotch1jTMD were critical contributors to the receptor ability to act as a mechanoreceptor, we generated hybrid constructs containing the sequences SV**E**GT**E**LDFAC (modif. 3) and SV**E**GT**EPPPPAQ** (modif. 4) (Figure 3.16A)**.** However, these hybrid constructs did not show any inducibility, suggesting that the amino acids close to the N-terminus of the hNotch1jTMD could be critical to determine if a sequence can act as a mechanoreceptor (Figure 3.16B and C and Fig. Sup 3.16). On the other hand, we also observed that constructs with changes close to the N-terminus had normal inducibility **(i)** Q***A***ETVEPPPPAQ, **(ii)** Q***E***ETVEPPPPAQ, **(iii)** QS***S***TVEPPPPAQ, (Figure 3.15B).

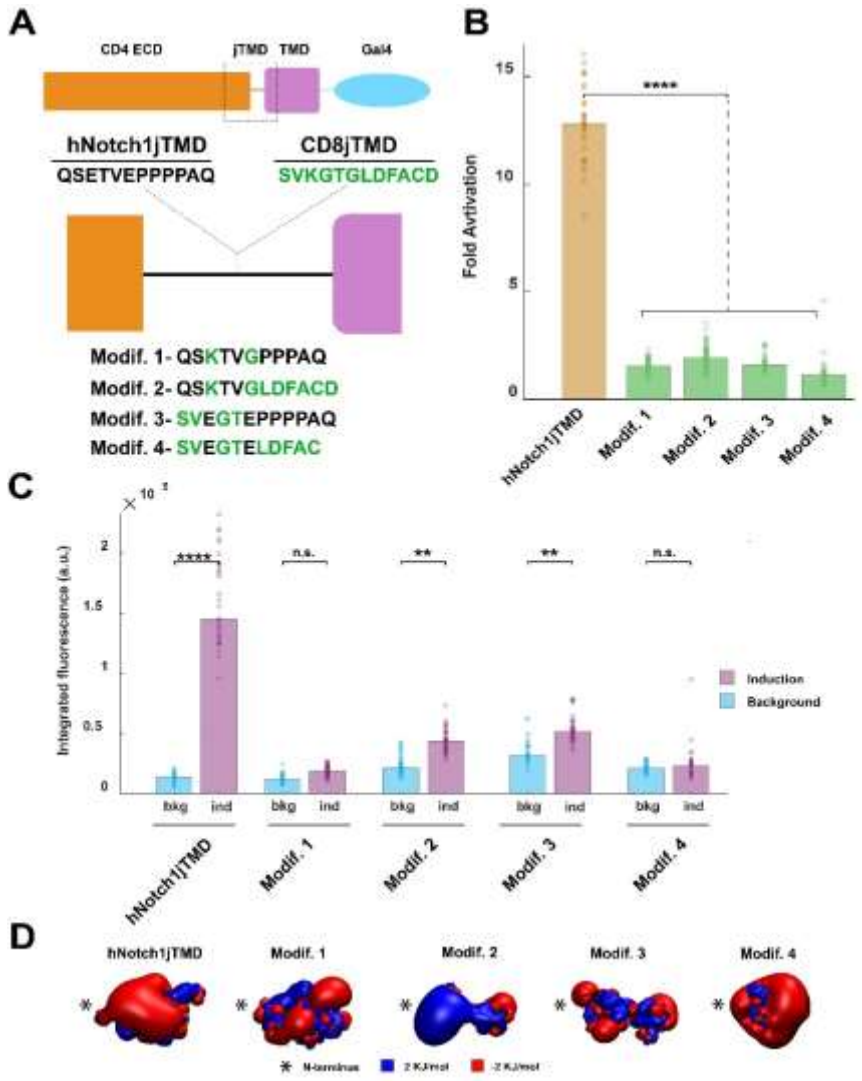

Figure 3.16. Ligand dependent induction by jTMD modifications based on electrostatic properties of amino acids composition of CD8jTMD and hNotch1jTMD. (A) Diagram showing the different jTMD modifications based on CD8jTMD and hNotch1jTMD (amino acids highlighted in green are from CD8jTMD). **(B)** Fold activation was minimal for all the modifications: modif. 1=1.57-fold, modfi. 2=1.93-fold, modif. 3=1.58-fold; modif. 4=1.12-fold. p-values compared to hNotch1jTMD: modif1=1.50 x 10^{-14}, modfi. 2=6.53 x 10^{-15}, modif. 3=7.94 x 10^{-13}, modif. 4=1.34 x 10^{-13}. **(C)** Note that there is a small difference between the induction and background for modifications 2 and 3 (see Table 8A from ANNEX 3). **(D)** Model of electrostatic charges predictions showed an overall positive charged jTMD for modification 2.

3.3.4. Influence of the Length of Human Notch1 jTMD in Receptor Activation.

Our experiments showed that not all jTMDs were equally efficient as mechanosensors, being the hNotch1jTMD the most efficient (~12-fold induction), and the CD4jTMD totally inactive. One can imagine several scenarios that could explain

the inability of the CD4jTMD to act as a mechanosensor. For example, the sequence of the CD4jTMD could not be cleaved by proteases after ligand binding. Alternatively, this jTMD could actively inhibit the cleavages by ADAM proteases. To distinguish between these two scenarios, we generated constructs that contained the CD4 LBD followed by the hNotch1NRR (including the S2 cleavage site), the CD4jTMD, the hNotch1 TMD and the Gal4 ICD, or a double jTMD: combining the hNotch1jTMD (12 aa) plus the CD4jTMD (12 aa) (Figure 3.17A). Cell-cell interaction experiments showed that both receptors could be induced by ligand binding similar to CD4NRRhNotch1jTMD with higher, but not significant, fold activation when the receptor has two jTMDs (24aa) (NotchJtmd=4.45-fold, CD4jTMD4.17-fold, and CD4+NotchjTMD (24aa)=5.40-fold, respectively). It indicates that CD4jTMD did not inhibit the ability of the Notch1NRR to be cleaved in its S2 site (Figure 3.17B and Table 6A from ANNEX 4). Interestingly, this experiment shows that hNotch1NRR and/or hNotch1jTMD can be cleaved even when they are placed farther away from the cell membrane than in its original location (24 aa versus 12 aa).

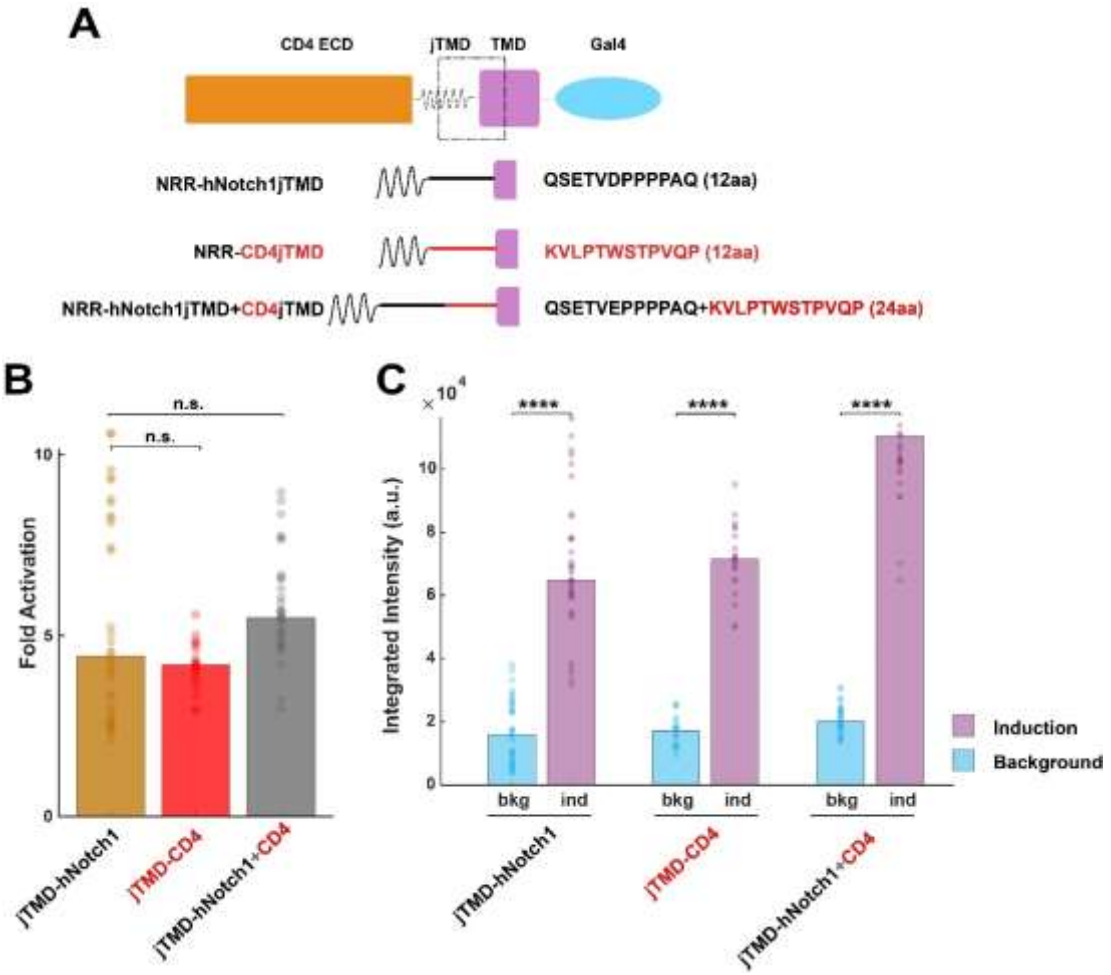

Figure 3.17. Ligand dependent induction of CD4-hNotch1NRR receptor with CD4jTMD (12 aa) or CD4jTMD+hNoth1jTMD (24 aa). (A) Diagram showing the amino acids sequence from CD4jTMD and the combination of hNotch1 and CD4jTMDs. **(B)** Fold activation did not show significant differences of both receptors compared to CD4hNRRhNotch1jTMDG4 receptor (CD4NRRhNotch1jTMDG4=4.43-fold; CD4NRRCD4jTMD=4.17-fold; CD4NRRCD4jTMDhNotch1jTMD=5.46-fold). p-values compared to CD4NRRhNotch1jTMDG4: CD4NRRCD4jTMD=0.520; CD4NRRCD4jTMDhNotch1jTMD=0.108. **(C)** Integrated Intensity graphs showed a higher level of background and induction for the receptor carrying the jTMDs from hNotch1 and CD4 (see Table 6 from ANNEX 3).

Our data indicate that multiple sequences of around 12 aa can act as mechanosensors when replaced by the hNotch1jTMD without requiring hNotch1NRR. In addition, we observed activation of the receptor when that hNRR domain was located further than in normal conditions. Next, we decided to evaluate whether reducing the jTMD length affects the function of the hNotch1NRR as a mechanoreceptor. For that, we generated new receptors consisted of CD4 LBD, Notch1NRR, and Notch1jTMD between 5 to 12 aa (5 aa (QSEAQ), 6 aa (QSEPAQ), 7 aa (QSEPPAQ), 8 aa (QSEPPPAQ), 9 aa (QSEPPPPAQ), 10 aa (QSEEPPPPAQ), 11 aa (QSETEPPPPAQ), and 12 aa (QSETVEPPPPAQ; the hNotch1jTMD), followed by hNotch1TMD and Gal4 (Figure 3.18A). Cell-cell interaction experiments showed that the shortest jTMDs with only 5 aa and 6 aa prevented receptor activation despite the presence of a complete NRR domain (including the S2 cleavage site) (Figure 3.18B, see Table 7 from ANNEX 3). Receptors with either 7 aa or 8 aa in the jTMD showed a low ligand dependent activity (2-fold and 2.3-fold, respectively). Moreover, these constructs showed a higher background than hNotch1jTMD (12aa) (Figure 3.14C and Sup. 3.18. See also table 7A from ANNEX 3 for values). In contrast, jTMDs with 9 aa,10 aa, and 11 aa had ligand dependent induction comparable to those observed with the hNotch1jTMD (12aa) (Figure 3.18B). Similar results were observed with 5aa, 6aa and 12 aa jTMD when the extracellular domain of CD4 was replaced by 1d3 (Figure 3.19). This experiment indicates that for NRR to act as a mechanoreceptor, a jTMD with a minimum length is required. However, we still do not know if this requirement depends on a specific amino acid sequence, or only on a minimum size of separation between the NRR and the cell membrane. It is well known that mutations in the NRR domain of hNotch1 induce ligand independent cleavage responsible for a specific type of leukaemia: T-cell acute lymphoblastic leukemia (T-ALL).

These types of mutations happened in the heterodimerization domain mainly due to a single amino acid substitution and in-frame insertions or deletions that induce ligand independent activation (Weng et al. 2004; Malecki et al. 2006). A new class of activating mutations in hNotch1 T-ALL was reported (Sulis et al. 2008). In fact, this mutation results in expansion of the juxta-transmembrane domain region, called juxta-transmembrane expansion (JME), spacing the HD (S2 cleavage site) from the transmembrane domain. Their results suggested that an aberrant proteolytic cleavage at the canonical Notch S2 site is occurring. From our results, the presence of jTMD appears to be important for Notch receptor signalling: either due to its aa composition or its length, which determines the distance of the S2 cleavage site from the cell membrane (Figure 3.17). Moreover, these results showed that spacing the length between the S2 site and the plasma membrane by adding the CD4jTMD increased ligand independent cleavage (Figure 3.16C and Fig Sup. 3.16).

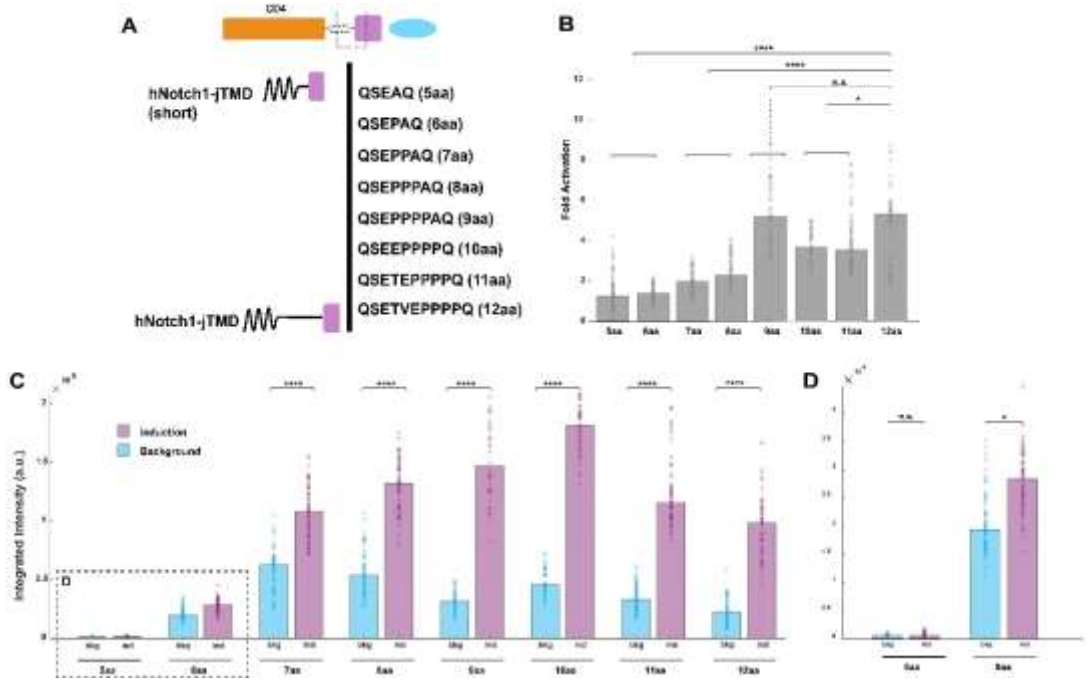

Figure 3.18. Ligand dependent induction of CD4hNRRhNotch1jTMDG4 with different lengths of jTMD. (A) Diagram showing the amino acid sequences of the different lengths of hNotch1jTMDs tested. **(B)** Fold activation chart showing an increase of the receptor activation upon ligand binding while increasing the length of the jTMD being 12aa length (hNotch1jTMD) the highest fold activation (5aa=1.24-fold; 6aa=1.38-fold; 7aa=1.97-fold; 8aa=2.30-fold; 9aa=5.05-fold; 10aa=3.64-fold; 11aa=3.47-fold; and 12aa=5.20-fold). **(C)** Integrated intensity for the different receptors with variation on the jTMD length. Note that the background for jTMD with 7aa and 8aa showed the highest level of integrated intensity while the lowest level were observed in the jTMD with 5aa (See Table 7A from ANNEX 3) (p-values between induction and background: 5aa=0.41 6aa=0.004

7aa=1.43x10^{-8} 8aa=3.06x10^{-9} 9aa=1.51x10^{-9} 10aa=3.47x10^{-9} 11aa=3.06x10^{-9} 12aa=6.63x10^{-9}). **(D)** Smaller scale of the integrated intensity better appreciates the difference between 5aa and 6aa from **C**.

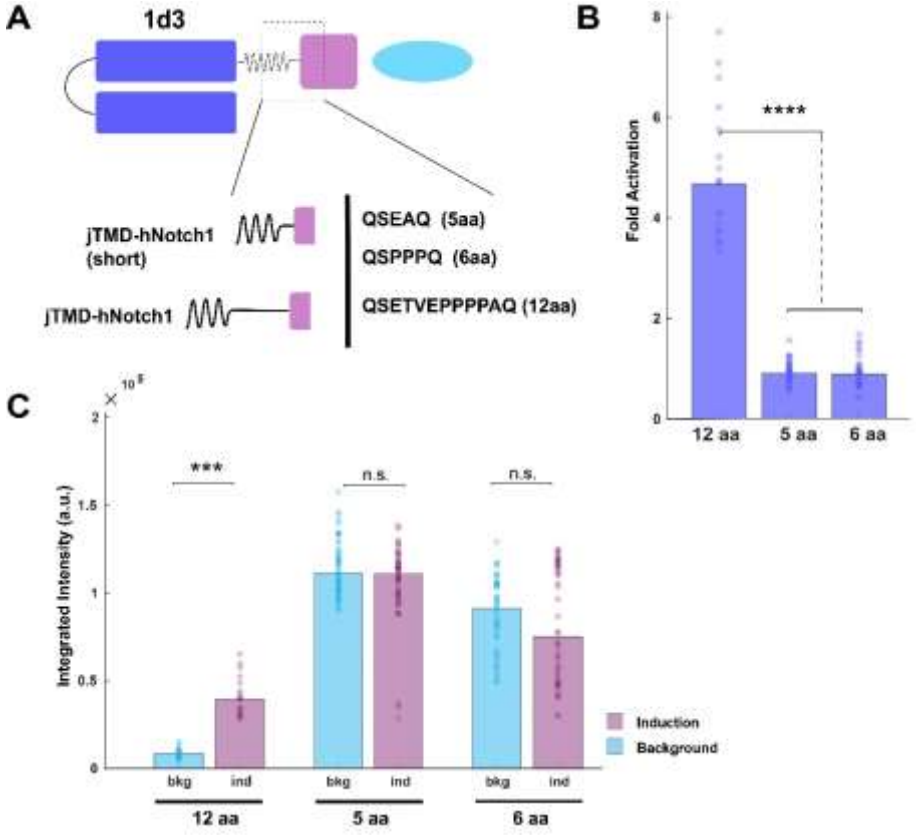

Figure 3.19. Ligand dependent induction of 1d3NRRhNotch1jTMDG4 with jTMD of 12 aa, 5 aa and 6 aa. (A) Diagram showing the amino acid sequences for the different lengths of hNotch1jTMDs. **(B)** Fold activation showed no induction for 5aa and 6aa jTMD compared to 12aa (hNotch1jTMD: 5aa=1.09-fold, 6aa=1.08-fold; p-values compared to hNotch1jTMD: 5aa=7.9 x 10^{-21}, and 6aa=3.9 x 10^{-21}). **(C)** Integrated intensity graphs showed a higher level of background for 5aa and 6aa jTMDs compared to the control hNotch1jTMD (hNotch1=3.41 x 10^{4}, 5aa =11.34 x 10^{4}, 6aa=9.12 x 10^{4}). We only observed significant different between background versus induction in the 12 aa jTMD (bkg=0.85x10^{4} and ind=3.96x10^{4}).

3.3.5 Replacement of Human Notch1 TMD.

Our previous result showed that Notch receptor can be activated without the NRR domain and that the jTMD length play an important role in the receptor activation. However, some experiments using the chimeric Notch receptor where Torso and Sevenless TMDs replaced its TMD, two tyrosine kinases receptors, induced UAS-lacZ expression, suggested that the TMD be cleaved (Struhl and Adachi 2000). Moreover, the truncated Notch receptor carrying the β-APP, another single-pass transmembrane

protein associated with Alzheimer's disease in humans (Selkoe and Wolfe 2007), also induced strong expression of UAS-LacZ gene (Struhl and Adachi 2000). To investigate whether hNotch1TMD is required for mechanotransduction (or can be cleavage upon ligand binding), we design two different strategies: **(i)** we replaced the hNotch1TMD from the previous constructs carrying the short-erbB4, long-erbB4 and E-cadherin jTMD (Figure 3.13) by their own TMDs (Figure 3.20A), and **(ii)** the TMD from CD4noNRRhNotch1jTMD was also replaced by three different proteins: SEVENLESS, TORSO and Amyloid Precursor Protein (β-APP) (Figure 3.21A). Cells expressing the receptor carrying short-erbB4, long-erbB4, or E-cadherin jTMD and TMD did not activate these receptors upon mixing with cells expressing the ligand gp160 (Figure 3.19B and 3.19C). Note that these receptors are also carrying the jTMD from the same proteins. However, those receptors with Sevenless, TORSO or β-APP TMD containing the hNotch1jTMD showed receptor activation (Figure 3.21B), with a similar level of induction among them, and much lower than the control (hNotch1TMD) (2.62-fold, 2.20-fold, and 3.24-fold activation, respectively). Notice that the ligand independent activation is higher in all these receptors compared to CD4NotchjTMD//TMD (Figure Sup.3.21 from ANNEX 4). These results indicate that hNotch1TMD is no essential to trigger ligand dependent activation of synthetic receptors without NRR but enhances the receptor inducibility.

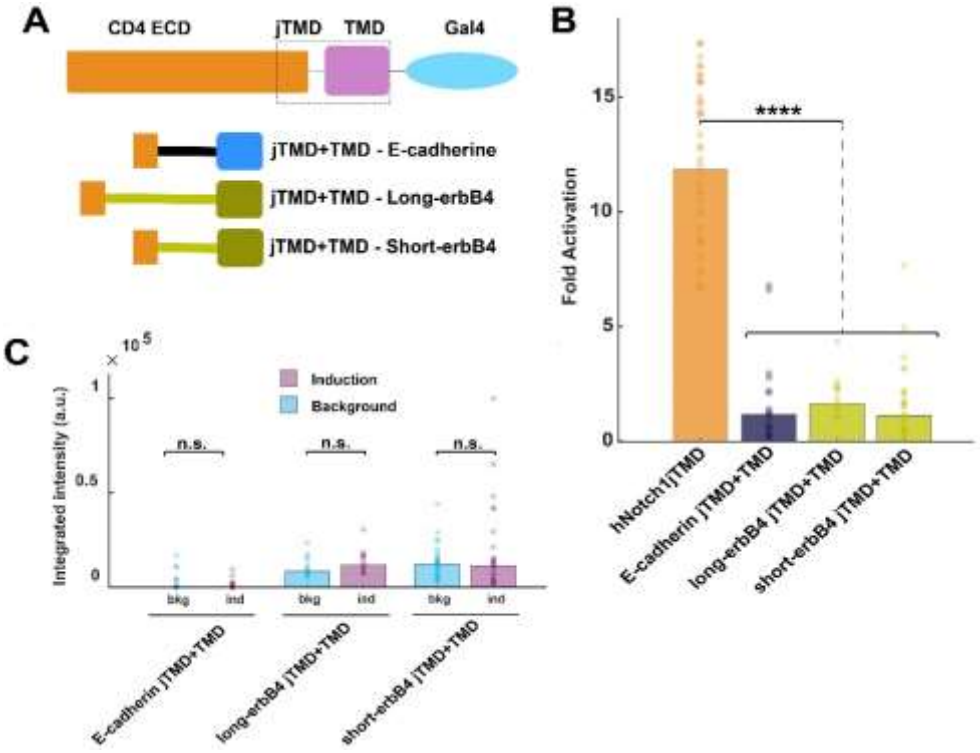

Figure 3.20. hNotch1TMD for mechanotransduction I. Ligand dependent induction of E-cadherin and erbB4 TMDs. (A) Diagram showing TMDs from different proteins (see sequences in Sequence ANNEX 1). **(B)** No induction was detected for any of the three engineered receptors (E-cadherin=1.18-fold, long-erbbB4=1.41-fold, and short-erbB4=1.09-fold; p-values compared to hNotch1TMD: E-cadherin=1.39 x 10^{-9}, long-erbbB4=1.20 x 10^{-8}, short-erbB4=6.47 x 10^{-13}. **(C)** No differences between the background and induction for integrated intensity was detected (see table 9A from ANNEX 3). Note the low level in integrated intensity of E-cadherin TMD receptor (bkg=0.13 x 10^4 ± 0.48 x 10^4 and ind=0.25 x 10^4 ± 2.1 x 10^4).

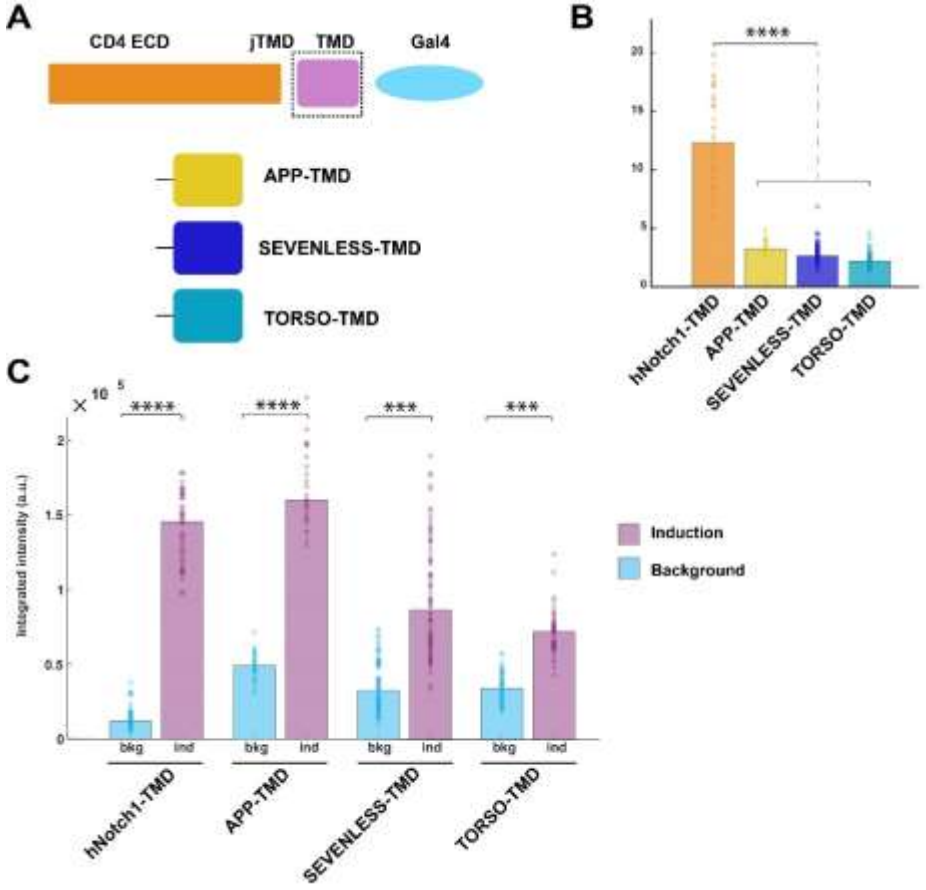

Figure 3.21. hNotch1TMD for mechanotransduction II. Ligand dependent induction of different TMDs, TORSO, SEVENLESS and β-APP. (A) Diagram showing TMDs from different proteins (see Table2 in Sequence ANNEX). **(B)** Fold activation showed some level of induction for the three receptors but significantly lower than the hNotch1TMD (TORSO=2.21-fold, SEVENLESS=2.73-fold, and β-APP=3.21-fold; p-values compared to hNotch1jTMD: TORSO=4.14 x 10^{-13}, SEVENLESS=9.76 x 10^{-15}; and β-APP=8.87 x 10^{-13}). **(C)** β-APP showed the highest level of background followed by SEVENLESS and TORSO in which the level of induction was significantly lower than the control hNotch1TMD (see table 9A from ANNEX 3).

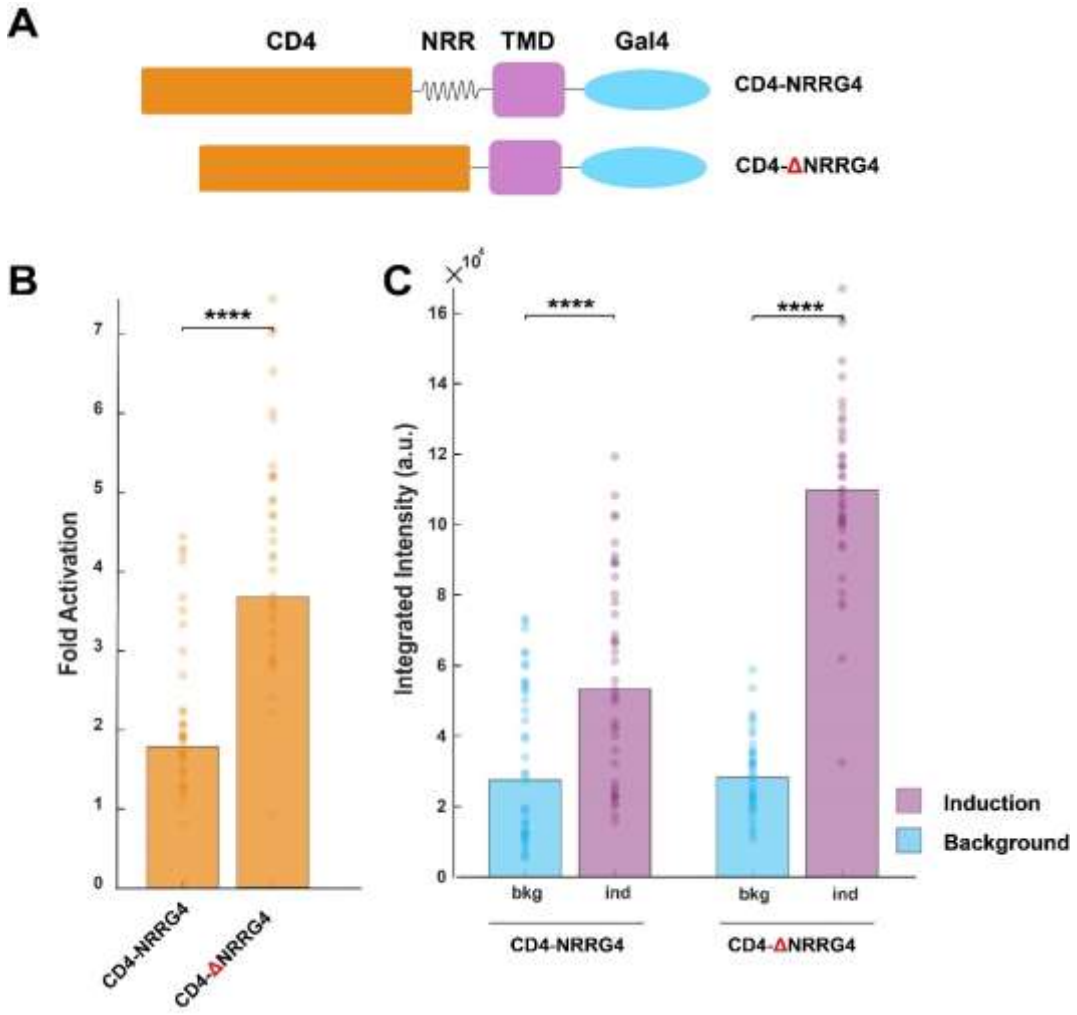

Figure 3.22. Ligand independent activation of CD4NRRG4 and CD4noNRRG4 receptors. **(A)** Diagram showing the different domains from both receptors. **(B)** Fold increase of the CD4noNRRG4 (3.67-fold) receptor was higher than CD4NRRG4 (1.78-fold), p-value=1.37 x 10^{-9}. **(C)** Integrated intensity of induction showed a significant difference in the level of background compared to the reporter cell line (CD4NRR: bkg=2.93 x 10^4; ind=5.33 x 10^4, p-value=5.92 x 10^{-5}; and CD4noNRR: bkg=2.60 x 10^4; ind=10.98 x 10^4, p-value=4.07 x 10^{-14}).

Our experiments indicate that Notch receptor can be induced without the NRR domain and that multiple short aa sequences replacing the hNotch1jTMD can act as ligand dependent mechanosensor. This statement raises the question about what is the function of NRR, a large protein domain (~300 aa) that appears to be conserved at the Notch receptor across all metazoans. We observed that although the ligand dependent activation of CD4noNRRG4 was higher than CD4NRRG4 (12-folds versus 4.9-folds activation), the ligand independent activation of CD4noNRRG4 was approximately 2-folds higher than CD4NRRG4 (Figure 3.22). In other molecules (hCARNRR and

hCARnoNRR, CD4NRR and CD4noNRR), we also observed that the NRR domain's addition also reduced the ligand independent signalling (Figure 3.7 and 3.22). It indicates that one of the NRR domain functions is reduced the ligand independent cleavage by ADAM proteases.

3.3.6 Dynamic of Synthetic Receptor *in vitro* and Evaluation of Notch Receptor Activity *in vivo*.

To investigate other potential functions of the NRR domain, we measured the temporal dynamics of ligand dependent activation of CD4NRRG4 and CD4noNRRG4. To this end, we performed time-lapse microscopy of cell-cell interaction experiment by mixing cell lines expressing the CD4NRRG4 and CD4noNRRG4 receptors with cells expressing gp160 ligand in a ratio 1:10, respectively (Figure 3.23A). We recorded them for 72 hours, starting three hours since the cells were plated. Cells expressing CD4NRRG4 receptor reached half-maximal induction significantly faster than CD4noNRRG4 (11 hours versus 22 hours), suggesting that the NRR domain could provide a quick signal activation by accelerating the action of ADAM proteases upon ligand binding (Figure 3.23B and C). One possible explanation is that after the mechanical tension has occurred, the NRR maintains the protein in an "open" state, to increase the amount of time that ADAMs can access and cleave the S2 site before it goes back its inactive conformation.

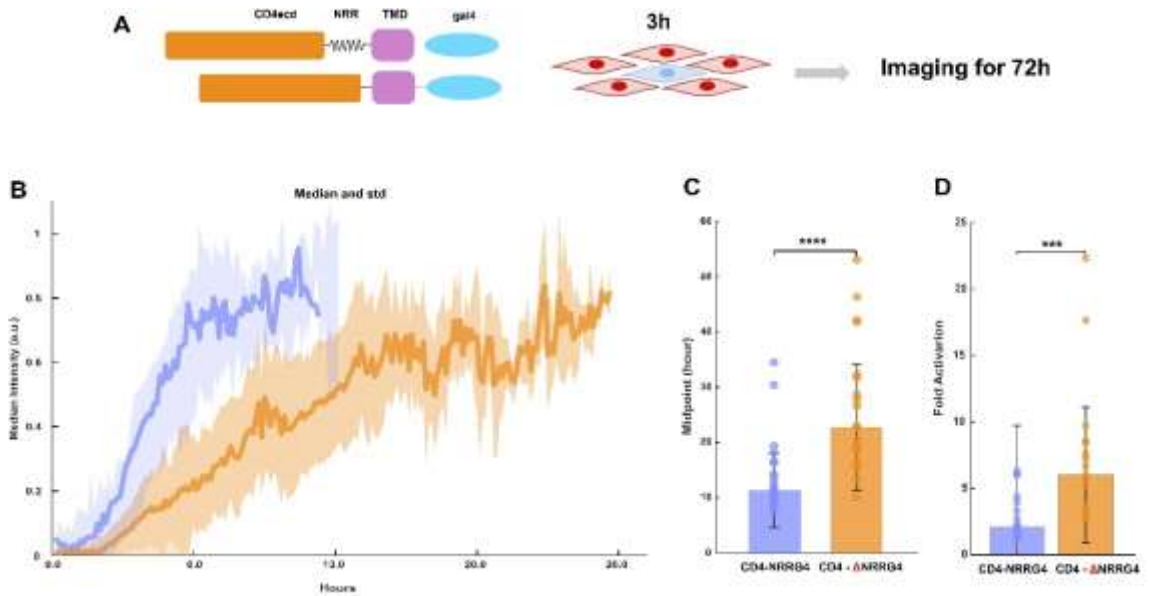

Figure 3.23. Temporal dynamics of ligand dependent activation of CD4NRRG4 and CD4noNRRG4. (A) Schematic representation showing how the experiment has been performed. **(B)** Histogram showing the median intensity versus time. Note that CD4noNRR reach half of its induction slower than CD4NRR, as it is shown in **C. (C)** Indicate the midpoint where the maximum intensity is reached (CD4NRR=11.64 ± 6.71 hours; CD4noNRR=22.68 ± 11.4 hours, p-value=3.24 x 10^{-5}). **(D)** Fold activation for CD4noNRRG4 is three times higher than CD4NRRG4 (6.02-fold and 2.07-fold, respectively; p-value=3.2 x 10^{-4}).

To investigate whether jTMDs could act as mechanosensors under physiological conditions when the NRR domain is absent in the Notch receptor, we generated transgenic *Drosophila* carrying Notch receptor with and without NRR domain under the heat-shock promoter (HSP-70) with Gal4 as intracellular domain. *Drosophila* embryos received heat shocks of different duration at several time points during development. At same developmental stages (12 hours), *Drosophila* embryos carrying Notch receptor with and without NRR domains showed a similar expression pattern of ligand dependent cleavage (Figure 3.24A-C and D-F). More experiments are necessary to obtain sufficient data to analyze the number of induced nucleus per stripe in each receptor. Moreover, *in vivo* time-lapse of *Drosophila* embryos would examine the temporal dynamics of ligand dependent activation through the development to confirm the faster activation of NotchNRRG4 observed *in vitro* experiments.

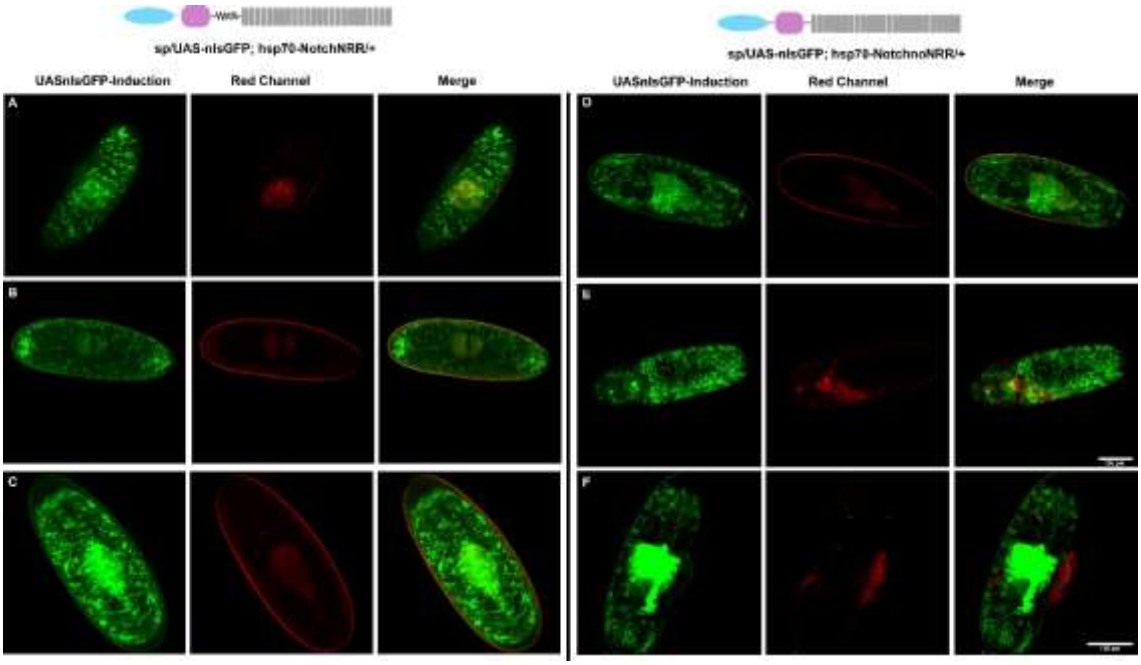

Figure 3.24. Expression pattern of ligand-dependent activation of NotchNRRG4 and NothnoNRRG4 under heat-shock promoter. (A), (B) and **(C)** are showing the *in vivo* expression pattern of the reporter UASnlsGFP once the NotchNRR receptor is activated upon ligand binding during Drosophila embryos development (stage of 12 hours). **(D), (E)** and **(F)** are showing *in vivo* the expression pattern of the reporter UASnlsGFP once the NotchnoNRR receptor is activated upon ligand binding during Drosophila embryos development (stage of 12 hours). No difference in the expression pattern of both receptors is detected. Scale bars in **(E)** corresponds to **(A), (B), (D) and (E)** images**.** Scale bar in **(F)** corresponds to **(C)** and **(F).**

3.3.7 Mass Spectrometry of Synthetic Receptor.

As we mentioned above, receptors lacking NRR with Notch1jTMD can be activated even though they do not have an S2 cleavage site. Experiments adding blockers for ADAMs, showed a substantial reduction of the ligand dependent activation of CD4noNRRG4 receptor (Figure 3.10). All these experiments suggest that synthetic and hNotch1 receptor without NRR may have a S2-like cleavage site in the jTMD. To test this hypothesis, we replaced the intracellular domain, Gal4, from CD4NRRG4 and CD4noNRRG4 receptors by the nuclear localization GFP (nlsGFP) (Figure 3.25A). CHO-K1 cell lines were transfected with both receptors, and after 4 hours of the transfection, DAPT (γ-secretase inhibitor) or DMSO were added to the fresh medium. After 24 hours, cells expressing the ligand gp160 were plated on top of the transfected cells with each receptor. Forty-eight hours after ligand cell line was plated, the cells were harvested, and the receptors were isolated by immunoprecipitation using nanobodies against the ICD (nlsGFP) (Pleiner et al. 2015). After digesting the purified receptors, mass spectrometry of the peptides was performed using Eclipse-Instrument. Mass spectrometry results showed 4 different peptide sizes of the jTMD from the receptors with and without NRR domains. These results suggest that there may be 4 potential S2-like sites in the jTMD (Figure 3.25B and C).

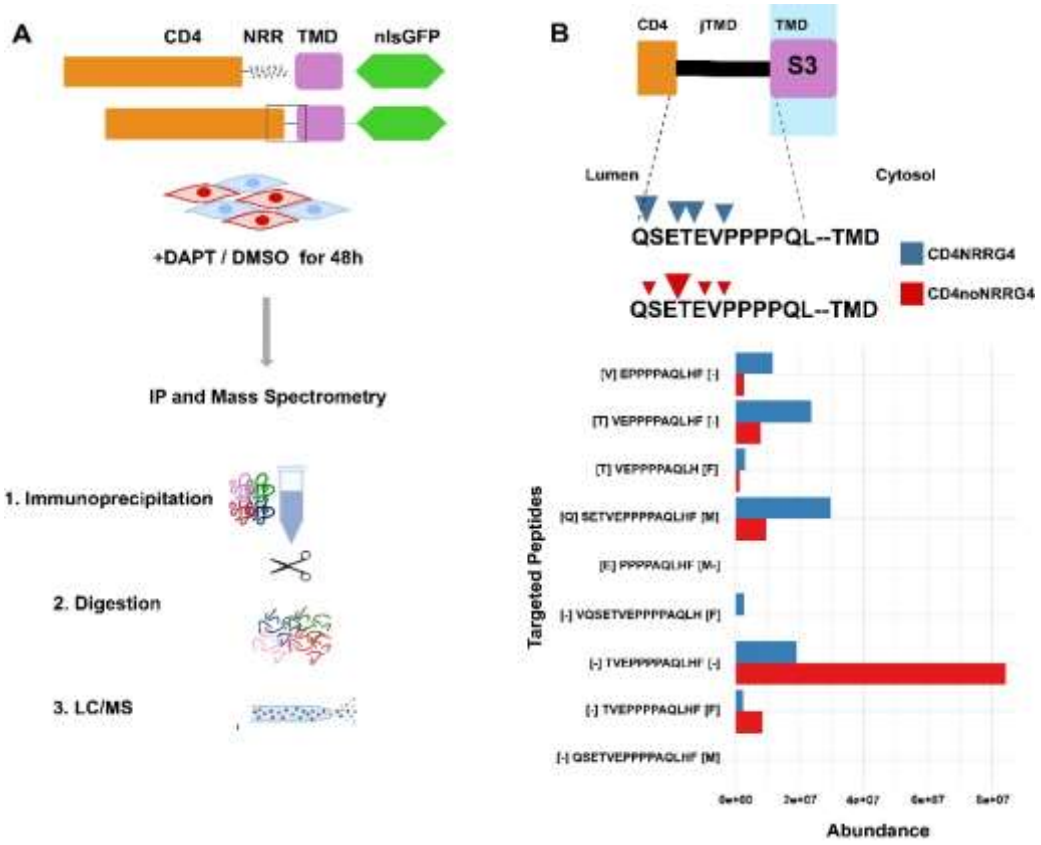

Figure 3.25. S2-like cleavage sites in hNotch1 jTMD. (A) Diagram showing the experiment strategy where the cell lines carrying the receptors (CD4NRRnlsGFP and CD4noNRRnlsGFP) were co-culture with gp160 cell line under DAPT or DMSO condition for 48 hours. **(B)** Schematic representation showing the abundance of the different cleavage site in CD4NRR (blue arrowheads) and CD4noNRR (red arrowheads) receptors. Note that the most abundant cleavage site in the jTMD for CD4NRR is located between glutamine (Q) and serine (S) and between 1st glutamic acid (E) and threonine (T) for cd4noNRR.

DISCUSSION

Las fuerzas mecánicas regulan muchos procesos biológicos y las células presentan múltiples mecanosensores para responder a estas fuerzas. El receptor Notch es uno de los mecanorreceptores mejor estudiados. En los últimos años, se ha demostrado que la región reguladora negativa de Notch (NRR) es esencial para la función de Notch como mecanorreceptor. Actualmente grandes números de evidencias indican que NRR, una secuencia de 300 aminoácidos entre las repeticiones de EGF y el dominio transmembrana, es esencial para la activación de Notch dependiente del ligando que se basa en varias líneas de evidencia (Parks et al. 2000a; Gordon et al. 2015b; Langridge y Struhl 2017). Primero, la estructura cristalográfica sugiere que el sitio de escisión S2 está dentro de NRR y protegido de metaloproteasas (Gordon et al. 2009b). El plegamiento apropiado del dominio NRR es posible debido a múltiples enlaces disulfuro que permiten dicho plegado oportuno. En segundo lugar, algunas mutaciones en el dominio NRR inducen la activación independiente del ligando del receptor Notch. Se cree que estas mutaciones cambian la conformación de la región NRR exponiendo el sitio de escisión S2 (Malecki et al. 2006; Sulis et al. 2008). Por tanto, todas las evidencias disponibles sugieren que NRR actúa como un inductor de escisión dependiente de ligando.

Durante más de tres décadas, se ha pensado que el dominio NRR es el elemento clave para desencadenar la activación dependiente del ligando del receptor Notch. Debido a su estructura plegada en condiciones normales que protege y bloquea el sitio S2, el dominio NRR se ha considerado un importante mecanosensor nativo. Por tanto, la activación de la vía de señalización de Notch necesita de una fuerza de tracción para desdoblar y exponer el sitio de escisión S2. Sin embargo, nuestros resultados indican que el dominio NRR no es necesario para la activación dependiente del ligando del receptor Notch y una pequeña secuencia de solo 12 aa, el dominio yuxtatransmembrana (jTMD), puede reemplazar la función mecanosensora llevada a cabo por el dominio NRR de 300 aa, siendo suficiente para lograr la escisión dependiente del ligando. Además, la inducción de receptores sintéticos basados en Notch que carecen del dominio NRR es inhibida por bloqueadores de metaloproteasas (ADAMs) y específicamente por ADAM10CRISPR-Cas9. Estos resultados indican que existe un sitio potencial de escisión similar a S2 en Notch jTMD que es accesible para las metaloproteasas ADAM10 tras la

unión del ligando. También hemos demostrado que la activación dependiente de ligando del receptor Notch no es producida por el dominio transmembrana hNotch1, lo que confirma que 12 aminoácidos de Notch jTMD son suficientes para actuar como un mecanosensor.

Aunque se sabe que NRR es un dominio específico y exclusivo del receptor Notch, un estudio reciente ha encontrado que dominios de proteólisis de varias proteínas de membrana con homología estructural con el receptor Notch (dominio similar a "SEA" en tándem) pueden reemplazar la función NRR y activar la vía de señalización de Notch (Hayward et al. 2019). Estos receptores quiméricos contienen repeticiones de EGF en su dominio extracelular y un dominio similar a SEA entre 120 y 900 aa, reemplazando el dominio NRR, seguido por el dominio transmembrana Notch y Gal4 como dominio intracelular. La mayoría de los receptores que contienen dominios similares a "SEA" con homología estructural con Notch tienen un mecanismo proteolítico similar al de Notch. La estructura cristalina de varios de estos dominios de tipo "SEA" revelan diferencias entre la conformación de NRR y estos dominios "SEA". Por ejemplo, las estructuras de tipo NRR y "SEA" de EpCAM presentan la hélice α cerca de la cadena β que contiene sitios proteolíticos putativos. Por el contrario, los dominios similares a cadherina en las proteínas protocadherinas interactúan con el lado opuesto del dominio similar a "SEA". Por lo tanto, el sitio proteolítico tendría diferentes formas de activarse y quizás requisitos adicionales de la fuerza necesaria para activarse. Entre todos los diferentes receptores seleccionados, han encontrado que la Protocadherina-15 (PCDH15) y la proteína 2 relacionada con Cadherina (CDHR2) mostraron una fuerte escisión dependiente de ligando en comparación con los demás receptores (Hayward et al. 2019).

Nuestros resultados demuestran que no hay un requisito estricto en la secuencia de solo 12 aminoácidos (jTMD) para permitir la escisión dependiente del ligando, ya que que múltiples cambios en varios aminoácidos del hNotch1 jTMD aún permiten la activación del receptor Notch al interaccionar con el ligando. Además, también demostramos que las secuencias cortas de solo 12 aa (jTMD) del receptor Notch de diferentes especies (pollo, pez cebra, Xenopus, Drosophila) y de otras proteínas de membrana como E-cadherina, NCAM o erbB4, que no se ha mostrado ser activadas por

fuerzas, también pueden actuar como mecanorreceptores dependientes de ligandos en moléculas heterólogas. Por ejemplo, el influjo de Ca2 + induce la activación de ADAM10 para activar la molécula de adhesión E-cadherina que afecta la adhesión celular y, por lo tanto, aumenta la migración celular (Maretzky et al. 2005). Además, TACE / ADAM17 participa en la activación de ErbB4 (receptor de tirosina quinasas) en las células epiteliales del colon. En este caso, ADAM17 es activado por ERK1 / 2, que fosforila TACE en T735 en su cola citoplásmica (Hilliard et al. 2011). Para la molécula de adhesión neural (NCAM), ADAM10 se activa en respuesta a ephrinA5 / EphA3 (Brennaman et al. 2014).

También observamos que incluso secuencias de aminoácidos intrínsecamente desordenadas (12 Ala o 12 Gly) también podrían actuar como activadores de escisión dependientes de ligandos. Nos gustaría sugerir que la observación de que los dominios cortos y no estructurados pueden actuar como mecanorreceptores es similar a la elucidación sobre los requisitos para los dominios de activación en los factores de transcripción. Originalmente, se pensó que los dominios de activación de los factores de transcripción (aproximadamente 881 aa) necesitarían tener estructuras definidas para interactuar con la ARN polimerasa II. Sin embargo, más tarde se descubrió que muchas secuencias de aminoácidos cortas y no estructuradas podrían actuar como potentes activadores de la transcripción (Ma y Ptashne 1987a). Se sabe que el 90% del factor de transcripción corresponde a un dominio de activación (AD). Estudios donde se analiza la deleción del factor de transcripción Gal4 mostró que dos fragmentos cortos de 49 aa y 114 aa son suficientes para activar la transcripción cuando se une al dominio de unión del ADN (Ma y Ptashne 1987a). Más tarde, Ma y Ptashne, (1987b) habían descubierto que secuencias más cortas (la más corta con 20 aa en su longitud) sin características aparentes similares entre ellas (excepto por la acidez) también pueden activar la transcripción. Además, se demostró que diferentes secuencias de péptidos que llevan un exceso de residuos ácidos (con algunos residuos hidrófobos cruciales) funcionaban como dominios de activación cuando se unen a dominios de unión al ADN (Regier et al. 1993; Ptashne 2004). De acuerdo con estos trabajos, nuestros resultados sugieren que un dominio complejo y estructurado no es esencial para detectar una fuerza mecánica y que los dominios de detección de fuerza mecánica en las proteínas pueden ser

bastante comunes, probablemente regulando muchos más procesos celulares de los que se sospechaba anteriormente.

Nuestros resultados donde se modificó la longitud del jTMD también revelan una característica esencial de la activación del receptor Notch. Observamos que el dominio jTMD con secuencias más cortas de 9 aa no era suficiente para activar el receptor Notch. Estos resultados sugieren una longitud mínima del jTMD y, por lo tanto, la distancia entre el sitio de escisión S2 y el TMD debe ser de al menos 9 aa para permitir que el NRR actúe como un mecanosensor. Además, los experimentos en los que el sitio de escisión S2 se encontraba alejado de la membrana celular mediante un jTMD de 24 aa, mostraron que longitudes mayores de 12 aa hacen que el receptor Notch sea más sensible para ser activado. Estos resultados pueden correlacionarse con una mutación relativamente nueva responsable de T-ALL en la que el sitio de escisión S2 está separado del dominio transmembrana debido a una expansión de la jTMD (Sulis et al. 2008). En general, nuestros resultados sugieren que NRR para actuar como mecanosensor no requiere estar ubicado a una distancia específica de la membrana, pero parece ser crítico para evitar cualquier activación aberrante e independiente del ligando, donde el jTMD juega un papel importante papel.

Los resultados de nuestros experimentos indican que múltiples secuencias cortas de aa pueden actuar como mecanosensores dependientes del ligando y que el receptor Notch puede inducirse sin el NRR. Esto plantea la cuestión de cuál es la función de NRR, un gran dominio proteico (~ 300 aa) que parece estar conservado en las moléculas Notch en todos los metazoos. Observamos que, aunque la activación dependiente del ligando de CD4noNRRG4 era mayor que la de CD4NRRG4 (activación de 12 veces frente a 4,9 veces), la activación de CD4noNRRG4 independiente del ligando era aproximadamente dos veces mayor que la de CD4NRRG4 (Figura 3.22), lo que sugiere que el dominio NRR juega un papel esencial previniendo la activación inespecífica de la vía de señalizaión de Notch. Además, los resultados del “time-lapse” indican que el receptor diseñado sin NRR presentó una dinámica más lenta que el receptor CD4NRR, lo que sugiere que la región reguladora negativa de Notch (NRR) podría facilitar la interacción entre las ADAM y el sitio de escisión S2, lo que permite un corte proteolítico más eficiente. Otra posibilidad es que después de que se haya producido la tensión mecánica, el NRR mantenga la

proteína en un estado "abierto" aumentando la cantidad de tiempo que las proteasas ADAM pueden acceder al sitio de escisión S2 y por tanto su actividad proteolítica. Basado en este modelo, tener el NRR mejoraría la escisión en el sitio S2 tras la exposición del ligando. Sin embargo, nuestros resultados preliminares *in vivo* no mostraron diferencias significativas en el patrón de activación de embriónes de *Drosophila* con el receptor Notch con y sin NRR. Es necesario realizar experimentos de "time-lapse" *in vivo* para evaluar si la dinámica del receptor Notch también se ve afectada por el dominio NRR.

Finalmente, nuestros resultados de espectrometría de masas mostraron cuatro péptidos diferentes en el jTMD de los receptores sintéticos con y sin NRR. Esto sugiere que hay cuatro sitios potenciales de escisión similares a S2 en el hNotch1 jTMD en nuestro receptor. Serían necesarios más experimentos para revelar si existe una preferencia de qué sitio de escisión es reconocido por las ADAM dependiendo del contexto celular, como se muestra para los diferentes sitios de escisión de S3 en el dominio transmembrana de Notch (Tagami et al.2008) y, por lo tanto, el ligando que se une al receptor Notch. La activación del receptor Notch por diferentes ligandos podría desencadenar una escisión específica en el jTMD, lo que sugiere un control interno nativo de la vía de señalización Notch. Esta hipótesis podría explicar por qué una proteína simple como el receptor Notch puede inducir una vía de señalización compleja al unirse al ligando.

CONCLUSIONS

After analyzing the role of the negative regulatory region (NRR) in Notch receptor as a mechanosensor, we have reached the following conclusions:

1. CD4noNRRG4 receptor, without the canonical S2 cleavage site, is activated upon ligand binding suggesting that NRR domain is not essential for receptor signal activation. Furthermore, the CD4noNRRG4 receptor exhibits higher fold activation than CD4NRR receptor, even showing both receptors similar displayed on the cell surface.
2. The induction from CD4noNRRG4, CD4NRRG4, NotchnoNRRG4, and NotchNRRG4 receptors is strongly reduced by adding ADAM blockers, suggesting that these proteases also trigger the activation of the receptors lacking the S2 site.
3. Ablation of the ADAM10 protease by CRISPR/Cas9 technology blocks the activation of CD4noNRRG4 and CD4NRRG4 receptors indicating the activation of the CD4noNRRG4 receptor occurs by a mechanism similar to that observed in Notch-ligand interactions in a potential S2-like cleavage site.
4. Replacing the juxtatransmembrane domain (jTMD) from hNotch1 by the CD4jTMD shows not induction upon ligand binding, indicating that hNotch1 TMD is not sufficient for the ligand dependent activation of the engineered receptor. This result suggests that the 12 aa of the hNotch1jTMD, N-terminal to the TMD, can act as a ligand dependent mechanosensory in the absence of the NRR domain.
5. Notch receptors lacking the NRR domain, where the humanNotch1jTMD is replaced by different Notch species-jTMD, can trigger activation of the receptor, indicating that these different jTMDs can act as ligand dependent mechanosensors when are placed in heterologous molecules.
6. The jTMD from membrane proteins such as NCAM, E-cadherin or ErbB4 can also trigger receptor activation upon ligand binding, suggesting that can also work as mechanosensors.
7. Synthetic receptors without NRR and the jTMD from CD4 and CD8 cannot be induced upon ligand binding indicating that these 12 aa sequences (jTMD) from all the membrane proteins cannot act as mechanosensors. However, these

jTMDs do not inhibit the ability of the synthetic receptor when the NRR is present.

8. Modifications of the amino acid sequence from hNotch1jTMD do not block the activation of the synthetic receptors even when the sequences of the jTMD are either 12 Alanines or Glycines which do not have any defined structure.
9. Hybrids jTMD in which the Lysine, Glycine and last seven amino acids from CD8jTMD are substituted by Glutamic acid and the last seven amino acids from hNotch1jTMD respectively, do not show any inducibility. It suggests that amino acids at the hNotch1jTMD N-terminus may play an essential role for hNotch1jTMD to act as a mechanosensor.
10. We find that the S2 cleavage site needs to be placed to a minimal distance, at least 9 aa, from the plasma membrane to trigger Notch receptor activation. Moreover, NRR can be cleaved when it is placed at 24 aa from the plasma membrane.
11. Cell-cell interaction time-lapse reveals that receptors containing the NRR domain reached half-maximal induction over time faster than without it (11 hours versus 22 hours), suggesting that NRR conformation could enhance the efficiency of the proteolytic activity of the ADAMs.
12. Mass spectrometry experiments show four different peptides from the jTMD of CD4NRRnlsGFP and CD4noNRRnlsGFP receptors, indicating that there may be four potential S2-like sites in humans Notch1jTMD.
13. *Drosophila* embryos carrying Notch receptors with and without NRR seem to show a similar cell pattern induced by ligand dependent cleavage.

Tras analizar el papel de la región reguladora negativa (NRR) en el receptor Notch como mecanosensor, hemos llegado a las siguientes conclusiones:

1. El receptor CD4noNRRG4, sin el sitio de escisión canónico S2, se activa tras la unión del ligando, lo que sugiere que el dominio NRR no es esencial para la activación de la señal del receptor. Además, el receptor CD4noNRRG4 exhibe una mayor activación que el receptor CD4NRR, incluso mostrando ambos receptores de manera similar en la superficie celular.
2. La inducción de los receptores CD4noNRRG4, CD4NRRG4, NotchnoNRRG4 y NotchNRRG4 se reduce fuertemente al agregar bloqueadores de las proteasas ADAM, lo que sugiere que estas proteasas también desencadenan la activación de los receptores que carecen del sitio de corte S2.
3. La ablación de la proteasa ADAM10 mediante tecnología CRISPR / Cas9 bloquea la activación de los receptores CD4noNRRG4 y CD4NRRG4, lo que indica que la activación del receptor CD4noNRRG4 se produce mediante un mecanismo similar al observado en las interacciones Notch-ligando en un potencial sitio de escisión similar a S2.
4. La sustitución del dominio juxtatransmembrana (jTMD) de hNotch1 por CD4jTMD no muestra inducción tras la unión del ligando, lo que indica que hNotch1 TMD no es suficiente para la activación dependiente del ligando de dicho receptor sintético. Este resultado sugiere que los 12 aa del hNotch1jTMD, N-terminal del TMD, pueden actuar como un mecanismo sensorial dependiente de ligando en ausencia del dominio NRR.
5. Los receptores Notch que carecen del dominio NRR, donde el HumanNotch1jTMD se reemplaza por diferentes especies del jTMD de Notch, pueden desencadenar la activación del receptor, lo que indica que estos diferentes jTMDs pueden actuar como mecanosensores dependientes de ligandos cuando se colocan en moléculas heterólogas.
6. El dominio jTMD de proteínas de membrana como NCAM, E-cadherina o ErbB4 también puede desencadenar la activación del receptor al unirse al ligando, lo que sugiere que también puede funcionar como mecanosensores.

7. Los receptores sintéticos sin NRR y con el jTMD de CD4 y CD8 no pueden inducirse tras la unión del ligando, lo que indica que estas secuencias de 12 aa (jTMD) de todas las proteínas de membrana no pueden actuar como mecanosensores. Sin embargo, estos jTMD no inhiben la capacidad del receptor sintético cuando está presente el dominio NRR.
8. Las modificaciones de la secuencia de aminoácidos de hNotch1jTMD no bloquean la activación de estos receptores sintéticos incluso cuando las secuencias de jTMD son 12 alaninas o glicinas que no tienen ninguna estructura definida.
9. Los dominios híbridos jTMD en los que la lisina, la glicina y los últimos siete aminoácidos de CD8jTMD están sustituidos por ácido glutámico y los últimos siete aminoácidos de hNotch1jTMD, respectivamente, no muestran ninguna inducibilidad. Sugiere que los aminoácidos en el extremo N-terminal de hNotch1jTMD pueden desempeñar un papel esencial para que hNotch1jTMD actúe como un mecanosensor.
10. Encontramos que el sitio de escisión S2 debe estar a una distancia mínima, al menos 9 aa, de la membrana plasmática para desencadenar la activación del receptor Notch. Además, NRR se puede escindir cuando se coloca a 24 aa de la membrana plasmática.
11. Experimento de “time-lapse” de interacción celular revelan que los receptores que contienen el dominio NRR alcanzan la inducción media máxima más rápido que el receptor sin NRR (11 horas frente a 22 horas), lo que sugiere que la conformación de la región NRR podría mejorar la eficiencia de la actividad proteolítica de las ADAMs.
12. Los experimentos de espectrometría de masas muestran cuatro péptidos diferentes en el jTMD de los receptores CD4NRRnlsGFP y CD4noNRRnlsGFP, lo que indica que puede haber cuatro sitios potenciales similares a S2 en el dominio jTMD de Notch 1 dehumano.
13. Los embriones de *Drosophila* que llevan receptores Notch con y sin NRR parecen mostrar un patrón de inducción dependiente de ligando similar entre ellos.

METHODS

Gene constructs

All constructs used in this thesis were assembled using standard restriction enzyme-based cloning and Gibson cloning (Gibson et al. 2008). 1d3NRRG4 has been described previously (Huang et al. 2016). All the constructs were subcloned into the FUW lentiviral backbone (Lois et al. 2002).

TRACT engineered construct: 1d3NRRG4 was constructed by fusing a single-chain antibody (SCAD) that recognizes the mouse CD19, the NRR and TMD from human notch1, and Gal4 as the intracellular domain. The SCAD included amino acids 1-289 from the monoclonal 1d3-28z.1-3 (Kochenderfer et al. 2009). The NRR domain and TMD comprised amino acid 1446-1880 of human Notch1. Gal4 transcription Factor was then fused after the Notch1 TMD, and the entire 1d3NRRG4 was subcloned into the FUW lentiviral backbone (Lois et al. 2002). All the receptors were cloned following the same logic, introducing different modifications described in the figures or Supplementary Tables. All the gene blocks were generated from Integrated DNA Technologies (IDT).

Different modifications on 1d3NRRG4 or CD4NRRG4 to improve TRACT function are listed in the followings:

For the different modifications of the transmembrane domain and 1d3HybdridG4 receptors, the insert of the hNotch1jTMD and TMD modifications were a gene block from Integrated DNA Technologies (IDT). These inserts were subcloned into 1d3NotchjTMD/TMD (2xBamHI) digested with BamHI.

1d3NRResn63GS and 1d3NRResnGCN4S: The insert TMD esn63GSGCN4 was a gene block from Integrated DNA Technologies (IDT) and the inserts for 1d3NRResnGCN4S were GCN gene block and TMDesn63GS which was generated by PCR. The esn63GSGCN4 gene block or the PCR fragment and the GCN gene block and TMDesn63GS were subcloned into FU1D3NRResn digested with Xba and AscI.

Construct where the jTMD were snorkelled FUCD4NRRqseRKR, FUCD4NRRqseLWFRR: the inserts, QSERKR, QSELWFRR, were gene blocks from IDT that were subcloned into FUCD4NRRqseaqESN digested with BamHI.

The inserts of dimerized receptors (DBD, zipV16AD and VP16ADzip) by leucine-zipper in their intracellular domain (1d3NRRDBD, 1d3NRRZIPVP16 and 1d3NRRVP16ZIP, respectively), were subcloned into 1d3NRRG4 digested with BamHI and AscI.

The inserts were gene blocks for the different variations of DHFR: SmaI tet DHFR gene block for hCARNRRtetDHFR and SmaI tet DHFR 100I and Sma I tet DHFR 100Y for hCARNRRtetDHFR100I (WT) and hCARNRRtetDHFR100Y, respectively. These inserts were subcloned into Fsynotchtet digested with SmaI.

Most of the receptors where the insert was a gene-block of a juxtatransmembrane domain (jTMD): CD8, CD4, NCAM, erbB4, e-cadherin, chicken, Xenopus, zebrafish, *Drosophila*, modifications of NotcjTMD (from modif.1 to modif.6) 12 Alanines and 12 Glycines, were designed by IDT. These inserts were subcloned into CD4noNRRhN1jTMD digested with BamHI.

For the receptor CD4NRRQSEAQ (5aajTMD), the insert of 5aa (QSEAQ) from IDT were subcloned into CD4NRRG4 digested with BamHI.

For those receptors with different length of the jTMD carrying NRR, the inserts (6aa, 7aa, 8aa, 9aa, 10aa, 11aa, 12aa) from IDT were subcloned into CD4NRRQSEAQ(5aajTMD) digested with BamHI.

The insert from the three constructs with the TMD from TORSO, SEVENLESS or APP were gene blocks inserted into FUCD4hN1TMDesn (2x BamHI) digested with BamHI-HF.

Cell culture.

CHO-K1 and UAS-H2B-citrine reporter CHO cells (kindly provided by Dr. Elowitz (Caltech)) and their derivatives were grown on tissue-culture grade plastic plates (Thermo Scientific) in MEM (10-010-CV, Corning Cellgro), supplemented with 10% FBS (Corning), and 1% penicillin, streptomycin, and L-glutamine (30-009-CI, Corning). HEK293 (used to make lentiviruses; 293T, ATCC, No. CRL-3216), HeLa cells (CCL-2, ATTC) and their derivatives cell lines were grown in DMEM (Corning Cellgro), supplemented with 10% FBS (Corning), 1% penicillin, streptomycin, and L-glutamine (30-009-CI,

Corning) and 1% sodium pyruvate (25-000-CI, Corning Cellgro). All cells were grown at 37°C in 5% CO_2 in a humidified atmosphere. Cells were passaged every 1-2 days, depending on confluency, using 0.05% Trypsin-EDTA (25300-62, Life Technologies).

Lentivirus production.

We used human embryonic kidney cells (HEK 293T cells) from ATCC (reference above) to generate all the lentivirus for this thesis.

Cell thawing: A frozen vial from liquid nitrogen container was incubated in a 37°C water bath for less than 2 minutes. The cells were transferred into a 15 ml tube, and added dropwise, 10 ml of pre-warmed. After layering the medium, cells were spined for 5 minutes at 1000 rpm in a table-top centrifuge. The supernatant medium was discarded, and 4 ml of 10% FBS medium was added on top the pellet, and cells were resuspended by pipetting 5-6 times. Then, cells were seeded on a 6 cm tissue culture plate and placed in a tissue culture incubator (humidified, 37°C and 5% CO_2). Next day, cells were trypsinized and split into a 10 cm plate.

Cells transfection: The day before the transfection, we trypsinized, counted and diluted the cells to 0.5 x 10^6 cells/ ml. Then, cells were seeded on 10 cm plates. Approximately 16 to 20 hours after seeding the cells, we removed 2 ml (10 cm plate) of medium and leaved cells in the incubator for at least 1 hour. Then, in a 5 ml polypropylene tube, we mixed 20 µl of transfer vector, 15 µl of Δ 8.9 plasmid, plus 5 µl of VSVg plasmid. Added 100 µl of 2.5M $CaCl_2$ and filled up to 1 ml with ddH_20, and mixed. In a separate 5 ml polypropylene tubes, we added 1 ml of 2x HBSS pH 7.05 (280mM NaCl, 50mM HEPES, 1.42mM $Na_2HPO_4 \bullet 7H_2O$ and carefully adjust the pH to 7.02, 7.03, 6.04 and 7.05 making fours solutions with different pHs). Then, we took out of the incubator one plate at a time and placed it is the hood. We added 1 ml of the DNA+$CaCl_2$+H_2O into the tube with 1ml of 2x HBSS pH 7.05 and mixed. Once mixed, we added the DNA+$CaCl_2$+HBSS mixture to the side of a plate while swirling and putting the dish back in the incubator. We always used 3 x 10 cm plate for each virus. 4 hours after adding the DNA+CaCl2+HBSS mix to the cells, the medium was aspirated, and cells were washed twice with pre-warmed PBS, and changed to 12 ml (10 cm plate) of new pre-

warmed DMEM+10% FBS medium. Then, plates were returned to the incubator and left there for 72 hours until the supernatant is collected.

Virus collection: To collect the viral supernatant, we took the plates from the incubator, and poured the medium into 50 ml conical tubes. Tubes were spinned at 1000 rpm in a table-top centrifuge for 5 minutes to remove large cellular debris. After this spinning, the viral supernatant was filtered using a pre-wetted 0.8µm syringe filter (PN4618, from PALL). The filtered suspension was added into a 30 ml ultraclear Beckman tubes (358126, from BECKMAN COULTER). The tubes were sealed with parafilm, placed into the ultracentrifuge buckets, and equilibrated before introducing in the ultracentrifuge to prevent spilling during spinning. The centrifuge was adjusted to spin for 90 minutes at 4°C, 25,000 rpm. When spin finished, the viral supernatant was poured into a 500 ml beaker containing 10 ml of bleach 10%. Then, tubes were inverted over a sterile Kimwipe to drain remnants of medium. Finally, we added 30 µl of cold PBS to the tube's bottom and sealed with parafilm to prevent evaporation. The tubes were placed at 4°C in a rotating rocker at least 24 hours to dissolve the pellet. After that, pipette up and down gently to dissolve the pellet, aliquot the virus into 3 µl aliquots, and freeze at –80°C.

Generation of Stable Cell lines.

Citrine is a variant of YFP, and we will refer to this reporter as UAS-H2BmCitrine. UAS-H2BmCitrine cells were grown as described previously (Sprinzak et al. 2010).

Lentiviral vectors were produced and stored as previously described, using the plasmids described above. The viral titer was determined by serial dilution. We calculated the volume of lentiviral prep from this viral titer that we need to add to the cells in suspension to generate every cell line with approximately the same number of viral particles to be comparable. To stably express the receptors or ligands, UAS-H2B-citrine reporter CHO (receptors) or CHO-K1 (ligands) cell lines were resuspended in MEM culture media (with 10% FBS and 10x Pen, Strep-Glut) at a density of 300,000 cells/ml. The cells were infected by mixing with the specific receptor/ligand lentivirus. Then, the cells were cultured in a 96-well plate for 3 days, without changing the media. Subsequently, the cells were expanded in fresh media and used for the experiments. To

generate stable lines of emitter cells, CHO-K1 cells were infected by retrovirus expressing either mCD19mCherry, hCD19tdTomato or gp160mCherry. To generate UAS-GFP reporter HeLa cell line (used for ADAM10 experiments), HeLa cells were infected with UAS-GFP lentivirus. UAS-GFP reporter HeLa cells were sorted into three different populations based on GFP intensity to generated more homogenous stable cell lines.

Cell-cell interaction experiments.

Receptor cell lines (modifications indicated in 2nd and 3rd Chapters) were co-cultured with either mCD19mCherry, gp160mCherry or hCD19tdTtomato cells at 1:1 ratio in 24-well plates (at 300,000 cells/ml), depending on the extracellular domain of the receptor which will be recognized by one of these three ligands. After 48 hours of cells plating, pictures were taken under an inverted epifluorescence microscope with 10x objective. At least three experiments were done for each receptor.

Co-culture assays and time-lapse microscopy.

24 Glass-bottom multi-well plates (CLS-1812-024 from Chemglass Life Sciences) were coated with 5 µg/ml Hamster Fibronectin (Oxford Biomedical Research) diluted in 1x phosphate-buffered saline (PBS) for 30 minutes at room temperature. Emitter cells (pre-induced for 48h with 4-epiTc (kind gift from Michael Elowitz laboratory) or CHO-K1 cells were mixed in suspension with similarly trypsinized receptor cell line (CD4NRR or CD4noNR) at a ratio of 20:1. A total of 10 x 10^4 cells (70% confluence) were plated for each experiment, with continued 4-epiTc induction. Imaging starts 2-4h post-plating.

Time-lapse microscopy: Movies were acquired at 20X (0.75 NA) on an Olympus IX81 inverted epifluorescence microscope equipped with hardware autofocus (ZDC2) and an environmental chamber maintaining cells at 37°C, 5% CO_2. Automated acquisition software (METAMORPH, Molecular Devices) was used to acquire images every 30 minutes in multiple colours (YFP, RFP) or differential interference contrast (DIC), from multiple stage positions.

Induction experiments by substrate-attached ligand on ELISA plates.

Mouse anti-CD4 (monoclonal-CD4 (MHCD0400 from Thermo Fisher), mouse anti-humanNotch1 (MAB5317, R&D Systems) and anti-rabbit anti-mouse IgG F(ab')2 (315-005-047 Jackson ImmunoResearch) antibodies were diluted at 10 µg/ml. Diluted antibodies were used to coat 96-well ELISA plates (442404, Thermo Scientific) at 4°C overnight. Next day the ELISA plates were gently washed with PBS, and 10mg/ml BSA was added to block the plates at 37°C for 2 hours. Then, receptor cell lines (CD4NRR, CD4noNRR, NotchNRR and NotchnoNRR) carrying the reporter (UAS-H2BmCitrine) were plated at (2×10^4).

For S2 inhibitor experiments, we incubated the cells with the batimastat (BB94, 50 µM; SML0041, Sigma-Aldrich), GM6001 (50 µM; SC203979, Santa Cruz Biotechnology), TAPI (100 µM; SC20585, Santa Cruz Biotechnology), while for S3 inhibitor experiments we added DAPT (10 µM) into growth medium when cells were plated. Cells were analyzed 48 hours after the cells were plated using an inverted epifluorescence microscope with 10x magnification.

ADAM10 and Scrambled CRISPR-CAS9 induction experiments.

There are currently several tools to edit the genome, but the CRISPR/Cas9 system has become the most popular, owing to its ease of use and rapidity. The CRISPR/Cas9 (clustered regularly interspaced short palindromic repeats) system was first described in prokaryotes as an adaptative immunity strategy against foreign elements (Barrangou, 2015). The CRISPR/Cas9 system comprises two components: the guide RNA (gRNA) and the endonuclease Cas9.

We used this system to knockout the ADAM10 gene. For that, we tested 3 different gRNAs (#1 346-CATGGGTCTGTTATTGA; #2 982-CTTGGTCTGGCTTGGGT; #3 1123-GTAATGTGAGAGACTTT; abm, 1130711; HGNC ID:188). We made lentiviruses, infected Hela cells, and verified the CRISPR/Cas9 system's efficiency by western blot (antibody against ADAM10). We used the #3 gRNA to infect the receptor cell lines CD4NRRG4 and CD4NoNRRG4. Then, we performed induction experiments by substrate-attached ligand and images were taken after 48 hours of cells were plated.

Induction experiments by recombinant enzymes.

Reporter cell lines carrying the receptors SUMOubi, 2xSUMO, CD4SUMO and 1d3NRRG4 were plated at 60% confluency 24 hours before adding different concentrations of recombinant SUMO protease (0.5 U, 2.5 U, 5 U, 10 U and 20 U). For CD4LPETGG4 receptor, recombinant SorteaseA was used. After 24h of adding the enzymes, images were taken using an inverted epifluorescence microscope (10x).

Western Blots.

Sample preparation: Cells were washed with PBS before adding 500 µl of RIPA (Radio Immuno Precipitation Assay) Buffer (50mM Tris, pH8.0, 150mM NaCl, 1% Triton X-100, 0.5% sodium deoxycholate, 0.1% SDS and EDTA-free protease inhibitor cocktail) at room temperature into a 6 cm plate. Cells were scraped with the lysis buffer and incubate during 5 minutes before sheared the genomic DNA by passing 15-20 times through a 26g needle. Then, the cell lysate was either boiled for 3 minutes (ADAM10 detection) or incubate at 37°C for 30 minutes (Receptors detection) and spinned down at 4°C 14.000 rpm for 5 minutes to discard the insoluble cell debris. The lysate supernatant was transferred to a new Eppendorf and used immediately or stored at -20°C until its use. If the samples were frozen, it was boiled for 2 minutes and spin down before loading.

Measurement of protein concentration: The protein concentration of the cell extracts is determined by the Bradford colourimetric method, using bovine serum albumin (BSA) as standard. The protein concentration is determined by measuring the samples' absorbance at 594 nm and extrapolating the values obtained in a standard line constructed with known BSA amounts (125-2000 µg).

Assembly and gel casting: The running gel 8% was prepared by mixing: 3 ml of 30% acrylamide/bis solution; 3.75 ml of 1.5M TRIS pH 8.8; 8.25 ml of ddH_2O; 50 µl of 10% ammonium persulfate; 15 µl of TEMED. Then, the solution was pipetted into the assemble gel cassette. 0.5ml of isopropanol was added at the top of the gel to level it out and waited 30 minutes for the gel to polymerize. Once running gel has solidified, isopropanol was decanted. Using the corner of a Kim wipe, we drained the residual

alcohol off the top of the gel. Next, the reagents for the stacking gel were added to a 15ml conical tube and mixed gently (stacking gel 5%: 0.65 ml of 30% acrylamide/bis solution; 1.25 of 4x Tris pH 6.8; 3.05 ml of H_2O; 25 µl of 10% APS; 10 µl OF TEMED). Between 2 and 3 ml of the stacking gel solution were added into the running gel, and then the combs were inserted into the gel and waited 10 minutes for the gel to polymerize.

Loading and gel electrophoresis: After stacking gel was polymerized, the assemble gel cassette was inserted into the electrophoresis apparatus. The electrophoresis cobette was filled up with electrophoresis running buffer (15.1 g TRIS base, 72 g glycine, 5 g SDS, H20 up to 1000 ml to make 5X STOCK. Dilute 1:5 before using). Samples containing equal protein amounts (30 µg of total protein) were loaded per lane, a line was also loaded with 3-5 µl of pre-stained standards. The samples were stacked by running at 90 volts for 15-20 minutes, then at 150 volts for an additional 2 hours.

Transfer Assembly: Once the proteins have been separated according to their molecular weight by electrophoresis, the proteins present in the gel are transferred to nitrocellulose membranes by applying a constant current (300 milliamps). The transfer cobette was filled up with the transfer Buffer (29 g glycine, 58 g Tris-base, 3.7 g SDS to make 10x STOCK. The working solution is diluted in water (1:10) and 200ml ethanol are added per liter). The transfer efficiency was then checked by incubating the membrane for 5 minutes in Ponceau S staining solution (0.1% Ponceau in 5% acetic acid). Next, we blocked membrane with 4 % of blocking solution (skimmed milk powder dissolved in TBS-T (24 g Tris-HCl, 5.6 g Tris-base, 88 g NaCl, H_2O up to 900 ml and adjust the pH to 7.6 making 10x STOCK. Dilute 1:10 before use. And add 1 ml of Tween20) for 1 hour at room temperature. Then, the membranes were incubated with antibodies against ADAM10 (rabbit polyclonal (abcam, ab1997, diluted 1:800), alpha-tubulin (mouse monoclonal (DM1A (ThermoFisher) diluted 1:500) or GFP primary antibody (rabbit polyclonal (AB3080P 1:1500 (Millipore) diluted 1:1000) overnight in 1% of blocking solution at 4°C. Next day, the membrane was washed 3 times with TBST for 5 minutes each wash and incubated with secondary antibody conjugated to the enzyme horseradish peroxidase (HRP) (goat anti-rabbit (1706515, BIO-RAD diluted 1:2000) and

anti-mouse (1706516, BIO-RAD diluted 1:2000) in 1% of blocking solution for 1 hour at room temperature. After the incubation with the secondary antibody, the membrane was washed 3 times for 5 minutes in TBST buffer. Finally, the chemiluminescent substrate (1705061, BIO-RAD) is added for 2 minutes at room temperature. The membranes are imaged in Western Blot imager (Azure c-400 from Azure system) at different exposure times. The bands corresponding to the proteins of interest are observed where there has been luminescent emission.

Cell surface and regular immunostaining.

The cell for immunostaining was first seeded on coverslip glasses pre-coated by poly-D-lysine in water for 30 minutes at room temperature before the seeding. For cell surface staining, the cells were first pre-treated with Dynasore (100 µM, D7693, Sigma) for 30 minutes at 37°C in the incubator to block the endocytosis. The cells were then washed by the surface staining buffer (1x PBS with 2% fetal bovine serum (FBS), 0.1% sodium azide and 100µM Dynasore) for 5 minutes on ice. After the wash, the cells were incubated with different primary antibodies depend on the receptor cell line: anti-human CD4 (1:50 dilution, monoclonal-CD4 (MHCD0400 from Thermo Fisher) or rabbit anti-mouse IgG F(ab')2 (1:50 dilution in the surface staining buffer, 315-005-047 Jackson ImmunoResearch) for 45 minutes on ice. The cells were washed three times for 5 minutes each on ice after the antibody incubation. Subsequently, the cells were incubated with the secondary antibody, goat anti-rabbit or anti-mouse (Alexa555, 1:250 dilution) for 45 minutes on ice. After this, the cells were washed three times for 10 minutes each. After the cell surface staining, the cells were fixed with 4% paraformaldehyde for 10 minutes at room temperature and followed by the regular immunostaining procedures or incubate with 499 fluor Membrite (30093-T, Boitium) for 30 minutes at 4°C and DAPI (4',6-diamidino-2-phenylindole, 1:50,000) for 10 minutes at room temperature. The cells were washed in PBS three times for 5 minutes each and permeabilized with PBS/0.05% triton X-100 (PBST) for 20 minutes for the regular immunostaining. After the permeabilization process, blocking solution with 10% FBS in PBST were added to the cells for 40 minutes. Subsequently, the cells were incubated with different primary antibodies depending on the experiment: antibodies against Gal4DBD (DNA binding domain, mouse monoclonal IgG2a, (RK5C1) sc-510. Santa Cruz

Biotechnology diluted at 1:200) or mCherry/tdTomato (Rat monoclonal [5F8] to Red Fluorescent Proteins (RFP), Chromotek; diluted at 1:1000) diluted in 1% serum/PBST. The incubation duration is overnight at 4°C. Next day, the cells were washed three times in PBST and incubated with secondary antibody (555 goat anti-mouse or rat, Life Technologies, diluted at 1:800) for 90 minutes. Finally, the cells were washed 3 times in PBST and analyzed under an inverted epifluorescence microscope or imaged using confocal microscope (Zeiss LSM 800) under 63x or 100x objective.

Co-culture Induction Assay for cleavage site.

CHO-K1 cell lines were transfected with two different receptors: CD4-NRR-Notch1TMD-nlsGFP or CD4-NRR-Notch1TMD-nlsGFP using lipofectamine 2000 reagent (Invitrogen, 11668027). The cells were seeded 24h before the transfection to be 70-90% confluent the day of transfection. The Lipofectamine 2000 were diluted in Opti-MEM in a ratio 1:5 respectively. The DNA was also diluted in the same medium: 5 µg of DNA in 250 µl of medium for 24 well plates). Both dilutions were at room temperature for 5 minutes and then mixed and incubated for at least 20 minutes at room temperature. Then, the lipid-DNA complex was added to the cells. After 4 hours, the cells were washed with fresh medium containing DAPT (γ-secretase blocker) or DMSO as a control. In order to find the S2-like site of the receptor without NRR, the S3 cleavage site must be blocked, so this inhibitor of secretase was added to the medium after 4 hours of transfection. Twenty-four hours after the washes, ligand cell lines expressing gp160mCherry or mCD19mCherry (as a control) were plated on top of the transfected CHO-K1 cells. The cells were harvested after 48 hours of adding the ligand cell lines.

Purification of receptors from transfected CHO-K1 cell lines.

The cells were washed with DPBS without calcium and magnesium at room temperature and collected with a scrapper. Cells in suspension were centrifuged for 5 minutes at 1000 rpm with two washes in between. The pellet was frozen at -80°C.

The next day, the pellet was thawed and diluted in solubilization buffer (0.05M HEPES pH 7.5, 0.2M NaCl, 2mM MgoAc (Millipore Sigma, 63052-100), Triton 1%, 25x EDTA-free protease inhibitor cocktail (PI, Millipore Sigma, 11873580001), 1mM DTT

(1,4-dithiothreitol, Millipore Sigma)**,** and 4M UREA) and incubated at 4°C for minutes. The pellet was then centrifuged at 18,213 relative centrifugal force (rcf) for 20 minutes in table-top Eppendorf centrifuge at 4°C.

Biotinylated nanobodies (kind gift from Voorhees lab), which target the intracellular domain of the receptors (nls GFP), were immobilized on magnetic Pierce Streptavidin Beads (Thermo Fisher) in wash buffer (0.05M HEPES pH 7.5, 0.2M NaCl, 2mM MgoAc (Millipore Sigma, 63052-100), Triton 0.1%, 25x EDTA-free protease inhibitor cocktail (PI, Millipore Sigma, 11873580001), and 1mM DTT (1,4-dithiothreitol, Millipore Sigma) for 30 minutes at 4°C. The remaining biotin-binding sites on the beads we subsequently blocked with 50 µM Biotin-PEG-COOH (Iris Biotech) in S250 buffer for 15 minutes in solubilization buffer. The blocked beads were incubated with the Protein Extract for 1h at 4°C. After the incubation, the beads were separated from the extract using a magnetic rack and were washed twice in solubilization buffer followed by two washes in wash buffer. Nanobody-target protein complexes were then eluted by adding 0.5 µM SUMOStar protease (Liu et al. 2008) in wash buffer for 30 minutes at 4°C. Once the proteins were purified, Digestion in solution with Chymotrypsin and trypsin was performed.

The four samples (induction and control for CD4NRRG4 and CD4noNRRG4) were digested following a reduction process with 1 µl of TCEP (Tris(2-carboxyethyl) phosphine, reducing agent) in MS buffers for 20 minutes at room temperature and alkylation with 3.6 µl OF 500 mM 2-chloro-acetamide for 15 minutes at room temperature. After this, the samples were incubated with 2 µl Lys-C endoprotease for 4 hours at 37 °C. Then, the samples were incubated with trypsin (100 ng/µl) and Chymotrypsin (100ng/ µl) for 18 hours at 37°C and at 25°C for 18 hours, respectively. The next day, the samples were desalted using Pierce C18 spin columns (cat #89870). 10 µL of 20% TFA were added to the samples to adjust pH=2. Then, an activated Resin process of the columns was performed. After the Resin equilibration, the samples were added to the columns and centrifuge for 2 minutes at 1500 g three times. Then, the samples were washed (200 µL 5% CAN (acetonitrile) and 0.5% TFA (*Trifluoroacetic acid*) and eluted with 50 µL 70% ACN 0.2% FA (formic acid). Finally, the samples were dried and stored at -80°C for Mass Spectrometry.

Liquid Chromatography-Mass Spectrometry (LC-MS) analysis.

Liquid chromatography-mass spectrometry (LC-MS) analysis was carried out on an EASY-nLC 1200 (Thermo Fisher Scientific, San Jose, CA) coupled to an Orbitrap Eclipse Tribrid mass spectrometer (Thermo Fisher Scientific, San Jose, CA). Digested and desalted peptides were resuspended in 20 µL 0.2% formic acid, and 5 µL peptides per sample were loaded onto an Aurora 25 cm x 75 µm ID, 1.6 µm C18 reversed-phase column (IonOpticks, Parkville, Victoria, Australia) and separated over 43 minutes at a flow rate of 350 nl/min with the following gradient: 2–6% Solvent B (3 minutes), 6-25% B (20 minutes), 25-40% B (7 minutes), 40-98% B (1 minute), and 98% B (12 minutes). Solvent A consisted of 97.8% H2O, 2% ACN, and 0.2% formic acid, and solvent B consisted of 19.8% H_2O, 80% ACN, and 0.2% formic acid.

MS1 spectra were acquired in the Orbitrap at 120K resolution with a scan range from 350-2000 m/z, an AGC target of 1e6, and a maximum injection time of 50 milliseconds in Profile mode. Features were filtered for monoisotopic peaks with a charge state of 2-7 and a minimum intensity of 1e4, with dynamic exclusion set to exclude features after 1 time for 45 seconds with a 5-ppm mass tolerance. HCD fragmentation was performed with collision energy of 28% after quadrupole isolation of features using an isolation window of 0.7 m/z, an AGC target of 1e4, and a maximum injection time of 35 milliseconds. MS2 scans were then acquired in the ion trap at Rapid rate in Centroid mode and with auto scan range. Cycle time was set at 3 seconds.

Cell-cell interaction and induction experiments by the substrate-attached ligand on ELISA plates Imaging.

For all *in vitro* experiments, images were taken under an inverted fluorescence microscope with 10× or 20x objective lenses with an exposure time of 200 milliseconds and 1 binning under the same condition among constructs and experiments.

***In vivo* experiments (*Drosophila melanogaster*).**

For all experiments using transgenic flies, we modified the 1d3NRRG4 receptor described in Results from 2nd Chapter (Figure 2.17, 2.18 and 2.19) and 3rd Chapter (Figure 3.24) and we generated transgenic flies with new receptors called: nSyb-

1d3NRR::dNlg2lexAGADDHFR7 and nSyb-1d3NRR::dNlg2lexAGADDHFR30 (Figure 2.17) ; nSyb-1d3NRR::G4; nSyb-1d3NRR::dNlg2ICD::G4; nSyb-1d3NRRHyb::dNlg2ICD::G4 (Figure 2.18); nSyb-1d3NRR (Figure 2.19) and hsp70-NotchNRR and hsp70-NotchnoNRR.

For DHFR flies, were given drosophila formula with different concentrations of TMP. After the treatment, the flies were dissected and imaged for GFP signal under an inverted epifluorescence microscope (4x). More details in results from Figure 2.17 (2nd Chapter).

Transgenic flies used to analyze some *in vitro* modifications of the receptor (Figure 2.18) were dissected in adult stages and stained against nc82 and GFP antibody. On the other hand, the transgenic flies used to test the capability of TRACT method as a retrograde tracer (Figure 2.19) were cryo-dissected and stained against OLLAS tag antibody.

For HSP70-NotchNRRG4 and NotchnoNRRG4 (Figure 3.24) transgenic flies' analysis by live imaging, the embryos were collected for 1-2 hours at 25C. Then, the outer chorion layer was removed to visualize both receptors' expression pattern for live imaging. The *Drosophila* embryos were dechorionated with 50% bleach for 3 minutes agitating gently followed by 3 washes with dH2O. After that, mount the embryos in holocarbon oil (H8898 from Sigma). Dechorionated embryos were imaged using confocal microscope (Zeiss LSM 800) under 20X objective. Z-stacks were merged and analyzed using ImageJ and edited with Photoshop (Adobe) software. All the crosses were maintained at room temperature and were repeated at least 3 times.

Cryoprotection and freezing.

The flies were fixed with 4% paraformaldehyde (PFA) for 10 minutes at washed repeatedly with 0.1M PBS for 1 hour. They were then transferred to a solution of 0.1M PBS and sucrose (10%) between 24-48 hours at 4°C to cryoprotect the samples.

Subsequently, the pieces were transferred to another solution composed of 0.1M PBS, sucrose (10%) and gelatin (10%), for 30 minutes at 37°C. With this step, we

achieve that the sucrose/gelatin solution completely envelops the piece and gives it consistency.

While the flies were soaked in the sucrose/gelatin solution, the sucrose/gelatin solution was added in a 2x2 cm plastic tray and placed at 4°C until the mixture solidified. Next, the sucrose/gelatin solution flies were placed in the plastic tray on the solid sucrose/gelatin base. Then, more solution was added to the piece until it was covered entirely and left 15 minutes at 4°C until it was solidified. After this process, the gelatin piece was removed from the plastic tray and cut into cubic blocks with a blade with the proper orientation. The block was then frozen at -70°C. For this process, isopropyl alcohol (2-propanol) was used to which dry ice was added to reach a temperature between -60°C and -75°C.

Previously, we had cut out a 2x2 cm square from a 3 mm thick sheet of cork and labelled properly with the specimen's name to be frozen. Then, we added a few drops of Tissu-Tek on the reverse side of the sheet on which the sucrose/gelatin block containing the sample was placed. This whole set (cork/Tissu-Tek/block) was immersed in isopropyl alcohol (-70°C) for 2 minutes. Tissu-Tek solidifies at low temperatures, acting as a glue.

After freezing, we took out the block attached to the cork sheet, let it dry dried and wrapped in aluminium foil. The pieces were stored at -80°C until they were cut in the cryostat microtome.

Microtomy.

The cuts were made on a cryostat microtome with a thickness of 40 µm. Consecutive series were obtained to perform the different immunocytochemical reactions subsequently. Sections were collected on superfrost slides and allowed them to dry for 2 hours and later stored at -80°C until use.

Immunostaining and microscopy of fly brain.

The brains of the wandering larvae were dissected in 1x PBS under a dissection microscope. Brains were fixed by immersing them in a 4% paraformaldehyde solution in

PBS for 15 minutes at room temperature. Brains were washed in PBS three times for 10 minutes each, followed by permeabilization with PBS/0.5% triton X-100 (PBST) for 30 minutes and blocking with 5% serum in PBST for 30 minutes. The brain samples were stained with different antibodies depending on the experiment: antibodies against GFP (rabbit polyclonal from Millipore, AB3080, diluted at 1:1,000), mCherry (rat monoclonal, 5F8, from Chromotek diluted at 1:1,000), Brp (mouse monoclonal, nc82, from DSHB diluted at 1:50) and OLLAS tag (rat monoclonal L2 NBP106713 (Novus) diluted at 1:300) diluted in 5% horse serum /PBST. Brains were incubated with primary antibodies overnight at 4°C, washed three times in PBST, incubated with secondary (goat secondary antibodies, Life Technologies, 1:500) for two hours at room temperature, washed in PBST and mounted on glass slides with a clearing solution (Slowfade Gold antifade reagent, Invitrogen).

Stained brains, VNC or muscles were imaged with confocal microscopes (Olympus Fluoview 300) under either 20X or 40X. We imaged 150 sections with an optical thickness of 0.3-0.5 µm from dorsal or ventral sides in a typical experiment. Confocal stacks were processed with Fiji to obtain maximal projections, and images were processed with Photoshop.

Image segmentation.

Images were acquired in uint8 or uint16 format. The images were smoothed with a Gaussian filter (standard deviation 2) and divided by the same image smoothed with a Gaussian filter using a standard deviation of 3. The resulting ratiometric image was normalized by dividing each pixel by the maximum intensity in the image. The normalized imaged was then converted to a binary using a threshold of 0.501. The Gaussian filters and threshold size were empirically determined and kept constant for all experiments unless stated otherwise. The binary image was then segmented using the MATLAB function *regionprops,* and each ROI was labelled with a unique identifier. The Euclidean distance transform of the labelled image was then calculated to obtain the interpixel distance between all pixels in an ROI. This approach assigns pixels at the core of an ROI with a higher value than pixels at the periphery. The Euclidean distance matrix was inverted, and the watershed approach was used to segment the matrix into

a series of segments, some of which contain the expected ROIs. This step is necessary to capture features of the ROIs which may not be Gaussian in nature. The fully segmented image was then multiplied by the original labelled binary image and relabeled with unique identifiers. The resulting segmentation contains the non-Gaussian shape of ROIs above a threshold. The same approach was applied to the induction and background images. The ROIs from each image were pooled together, and unless stated otherwise, were analyzed as a population. The distribution of area and intensity was plotted and used to manually select areas corresponding to the size of a cell. The same area limits were used to analyze the induction and background datasets but varied across experiments (usually in the range of 10 and 2000 pixels^2).

The mean intensity of each ROI was calculated and summed across all ROIs in an image to obtain the integrated intensity for each image. The median and standard deviation of the integrated intensity was calculated across all images in multiple experiments performed under identical conditions. The fold induction was obtained by calculating the ratio of integrated intensities at different conditions. The first step was to obtain the probability distribution of ROIs with a specific mean intensity. To obtain a proper sampling of all intensities, the ROIs from 5 images were pooled together. The probability distribution represents the median and standard deviation across multiple sets of 5 images each. The same approach was used for the induction and background images. A threshold was selected by identifying a particular intensity with equal probability in both the induction and background images. In cases where the intensity probabilities did not intercept at any intensity, a threshold was selected based on the curvature of the distribution. The fold activation was calculated by dividing the integrated intensity of ROIs above the threshold in the induction images by the integrated intensity of ROIs above the same threshold in the background images. The intensity fold induction was taken across all possible induction-background image pairs in experiments performed within the same day.

In some experiments where segmentation was not possible due to cytosolic expression of the fluorescent reporter, we only determined the overall intensity of the images by summing the intensity of every pixel in the images. The fold-change in

intensity in when the blockers are applied or knocking down the ADAMS gene with CRISPR-CAS9 were calculated by the following equation

Fold change = |A_- B|/(A-C)

A is the summed intensity of an image with ADAMS in the ligand cell line's presence. B is the receptor cell line with knocked down ADAMS in the presence of the ligand cell line. The letter C represents the summed image intensity of the receptor line with knocked down ADAMS in the absence of the ligand cell line. To investigate the effect of distinct manipulations on the overall intensity of induction, we divided the summed intensity of the images in the blocker's presence by the summed intensity of the images without the blockers. Because all images were taken under identical conditions, the equation shown above was applied between randomly selected pairs of images.

Time lapse.

To investigate the time evolution of intensity changes upon cell-cell interactions, we performed live imaging of 25 cells for each construct and obtained images at 512 by 512 pixels every 25 minutes. The analysis of intensity changes across time was performed by tracking the changes in intensity upon induction of individual cells. The intensity changes of individually tracked cells was determined by manually drawing a boundary around a subset of selected cells in each image. Only cells which were visible in all frames were selected. Whenever a cell would divide into two cells one arbitrarily selected cell would be tracked for the remaining of the video. The manually drawn boundaries were refined automatically by applying the contour region growing technique (Chan and Vese, 2001) on the Gaussian filtered image (1-pixel sigma) at each frame. The refined boundary's median intensity was calculated and averaged across tracked cells in the induction and background conditions. Individual tracking: the changes in intensities of individually tracked cells were monitored by calculating the median intensity within the refined cell boundary of a cell in each frame. The median intensity within the refined boundary as a function of time was fitted with a shifted logistic equation (eqn. 2).

Equation 2: a/(1+exp(-k*(x-b))) + c

Where **x** is time, **b** is the median intensity at half-saturation, (**a + c**) represents the maximum median intensity, **c** is the initial median intensity, and **K** is the rate of change. The fold induction for a cell was calculated by dividing the maximum median intensity of the ROI (a+c) by the initial median ROI intensity (c). Because the median intensity of an ROI would change abruptly following a cell division event, we ignored periods after cell division. Changes in intensities during these manually selected time windows were fitted with the above equation, and the rate constant was recovered for each individually tracked cell. The median and standard deviation of the half-saturation midpoint (b) or the fold induction were pooled across trials and statistical significance was determined as described below.

Peptide Charges.

The peptides' secondary structure in aqueous solution was predicted using the PEP-FOLD2 algorithm (Lamiable et al., 2016). In all cases, the model most likely to be present in water was utilized. Protein structure files (psf) and protein databank files (pdb) were generated with the built-in (AutoPSF) function from VMD (Humphrey et al., 1996). Default AutoPSF parameters were utilized. Missing non-hydrogen atoms in the resulting pdb files and their physical properties were automatically added using the PDB2PQR server implementing the CHARMM force field parameters (Jurrus et al., 2017). The solvent electrostatic distribution on the peptides was determined using the Adaptive Poisson-Boltzmann Solver (APBS, Unni et al., 2011). Recovered isoelectric charge distributions were plotted using VMD.

Statistics.

The integrated intensity and/or fold-induction were compared across constructs by calculating each construct's median integrated intensity or fold-induction for each trial. A two-sided Wilcoxon rank-sum test was performed to test the hypothesis that each construct's median values belonged to distinct distributions with unequal medians. Unless stated otherwise, all statistical tests were performed using nonparametric tests.

The Symbols for the p-values are indicated in the next table:

ns	*	**	***	****
p > 0.05	p ≤ 0.05	p ≤ 0.01	p ≤ 0.001	p ≤ 0.0001

Figures were elaborated using Adobe Illustrator and Schemas from Figures in General Introduction using MOTIFOLIO as a template.

TRANSGENIC FLIES:

-nSyb-1d3NRR::dNlg2ICD::G4V5 and nSyb-1d3NRRG4V5: The 1d3NRR::dNlg2ICD::G4V5 fragment was directly amplifyied from GH146-1d3NRR::dNlg2ICD::G4V5, and was subcloned into pattNSYBBN digested by EcoRI and AatII. The SNTG4V5 construct was generated by amplifying FU-SdNTG4-W with the reverse primer having a V5 tag sequence, and the SNTG4V5 PCR fragment was subcloned into pattNSYBBN digested by EcoRI and AatII. Transgenic nSyb- 1d3NRR::dNlg2ICD::G4V5 and nSyb-1d3NRRG4V5 flies were produced by attb site specific integration in attP40 site.

-OR83b-LexA: kind gift from Freeman's lab. It has been generated by Tzumin Lee (FlyBase Recombinant Construct Report: P{Orco-LexA-VP16}).

-LexAop-CD19: We did the subcloning and generated it. This transgenic fly line was produced by attb site specific integration in attP2 site.

-nSyb-nlgSNTlexAGADDHFR7(P40), nSyb-nlgSNTlexAGADDHFR7(P2), nSyb-nlgSNTlexAGADDHFR30(P40). dNRRdNLGNlexAD insert was from the figestion of pattBnSyb1d3dNRRdNLGNlexAD with NicoI and StuI. DHFR30, DHFR7 and nSybsyn211d3 were geneblocks synthesized by IDT. The pattB backbone was digested with EcoRI-HF, NotI-HF. Al the inserts and the neckbone pattB were fused using the Gibson Assembly kit to generate these three different constructs. They were produced by attB site-specific integration in the attp40 and attp2 insertion sites. All transgenic Drosophila were generated by BestGene Inc.

-UAS-sp-nSybCD19(P2). A fragment comprising the intracellular and transmembrane domains of nSyb was synthesized (Gene blocks, IDT inc), fused a fragment containing the extracellular domain of CD19 (Gene blocks, IDT inc.), and inserted into the UAS vector. Transgenic flies were produced by attb site-specific integration in attP2 site.

-VglutGal4. This transgenic fly line was gotten from Bloomington Stock Center. The donor is Hermann Aberle, from the University of Munster.

-13xlexAopCD4tdGFP (VK33). This transgenic fly line was gotten from Bloomington Stock Center. See details in Poe et al., 2017.

-5xUASCD4::tdGFP reporter was a gift from Dr Freeman, Oregon Health and Science University.

BIBLIOGRAFY

Adams JA, Fierke CA, Benkovic SJ (1991) The function of amino acid residues contacting the nicotinamide ring of NADPH in dihydrofolate reductase from Escherichia coli. Biochemistry 30:11046–11054.

Agrawal N, Frederick MJ, Pickering CR, et al (2011) Exome sequencing of head and neck squamous cell carcinoma reveals inactivating mutations in NOTCH1. Science 333:1154–1157. https://doi.org/10.1126/science.1206923

Agrawal N, Jiao Y, Bettegowda C, et al (2012) Comparative genomic analysis of esophageal adenocarcinoma and squamous cell carcinoma. Cancer Discov 2:899–905.

Akin O, Zipursky SL (2016) Frazzled promotes growth cone attachment at the source of a Netrin gradient in the Drosophila visual system. eLife 5:e20762.

Alberts B, Johnson A, Lewis J, et al (2002) Molecular Biology of the Cell, 4th edn. Garland Science

Anderson KV, Ingham PW (2003) The transformation of the model organism: a decade of developmental genetics. Nature Genetics 33:285–293.

Arcaini L, Rossi D, Lucioni M, et al (2015) The NOTCH pathway is recurrently mutated in diffuse large B-cell lymphoma associated with hepatitis C virus infection. Haematologica 100:246–252. https://doi.org/10.3324/haematol.2014.116855

Armstrong F, Brunet de la Grange P, Gerby B, et al (2009) NOTCH is a key regulator of human T-cell acute leukemia initiating cell activity. Blood 113:1730–1740. https://doi.org/10.1182/blood-2008-02-138172

Artavanis-Tsakonas S, Muskavitch MA, Yedvobnick B (1983) Molecular cloning of Notch, a locus affecting neurogenesis in Drosophila melanogaster. Proc Natl Acad Sci U S A 80:1977–1981.

Asnafi V, Buzyn A, Le Noir S, et al (2009) NOTCH1/FBXW7 mutation identifies a large subgroup with favorable outcome in adult T-cell acute lymphoblastic leukemia (T-ALL): a Group for Research on Adult Acute Lymphoblastic Leukemia (GRAALL) study. Blood 113:3918–3924.

Aster JC, Pear WS, Blacklow SC (2008) Notch signaling in leukemia. Annu Rev Pathol 3:587–613.

Aster JC, Pear WS, Blacklow SC (2017) The Varied Roles of Notch in Cancer. Annu Rev Pathol 12:245–275. https://doi.org/10.1146/annurev-pathol-052016-100127

Astic L, Saucier D, Coulon P, et al (1993) The CVS strain of rabies virus as transneuronal tracer in the olfactory system of mice. Brain Research 619:146–156.

Bachmair A, Finley D, Varshavsky A (1986) In vivo half-life of a protein is a function of its amino-terminal residue. Science 234:179–186.

Bang ML, Owczarek S (2013) A matter of balance: role of neurexin and neuroligin at the synapse. Neurochem Res 38:1174–1189.

Banks SML, Cho B, Eun SH, et al (2011) The functions of auxilin and Rab11 in Drosophila suggest that the fundamental role of ligand endocytosis in notch signaling cells is not recycling. PLoS One 6:e18259.

Barnea G, Strapps W, Herrada G, et al (2008) The genetic design of signaling cascades to record receptor activation. PNAS 105:64–69.

Barrangou R (2015) The roles of CRISPR-Cas systems in adaptive immunity and beyond. Curr Opin Immunol 32:36–41.

Bellen HJ, Tong C, Tsuda H (2010) 100 years of Drosophila research and its impact on vertebrate neuroscience: a history lesson for the future. Nat Rev Neurosci 11:514–522. https://doi.org/10.1038/nrn2839

Benhra N, Vignaux F, Dussert A, et al (2010) Neuralized promotes basal to apical transcytosis of delta in epithelial cells. Mol Biol Cell 21:2078–2086.

Benson DL, Yoshihara Y, Mori K (1998) Polarized distribution and cell type-specific localization of telencephalin, an intercellular adhesion molecule. J Neurosci Res 52:43–53.

Berck ME, Khandelwal A, Claus L, et al (2016) The wiring diagram of a glomerular olfactory system. eLife 5:e14859.

Berlin S, Carroll EC, Newman ZL, et al (2015) Photoactivatable genetically encoded calcium indicators for targeted neuronal imaging. Nature Methods 12:852–858.

Bernasconi-Elias P, Hu T, Jenkins D, et al (2016) Characterization of activating mutations of NOTCH3 in T-cell acute lymphoblastic leukemia and anti-leukemic activity of NOTCH3 inhibitory antibodies. Oncogene 35:6077–6086.

Bidaye SS, Machacek C, Wu Y, Dickson BJ (2014) Neuronal control of Drosophila walking direction. Science 344:97–101.

Blaumueller CM, Qi H, Zagouras P, Artavanis-Tsakonas S (1997) Intracellular Cleavage of Notch Leads to a Heterodimeric Receptor on the Plasma Membrane. Cell 90:281–291.

Bossis G, Melchior F (2006) Regulation of SUMOylation by reversible oxidation of SUMO conjugating enzymes. Mol Cell 21:349–357.

Bozkulak EC, Weinmaster G (2009) Selective use of ADAM10 and ADAM17 in activation of Notch1 signaling. Mol Cell Biol 29:5679–5695.

Brennaman LH, Moss ML, Maness PF (2014) EphrinA/EphA-induced ectodomain shedding of neural cell adhesion molecule regulates growth cone repulsion through ADAM10 metalloprotease. J Neurochem 128:267–279.

Brou C, Logeat F, Gupta N, et al (2000) A Novel Proteolytic Cleavage Involved in Notch Signaling: The Role of the Disintegrin-Metalloprotease TACE. Molecular Cell 5:207–216.

Bush G, diSibio G, Miyamoto A, et al (2001) Ligand-induced signaling in the absence of furin processing of Notch1. Dev Biol 229:494–502.

Butcher NJ, Friedrich AB, Lu Z, et al (2012) Different classes of input and output neurons reveal new features in microglomeruli of the adult Drosophila mushroom body calyx. J Comp Neurol 520:2185–2201.

Calvo A (2015) Biología celular biomédica.

Card JP, Enquist LW (2001) Transneuronal circuit analysis with pseudorabies viruses. Curr Protoc Neurosci Chapter 1:Unit1.5. https://doi.org/10.1002/0471142301.ns0105s09

Card JP, Whealy ME, Robbins AK, Enquist LW (1992) Pseudorabies virus envelope glycoprotein gI influences both neurotropism and virulence during infection of the rat visual system. J Virol 66:3032–3041

Cavanaugh DJ, Geratowski JD, Wooltorton JRA, et al (2014) Identification of a Circadian Output Circuit for Rest:Activity Rhythms in Drosophila. Cell 157:689–701.

Caveney S (1985) The role of gap junctions in development. Annu Rev Physiol 47:319–335.

Chan TF, and Vese LA (2001) Active Contours Without Edges. IEEE Trans Image Process 10(2):266-77.

Chandu D, Huppert SS, Kopan R (2006) Analysis of transmembrane domain mutants is consistent with sequential cleavage of Notch by gamma-secretase. J Neurochem 96:228–235.

Chatterjee S, Sullivan HA, MacLennan BJ, et al (2018) Nontoxic, double-deletion-mutant rabies viral vectors for retrograde targeting of projection neurons. Nature Neuroscience 21:638–646.

Chen T-W, Wardill TJ, Sun Y, et al (2013) Ultrasensitive fluorescent proteins for imaging neuronal activity. Nature 499:295–300.

Chen Y, Akin O, Nern A, et al (2014) Cell-type-Specific Labeling of Synapses In Vivo through Synaptic Tagging with Recombination. Neuron 81:280–293.

Chen Y, Ju L, Rushdi M, et al (2017) Receptor-mediated cell mechanosensing. Mol Biol Cell 28:3134–3155.

Chiang MY, Radojcic V, Maillard I (2016) Oncogenic Notch signaling in T-cell and B-cell lymphoproliferative disorders. Curr Opin Hematol 23:362–370.

Chiang MY, Xu ML, Histen G, et al (2006) Identification of a conserved negative regulatory sequence that influences the leukemogenic activity of NOTCH1. Mol Cell Biol 26:6261–6271.

Chklovskii DB, Vitaladevuni S, Scheffer LK (2010) Semi-automated reconstruction of neural circuits using electron microscopy. Current Opinion in Neurobiology 20:667–675.

Cho U, Zimmerman SM, Chen L, et al (2013) Rapid and tunable control of protein stability in Caenorhabditis elegans using a small molecule. PLoS One 8:e72393.

Choi J, Young JAT, Callaway EM (2010) Selective viral vector transduction of ErbB4 expressing cortical interneurons in vivo with a viral receptor-ligand bridge protein. Proc Natl Acad Sci U S A 107:16703–16708.

Chowdhury F, Li ITS, Ngo TTM, et al (2016) Defining Single Molecular Forces Required for Notch Activation Using Nano Yoyo. Nano Lett 16:3892–3897.

Christiansen F, Zube C, Andlauer TFM, et al (2011) Presynapses in Kenyon Cell Dendrites in the Mushroom Body Calyx of Drosophila. J Neurosci 31:9696–9707.

Clowney EJ, Iguchi S, Bussell JJ, et al (2015) Multimodal Chemosensory Circuits Controlling Male Courtship in Drosophila. Neuron 87:1036–1049.

Cooper GM, Cooper GM (2000) The Cell, 2nd edn. Sinauer Associates

Cordle J, Redfieldz C, Stacey M, et al (2008) Localization of the delta-like-1-binding site in human Notch-1 and its modulation by calcium affinity. J Biol Chem 283:11785–11793.

Coustan-Smith E, Mullighan CG, Onciu M, et al (2009) Early T-cell precursor leukaemia: a subtype of very high-risk acute lymphoblastic leukaemia. Lancet Oncol 10:147–156.

Cowan WM, Gottlieb DI, Hendrickson AE, et al (1972) The autoradiographic demonstration of axonal connections in the central nervous system. Brain Res 37:21–51.

de Olmos JS, Ebbesson SOE, Heimer L (1981) Silver Methods for the Impregnation of Degenerating Axoplasm. In: Heimer L, Robards MJ (eds) Neuroanatomical Tract-Tracing Methods. Springer US, Boston, MA, pp 117–170

De Strooper B, Annaert W, Cupers P, et al (1999) A presenilin-1-dependent gamma-secretase-like protease mediates release of Notch intracellular domain. Nature 398:518–522.

Deatherage CL, Lu Z, Kim J-H, Sanders CR (2015) Notch Transmembrane Domain: Secondary Structure and Topology. Biochemistry 54:3565–3568.

DeFalco J, Tomishima M, Liu H, et al (2001) Virus-assisted mapping of neural inputs to a feeding center in the hypothalamus. Science 291:2608–2613.

del Amo FF, Gendron-Maguire M, Swiatek PJ, et al (1993) Cloning, analysis, and chromosomal localization of Notch-1, a mouse homolog of Drosophila Notch. Genomics 15:259–264.

Denk W, Horstmann H (2004) Serial block-face scanning electron microscopy to reconstruct three-dimensional tissue nanostructure. PLoS Biol 2:e329. https://doi.org/10.1371/journal.pbio.0020329

Desbois M, Cook SJ, Emmons SW, Bülow HE (2015) Directional Trans-Synaptic Labeling of Specific Neuronal Connections in Live Animals. Genetics 200:697–705.

Dolan M-J, Luan H, Shropshire WC, et al (2017) Facilitating Neuron-Specific Genetic Manipulations in Drosophila melanogaster Using a Split GAL4 Repressor. Genetics 206:775–784.

D'Souza B, Miyamoto A, Weinmaster G (2008) The many facets of Notch ligands. Oncogene 27:5148–5167.

Ellisen LW, Bird J, West DC, et al (1991) TAN-1, the human homolog of the Drosophila notch gene, is broken by chromosomal translocations in T lymphoblastic neoplasms. Cell 66:649–661.

Ellison C, Brun YV (2015) Mechanosensing: a regulation sensation. Curr Biol 25:R113–R115.

Emery G, Hutterer A, Berdnik D, et al (2005) Asymmetric Rab 11 endosomes regulate delta recycling and specify cell fate in the Drosophila nervous system. Cell 122:763–773.

Fabbri G, Rasi S, Rossi D, et al (2011) Analysis of the chronic lymphocytic leukemia coding genome: role of NOTCH1 mutational activation. J Exp Med 208:1389–1401.

Fehon RG, Kooh PJ, Rebay I, et al (1990) Molecular interactions between the protein products of the neurogenic loci Notch and Delta, two EGF-homologous genes in Drosophila. Cell 61:523–534.

Feinberg EH, VanHoven MK, Bendesky A, et al (2008) GFP Reconstitution Across Synaptic Partners (GRASP) Defines Cell Contacts and Synapses in Living Nervous Systems. Neuron 57:353–363.

Fetcho JR, Liu KS (1998) Zebrafish as a model system for studying neuronal circuits and behavior. Ann N Y Acad Sci 860:333–345.

Fişek M, Wilson RI (2014) Stereotyped connectivity and computations in higher-order olfactory neurons. Nature Neuroscience 17:280–288.

Georgakopoulos A, Litterst C, Ghersi E, et al (2006) Metalloproteinase/Presenilin1 processing of ephrinB regulates EphB-induced Src phosphorylation and signaling. EMBO J 25:1242–1252.

George J, Lim JS, Jang SJ, et al (2015) Comprehensive genomic profiles of small cell lung cancer. Nature 524:47–53.

Gerfen CR, Sawchenko PE (1984) An anterograde neuroanatomical tracing method that shows the detailed morphology of neurons, their axons and terminals: immunohistochemical localization of an axonally transported plant lectin, Phaseolus vulgaris leucoagglutinin (PHA-L). Brain Res 290:219–238.

Giannone G, Jiang G, Sutton DH, et al (2003) Talin1 is critical for force-dependent reinforcement of initial integrin-cytoskeleton bonds but not tyrosine kinase activation. J Cell Biol 163:409–419.

Gibson DG, Benders GA, Andrews-Pfannkoch C, et al (2008) Complete Chemical Synthesis, Assembly, and Cloning of a Mycoplasma genitalium Genome. Science 319:1215–1220.

Giebeler N, Zigrino P (2016) A Disintegrin and Metalloprotease (ADAM): Historical Overview of Their Functions. Toxins (Basel) 8:122.

Glomski K, Monette S, Manova K, et al (2011) Deletion of Adam10 in endothelial cells leads to defects in organ-specific vascular structures. Blood 118:1163–1174.

Glover JC, Petursdottir G, Jansen JKS (1986) Fluorescent dextran-amines used as axonal tracers in the nervous system of the chicken embryo. Journal of Neuroscience Methods 18:243–254. https://doi.org/10.1016/0165-0270(86)90011-7

Gordon WR, Roy M, Vardar-Ulu D, et al (2009a) Structure of the Notch1-negative regulatory region: implications for normal activation and pathogenic signaling in T-ALL. Blood 113:4381–4390.

Gordon WR, Vardar-Ulu D, Histen G, et al (2007) Structural basis for autoinhibition of Notch. Nature Structural & Molecular Biology 14:295–300.

Gordon WR, Vardar-Ulu D, L'Heureux S, et al (2009b) Effects of S1 Cleavage on the Structure, Surface Export, and Signaling Activity of Human Notch1 and Notch2. PLOS ONE 4:e6613.

Gordon WR, Zimmerman B, He L, et al (2015) Mechanical Allostery: Evidence for a Force Requirement in the Proteolytic Activation of Notch. Developmental Cell 33:729–736.

Gorostiza EA, Depetris-Chauvin A, Frenkel L, et al (2014) Circadian Pacemaker Neurons Change Synaptic Contacts across the Day. Current Biology 24:2161–2167.

Gradinaru V, Zhang F, Ramakrishnan C, et al (2010) Molecular and Cellular Approaches for Diversifying and Extending Optogenetics. Cell 141:154–165.

Greenwald I, Seydoux G (1990) Analysis of gain-of-function mutations of the lin-12 gene of Caenorhabditis elegans. Nature 346:197–199. https://doi.org/10.1038/346197a0

Haass C, Selkoe DJ (1993) Cellular processing of beta-amyloid precursor protein and the genesis of amyloid beta-peptide. Cell 75:1039–1042. h

Hambleton S, Valeyev NV, Muranyi A, et al (2004) Structural and functional properties of the human notch-1 ligand binding region. Structure 12:2173–2183.

Han Z-J, Feng Y-H, Gu B-H, et al (2018) The post-translational modification, SUMOylation, and cancer (Review). Int J Oncol 52:1081–1094.

Hansson EM, Lanner F, Das D, et al (2010) Control of Notch-ligand endocytosis by ligand-receptor interaction. J Cell Sci 123:2931–2942.

Hardie D (1991) Biochemical Messengers: Hormones, neurotransmitters and growth factors. Springer Netherlands

Hasegawa E, Truman JW, Nose A (2016) Identification of excitatory premotor interneurons which regulate local muscle contraction during Drosophila larval locomotion. Scientific Reports 6:30806. https://doi.org/10.1038/srep30806

Hassinger JE, Oster G, Drubin DG, Rangamani P (2017) Design principles for robust vesiculation in clathrin-mediated endocytosis. Proc Natl Acad Sci U S A 114:E1118–E1127.

Hayward AN, Aird EJ, Gordon WR (2019) A toolkit for studying cell surface shedding of diverse transmembrane receptors. eLife 8:e46983.

Hell SW, Wichmann J (1994) Breaking the diffraction resolution limit by stimulated emission: stimulated-emission-depletion fluorescence microscopy. Opt Lett 19:780.

Henrique D, Schweisguth F (2019) Mechanisms of Notch signaling: a simple logic deployed in time and space. Development 146:.

Higashiyama S, Nanba D, Nakayama H, et al (2011) Ectodomain shedding and remnant peptide signalling of EGFRs and their ligands. J Biochem 150:15–22.

Hilliard VC, Frey MR, Dempsey PJ, et al (2011) TNF-α converting enzyme-mediated ErbB4 transactivation by TNF promotes colonic epithelial cell survival. Am J Physiol Gastrointest Liver Physiol 301:G338-346.

Horiuchi K, Kimura T, Miyamoto T, et al (2007) Cutting edge: TNF-alpha-converting enzyme (TACE/ADAM17) inactivation in mouse myeloid cells prevents lethality from endotoxin shock. J Immunol 179:2686–2689.

Huang B, Babcock H, Zhuang X (2010) Breaking the Diffraction Barrier: Super-Resolution Imaging of Cells. Cell 143:1047–1058.

Huang T-H (2017) A Synthetic Genetic System to Investigate Brain Connectivity and Genetically Manipulate Interacting Cells.

Huang T-H, Niesman P, Arasu D, et al (2017) Tracing neuronal circuits in transgenic animals by transneuronal control of transcription (TRACT). Elife 6:. https://doi.org/10.7554/eLife.32027

Huang T-H, Velho T, Lois C (2016) Monitoring cell-cell contacts in vivo in transgenic animals. Development 143:4073–4084.

Hubel DH, Wiesel TN, Stryker MP (1977) Orientation columns in macaque monkey visual cortex demonstrated by the 2-deoxyglucose autoradiographic technique. Nature 269:328–330.

Huh Y, Oh MS, Leblanc P, Kim K-S (2010) Gene transfer in the nervous system and implications for transsynaptic neuronal tracing. Expert Opinion on Biological Therapy 10:763–772.

Humphrey W, Dalke A, and Schulten K (1996). VMD: visual molecular dynamics. J Mol Graph 14(1):33-8, 27-8.

Huppert SS, Le A, Schroeter EH, et al (2000) Embryonic lethality in mice homozygous for a processing-deficient allele of Notch1. Nature 405:966–970.

Huxley-Jones J, Clarke T-K, Beck C, et al (2007) The evolution of the vertebrate metzincins; insights from Ciona intestinalis and Danio rerio. BMC Evol Biol 7:63.

Inagaki HK, Ben-Tabou de-Leon S, Wong AM, et al (2012) Visualizing Neuromodulation In Vivo: TANGO-Mapping of Dopamine Signaling Reveals Appetite Control of Sugar Sensing. Cell 148:583–595.

Iskratsch T, Wolfenson H, Sheetz MP (2014) Appreciating force and shape—the rise of mechanotransduction in cell biology. Nat Rev Mol Cell Biol 15:825–833.

Itakura Y, Kohsaka H, Ohyama T, et al (2015) Identification of Inhibitory Premotor Interneurons Activated at a Late Phase in a Motor Cycle during Drosophila Larval Locomotion. PLOS ONE 10:e0136660.

Itoh M, Kim C-H, Palardy G, et al (2003) Mind Bomb Is a Ubiquitin Ligase that Is Essential for Efficient Activation of Notch Signaling by Delta. Developmental Cell 4:67–82.

Iwamoto M, Björklund T, Lundberg C, et al (2010) A general chemical method to regulate protein stability in the mammalian central nervous system. Chem Biol 17:981–988.

Jacob F, Monod J (1961) Genetic regulatory mechanisms in the synthesis of proteins. J Mol Biol 3:318–356. https://doi.org/10.1016/s0022-2836(61)80072-7

Jafar-Nejad H, Andrews HK, Acar M, et al (2005) Sec15, a component of the exocyst, promotes notch signaling during the asymmetric division of Drosophila sensory organ precursors. Dev Cell 9:351–363.

Jagadish S, Barnea G, Clandinin TR, Axel R (2014) Identifying Functional Connections of the Inner Photoreceptors in Drosophila using Tango-Trace. Neuron 83:630–644.

Jarriault S, Brou C, Logeat F, et al (1995) Signalling downstream of activated mammalian Notch. Nature 377:355–358.

Jarriault S, Greenwald I (2005) Evidence for functional redundancy between C. elegans ADAM proteins SUP-17/Kuzbanian and ADM-4/TACE. Dev Biol 287:1–10.

Jurrus E, Engel D, Star K , et al (2017). Improvements to the APBS biomolecular solvation software suite. Protein Sci27(1):112-128.

Kalus I, Bormann U, Mzoughi M, et al (2006) Proteolytic cleavage of the neural cell adhesion molecule by ADAM17/TACE is involved in neurite outgrowth. J Neurochem 98:78–88.

Kao HY, Ordentlich P, Koyano-Nakagawa N, et al (1998) A histone deacetylase corepressor complex regulates the Notch signal transduction pathway. Genes Dev 12:2269–2277.

Katz LC, Burkhalter A, Dreyer WJ (1984) Fluorescent latex microspheres as a retrograde neuronal marker for in vivo and in vitro studies of visual cortex. Nature 310:498–500.

Kawasaki F, Zou B, Xu X, Ordway RW (2004) Active zone localization of presynaptic calcium channels encoded by the cacophony locus of Drosophila. J Neurosci 24:282–285.

Kelly RM, Strick PL (2000) Rabies as a transneuronal tracer of circuits in the central nervous system. J Neurosci Methods 103:63–71.

Kidd S, Kelley MR, Young MW (1986) Sequence of the notch locus of Drosophila melanogaster: relationship of the encoded protein to mammalian clotting and growth factors. Mol Cell Biol 6:3094–3108.

Kidd S, Lieber T (2002) Furin cleavage is not a requirement for Drosophila Notch function. Mech Dev 115:41–51.

Kiel MJ, Velusamy T, Betz BL, et al (2012) Whole-genome sequencing identifies recurrent somatic NOTCH2 mutations in splenic marginal zone lymphoma. J Exp Med 209:1553–1565.

Kile BT, Hilton DJ (2005) The art and design of genetic screens: mouse. Nature Reviews Genetics 6:557–567.

Kim CK, Adhikari A, Deisseroth K (2017) Integration of optogenetics with complementary methodologies in systems neuroscience. Nat Rev Neurosci 18:222–235.

Kim J, Zhao T, Petralia RS, et al (2011) mGRASP enables mapping mammalian synaptic connectivity with light microscopy. Nat Methods 9:96–102.

Klar TA, Hell SW (1999) Subdiffraction resolution in far-field fluorescence microscopy. Opt Lett 24:954.

Klinakis A, Lobry C, Abdel-Wahab O, et al (2011) A novel tumour-suppressor function for the Notch pathway in myeloid leukaemia. Nature 473:230–233.

Knight D, Xie W, Boulianne GL (2011) Neurexins and neuroligins: recent insights from invertebrates. Mol Neurobiol 44:426–440.

Knöll R, Hoshijima M, Hoffman HM, et al (2002) The cardiac mechanical stretch sensor machinery involves a Z disc complex that is defective in a subset of human dilated cardiomyopathy. Cell 111:943–955.

Kochenderfer JN, Feldman SA, Zhao Y, et al (2009) Construction and preclinical evaluation of an anti-CD19 chimeric antigen receptor. J Immunother 32:689–702.

Koo EH, Kopan R (2004) Potential role of presenilin-regulated signaling pathways in sporadic neurodegeneration. Nat Med 10 Suppl:S26-33.

Kopan R, Ilagan MaXG (2009) The Canonical Notch Signaling Pathway: Unfolding the Activation Mechanism. Cell 137:216–233.

Kremer MC, Christiansen F, Leiss F, et al (2010) Structural Long-Term Changes at Mushroom Body Input Synapses. Current Biology 20:1938–1944.

Kridel R, Meissner B, Rogic S, et al (2012) Whole transcriptome sequencing reveals recurrent NOTCH1 mutations in mantle cell lymphoma. Blood 119:1963–1971.

Kristensson K, Olsson Y (1975) Retrograde transport of horseradish peroxidase in transected axons. II. Relations between rate of transfer from the site of injury to the perikaryon and onset of chromatolysis. J Neurocytol 4:653–661.

Kristensson K, Olsson Y (1971) Retrograde axonal transport of protein. Brain Res 29:363–365.

Kurjan J (1992) Pheromone response in yeast. Annu Rev Biochem 61:1097–1129.

Lai JS-Y, Lo S-J, Dickson BJ, Chiang A-S (2012) Auditory circuit in the Drosophila brain. PNAS 109:2607–2612.

Lai S-L, Lee T (2006) Genetic mosaic with dual binary transcriptional systems in Drosophila. Nat Neurosci 9:703–709.

Lake RJ, Grimm LM, Veraksa A, et al (2009) In vivo analysis of the Notch receptor S1 cleavage. PLoS One 4:e6728.

Lamiable A, Thévenet P, Rey J, et al (2016) PEP-FOLD3: faster de novo structure prediction for linear peptides in solution and in complex. Nucleic Acids Res 8;44(W1):W449-54.

Lanciego JL, Wouterlood FG (2020) Neuroanatomical tract-tracing techniques that did go viral. Brain Struct Funct 225:1193–1224.

Langridge PD, Struhl G (2017) Epsin-Dependent Ligand Endocytosis Activates Notch by Force. Cell 171:1383-1396.e12.

Lasek R, Joseph BS, Whitlock DG (1968) Evaluation of a radioautographic neuroanatomical tracing method. Brain Res 8:319–336.

Lee S, Kumano K, Nakazaki K, et al (2009) Gain-of-function mutations and copy number increases of Notch2 in diffuse large B-cell lymphoma. Cancer Sci 100:920–926.

Levine JD, Zhao XS, Miselis RR (1994) Direct and indirect retinohypothalamic projections to the supraoptic nucleus in the female albino rat. J Comp Neurol 341:214–224.

Lewis RN, Zhang YP, Hodges RS, et al (2001) A polyalanine-based peptide cannot form a stable transmembrane alpha-helix in fully hydrated phospholipid bilayers. Biochemistry 40:12103–12111.

Li S-J, Vaughan A, Sturgill JF, Kepecs A (2018) A Viral Receptor Complementation Strategy to Overcome CAV-2 Tropism for Efficient Retrograde Targeting of Neurons. Neuron 98:905-917.e5.

Libbrecht S, Van den Haute C, Malinouskaya L, et al (2017) Evaluation of WGA–Cre-dependent topological transgene expression in the rodent brain. Brain Struct Funct 222:717–733.

Lieber T, Kidd S, Young MW (2002) kuzbanian-mediated cleavage of Drosophila Notch. Genes Dev 16:209–221.

Lin T-Y, Luo J, Shinomiya K, et al (2016) Mapping chromatic pathways in the Drosophila visual system. J Comp Neurol 524:213–227.

Lis JT, Simon JA, Sutton CA (1983) New heat shock puffs and beta-galactosidase activity resulting from transformation of Drosophila with an hsp70-lacZ hybrid gene. Cell 35:403–410.

Liu L, Spurrier J, Butt TR, Strickler JE (2008) Enhanced protein expression in the baculovirus/insect cell system using engineered SUMO fusions. Protein Expr Purif 62:21–28.

Liu S, Liu Q, Tabuchi M, Wu MN (2016) Sleep Drive Is Encoded by Neural Plastic Changes in a Dedicated Circuit. Cell 165:1347–1360.

Lo L, Anderson DJ (2011) A Cre-dependent, anterograde transsynaptic viral tracer for mapping output pathways of genetically marked neurons. Neuron 72:938–950.

Logeat F, Bessia C, Brou C, et al (1998) The Notch1 receptor is cleaved constitutively by a furin-like convertase. Proc Natl Acad Sci U S A 95:8108–8112.

Lois C, Hong EJ, Pease S, et al (2002) Germline Transmission and Tissue-Specific Expression of Transgenes Delivered by Lentiviral Vectors. Science 295:868–872.

Lovendahl KN, Blacklow SC, Gordon WR (2018) The Molecular Mechanism of Notch Activation. Adv Exp Med Biol 1066:47–58.

Luan H, Peabody NC, Vinson CR, White BH (2006) Refined Spatial Manipulation of Neuronal Function by Combinatorial Restriction of Transgene Expression. Neuron 52:425–436.

Luca VC, Kim BC, Ge C, et al (2017) Notch-Jagged complex structure implicates a catch bond in tuning ligand sensitivity. Science 355:1320–1324.

Ma J, Ptashne M (1987a) Deletion analysis of GAL4 defines two transcriptional activating segments. Cell 48:847–853. https://doi.org/10.1016/0092-8674(87)90081-x

Ma J, Ptashne M (1987b) A new class of yeast transcriptional activators. Cell 51:113–119.

Macpherson LJ, Zaharieva EE, Kearney PJ, et al (2015) Dynamic labelling of neural connections in multiple colours by trans-synaptic fluorescence complementation. Nature Communications 6:10024.

Maday S, Twelvetrees AE, Moughamian AJ, Holzbaur ELF (2014) Axonal transport: cargo-specific mechanisms of motility and regulation. Neuron 84:292–309.

Malecki MJ, Sanchez-Irizarry C, Mitchell JL, et al (2006) Leukemia-associated mutations within the NOTCH1 heterodimerization domain fall into at least two distinct mechanistic classes. Mol Cell Biol 26:4642–4651.

Mamiya A, Gurung P, Tuthill JC (2018) Neural Coding of Leg Proprioception in Drosophila. Neuron 100:636-650.e6.

Mansour MR, Linch DC, Foroni L, et al (2006) High incidence of Notch-1 mutations in adult patients with T-cell acute lymphoblastic leukemia. Leukemia 20:537–539.

Mansour MR, Sulis ML, Duke V, et al (2009) Prognostic implications of NOTCH1 and FBXW7 mutations in adults with T-cell acute lymphoblastic leukemia treated on the MRC UKALLXII/ECOG E2993 protocol. J Clin Oncol 27:4352–4356.

Mao Y, Wang L, Gu C, et al (2012) Subunit organization of the membrane-bound HIV-1 envelope glycoprotein trimer. Nat Struct Mol Biol 19:893–899.

Marambaud P, Shioi J, Serban G, et al (2002) A presenilin-1/gamma-secretase cleavage releases the E-cadherin intracellular domain and regulates disassembly of adherens junctions. EMBO J 21:1948–1956.

Marambaud P, Wen PH, Dutt A, et al (2003) A CBP binding transcriptional repressor produced by the PS1/epsilon-cleavage of N-cadherin is inhibited by PS1 FAD mutations. Cell 114:635–645.

Maretzky T, Reiss K, Ludwig A, et al (2005) ADAM10 mediates E-cadherin shedding and regulates epithelial cell-cell adhesion, migration, and beta-catenin translocation. Proc Natl Acad Sci U S A 102:9182–9187.

Marsh L, Neiman AM, Herskowitz I (1991) Signal transduction during pheromone response in yeast. Annu Rev Cell Biol 7:699–728.

Masuda-Nakagawa LM, Ito K, Awasaki T, O'Kane CJ (2014) A single GABAergic neuron mediates feedback of odor-evoked signals in the mushroom body of larval Drosophila. Front Neural Circuits 8:.

McCarter AC, Wang Q, Chiang M (2018) Notch in Leukemia. Adv Exp Med Biol 1066:355–394.

McGuire SE, Le PT, Osborn AJ, et al (2003) Spatiotemporal rescue of memory dysfunction in Drosophila. Science 302:1765–1768.

Meloty-Kapella L, Shergill B, Kuon J, et al (2012) Notch Ligand Endocytosis Generates Mechanical Pulling Force Dependent on Dynamin, Epsins, and Actin. Developmental Cell 22:1299–1312.

Mendes CS, Bartos I, Akay T, et al (2013) Quantification of gait parameters in freely walking wild type and sensory deprived Drosophila melanogaster. Elife 2:e00231.

Minuzzo S, Agnusdei V, Pusceddu I, et al (2015) DLL4 regulates NOTCH signaling and growth of T acute lymphoblastic leukemia cells in NOD/SCID mice. Carcinogenesis 36:115–121.

Mitsui S, Saito M, Hayashi K, et al (2005) A novel phenylalanine-based targeting signal directs telencephalin to neuronal dendrites. J Neurosci 25:1122–1131.

Mohr SE, Smith JA, Shamu CE, et al (2014) RNAi screening comes of age: improved techniques and complementary approaches. Nat Rev Mol Cell Biol 15:591–600.

Moore RY, Speh JC, Card JP (1995) The retinohypothalamic tract originates from a distinct subset of retinal ganglion cells. J Comp Neurol 352:351–366.

Morgan TH (1917) The Theory of the Gene. The American Naturalist 51:513–544

Mori K, Fujita SC, Watanabe Y, et al (1987) Telencephalon-specific antigen identified by monoclonal antibody. Proc Natl Acad Sci U S A 84:3921–3925.

Response Behaviors Using Synthetic Notch Receptors. Cell 164:780–791.

Mosca TJ, Luo L (2014) Synaptic organization of the Drosophila antennal lobe and its regulation by the Teneurins. eLife 3:e03726.

Mumm JS, Schroeter EH, Saxena MT, et al (2000) A Ligand-Induced Extracellular Cleavage Regulates γ-Secretase-like Proteolytic Activation of Notch1. Molecular Cell 5:197–206.

Musse AA, Meloty-Kapella L, Weinmaster G (2012) Notch ligand endocytosis: Mechanistic basis of signaling activity. Semin Cell Dev Biol 23:429–436.

Naidoo J, Stanek LM, Ohno K, et al (2018) Extensive Transduction and Enhanced Spread of a Modified AAV2 Capsid in the Non-human Primate CNS. Mol Ther 26:2418–2430.

Nassi JJ, Cepko CL, Born RT, Beier KT (2015) Neuroanatomy goes viral! Front Neuroanat 9:80.

Nauta WJ, Gygax PA (1954) Silver impregnation of degenerating axons in the central nervous system: a modified technic. Stain Technol 29:91–93.

Nauta WJH, Gygax PA (1951) Silver impregnation of degenerating axon terminals in the central nervous system: (1) Technic. (2) Chemical notes. Stain Technol 26:5–11.

Ni CY, Murphy MP, Golde TE, Carpenter G (2001) gamma -Secretase cleavage and nuclear localization of ErbB-4 receptor tyrosine kinase. Science 294:2179–2181.

Nichols JT, Miyamoto A, Olsen SL, et al (2007) DSL Ligand Endocytosis Physically Dissociates Notch1 Heterodimers before Activating Proteolysis Can Occur. The Journal of Cell Biology 176:445–458

Nienhaus K, Nienhaus GU (2014) Fluorescent proteins for live-cell imaging with super-resolution. Chem Soc Rev 43:1088–1106.

Nowell CS, Radtke F (2017) Notch as a tumour suppressor. Nat Rev Cancer 17:145–159.

Oka S, Mori K, Watanabe Y (1990) Mammalian telencephalic neurons express a segment-specific membrane glycoprotein, telencephalin. Neuroscience 35:93–103.

Okochi M, Steiner H, Fukumori A, et al (2002) Presenilins mediate a dual intramembranous γ-secretase cleavage of Notch-1. The EMBO Journal 21:5408–5416.

O'Neil J, Grim J, Strack P, et al (2007) FBW7 mutations in leukemic cells mediate NOTCH pathway activation and resistance to gamma-secretase inhibitors. J Exp Med 204:1813–1824.

Pagliaro L, Sorrentino C, Roti G (2020) Targeting Notch Trafficking and Processing in Cancers. Cells 9:.

Palmer WH, Deng W-M (2015) Ligand-Independent Mechanisms of Notch Activity. Trends Cell Biol 25:697–707.

Pancewicz J, Taylor JM, Datta A, et al (2010) Notch signaling contributes to proliferation and tumor formation of human T-cell leukemia virus type 1-associated adult T-cell leukemia. Proc Natl Acad Sci U S A 107:16619–16624.

Parks AL, Klueg KM, Stout JR, Muskavitch MA (2000a) Ligand endocytosis drives receptor dissociation and activation in the Notch pathway. Development 127:1373–1385

Patterson GH, Lippincott-Schwartz J (2002) A photoactivatable GFP for selective photolabeling of proteins and cells. Science 297:1873–1877.

Patton EE, Zon LI (2001) The art and design of genetic screens: zebrafish. Nature Reviews Genetics 2:956–966. https://doi.org/10.1038/35103567

Peschon JJ, Slack JL, Reddy P, et al (1998) An essential role for ectodomain shedding in mammalian development. Science 282:1281–1284.

Pfeiffer BD, Ngo T-TB, Hibbard KL, et al (2010) Refinement of tools for targeted gene expression in Drosophila. Genetics 186:735–755.

Pleiner T, Bates M, Trakhanov S, et al (2015) Nanobodies: site-specific labeling for super-resolution imaging, rapid epitope-mapping and native protein complex isolation. Elife 4:e11349.

Porter DL, Levine BL, Kalos M, et al (2011) Chimeric antigen receptor-modified T cells in chronic lymphoid leukemia. N Engl J Med 365:725–733.

Preuße K, Tveriakhina L, Schuster-Gossler K, et al (2015) Context-Dependent Functional Divergence of the Notch Ligands DLL1 and DLL4 In Vivo. PLoS Genet 11:e1005328.

Ptashne M (2004) Two “what if” experiments. Cell 116:S71-72, 2 p following S76.

Puente XS, Pinyol M, Quesada V, et al (2011) Whole-genome sequencing identifies recurrent mutations in chronic lymphocytic leukaemia. Nature 475:101–105.

Qi H, Rand MD, Wu X, et al (1999) Processing of the notch ligand delta by the metalloprotease Kuzbanian. Science 283:91–94.

Rana A, Westein E, Niego B, Hagemeyer CE (2019) Shear-Dependent Platelet Aggregation: Mechanisms and Therapeutic Opportunities. Front Cardiovasc Med 6:141.

Reece JB, Urry LA, Cain, ML, et al (2014) Campbell Biology, Books a la Carte Edition.

Regier JL, Shen F, Triezenberg SJ (1993) Pattern of aromatic and hydrophobic amino acids critical for one of two subdomains of the VP16 transcriptional activator. Proc Natl Acad Sci U S A 90:883–887.

Reiss K, Saftig P (2009) The “a disintegrin and metalloprotease” (ADAM) family of sheddases: physiological and cellular functions. Semin Cell Dev Biol 20:126–137.

Rooke J, Pan D, Xu T, Rubin GM (1996) KUZ, a conserved metalloprotease-disintegrin protein with two roles in Drosophila neurogenesis. Science 273:1227–1231.

Roybal KT, Williams JZ, Morsut L, et al (2016) Engineering T Cells with Customized Therapeutic Response Programs Using Synthetic Notch Receptors. Cell 167:419-432.e16.

Ruta V, Datta SR, Vasconcelos ML, et al (2010) A dimorphic pheromone circuit in Drosophila from sensory input to descending output. Nature 468:686–690.

Sadler JE (1998) Biochemistry and genetics of von Willebrand factor. Annu Rev Biochem 67:395–424.

Sadler JE (2005) von Willebrand factor: two sides of a coin. J Thromb Haemost 3:1702–1709.

Sanchez-Irizarry C, Carpenter AC, Weng AP, et al (2004) Notch subunit heterodimerization and prevention of ligand-independent proteolytic activation depend, respectively, on a novel domain and the LNR repeats. Mol Cell Biol 24:9265–9273.

Sando R, Baumgaertel K, Pieraut S, et al (2013) Inducible control of gene expression with destabilized Cre. Nat Methods 10:1085–1088. https://doi.org/10.1038/nmeth.2640

Sawada Y, Sheetz MP (2002) Force transduction by Triton cytoskeletons. J Cell Biol 156:609–615.

Schlöndorff J, Blobel CP (1999) Metalloprotease-disintegrins: modular proteins capable of promoting cell-cell interactions and triggering signals by protein-ectodomain shedding. J Cell Sci 112 (Pt 21):3603–3617

Schmidpeter PAM, Koch JR, Schmid FX (2015) Control of protein function by prolyl isomerization. Biochim Biophys Acta 1850:1973–1982.

Schmued LC, Fallon JH (1986) Fluoro-Gold: a new fluorescent retrograde axonal tracer with numerous unique properties. Brain Res 377:147–154.

Schneider-Mizell CM, Gerhard S, Longair M, et al (2016) Quantitative neuroanatomy for connectomics in Drosophila. eLife 5:e12059.

Schrader EK, Wilmington SR, Matouschek A (2010) Making it easier to regulate protein stability. Chem Biol 17:917–918.

Schweisguth F (2004) Regulation of notch signaling activity. Curr Biol 14:R129-138

Seals DF, Courtneidge SA (2003) The ADAMs family of metalloproteases: multidomain proteins with multiple functions. Genes Dev 17:7–30.

Selkoe DJ, Wolfe MS (2007) Presenilin: running with scissors in the membrane. Cell 131:215–221.

Sen A, Madhivanan K, Mukherjee D, Aguilar RC (2012) The epsin protein family: coordinators of endocytosis and signaling. Biomol Concepts 3:117–126.

Seo D, Southard KM, Kim J-W, et al (2017) A Mechanogenetic Toolkit for Interrogating Cell Signaling in Space and Time. Cell 169:1357.

Sethi S, Wang JW (2017) A versatile genetic tool for post-translational control of gene expression in Drosophila melanogaster. Elife 6:.

Seugnet L, Simpson P, Haenlin M (1997) Requirement for dynamin during Notch signaling in Drosophila neurogenesis. Dev Biol 192:585–598.

Sharpe HJ, Stevens TJ, Munro S (2010) A comprehensive comparison of transmembrane domains reveals organelle-specific properties. Cell 142:158–169.

Shaya O, Binshtok U, Hersch M, et al (2017) Cell-Cell Contact Area Affects Notch Signaling and Notch-Dependent Patterning. Dev Cell 40:505-511.e6.

Shergill B, Meloty-Kapella L, Musse AA, et al (2012) Optical tweezers studies on Notch: single-molecule interaction strength is independent of ligand endocytosis. Dev Cell 22:1313–1320.

Singh S, Mittal A (2016) Transmembrane Domain Lengths Serve as Signatures of Organismal Complexity and Viral Transport Mechanisms. Sci Rep 6:22352.

Snyder SH (1985) The molecular basis of communication between cells. Sci Am 253:132–141.

Sotillos S, Roch F, Campuzano S (1997) The metalloprotease-disintegrin Kuzbanian participates in Notch activation during growth and patterning of Drosophila imaginal discs. Development 124:4769–4779

Soudais C, Laplace-Builhe C, Kissa K, Kremer EJ (2001) Preferential transduction of neurons by canine adenovirus vectors and their efficient retrograde transport in vivo. FASEB J 15:2283–2285.

Sporns O, Tononi G, Kötter R (2005) The human connectome: A structural description of the human brain. PLoS Comput Biol 1:e42.

Sprinzak D, Lakhanpal A, Lebon L, et al (2010) Cis-interactions between Notch and Delta generate mutually exclusive signalling states. Nature 465:86–90.

St Johnston D (2002) The art and design of genetic screens: Drosophila melanogaster. Nature Reviews Genetics 3:176–188.

Stephenson NL, Avis JM (2012) Direct observation of proteolytic cleavage at the S2 site upon forced unfolding of the Notch negative regulatory region. PNAS 109:E2757–E2765.

Stöcker W, Grams F, Baumann U, et al (1995) The metzincins--topological and sequential relations between the astacins, adamalysins, serralysins, and matrixins (collagenases) define a superfamily of zinc-peptidases. Protein Sci 4:823–840.

Struhl G, Adachi A (1998) Nuclear access and action of notch in vivo. Cell 93:649–660.

Struhl G, Adachi A (2000) Requirements for Presenilin-Dependent Cleavage of Notch and Other Transmembrane Proteins. Molecular Cell 6:625–636.

Sulis ML, Williams O, Palomero T, et al (2008) NOTCH1 extracellular juxtamembrane expansion mutations in T-ALL. Blood 112:733–740.

Sun N, Cassell MD, Perlman S (1996) Anterograde, transneuronal transport of herpes simplex virus type 1 strain H129 in the murine visual system. J Virol 70:5405–5413

Tabuchi K, Sawamoto K, Suzuki E, et al (2000) GAL4/UAS-WGA system as a powerful tool for tracing Drosophila transsynaptic neural pathways. Journal of Neuroscience Research 59:94–99.

Tagami S, Okochi M, Yanagida K, et al (2008) Regulation of Notch signaling by dynamic changes in the precision of S3 cleavage of Notch-1. Mol Cell Biol 28:165–176.

Takano T, Xu C, Funahashi Y, et al (2015) Neuronal polarization. Development 142:2088–2093. https://doi.org/10.1242/dev.114454

Takemura S, Bharioke A, Lu Z, et al (2013) A visual motion detection circuit suggested by Drosophila connectomics. Nature 500:175–181.

Talay M, Richman EB, Snell NJ, et al (2017) Transsynaptic Mapping of Second-Order Taste Neurons in Flies by trans-Tango. Neuron 96:783-795.e4.

Taylor AC, Weiss P (1965) Demonstration of axonal flow by the movement of tritium-labeled protein in mature optic nerve fibers. Proc Natl Acad Sci U S A 54:1521–1527.

Tervo DGR, Hwang B-Y, Viswanathan S, et al (2016) A Designer AAV Variant Permits Efficient Retrograde Access to Projection Neurons. Neuron 92:372–382.

Thompson BJ, Buonamici S, Sulis ML, et al (2007) The SCFFBW7 ubiquitin ligase complex as a tumor suppressor in T cell leukemia. J Exp Med 204:1825–1835.

Tian L, Wu X, Chi C, et al (2008) ADAM10 is essential for proteolytic activation of Notch during thymocyte development. Int Immunol 20:1181–1187.

Tiyanont K, Wales TE, Aste-Amezaga M, et al (2011) Evidence for Increased Exposure of the Notch1 Metalloprotease Cleavage Site upon Conversion to an Activated Conformation. Structure 19:546–554.

Toonen JA, Ronchetti A, Sidjanin DJ (2016) A Disintegrin and Metalloproteinase10 (ADAM10) Regulates NOTCH Signaling during Early Retinal Development. PLoS One 11:e0156184.

Tootell RB, Hamilton SL, Silverman MS, Switkes E (1988) Functional anatomy of macaque striate cortex. I. Ocular dominance, binocular interactions, and baseline conditions. J Neurosci 8:1500–1530.

Tordo J, O'Leary C, Antunes ASLM, et al (2018) A novel adeno-associated virus capsid with enhanced neurotropism corrects a lysosomal transmembrane enzyme deficiency. Brain 141:2014–2031.

Tousseyn T, Jorissen E, Reiss K, Hartmann D (2006) (Make) stick and cut loose--disintegrin metalloproteases in development and disease. Birth Defects Res C Embryo Today 78:24–46.

Tousseyn T, Thathiah A, Jorissen E, et al (2009) ADAM10, the rate-limiting protease of regulated intramembrane proteolysis of Notch and other proteins, is processed by ADAMS-9, ADAMS-15, and the gamma-secretase. J Biol Chem 284:11738–11747.

Trinquand A, Tanguy-Schmidt A, Ben Abdelali R, et al (2013) Toward a NOTCH1/FBXW7/RAS/PTEN-based oncogenetic risk classification of adult T-cell acute lymphoblastic leukemia: a Group for Research in Adult Acute Lymphoblastic Leukemia study. J Clin Oncol 31:4333–4342.

Trojanowski JQ (1983) Native and derivatized lectins for in vivo studies of neuronal connectivity and neuronal cell biology. J Neurosci Methods 9:185–204.

Trojanowski JQ, Gonatas JO, Gonatas NK (1981) Conjugates of horseradish peroxidase (HRP) with cholera toxin and wheat germ agglutinin are superior to free HRP as orthogradely transported markers. Brain Res 223:381–385.

Tsai Y-H, VanDussen KL, Sawey ET, et al (2014) ADAM10 regulates Notch function in intestinal stem cells of mice. Gastroenterology 147:822-834.e13.

Ugolini G (1995) Specificity of rabies virus as a transneuronal tracer of motor networks: transfer from hypoglossal motoneurons to connected second-order and higher order central nervous system cell groups. J Comp Neurol 356:457–480.

Ugolini G, Kuypers HG, Strick PL (1989) Transneuronal transfer of herpes virus from peripheral nerves to cortex and brainstem. Science 243:89–91.

Urban DJ, Roth BL (2015) DREADDs (designer receptors exclusively activated by designer drugs): chemogenetic tools with therapeutic utility. Annu Rev Pharmacol Toxicol 55:399–417. https://doi.org/10.1146/annurev-pharmtox-010814-124803

Unni S, Huang Y, Hanson R, et al (2011). Web servers and services for electrostatics calculations with APBS and PDB2PQR. Comput Chem 32(7):1488-91

Vadillo E, Dorantes-Acosta E, Pelayo R, Schnoor M (2018) T cell acute lymphoblastic leukemia (T-ALL): New insights into the cellular origins and infiltration mechanisms common and unique among hematologic malignancies. Blood Rev 32:36–51.

van Tetering G, Vooijs M (2011) Proteolytic Cleavage of Notch: "HIT and RUN." Curr Mol Med 11:255–269

Varnum-Finney B, Wu L, Yu M, et al (2000) Immobilization of Notch ligand, Delta-1, is required for induction of notch signaling. J Cell Sci 113 Pt 23:4313–4318

von Willebrand (1926) Hereditar pseudohemofili. Fin Laekaresaellsk Hand 87–112

Walani N, Torres J, Agrawal A (2015) Endocytic proteins drive vesicle growth via instability in high membrane tension environment. Proc Natl Acad Sci U S A 112:E1423-1432.

Waller AV, Owen R (1850) XX. Experiments on the section of the glossopharyngeal and hypoglossal nerves of the frog, and observations of the alterations produced thereby in the structure of their primitive fibres. Philosophical Transactions of the Royal Society of London 140:423–429.

Wang H, Liu J, Yuet KP, et al (2018) Split cGAL, an intersectional strategy using a split intein for refined spatiotemporal transgene control in Caenorhabditis elegans. Proc Natl Acad Sci U S A 115:3900–3905.

Wang NJ, Sanborn Z, Arnett KL, et al (2011) Loss-of-function mutations in Notch receptors in cutaneous and lung squamous cell carcinoma. Proc Natl Acad Sci U S A 108:17761–17766.

Wang W, Struhl G (2005) Distinct roles for Mind bomb, Neuralized and Epsin in mediating DSL endocytosis and signaling in Drosophila. Development 132:2883–2894.

Wang W, Struhl G (2004) Drosophila Epsin mediates a select endocytic pathway that DSL ligands must enter to activate Notch. Development 131:5367–5380.

Weinmaster G, Fischer JA (2011) Notch ligand ubiquitylation: what is it good for? Dev Cell 21:134–144.

Weng AP, Ferrando AA, Lee W, et al (2004) Activating Mutations of NOTCH1 in Human T Cell Acute Lymphoblastic Leukemia. Science 306:269–271.

Wharton KA, Johansen KM, Xu T, Artavanis-Tsakonas S (1985) Nucleotide sequence from the neurogenic locus notch implies a gene product that shares homology with proteins containing EGF-like repeats. Cell 43:567–581.

Whiteman P, de Madrid BH, Taylor P, et al (2013) Molecular basis for Jagged-1/Serrate ligand recognition by the Notch receptor. J Biol Chem 288:7305–7312.

Wickersham IR, Lyon DC, Barnard RJO, et al (2007) Monosynaptic restriction of transsynaptic tracing from single, genetically targeted neurons. Neuron 53:639–647.

Windler SL, Bilder D (2010) Endocytic internalization routes required for delta/notch signaling. Curr Biol 20:538–543.

Xia W, Wolfe MS (2003) Intramembrane proteolysis by presenilin and presenilin-like proteases. J Cell Sci 116:2839–2844.

Xu X, Choi SH, Hu T, et al (2015) Insights into Autoregulation of Notch3 from Structural and Functional Studies of Its Negative Regulatory Region. Structure 23:1227–1235.

Xu X, Holmes TC, Luo M-H, et al (2020) Viral Vectors for Neural Circuit Mapping and Recent Advances in Trans-synaptic Anterograde Tracers. Neuron 107:1029–1047.

Xu Z, Lam LSM, Lam LH, et al (2008) Molecular basis of the redox regulation of SUMO proteases: a protective mechanism of intermolecular disulfide linkage against irreversible sulfhydryl oxidation. FASEB J 22:127–137.

Yamagata M, Sanes JR (2012) Transgenic strategy for identifying synaptic connections in mice by fluorescence complementation (GRASP). Front Mol Neurosci 5:18.

Yamanaka M, Smith NI, Fujita K (2014) Introduction to super-resolution microscopy. Microscopy (Oxf) 63:177–192.

Yang Z-J, Yu Z-Y, Cai Y-M, et al (2020) Engineering of an enhanced synthetic Notch receptor by reducing ligand-independent activation. Commun Biol 3:116.

Yizhar O, Fenno LE, Davidson TJ, et al (2011) Optogenetics in neural systems. Neuron 71:9–34.

Yoshihara Y, Mori K (1994) Telencephalin: a neuronal area code molecule? Neurosci Res 21:119–124.

Yoshihara Y, Oka S, Nemoto Y, et al (1994) An ICAM-related neuronal glycoprotein, telencephalin, with brain segment-specific expression. Neuron 12:541–553.

Zacharioudaki E, Bray SJ (2014) Tools and methods for studying Notch signaling in Drosophila melanogaster. Methods 68:173–182.

Zemanick MC, Strick PL, Dix RD (1991) Direction of transneuronal transport of herpes simplex virus 1 in the primate motor system is strain-dependent. Proc Natl Acad Sci U S A 88:8048–8051.

Zeng F, Zhang M-Z, Singh AB, et al (2007) ErbB4 isoforms selectively regulate growth factor induced Madin-Darby canine kidney cell tubulogenesis. Mol Biol Cell 18:4446–4456.

Zhang X, Halvorsen K, Zhang C-Z, et al (2009) Mechanoenzymatic cleavage of the ultralarge vascular protein von Willebrand factor. Science 324:1330–1334.

ANNEXS

ANNEX 1. Transmembrane Domain Sequences.

Table1-Figure 2.8. Amino acid sequence of the different TMD modifications.

Modifications **TMD**	N-terminal sequences C-terminal
hNotch1TMD	**LHFMYVAAAAFVLLFFVGCGVLLS**
CD4TMD	MALIVLGGVAGLLLFIGLIFFCV
HybTMD	MALIVLGGVAGLLLFIGLIFFCV + **GVLLS**
24noC	MALIVLGGVAGLLLFIGL + **GVLLS**
24noC, ILE	MALIVLGGVAGLLLFIGL + V**GVLLI**
24noC, SER	MALIVLGGVAGLLLFIGL + V**GVLLS**
28noC	MALIVLGGVAGLLLFIGLGIFF**C**V + **GVLLS**
28noC, noSER	MALIVLGGVAGLLLFIGLGIFF**C**V + **GVLLI**

Amino acid substitution

Amino acid elimination

Sequences from E-cadherin and ErbB4 TMD (Figure 3.20):

E-cadherin TMD: AILGILGGILALLILILLLLLFL

Erbb4 TMD: LIAAGVIGGLFILVIVGLTFAVYV

Table2-Figure 3.21: Amino acid sequence of *Drosophila* Seveneles and Torso receptors and Amyloid precursor protein.

MB proteins **TMD**	N-terminal sequences C-terminal
NotchTMD	**LHFMYVAAAAFVLLFFVGCGVLLS**
APP	IIGLMVGGVVIATVIVITLVM
dSEVENLESS	GSLVLAIIAPAAIVSSCVLALVLV
dTORSO	LVLFIIVPICCILMLCSLTFC

ANNEX 2. Statistical DATA Tables – Chapter 2

Table 1 – Figure 2.8: TMD modifications.

1A: Integrated intensity and fold activation of the TMD modifications.

RECEPTOR	INTEGRATED INTENSITY		FOLD ACTIVATION
	Bkg	Ind	
hNotch1 TMD	$3.45 \times 10^5 \pm 1.78 \times 10^5$	$17.20 \times 10^5 \pm 3.09 \times 10^5$	4.95 ± 0.88
24noC	$1.20 \times 10^5 \pm 2.20 \times 10^5$	$9.37 \times 10^5 \pm 2.50 \times 10^5$	7.62 ± 2.11
24noC, ILE	$2.02 \times 10^5 \pm 0.79 \times 10^5$	$14.34 \times 10^5 \pm 6.94 \times 10^5$	7.10 ± 3.23
24noC, SER	$1.91 \times 10^5 \pm 1.04 \times 10^5$	$12.34 \times 10^5 \pm 3.12 \times 10^5$	6.44 ± 1.63
28noC	$1.10 \times 10^5 \pm 2.37 \times 10^5$	$4.75 \times 10^5 \pm 1.66 \times 10^5$	4.30 ± 1.50
28noC, SER	$0.88 \times 10^5 \pm 0.66 \times 10^5$	$2.25 \times 10^5 \pm 0.91 \times 10^5$	2.56 ± 1.03

1B: p-value of fold activation comparisons.

p-value, Fold Activation	hNotch1 TMD	24noC	24noC, ILE	24noC, SER	28noC	28noC, SER
hNotch1 TMD	-	-	-	-	-	-
24noC	0.017	-	-	-	-	-
24noC, ILE	0.222	0.638	-	-	-	-
24noC, SER	0.202	0.165	0.530	-	-	-
28noC	0.202	5.83×10^{-4}	0.073	0.037	-	-
28noC, SER	0.031	0.002	0.015	0.005	0.431	-

Table 2 – Figure 2.9. ECD modifications.

2A: Integrated intensity and fold activation of the ECD modifications.

RECEPTOR	INTEGRATED INTENSITY		FOLD ACTIVATION
	Bkg	Ind	
1d3NRR	$8.75 \times 10^5 \pm 1.28 \times 10^5$	$42.6 \times 10^5 \pm 6.56 \times 10^5$	4.86 ± 0.75
1d3S1LO	$3.21 \times 10^5 \pm 0.55 \times 10^5$	$7.25 \times 10^5 \pm 1.89 \times 10^5$	2.24 ± 0.59
1d3NRRLZ	$1.31 \times 10^5 \pm 0.63 \times 10^5$	$8.12 \times 10^5 \pm 3.16 \times 10^5$	6.22 ± 2.42
1d3Hyb	$2.71 \times 10^5 \pm 1.61 \times 10^5$	$33.99 \times 10^5 \pm 3.52 \times 10^5$	13.55 ± 1.40

2B: p-value of fold activation comparisons.

p-value	1d3NRR	1d3S1LO	1d3NRRLZ	1d3Hyb
1d3NRR	-	-	-	-
1d3S1LO	0.007	-	-	-
1d3NRRLZ	0.204	6.6×10^{-4}	-	-
1d3Hyb	0.015	0.016	0.003	-

Table 3 – Figure 2.10. ECD modifications (EGF-like repeats).

3A: Integrated intensity and fold activation of EGF repetas modifications.

RECEPTOR	INTEGRATED INTENSITY		FOLD ACTIVATION
	Bkg	Ind	
1d3NRR	$1.30 \times 10^4 \pm 0.42 \times 10^4$	$7.96 \times 10^4 \pm 1.26 \times 10^4$	6.12 ± 0.97
1d3EGF30-36NRR	$1.46 \times 10^4 \pm 0.45 \times 10^4$	$8.69 \times 10^4 \pm 0.21 \times 10^4$	5.96 ± 1.42
1d3EGF33-36NRR	$1.75 \times 10^4 \pm 0.70 \times 10^4$	$7.50 \times 10^4 \pm 1.51 \times 10^4$	4.27 ± 0.87
1d3EGF36NRR	$1.07 \times 10^4 \pm 0.59 \times 10^4$	$8.51 \times 10^4 \pm 0.92 \times 10^4$	7.91 ± 0.86

3B: p-value of fold activation comparisons.

p-value	1d3NRR	1d3EGF33-36NRR	1d3EGF33-36NRR	1d3EGF36NRR
1d3NRR	-	-	-	-
1d3EGF30-36NRR	5.90×10^{-4}	-	-	-
1d3EGF33-36NRR	3.90×10^{-5}	9.90×10^{-4}	-	
1d3EGF36NRR	2.61×10^{-5}	1.13×10^{-3}	0.77	-

Table 4 – Figure 2.12: Snorkelling and adding RKR motif in the jTMD.

4A: Integrated intensity and fold activation.

RECEPTOR	INTEGRATED INTENSITY		FOLD ACTIVATION
	Bkg	Ind	
WTNotch jTMD	$1.34 \times 10^4 \pm 0.44 \times 10^4$	$7.21 \times 10^4 \pm 1.23 \times 10^4$	5.43 ± 0.43
LWFRRGS jTMD	$1.93 \times 10^4 \pm 0.38 \times 10^4$	$4.92 \times 10^4 \pm 0.95 \times 10^4$	2.55 ± 0.759
RKRGGGGS jTMD	$3.30 \times 10^4 \pm 0.476 \times 10^4$	$7.11 \times 10^4 \pm 2.44 \times 10^4$	2.15 ± 0.74

p-value LWFRRGS vs RKRGGGGGGSjTMD: 0.048

p-value WTNotch jTMD vs RKRGGGGGGSjTMD: 4.81×10^{-8}

p-value WTNotch jTMD vs LWFRRGS: 1.54×10^{-7}

Table 5 – Figure 2.13: Dimerizing the ICD of the synthetic receptor (LZ).

5A: Integrated intensity and fold activation.

RECEPTOR	INTEGRATED INTENSITY		FOLD ACTIVATION
	Bkg	Ind	
1d3NRR	$1.36 \times 10^4 \pm 0.19 \times 10^4$	$8.93 \times 10^4 \pm 1.24 \times 10^4$	6.56 ± 0.91
1d3NRR-GCN4icd	$0.77 \times 10^4 \pm 0.13 \times 10^4$	$7.85 \times 10^4 \pm 2.08 \times 10^4$	10.09 ± 2.66
1d3NRR-63GS	$1.07 \times 10^4 \pm 0.56 \times 10^4$	$10.98 \times 10^4 \pm 3.09 \times 10^4$	10.20 ± 2.87

p-value 1d3NRR-GCN4 vs 1d3NRR-63GS: 0.89

p-value 1d3NRR vs 1d3NRR- GCN4: 8.73×10^{-5}

p-value 1d3NRR vs 1d3NRR-63GS: 8.21×10^{-5}

Table 6 – Figure 2.14. Split Gal4 strategy.

6A: Integrated intensity and fold activation.

RECEPTOR	INTEGRATED INTENSITY		FOLD ACTIVATION
	Bkg	Ind	
72 hours			
1d3NRR50%	$2.39 \times 10^4 \pm 0.56 \times 10^4$	$20.36 \times 10^4 \pm 4.40 \times 10^4$	8.50 ± 1.85
DbdZIPVP16-33%	$0.29 \times 10^4 \pm 0.12 \times 10^4$	$0.54 \times 10^4 \pm 0.09 \times 10^4$	1.87 ± 0.31
DbdZIPVP16-45%	$0.44 \times 10^4 \pm 0.04 \times 10^4$	$1.02 \times 10^4 \pm 0.34 \times 10^4$	2.32 ± 0.76
DbdZIPVP16-95%	$0.96 \times 10^4 \pm 0.38 \times 10^4$	$3.47 \times 10^4 \pm 0.67 \times 10^4$	3.59 ± 0.69

6B: p-value of fold activation comparisons.

p-value	1d3NRR-50%	DbdZIPVP16-33%	DbdZIPVP16-45%	DbdZIPVP16-95%
72 hours				
1d3NRR50%	-	-	-	-
DbdZIPVP16-33%	2.16×10^{-3}	-	-	-
DbdZIPVP16-45%	2.16×10^{-3}	0.25	-	-
DbdZIPVP16-95%	2.16×10^{-3}	1.16×10^{-3}	2.52×10^{-3}	-

Table 7 – Figure 2.16. Destabilization domain (DHFR).

7A: Integrated intensity and fol activation.

RECEPTOR	INTEGRATED INTENSITY		FOLD ACTIVATION
	Bkg	Ind	
Tta - TMP	$7.14 \times 10^6 \pm 3.49 \times 10^6$	$96.15 \times 10^6 \pm 1.99 \times 10^6$	---
Tta - DMSO	$76.51 \times 10^6 \pm 3.72 \times 10^6$	$93.79 \times 10^6 \pm 4.04 \times 10^6$	---
DHFR - TMP	$73.86 \times 10^6 \pm 3.01 \times 10^6$	$79.69 \times 10^6 \pm 3.67 \times 10^6$	119% ± 38%
DHFR - DMSO	$74.04 \times 10^6 \pm 2.84 \times 10^6$	$82.23 \times 10^6 \pm 2.92 \times 10^6$	98% ± 43%
100I - TMP	$71.45 \times 10^6 \pm 1.43 \times 10^6$	$86.68 \times 10^6 \pm 4.96 \times 10^6$	30% ± 21%
100I - DMSO	$76.04 \times 10^6 \pm 2.22 \times 10^6$	$71.86 \times 10^6 \pm 4.05 \times 10^6$	45% ± 28%
100Y - TMP	$73.79 \times 10^6 \pm 1.76 \times 10^6$	$92.93 \times 10^6 \pm 3.41 \times 10^6$	+5% no reduction
100Y - DMSO	$73.92 \times 10^6 \pm 2.70 \times 10^6$	$90.51 \times 10^6 \pm 4.48 \times 10^6$	10% ± 5%

%: percent change in total intensity upon induction

7B: p-value of fold activation comparisons.

p-value % Reduction	tTA - TMP	tTA - DMSO	DHFR - TMP	DHFR - DMSO	100I - TMP	100I - DMSO	100Y - TMP	100Y - DMSO
tTA - TMP	-	-	-	-	-	-	-	-
tTA - DMSO		-	-	-	-	-	-	-
DHFR - TMP	1.51×10^{-5}		-	-	-	-	-	-
DHFR - DMSO				-	-	-	-	-
100I - TMP	0.027		0.37		-	-	-	-
100I - DMSO				3.29×10^4		-	-	-
100Y - TMP	0.076				0.015		-	-
100Y - DMSO			0.091	1.24×10^4		0.022		-

Values represent the percent change in total intensity upon induction

ANNEX 3. Statistical DATA Tables – Chapter 3

Table 1 – Figure 3.7: Synthetic receptor with and without NRR.

1A: Integrated intensity and fold activation.

RECEPTOR	INTEGRATED INTENSITY		FOLD ACTIVATION
	Bkg	Ind	
hCARNRRG4	$1.43 \times 10^4 \pm 1.52 \times 10^4$	$6.25 \times 10^4 \pm 2.56 \times 10^4$	4.35 ± 1.24
hCARnoNRRG4	$1.84 \times 10^4 \pm 0.86 \times 10^4$	$18.95 \times 10^4 \pm 2.56 \times 10^4$	10.68 ± 1.91
CD4NRRG4	$0.63 \times 10^4 \pm 0.78 \times 10^4$	$3.15 \times 10^4 \pm 1.99 \times 10^4$	4.90 ± 1.58
CD4noNRRG4	$1.33 \times 10^4 \pm 0.78 \times 10^4$	$16.91 \times 10^4 \pm 4.67 \times 10^4$	12.05 ± 5.18

1B: p-value of fold activation comparisons.

p-value, **Fold Activation**	hCARNRRG4	HCARnoNRRG4	CD4NRRG4	CD4noNRRG4
hCARNRRG4	-	-	-	-
hCARnoNRRG4	2.60×10^{-7}	-	-	-
CD4NRRG4	0.59	2.95×10^{-9}	-	-
CD4noNRRG4	3.64×10^{-13}	7.7×10^{-4}	3.89×10^{-8}	-

Table 2 - Figure 3.13: Notch species jTMD

2A: Integrated intensity and fold activation.

RECEPTOR	INTEGRATED INTENSITY		FOLD ACTIVATION
	Bkg	Ind	
hNotch1	$1.58 \times 10^4 \pm 0.44 \times 10^4$	$18.72 \times 10^4 \pm 4.35 \times 10^4$	11.63 ± 3.57
hNotch2	$1.50 \times 10^4 \pm 1.85 \times 10^4$	$6.03 \times 10^4 \pm 5 \times 10^4$	4.16 ± 2.17
ChNotch1	$3.94 \times 10^4 \pm 0.91 \times 10^4$	$29.31 \times 10^4 \pm 3.85 \times 10^4$	7.43 ± 1.01
ZFNotch1	$3.69 \times 10^4 \pm 0.86 \times 10^4$	$29.10 \times 10^4 \pm 4.66 \times 10^4$	7.97 ± 1.33
XNotch1	$3.77 \times 10^4 \pm 1.41 \times 10^4$	$28.46 \times 10^4 \pm 4.64 \times 10^4$	7.48 ± 2.30
dNotch	$7.63 \times 10^4 \pm 1.65 \times 10^4$	$27.01 \times 10^4 \pm 4.58 \times 10^4$	3.77 ± 1.03
dNotchnoPro	$9.96 \times 10^4 \pm 2.09 \times 10^4$	$22.12 \times 10^4 \pm 6.67 \times 10^4$	2.53 ± 0.55

2B: p-value of fold activation comparisons.

p-value, **Fold Activation**	hNotch2	ChNotch1	ZFNotch1	XNotch1	dNotch	dNotchnoPro
hNotch2	-	-	-	-	-	-
ChNotch1	7.61×10^{-8}	-	-	-	-	-
ZFNotch1	5.06×10^{-8}	0.1	-	-	-	-
XNotch1	3.5×10^{-5}	0.71	0.11	-	-	-
dNotch	0.019	4.61×10^{-11}	4.61×10^{-11}	4.13×10^{-8}	-	-
dNotchnoPro	1.58×10^{-8}	1.52×10^{-11}	1.77×10^{-11}	2.57×10^{-11}	0.02	-
hNotch1	3.85×10^{-10}	1.65×10^{-7}	5.10×10^{-6}	8.10×10^{-7}	7.35×10^{-10}	3.12×10^{-10}

Table 3A – Figure 3.10: Effect of ADAM and γ-secretase blockers of integrated intensity for synthetic receptors.

3A-1: Integrated intensity and fold activation.

Condition	Integrity Intensity		% Decrease
	Bkg	Ind	
CD4NRR	$24.15 \times 10^6 \pm 2.43 \times 10^6$	$77.55 \times 10^6 \pm 15.04 \times 10^6$	---
CD4NRR-ADAMs	---	$36.51 \times 10^6 \pm 5.82 \times 10^6$	81.30 ± 8.36
CD4NRR-γsecretase	---	$23.96 \times 10^6 \pm 2.86 \times 10^6$	98.15 ± 3.16
CD4NRR- ADAMs+ γsecretase	---	$25.40 \times 10^6 \pm 2.43 \times 10^6$	98.34 ± 3.18
CD4noNRR	$32.83 \times 10^6 \pm 3.45 \times 10^6$	$91.66 \times 10^6 \pm 15.26 \times 10^6$	---
CD4noNRR-ADAMs	---	$37.68 \times 10^6 \pm 9.47 \times 10^6$	93.34 ± 10.63
CD4noNRR-γsecretase	---	$29.23 \times 10^6 \pm 3.16 \times 10^6$	107.76 ± 3.24
CD4noNRR- ADAMs+ γ-secretase	---	$27.42 \times 10^6 \pm 3.39 \times 10^6$	109.59 ± 4.20

3A.2: p-value of fold activation comparisons.

p-value of % decrease	CD4NRR-ADAMs	CD4NRR-γsecretase	CD4NRR-ADAMs+ γsecretase	CD4noNRR-ADAMs	CD4noNRR-γsecretase	CD4noNRR-ADAMs+ γsecretase
CD4NRR-ADAMs	-	-	-	-	-	-
CD4NRR-γsecretase	1.45×10^{-7}	-		-	-	-
CD4NRR-ADAMs+ γsecretase	1.45×10^{-7}	0.529	-	-	-	-
CD4noNRR-ADAMs	3.50×10^{-4}		-	-	-	-
CD4noNRR-γsecretase	-	7.31×10^{-8}	-	1.34×10^{-5}	-	-
CD4noNRR-ADAMs+ γsecretase	-	-	4.14×10^{-8}	5.95×10^{-6}	0.132	-

Table 3B – Figure 3.10: Effect of ADAM and γ-secretase blockers of integrated intensity for Notch receptors.

3B.1: Integrated intensity and fold activation.

Condition	Intensity		% Decrease
	Bkg	Ind	
NotchNRR	$27.83 \times 10^6 \pm 3.44 \times 10^6$	$85.60 \times 10^6 \pm 10.64 \times 10^6$	---
NotchNRR-ADAMs	---	$31.31 \times 10^6 \pm 2.77 \times 10^6$	91.72 ± 4.27
NotchNRR-γsecretase	---	$30.79 \times 10^6 \pm 1.69 \times 10^6$	93.29 ± 5.22
NotchNRR- ADAMs+ γsecretase	---	$28.04 \times 10^6 \pm 1.53 \times 10^6$	97.20 ± 4.07
NotchnoNRR	$31.02 \times 10^6 \pm 2.63 \times 10^6$	$76.40 \times 10^6 \pm 9.45 \times 10^6$	---
NotchnoNRR-ADAMs	---	$29.71 \times 10^6 \pm 1.75 \times 10^6$	104.08 ± 4.27
NotchnoNRR-γsecretase	---	$29.30 \times 10^6 \pm 1.42 \times 10^6$	102.76 ± 3.90
NotchnoNRR- ADAMs+ γsecretase	---	$29.24 \times 10^6 \pm 14.13 \times 10^6$	104.39 ± 4.02

3B.2: p-value of fold activation comparisons.

p-value	NotchNRR-ADAMs	NotchNRR-γsecretase	NotchNRR-ADAMs+ γsecretase	NotchnoNRR-ADAMs	NotchnoNRR-γsecretase	NotchnoNRR- ADAMs+ γsecretase
NotchNRR-ADAMs	-	-	-	-	-	-
Notch-γsecretase	0.174	-		-	-	-
NotchNRR-ADAMs+ γsecretase	2.39×10^{-4}	0.015	-	-	-	-
NotchnoNRR-ADAMs	4.46×10^{-8}		-	-	-	-
NotchnoNRR-γsecretase	-	4.17×10^{-7}	-	0.796	-	
NotchnoNRR- ADAMs+ γsecretase	-	-	1.06×10^{-6}	0.369	0.190	-

Table 4 – Figure 3.14: Different membrane proteins jTMD.

4A: Integrated intensity and fold activation.

RECEPTOR	INTEGRATED INTENSITY		FOLD ACTIVATION
	Bkg	Ind	
hNotch1	$1.10 \times 10^4 \pm 0.72 \times 10^4$	$13.52 \times 10^4 \pm 2.38 \times 10^4$	11.87 ± 3.37
CD4	$0.10 \times 10^4 \pm 0.22 \times 10^4$	$0.12 \times 10^4 \pm 0.23 \times 10^4$	1.09 ± 0.38
E-cadherin	$2.10 \times 10^4 \pm 0.87 \times 10^4$	$13.01 \times 10^4 \pm 3.16 \times 10^4$	6.49 ± 1.84
NCAM	$1.23 \times 10^4 \pm 1.10 \times 10^4$	$10.3 \times 10^4 \pm 4.36 \times 10^4$	8.24 ± 1.44
Short-erbB4	$1.72 \times 10^4 \pm 1.46 \times 10^4$	$11.07 \times 10^4 \pm 2.65 \times 10^4$	6.43 ± 1.33
Long-erbB4	$7.29 \times 10^4 \pm 1.02 \times 10^4$	$8.63 \times 10^4 \pm 1.89 \times 10^4$	1.68 ± 0.77
CD8	$3.50 \times 10^4 \pm 2.68 \times 10^4$	$4.21 \times 10^4 \pm 3.27 \times 10^4$	1.40 ± 0.45

4B: p-value of fold activation comparisons.

p-value	E-cadherin	NACM	CD4	CD8	Long-erbB4	Short-erbB4
E-cadherin	-	-	-	-	-	-
NCAM	0.001	-	-	-	-	-
CD4	1.11×10^{-13}	7.05×10^{-9}	-	-	-	-
CD8	3.03×10^{-10}	2.19×10^{-7}	0.003	-	-	-
Long-erbB4	2.53×10^{-9}	6.32×10^{-7}	0.17	0.13	-	-
Short-erbB4	0.17	0.002	1.93×10^{-15}	3.79×10^{-11}	4.73×10^{-10}	-
NotchjTMD	1.55×10^{-10}	2×10^{-4}	1.09×10^{-17}	3.27×10^{-12}	6.87×10^{-11}	5.42×10^{-11}

Table 5 – Figure 3.15: hNotch1 modifications of jTMD.

5A: Integrated intensity and fold activation.

RECEPTOR	INTEGRATED INTENSITY		FOLD ACTIVATION
	Bkg	Ind	
hNotch1 QSETVEPPPPAQ	$1.36 \times 10^4 \pm 0.41 \times 10^4$	$14.48 \times 10^4 \pm 3.65 \times 10^4$	11.96 ± 1.71
Modif.1 Q**A**ETVEPPPPAQ	$1.21 \times 10^4 \pm 0.40 \times 10^4$	$14.27 \times 10^4 \pm 2.34 \times 10^4$	9.95 ± 1.81
Modif.2 Q**E**ETVEPPPPAQ	$1.15 \times 10^4 \pm 0.81 \times 10^4$	$10.78 \times 10^4 \pm 2.71 \times 10^4$	10.16 ± 2.81
Modif.3 QS**S**TVEPPPPAQ	$0.58 \times 10^4 \pm 0.43 * 10^4$	$6.07 \times 10^4 \pm 1.09 \times 10^4$	10.34 ± 2.03
Modif.6 QSETVE**AAAA**AQ	$1.44 \times 10^4 \pm 1.01 \times 10^4$	$15.11 \times 10^4 \pm 3.70 \times 10^4$	9.62 ± 3.40
Modif.4 QSETVE**AAAAAA**	$3.91 \times 10^4 \pm 1.74 \times 10^4$	$18.43 \times 10^4 \pm 3.71 \times 10^4$	5.80 ± 2.40
Modif.5 QSET**AAAAAAAA**	$3.40 \times 10^4 \pm 1.08 \times 10^4$	$16.20 \times 10^4 \pm 3.76 \times 10^4$	4.77 ± 1.11
Modif.7 12A	$2.75 \times 10^4 \pm 1.31 \times 10^4$	$9.75 \times 10^4 \pm 4.40 \times 10^4$	3.52 ± 0.43
Modif.8 12G	$4.24 \times 10^4 \pm 0.67 \times 10^4$	$13.17 \times 10^4 \pm 2.32 \times 10^4$	3.24 ± 0.33

p-value	Modif.1	Modif.2	Modif.3	Modif.6	Modif.4	Modif.5	Modif.7	Modif.8
Modif.1	-	-	-	-	-	-	-	-
Modif.2	0.38	-	-	-	-	-	-	-
Modif.3	0.26	0.69	-	-	-	-	-	-
Modif.6	0.81	0.69	0.64	-	-	-	-	-
Modif.4	3.09×10^{-9}	2.73×10^{-9}	3.03×10^{-6}	3.69×10^{-14}	-	-		
Modif.5	4.46×10^{-11}	9.26×10^{-11}	4.34×10^{-7}	5.20×10^{-11}	0.16	-	-	-
Modif.7	9.83×10^{-15}	2.78×10^{-14}	4.11×10^{-8}	1.54×10^{-14}	1.73×10^{-12}	8.26×10^{-11}	-	-
Modif.8	8.61×10^{-16}	2.87×10^{-15}	2.17×10^{-8}	1.56×10^{-16}	5.00×10^{-16}	7.54×10^{-13}	9.54×10^{-4}	-
hNotch1	8.00×10^{-3}	4.50×10^{-2}	6.58×10^{-2}	0.051	2.17×10^{-12}	5.20×10^{-11}	4.78×10^{-14}	2.46×10^{-13}

5B: p-value of fold activation comparisons.

Table 6 – Figure 3.17: CD4NRR with CD4jTMD (12 aa) or CD4jTMD+hNoth1jTMD.

6A: Integrated intensity and fold activation.

RECEPTOR	INTEGRATED INTENSITY		FOLD ACTIVATION
	Bkg	Ind	
hNotch1 QSETVEPPPAQ	$1.59 \times 10^4 \pm 1.01 \times 10^4$	$6.48 \times 10^4 \pm 2.15 \times 10^4$	4.43 ± 2.00
CD4 KVLPTWSTPVGP	$1.70 \times 10^4 \pm 0.47 \times 10^4$	$7.12 \times 10^4 \pm 1.11 \times 10^4$	4.17 ± 0.65
hNotch1 + CD4	$2.00 \times 10^4 \pm 0.44 \times 10^4$	$10.90 \times 10^4 \pm 2.43 \times 10^4$	5.46 ± 1.40

p-value CD4 vs hNotch1 + CD4: 3.03×10^{-3}

p-value hNotch1 vs CD4: 0.52

p-value hNotch1 vs hNotch1 + CD4: 0.108

Table 7 – Figure 3.18: Different length of jTMD in CD4NRR receptor.

7A: Integrated intensity and fold activation.

RECEPTOR	INTEGRATED INTENSITY		FOLD ACTIVATION
	Bkg	Ind	
5aa	$0.051 \times 10^4 \pm 0.021 \times 10^4$	$0.062 \times 10^4 \pm 0.023 \times 10^4$	1.24 ± 0.86
6aa	$1.93 \times 10^4 \pm 0.52 \times 10^4$	$2.83 \times 10^4 \pm 0.53 \times 10^4$	1.38 ± 0.36
7aa	$6.17 \times 10^4 \pm 1.78 \times 10^4$	$10.73 \times 10^4 \pm 2.23 \times 10^4$	1.97 ± 0.52
8aa	$5.30 \times 10^4 \pm 1.87 \times 10^4$	$13.15 \times 10^4 \pm 12.21 \times 10^4$	2.30 ± 0.73
9aa	$3.11 \times 10^4 \pm 0.87 \times 10^4$	$14.64 \times 10^4 \pm 4.12 \times 10^4$	5.05 ± 1.62
10aa	$4.51 \times 10^4 \pm 1.11 \times 10^4$	$18.08 \times 10^4 \pm 1.94 \times 10^4$	3.64 ± 0.76
11aa	$3.25 \times 10^4 \pm 1.04 \times 10^4$	$11.53 \times 10^4 \pm 2.83 \times 10^4$	3.47 ± 1.43
12aa	$2.16 \times 10^4 \pm 1.06 \times 10^4$	$9.73 \times 10^4 \pm 2.2 \times 10^4$	5.20 ± 2.50

7B: p-value of fold activation comparisons.

p-value	5aa	6aa	7aa	8aa	9aa	10aa	11aa
5aa	-	-	-	-	-	-	-
6aa	0.15	-	-	-	-	-	-
7aa	1.27×10^{-7}	6.25×10^{-10}	-	-	-	-	-
8aa	6.89×10^{-13}	4.00×10^{-17}	5.20×10^{-6}	-	-	-	-
9aa	5.60×10^{-18}	2.51×10^{-18}	3.81×10^{-18}	1.09×10^{-14}	-	-	-
10aa	1.44×10^{-17}	2.84×10^{-19}	6.04×10^{-18}	5.02×10^{-11}	1.32×10^{-5}	-	-
11aa	1.73×10^{-20}	1.85×10^{-23}	1.59×10^{-19}	5.56×10^{-10}	7.74×10^{-6}	0.36	-
CD4NRR-12aa	2.65×10^{-19}	1.69×10^{-21}	3.41×10^{-16}	4.82×10^{-10}	0.41	0.03	0.01

Table 8 – Figure 3.16: jTMD modifications based on electrostatic properties of amino acids composition of CD8jTMD and hNotch1jTMD.

8A: Integrated intensity and fold activation.

RECEPTOR	INTEGRATED INTENSITY		FOLD ACTIVATION
	Bkg	Ind	
hNotch1 QSETVEPPPAQ	$1.36 \times 10^4 \pm 0.41 \times 10^4$	$14.48 \times 10^4 \pm 3.65 \times 10^4$	11.96 ± 1.71
CD8: SVKGTGLDFACD	$3.50 \times 10^4 \pm 2.68 \times 10^4$	$4.21 \times 10^4 \pm 3.27 \times 10^4$	1.40 ± 0.45
Modif.1 QSKTVGPPPAQ	$1.14 \times 10^4 \pm 0.31 \times 10^4$	$1.85 \times 10^4 \pm 0.85 \times 10^4$	1.57 ± 0.29
Modif.2 QSKTVGLDFACD	$2.11 \times 10^4 \pm 0.73 \times 10^4$	$4.35 \times 10^4 \pm 0.83 \times 10^4$	1.93 ± 0.53
Modif.3 SVEGTEPPPPAQ	$3.21 \times 10^4 \pm 0.93 \times 10^4$	$5.18 \times 10^4 \pm 1.11 \times 10^4$	1.58 ± 0.36
Modif.4 SVEGTELDFAC	$2.07 \times 10^4 \pm 0.41 \times 10^4$	$2.33 \times 10^4 \pm 1.43 \times 10^4$	1.12 ± 0.69

8B: p-value of fold activation comparisons.

p-value	CD8 SVKGTGLDFACD	Modif.1 QSKTVGPPPAQ	Modif.2 QSKTVGLDFACD	Modif.3 SVEGTEPPPPAQ	Modif.4 SVEGTELDFAC
CD8 SVKGTGLDFACD	-	-	-	-	-
Modif.1 QSKTVGPPPAQ	0.033	-	-	-	-
Modif.2 QSKTVGLDFACD	2.02×10^{-9}	1.94×10^{-5}	-	-	-
Modif.3 SVEGTEPPPPAQ	0.033	9.64×10^{-10}	7.81×10^{-13}	-	-
Modif.4 SVEGTELDFAC	0.17	8.94×10^{-8}	1.18×10^{-9}	0.033	-
hNotch1jTMD	3.27×10^{-12}	1.50×10^{-14}	6.53×10^{-15}	7.94×10^{-13}	1.34×10^{-13}

Table 9 – Figure 3.20 and Figure 3.21: different membrane proteins TMD.

9A: Integrated intensity and fold activation.

RECEPTOR	INTEGRATED INTENSITY		FOLD ACTIVATION
	Bkg	Ind	
TORSO-TMD	$3.42 \times 10^4 \pm 0.99 \times 10^4$	$7.23 \times 10^4 \pm 1.42 \times 10^4$	2.21 ± 0.68
SEVENLESS-TMD	$3.25 \times 10^4 \pm 1.65 \times 10^4$	$8.63 \times 10^4 \pm 3.82 \times 10^4$	2.73 ± 0.80
APP-TMD 5W	$0.89 \times 10^4 \pm 0.40 \times 10^4$	$2.39 \times 10^4 \pm 0.85 \times 10^4$	3.21 ± 0.47
APP-TMD 4W	$4.93 \times 10^4 \pm 0.89 \times 10^4$	$16.02 \times 10^4 \pm 2.86 \times 10^4$	3.24 ± 0.58
hNotch1-TMD	$1.34 \times 10^4 \pm 0.76 \times 10^4$	$16.91 \times 10^4 \pm 4.67 \times 10^4$	12.05 ± 5.10
Long-erbB4-erbB4TMD	$0.81 \times 10^4 \pm 0.51 \times 10^4$	$1.151 \times 0^4 \pm 0.60 \times 10^4$	1.41 ± 0.74
Short-erbB4-erbB4TMD	$1.11 \times 10^4 \pm 0.86 \times 10^4$	$1.19 \times 10^4 \pm 1.90 \times 10^4$	1.09 ± 1.41
E-cadherin-TMD	$0.13 \times 10^4 \pm 0.48 \times 10^4$	$0.25 \times 10^4 \pm 2.1 \times 10^4$	1.18 ± 1.90
hNotch1jTMD	$1.10 \times 10^4 \pm 0.72 \times 10^4$	$13.52 \times 10^4 \pm 2.38 \times 10^4$	11.87 ± 3.37

9B: p-value of fold activation comparisons.

p-value	TORSO-TMD	SEVENLESS-TMD	APP-TMD 5W
TORSO-TMD	-	-	-
SEVENLESS-TMD	1.54×10^{-4}	-	-
APP-TMD	1.19×10^{-10}	2.76×10^{-6}	-
hNotch1-TMD	4.14×10^{-13}	9.76×10^{-15}	8.87×10^{-13}

p-value	Long-erbB4-erbB4TMD	Short-erbB4-erbB4TMD	E-cadherin-TMD
Long-erbB4-erbB4TMD			
Short-erbB4-erbB4TMD	0.06		
E-cadherin-TMD	0.34	0.67	
hNotch1-TMD	1.20×10^{-8}	6.47×10^{-13}	1.38×10^{-9}

Supplementary Figures. Histograms showing normalized probability distribution of intensities above the threshold (median shown as solid lines and standard deviation shown as shadow):

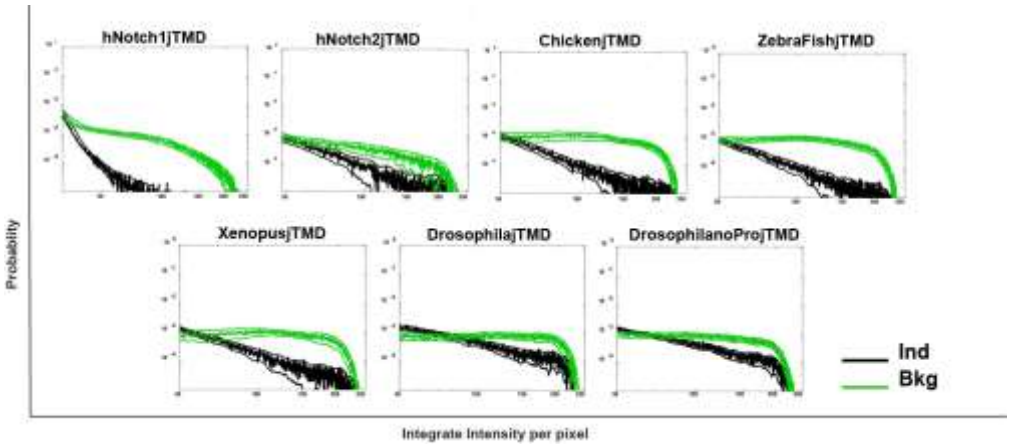

Figure Sup.3.13. Synthetic receptor with jTMD from different Notch species.

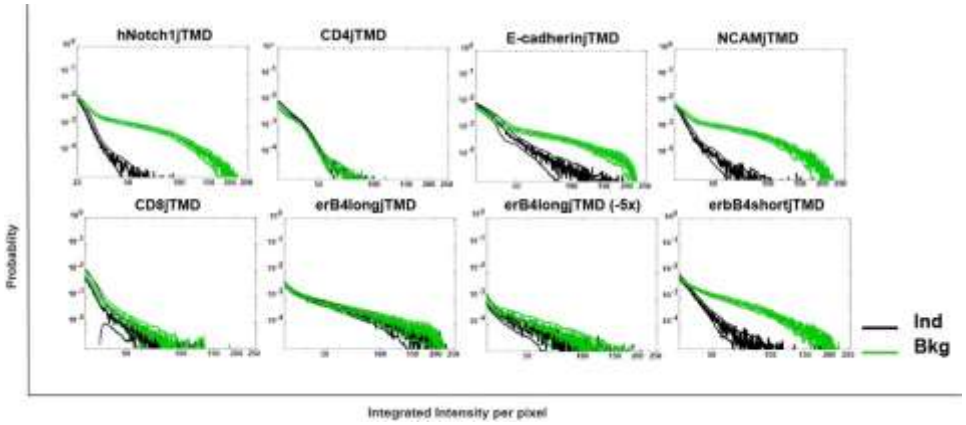

Figure Sup.3.14. Synthetic receptor with jTMD from different Notch membrane proteins.

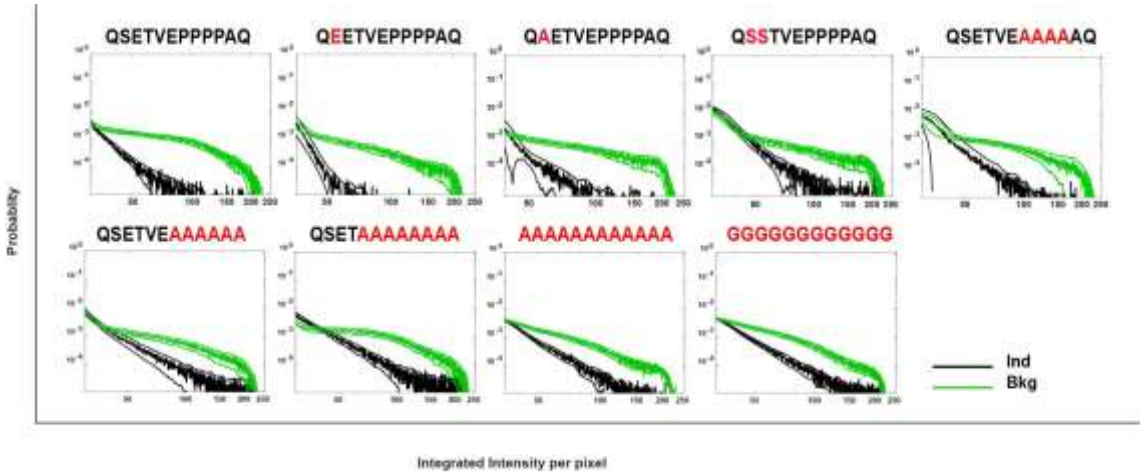

Figure Sup.3.15. Synthetic receptor with several modification of humanNotch1 jTMD.

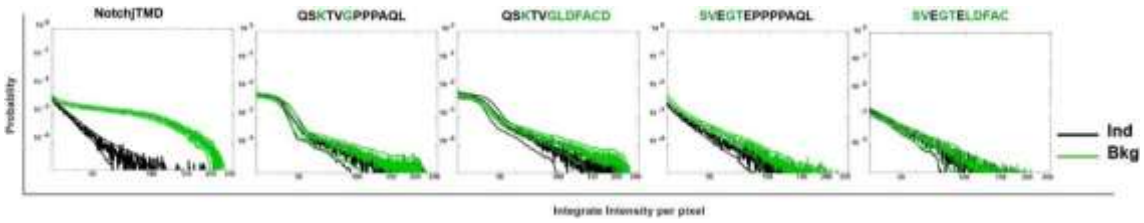

Figure Sup.3.16. Synthetic receptor with jTMD modifications based on electrostatic charges.

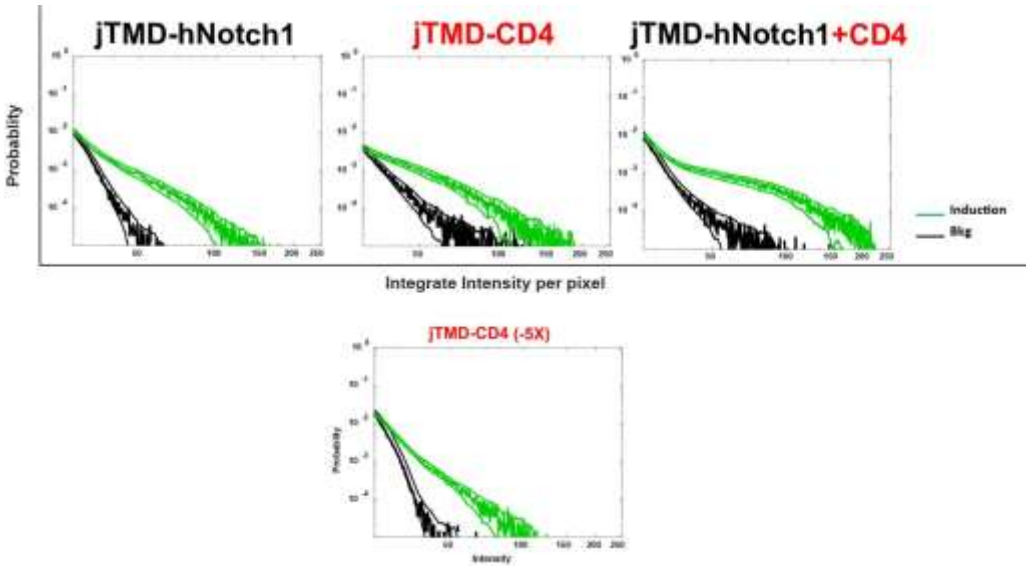

Figure Sup.3.17. Synthetic receptor with NRR and CD4jTMD or 24aa jTMD.

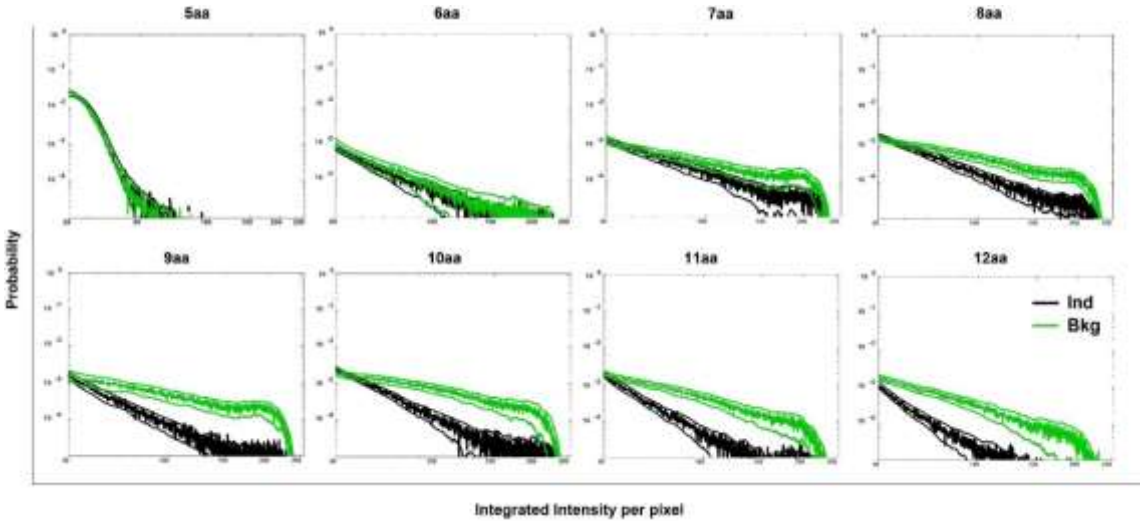

Figure Sup.3.18. Synthetic receptor with NRR in the absence of a full-length (12 aa) jTMD.

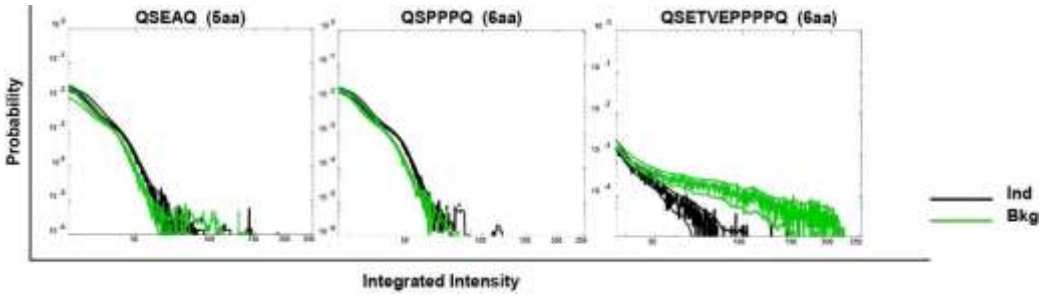

Figure Sup.3.19. Synthetic receptor 1d3NRRG4 with 5 and 6aa jTMD.

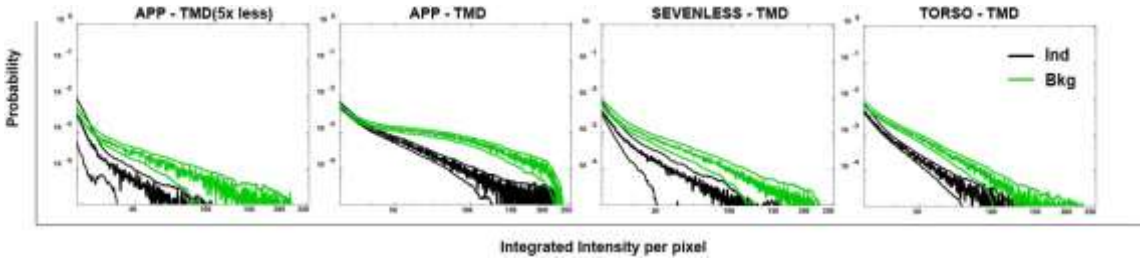

Figure Sup.3.21. Synthetic receptor with different TMDs: TORSO, SEVENLESS and β-APP.